Imperial College London

Department of Medicine

Division of Brain Sciences

Centre for Neuroinflammation and Neurodegeneration

Regulation of Cellular Energy Metabolism

–

Implications for Parkinson's Disease

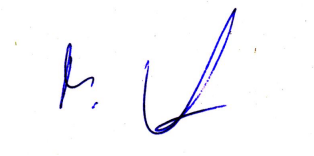
Maria Weinert

PhD thesis

June 2017

Declaration of Originality

I declare that this thesis is my own work and has not been submitted in any form for another degree or diploma at any university or other institution of tertiary education. Information derived from the published or unpublished work of others has been acknowledged in the text and a list of references is given.



Maria Weinert

24th May 2017

Copyright Declaration

The copyright of this thesis rests with the author and is made available under a Creative Commons Attribution Non-Commercial No Derivatives licence. Researchers are free to copy, distribute or transmit the thesis on the condition that they attribute it, that they do not use it for commercial purposes and that they do not alter, transform or build upon it. For any reuse or redistribution, researchers must make clear to others the licence terms of this work.

Acknowledgement

My foremost gratitude goes to my supervisor Kambiz Alavian who gave me the opportunity to work on this exciting project. It has been a privilege to work with Kambiz during these past 3 years, in which he shaped my expectations towards science as well as myself. He has provided constant support over the course of my PhD and has displayed endless patience with me on both good days and bad. His drive for success and perseverance are truly inspiring.

I would like to show my greatest appreciation also to my co-supervisor Prof. David Dexter, who generously shared his knowledge not only on the scientific side of this work, but also regarding all regulations and procedures set out by Imperial College London. His input has been of priceless value.

I owe a very important dept to my progress review panel, Prof. Simone Di Giovanni and Dr. Mark Ungless whose comments were always constructive and highly appreciated. I have greatly benefited from their feedback during key stages of my PhD project.

I want to thank my group for making the time at Imperial so pleasant and enjoyable. A particular thanks to Iain, who was never short of a word to cheer up our days. I would like to display a special appreciation to my colleague and friend Aurélie Millet, whose company on both my professional and personal way was and continues to be of the highest value. In continuation of this notion, I would like to acknowledge all my colleagues from the Division of Brain Sciences for making the years throughout my thesis so wonderful. A special thanks to my neighbours, the SDG group who not only were the best company on those many lunches together, but also were always, absolutely always keen to help. The same holds true for all members of Nel Syed's team. Without Nel's generous sharing of her resources, especially the hypoxia chamber, a substantial part of this thesis could not have been accomplished.

Several other figures deserve to be mentioned here in particular for their special support during this peace of work. Justyna offered her unconditional and very much appreciated help in particular during the first year of my thesis, where expertise and equipment was sparse in our new group. Ilaria has been my rock in the surf and a true inspiration for my future carrier. I am deeply indebted to both and hope to return all those little favours on many future occasions!

I am hugely grateful to my parents, as well as my sister and her family. They have encouraged my professional aspirations, always accepted my decisions – even the inconvenient ones – and offered the greatest support one could wish from a family. Mom, my success is your success. Without your faith in my skills and me I would never have been at this point right now!

Finally, I owe the deepest gratitude to Juanmi, Aurelia and Mateo. There is no better motivation to complete a PhD then your own family waiting for you at home to cheer you up with smiles and kisses on those few moments together. And Juanmi, what patience it took to complete this project – but yet again we did it! This work is dedicated to you and to our children. I wish from the bottom of my heart that one day it will pay off and I will be able to give back all the energy and commitment that you spend for me.

Abstract

Mutations in DJ-1 (PARK7) gene cause recessive, early-onset Parkinson‘s disease. DJ-1 is a neuroprotective oncogene that translocates from the cytoplasm to mitochondria under cellular stress conditions. The neuroprotective role of DJ-1 against reactive oxygen species has been extensively studied but its normal, physiological function is not fully understood. 14-3-3beta is a conserved protein of the 14-3-3 family of chaperones that are implicated in regulation of metabolism in part through regulation of subcellular localisation of their targets. We found that 14-3-3beta interacts with DJ-1 in a phosphorylation-dependent manner. Furthermore, 14-3-3beta inhibits the translocation of DJ-1 to mitochondria under normal cell physiological conditions. The knockdown of 14-3-3beta leads to increased mitochondrial membrane potential, likely through the enhanced mitochondrial translocation of DJ-1. 14-3-3beta knockdown cells show increased proliferation rates under normoxia and hypoxia and are more sensitive to chemical inhibition of mitochondrial ATP production compared to control cell lines. These results suggest that the interaction between DJ-1 and 14-3-3beta plays a role in cellular metabolic balance by influencing the cellular preference for glycolysis or oxidative phosphorylation as the two main modes of ATP production. We also postulate that the neuronal metabolic balance, regulated by the interaction between DJ-1 and 14-3-3beta, is required for cellular adaptation to environmental stress or synaptic activity.

Table of Contents

Preamble

Declaration of Originality **1**

Copyright Declaration **2**

Acknowledgement **3**

Abstract **5**

Table of Contents **7**

List of Figures **12**

List of Tables **14**

Abbreviations **15**

Publications and conference presentations **20**

1 Introduction 22

1.1 Mitochondria and metabolism **23**

1.1.1 Mitochondrial Physiology 24

i) The outer mitochondrial membrane *24*

ii) The intermembrane space and cristae *26*

iii) The inner mitochondrial membrane and matrix *28*

iv) Parameters for the assessment of mitochondrial integrity *30*

1.1.2 Mitochondrial phospholipids 32

i) Composition of the mitochondrial membranes *33*

ii) Lipid synthesis in mitochondria *34*

iii) Lipid import into mitochondria *34*

1.1.3 Protein import mechanisms 35

1.1.4 Mitochondrial genome and evolution 37

i) Mitochondrial genes *37*

ii) Mitochondrial inheritance *37*

1.1.5 Mitochondrial Metabolism 38

i) TCA cycle *39*

ii) Regulation of the TCA cycle *41*

iii) β-oxidation *46*

iv) Electron transport chain and oxidative phosphorylation *48*

v) Ketone body metabolism *49*

vi) Amino acid and pyrimidine synthesis in mitochondria *51*

vii) Urea cycle *52*

viii) NADH-shuttle *52*

1.1.6 Other mitochondrial functions 53
i) Mitochondria as calcium buffering organelles *53*
ii) ROS and Redox homeostasis *55*
iii) Mitochondria and cell death *58*
1.1.7 Mitochondrial dynamics, biogenesis, and degradation 61
i) Mitochondrial biogenesis *62*
ii) Degradation/mitophagy *63*
iii) Fission and fusion *65*
iv) Transport *66*
1.1.8 Role of mitochondria in neuronal metabolism 68
i) Substrates for neuronal metabolism *69*
ii) Neurons generate most ATP via OXPHOS *70*
iii) Neuron-astrocyte interplay *70*
1.2 Parkinson's disease 72
1.2.1 Clinical diagnosis of PD 72
i) Motor symptoms *73*
ii) Non-motor symptoms *74*
1.2.2 The motor circuits of the basal ganglia in PD 74
1.1.3 Treatment of PD 76
i) Pharmacological treatment *76*
ii) Invasive treatment *77*
1.2.4 Pathology 78
i) Neuropathology *78*
ii) Molecular alterations – human studies *79*
iii) Molecular alterations in animal models of PD *81*
iv) Hypotheses of PD pathogenesis *82*
1.2.5 Genetics of Parkinsonism 84
i) α-synuclein *85*
ii) LRRK2 *86*
iii) PINK1 *88*
iv) Parkin *90*
v) DJ-1 *92*
vi) Other genes *92*
1.3 14-3-3 β and its implication in Parkinson's disease 94
1.3.1 Structure and function of the family of 14-3-3 proteins 94
i) Structural determinants of 14-3-3 binding modes 94
ii) Expression 99
iii) 14-3-3 – Mechanisms of action 99
1.3.2 Functions of 14-3-3 proteins 101

i) Metabolic regulation 101
ii) Mitochondrial functions 104
iii) Neuronal functions of 14-3-3 and the implications in PD 105
1.4 DJ-1/Park7 110
1.4.1 Structure of DJ-1 111
1.4.2 Expression and translocation 113
1.4.3 Function of DJ-1 114
i) DJ-1 in cancer and cell proliferation 114
ii) DJ-1 in PD and protein homeostasis 115
iii) The role of DJ-1 in the regulation of peripheral metabolism 116
iv) DJ-1, reactive intermediates and the redox state 117
v) Metabolism and DJ-1 in PD 118
1.5 Hypothesis and aims 121
1.5.1 DJ-1 preliminary screen for novel interaction partners 121
1.5.2 Hypothesis 122
1.5.3 Aims 122

2 Materials and Methods 124
2.1 Tissue culture 125
2.1.1 General considerations 125
2.1.2 Coating of coverslips and culture dishes 126
2.1.3 Culture maintenance 126
i) Culture conditions 126
ii) Sub-culturing 126
iii) Counting cells 127
iv) Cryopreservation and reviving of cell lines 127
2.1.4 Genetic manipulation of cell lines 128
i) CaPO4 transfection 128
ii) Plasmids 129
2.1.5 Production of stable cell lines 130
i) Selection with puromycin – stable knockdown cell lines 130
ii) Selection with G418 – stable overexpression cell lines 130
iii) Transfection and selection of stably transfected cells 131
iv) Single clone isolation and expansion 131
v) Verification of knock down and overexpression 131
2.2 Interaction studies 132
2.2.1 Co-immunoprecepitation (IP) from HEK293T cells 132
i) Transfection and co-IP 132
ii) Phosphatase treatment of HEK293T lysate 133

iii) Interaction screen 133
2.2.2 co-immunoprecipitation (IP) from rat brain lysate 134
2.3 Subcellular fractionation of stable cell lines 135
2.4 Functional assays 137
i) Live cell imaging of mitochondrial potential 137
ii) Luciferase assay for ATP determination 138
iii) AnnexinV-PI cell death assay for flow cytometer 139
iv) Lactate dehydrogenase assay 140
v) SRB proliferation assay 141
2.5 Molecular biology 142
2.5.1 Propagation and purification of plasmid DNA 142
i) Preparation of LB-Agar plates 142
ii) Preparation of CaCl2 competent E.colis 142
iii) Bacterial transformation 143
iv) Preparation of bacterial glycerol stock 144
v) Plasmid propagation and purification 144
2.5.2 Plasmid generation 145
i) Site directed mutagenesis 145
ii) Plasmid sequencing 147
2.6 Biochemistry 147
2.6.1 Bradford assay 147
2.6.2 SDS-PAGE and Western blotting 148
2.7 Statistical analysis 150
2.8 Material 151
Reagents 151
Kits 153

3 Results – Interaction studies of DJ-1 and 14-3-3β 154
3.1 Introduction and Aims 155
3.2 In vitro and in vivo interaction between DJ-1 and 14-3-3β 155
3.3 The interaction of DJ-1 and 14-3-3β is mediated by phosphorylation of DJ-1 ... 156
3.3.1 Phosphorylation-dependence 156
3.3.2 Prediction of phosphorylation sites on DJ-1 157
3.3.3 Interaction of 14-3-3β with functional mutants of DJ-1 161
3.3.4 Summary of phosphorylation studies 163
3.4 Regulation of the interaction between DJ-1 and 14-3-3β by hypoxia 163
3.4.1 Conditions that alter cellular metabolism 163
3.4.2 Stress-inducing treatments 165

3.4.3 Interaction screen 166
3.4.4 Hypoxia is a modulator of 14-3-3β and DJ-1 interaction 168
3.4.5 Summary of the regulation studies 168
3.5 Summary and discussion 169

4 Results – The effect of 14-3-3β on the localisation of DJ-1 174
4.1 Introduction and Aims 175
4.2 Generation of stable cell lines 175
4.2.1 Verification of knockdown and overexpression of stable cell lines 176
4.3 Translocation studies 178
4.3.1 Knockdown of 14-3-3β increases mitochondrial levels of DJ-1 178
4.3.2 Overexpression of 14-3-3β decreases mitochondrial levels of DJ-1 180
4.4 Summary and discussion 182

5 Results – Metabolic co-operation of DJ-1 and 14-3-3β 186
5.1 Introduction 187
5.2 Effect of DJ-1 and 14-3-3β on cellular energy metabolism 187
5.2.1 Effect of DJ-1 and 14-3-3β on mitochondrial membrane potential 188
5.2.2 ΔΨm differences do not effect ATP levels or glycolytic activity 189
5.3 Proliferation and cell death 191
5.3.1 ΔΨm differences alter cell proliferation 191
5.3.2 Oligomycin sensitivity 193
5.3.3 The effect of DJ-1 and 14-3-3β on cell viability 196
5.4 Summary and discussion 198

6 Conclusions and future directions 202
6.1 Conclusions 203
6.1.1 Background and rational 204
6.1.2 Results and conclusions 206
6.1.3 Impact 208
6.2 Future directions 212

7 Supplement 216

8 References 221

9 Addendum - Effect of 14-3-3β on DJ-1 localisation in primary neurons 256
9.1 Introduction 257
9.2 Material and Methods 257
9.2.1 Neuronal isolation and culture 257
9.2.2 Cloning of rat 14-3-3β targeting Crispr/Cas9 vectors 259
9.2.3 Lentiviral pseudo-particle production 260
9.2.4 N27 cell culture and Crispr knockdown validation 261
9.2.5 Subcellular fractionation of primary neurons 262
9.2.6 Reagents and kits 263
9.3 Results: The effect of 14-3-3β on mitochondrial localisation of DJ-1 is cell type-dependent 265
9.3.1 Primary neuronal culture from rat cortex 265
9.3.2 Cas9-mediated gene depletion of rat 14-3-3β 265
9.3.3 14-3-3β enhances mitochondrial DJ-1 levels in primary cortical neurons 267
9.3.4 Cell type-specific expression of DJ-1 in mitochondria correlates with mitochondrial 14-3-3β 268
9.4 Discussion and future directions 271
9.5 References 274

List of Figures

1 Introduction

Figure 1.1 - Mitochondrial compartmentalisation 25
Figure 1.2 - Transport of selected mitochondrial metabolites across the IMM..... 29
Figure 1.3 - TCA cycle and related metabolic networks 40
Figure 1.4 - β-Oxidation of fatty acids 46
Figure 1.5 - Ketone body metabolism 50
Figure 1.6 - The motor circuits of the basal ganglia 75
Figure 1.7 - 14-3-3 sequence homology 96
Figure 1.8 - Structure of 14-3-3 97
Figure 1.9 - Sequence homology of different DJ-1 paralogues 110
Figure 1.10 - The crystal structure of human DJ-1 112

2 Material and Methods

Figure 2.1 - Cell fractionation 137

3 Results – Interaction studies of DJ-1 and 14-3-3β

Figure 3.1 - Interaction between DJ-1 and 14-3-3β 156
Figure 3.2 - Phospho-dependence of DJ-1 interaction with 14-3-3β 157
Figure 3.3 - Putative DJ-1 phosphorylation sites 160
Figure 3.4 - Interaction of 14-3-3β with functional mutants of DJ-1 162
Figure 3.5 - Screen for metabolic modulators of interaction 167
Figure 3.6 - Screen for stress-induced modulators of interaction 167
Figure 3.7 - Effect of hypoxia on the interaction between DJ-1 and 14-3-3β 168

4 Results – The effect of 14-3-3β on the localisation of DJ-1

Figure 4.1 - Generation of stable knockdown cell lines 176
Figure 4.2 - Quantification of knockdown efficiency 177
Figure 4.3 - Generation and verification of stable 14-3-3β overexpression cell lines 177
Figure 4.4 - 14-3-3β knockdown enhances the mitochondrial levels of DJ-1 179
Figure 4.5 - 14-3-3β overexpression decreases the mitochondrial levels of DJ-1 181

5 Results – Metabolic co-operation of DJ-1 and 14-3-3β

Figure 5.1 - DJ-1 and 14-3-3β knockdown have opposing effects on mitochondrial membrane potential 189
Figure 5.2 - Metabolic analysis of DJ-1 and 14-3-3β knockdown 190
Figure 5.3 - Effect of DJ-1 and 14-3-3β knockdown on cell proliferation 192
Figure 5.4 - Oligomycin sensitivity of DJ-1 and 14-3-3β knockdown cell lines 194
Figure 5.5 - Cell viability of stable cell lines 196

6 Conclusions and future directions

Figure 6.1 - Metabolic regulation of DJ-1 and 14-3-3β 205

7 Supplement

Figure S1 - Effect of EGF on the interaction of DJ-1 with 14-3-3β 217
Figure S2 - Oligomycin dose response in stable knockdown cell lines 218
Figure S3 - Cell size and internal complexity of stable knockdown cell lines 219
Figure S4 - Antibody specificity 220

9 Addendum – Effect of 14-3-3β on localisation of DJ-1 in primary neurons

Figure 9.1 - Primary neuronal culture from E18 rat cortex 265

Figure 9.2 - Cas9-mediated knockdown of 14-3-3β in rat N27 cells 266
Figure 9.3 - Cas9-mediated knockdown of 14-3-3β in cortical neurons 267
Figure 9.4 - Effect of 14-3-3β depletion on localisation of DJ-1 in neurons 268
Figure 9.5 - Cell type-specific expression of mitochondrial DJ-1 and 14-3-3β correlates .. 269

List of Tables

2 Material and Methods

Table 2.1 - Cell culture vessels 125
Table 2.2 - $CaPO_4$ transfection 129
Table 2.3 - DNA plasmids 129
Table 2.4 - Primers for DJ-1 functional mutations 146
Table 2.5 - PCR program for QuikChange Lightning 146
Table 2.6 - Antibodies 149

3 Results – Interaction studies of DJ-1 and 14-3-3β

Table 3.1 - Scansite 2.0 motif search 158

5 Results – Metabolic co-operation of DJ-1 and 14-3-3β

Table 5.1 – Overview of functional results 198

9 Addendum – Effect of 14-3-3β on DJ-1 localisation in primary neurons

Table 9.1 - Plasmids used for cloning and lentivirus pseudo-particle production 258
Table 9.2 - 14-3-3β guideRNA and primers used for pL-Crispr.EFS.GFP-r1433β cloning 258
Table 9.3 - PCR program for primer annealing 260
Table 9.4 - DNA/$CaPO_4$ transfection mix for lentiviral particle production 261

Abbreviations

6OHDA	6-hydroxydopamine
aa	amino acid
AD	Alzheimer's disease
ADP	adenosine diphosphate
AGC	asp/glu carrier, mitochondrial
AIF	apoptosis inducing factor
AMPK	AMP-activated protein kinase
ANLS	astrocyte to neuron lactate shuttle
Apaf	apoptotic protease activating factor
APC	ATP-Mg/P_i carrier, mitochondrial
ARNT	aryl hydrocarbon receptor nuclear translocator
AS160	Akt substrate 160
ATF4	autophagy-related factor 4
Atg	autophagy related protein
ATP	adenosine triphosphate
Bad	Bcl-2 antagonist of cell death
Bak	Bcl-2 homologous antagonist/killer
Bax	Bcl-2 associated X protein
BBB	blood brain barrier
Bcl-2	B-cell lymphoma 2
Bcl-x_L	Bcl2-like extra large
BH3	Bcl-2 homology 3
bHB	beta-hydroxybutyrate
Bid	BH3 interacting-domain death agonist
c-myc	cellular myelocytomatosis viral oncogene
$Ca^{2+}_{(c/m)}$	calcium (cytosolic/mitochondrial)
CARD	caspase recruitment domain
Cdc25	Cell Division Cycle 25
CDP	cytidine diphosphate
CK2	creatine kinase 2
CL	cardiolipin
CMV	cytomegalo virus
CoA	coenzyme A
COMT	catechol-O-methyltransferase
CREB	cAMP response element binding protein
Crispr	Clustered regularly interspaced short palindromic repeats
CRTC	cAMP-regulated transcriptional coactivator
CS	citrate synthase
Cys	cysteine
cytC	cytochrome c
DA	dopaminergic
DBS	deep brain stimulation
DIV	Days *in vitro*
DMEM	Dulbecco's modified essential medium
DMSO	dimethyl sulfoxide
DNA	deoxyribonucleic acid
DPBS	Dulbecco's phosphate buffered saline
Drp1	dynamin related protein 1

ECL	enhanced chemiluminescence
ECS	extracellular solution
EDTA	ethylene diamine tetra acetic acid
EGF	epidermal growth factor
EM	electron microscopy
ER	endoplasmic reticulum
Erk	extracellular signal regulated kinase
ERMES	ER mitochondria encounter structures
ERR	estrogen-related receptors
ETC	electron transport chain
FA	fatty acid
FADD	Fas-associated death domain containing protein
FADH2	Flavin adenine dinucleotide, reduced
Fbxo7	F-box only protein 7
FDG	fludeoxyglucose
Fe-S cluster	Iron-sulfur cluster
FEZ1	Fasciculation And Elongation Protein Zeta 1
Fis1	fission protein 1
fMRI	functional magnetic resonance imaging
FUNDC1	FUN14 Domain Containing 1
GABA	γ-aminobutyric acid
GAPDH	glyceraldehyde phosphate dehydrogenase
GBA	glucocerebrosidase
Gem1/Miro-1	GTPase EF-hand protein of Mitochondria/Mitochondrial Rho GTPase 1
GFP	green fluorescent protein
GLUT	glucose transporter
GPi/e	globus pallidus interna/externa
gRNA	guideRNA
GSH	Glutathione, reduced
GSK3	glycogen synthase kinase 3
GSSG	glutathione, oxidised
GWAS	genome-wide association study
H_2O_2	hydrogen peroxide
HEK	human embryonic kidney cells
HILIC	Hydrophilic interaction chromatography
HPLC	High performance liquid chromatography
HRP	horseradish peroxidase
ICS	intracristae space
IDH	isocitrate dehydrogenase
IF1	Inhibitor of F_1F_O ATP synthase
IMM	inner mitochondrial membrane
IMS	intermembrane space
IP	immunoprecipitation
IRS1	insulin receptor substrates 1
JNK	Jun N-terminal kinase
KGDH	alpha-ketoglutarat dehydrogenase (complex)
KIF/KLP	kinesin like protein
Km	Michaelis constant
L-dopa	levodopa
LB	lewy body

LKB1	liver kinase 1
LRRK2	leucine-rich repeat kinase 2
MAM	mitochondria-associated membranes
MAO B	monoamine oxidase B
MAP1LC3	microtubule associated protein 1 light chain 3
MARK	MAP/microtubule affinity-regulating kinase 1
MAT	methylacetoacetyl-CoA thiolase
Mcl-1	myeloid leukemia cell differentiation protein 1
MCU	mitochondrial calcium uniporter
MDH	malat dehydrogenase
Mdm	mitochondrial distribution and morphology protein
MEF2	myocyte enhancer factor-2
Mff	mitochondrial fission factor
Mfn	mitofusin
Mia	Melanoma Inhibitory Activity
MICOS	mitochondrial contact site and cristae organising system
Mid	mitochondrial dynamics protein
Mim	mitochondrial import protein
Mio10	mitochondrial inner membrane organization protein 10
Miro1	mitochondrial Rho GTPase
mitofilin/Fcj1	Formation of crista junctions protein 1
Mmm1	Mitochondrial outer membrane protein 1
MnSOD	manganese superoxide dismutase
MPP^+	1-methyl-4-phenylpyridinium
mPT(P)	mitochondrial permiability transition (pore)
MPTP	1-Methyl-4-phenyl-1,2,3, 6-tetrahydropyridin
mtDNA	mitochondrial DNA
mTOR	mammalian target of rapamycin
MW	molecular weight
NAC	non-amyloid beta component
NAD(P)H	nicotinamide adenine dinucleotide (phosphate), reduced
NALS	neuron to astrocyte lactate shuttle
NCBI	National Center for Biotechnology Information
Nrf	nuclear factor erythroid 2-related factor
OMM	outer mitochondrial membrane
OXPHOS	oxidative phosphorylation
p53	phospho-protein of 53 kDa
PA	phosphatidic acid
Pael-R	Parkin-associated endothelin receptor-like receptor
PAGE	polyacryl amide gel electrophoresis
PAM	presequence translocase-associated import motor
PAM sequence	protospacer adjacent motif
PAR	poly-(ADP ribose)
PARIS	Parkin interacting substrate
PARP	poly-(ADP ribose) polymerase
PC	phosphatidylcholine
PD	Parkinson's disease
PDC	pyruvate dehydrogenase complex
PDH	pyruvate dehydrogenase
PDK	PIP3-dependent protein kinase

PDL	poly-D-lysine
PE	phophatidylethanolamine
PES	polyethersulfone
PET	positron emission tomography
PFK	6-phosphofructo-2-kinase
PG	phosphatidylglycerol
PGAM5	phosphoglycerate mutase 5
PGC-1	peroxisome proliferator-activated receptor-_ coactivator-1
PHD	peptidyl prolyl hydroxylase
P_i	inorganic phosphate
PI	phosphatidylinositol
PI3K	phosphatidyl inositol 3 kinase
pIMS	peripheral intermembrane space
PINK1	PTEN-inducible putative kinase 1
PIP3	phosphatidylinositol-3,4,5-trisphosphate
PKC	protein kinase C
PL	phosoholipid
PMF	proton motive force
PPAR	peroxisome proliferator-activated receptors
PPP	pentose phosphate pathway
PRAS40	proline-rich Akt substrate 40
PTEN	phosphatase and tensin homolog
PUMA	p53 upragulated modulator of apoptosis
Raf	rapidly accelerated fibrosarcoma proto-oncogene
RANBP	Ran-specific binding protein 1
Ras	Rat sarcoma proto-oncogene
rcf	relative centrifugal force
REM	rapid eye movement
RGS3	regulator of G protein signaling 3
RIPK	receptor-interacting protein kinase
ROS	reactive oxygen species
rpm	rounds per minute
SAM	sorting and assembly machinery
SCOT	succinyl-CoA:3-CoA transferase
SDH	succinate dehydrogenase complex (complex II of the ETC)
Sdh	subunit of SDH complex
SDS	sodium dodecyl sulfate
SIK2	salt-inducible kinase 2
Slc25	solute carrier 25
SMAC	second mitochondria-derived activator of caspase
SNCA	gene ID for alpha-synuclein
SNpc	substantia nigra pars compacta
SOD	superoxide dismutase
SPECT	single-photon emission computer tomography
STN	subthalamic nucleus
TBS	tris buffered saline
TCA	trichloroacetic acid
Tfam	transcription factor A, mitochondrial
TFB2M	transcription factor B2, mitochondrial
TIM	translocase of the inner mitochondrial membrane

Tim	subunit of the TIM complex
TM	transmembrane
TMRE	Tetramethylrhodamine ethyl ester
TNF	tumour necrosis factor
TNFR	TNF receptor
TOM	translocase of the outer mitochondrial membrane
Tom	subunit of the TOM complex
TRADD	TNFR-associated death domain containing protein
TRAIL	TNF-related apoptosis-inducing ligand
TRX	thioredoxin
TSC	tuberous sclerosis complex
ULK1	unc51-like kinase1
VDAC	voltage-dependent anion channel
VHL	Von Hippel Lindau protein
WB	western blot
YWHAB	tyrosine and tryptophane hydroxylase activator beta
YY1	yin yang 1
ΔpH	proton gradient across the inner mitochondrial membrane
Δψm	membrane potential across inner mitochondrial membrane

Publications & conference presentations based on this work

Research article

Isolation, culture and long-term maintenance of primary mesencephalic dopaminergic neurons from embryonic mouse brain

Maria Weinert, Tharakeswari Selvakumar, Travis S Tierney, Kambiz N Alavian (2015). J Vis Exp.19;(96). doi: 10.3791/52475

DJ-1 mediated regulation of mitochondrial energy metabolism through direct binding to 14-3-3β

Maria Weinert, Kambiz N Alavian (2017). In preparation

Poster presentations

Biophysical Society Annual meeting 2017, New Orleans, US

Elizabeth A Jonas, Nelli Mnatsakanyan, Paige Miranda, Han-A-Park, Rongmin Chen, Pawel Licznerski, Maria Weinert, Peter JS Smith, Andres Chavez, Suzanne R Zukin, Valentin K Gribkoff, Kambiz N Alavian

Mitochondria and Memory: Bioenergetics, Synaptic Plasticity and Neurodegeneration

GRC Neurobiology of Brain Disorders 2017, Girona, Spain

Maria Weinert, Aurélie MC Millet, Elizabeth A Jonas, Kambiz N Alavian

DJ-1 interaction with 14-3-3β regulates cellular energy metabolism

Biophysical Society Annual meeting 2016, Los Angeles, US

Maria Weinert, Aurélie MC Millet, Elizabeth A Jonas, Kambiz N Alavian

DJ-1 interaction with 14-3-3β regulates cellular energy metabolism

Young Scientist Day 2016, Imperial College London, UK

Maria Weinert, Aurélie MC Millet, Elizabeth A Jonas, Kambiz N Alavian

DJ-1 interaction with 14-3-3β regulates cellular energy metabolism

Young Scientist Day 2015, Imperial College London, UK

Maria Weinert, Aurélie MC Millet, Elizabeth A Jonas, Kambiz N Alavian

Mechanisms of Modulation of cellular energetics by the Parkinson's disease protein DJ-1

1 Introduction

1.1 Mitochondria and metabolism

Since their discovery by Robert Altmann in 1890 (Ernster and Schatz, 1981) mitochondria have attracted the interest of numerous scientists due to their fascinating biology. The bacterial origin of mitochondria and their unique genetics has made them invaluable tools for unravelling eukaryotic evolution. The popular picture of mitochondria as the powerhouses of the cell reflects their key function in energy metabolism but the function of these organelles is not limited to adenosine triphosphate (ATP) production. Mitochondria are important hubs that integrate amino acid, lipid, and redox metabolism with energy production.

In the 1970s evidence for a role of mitochondria in calcium (Ca^{2+}) buffering (Lehninger, 1974; Nicholls, 1978) and reactive oxygen generation (Cadenas et al., 1977; Dionisi et al., 1975) accumulated. Finally, the discovery of the role of mitochondria in programmed cell death in the 1990s (Green and Reed, 1998; Liu et al., 1996; Richter, 1993; Susin et al., 1999) resulted in a shift of the research focus away from energy metabolism. This ultimately led to the identification of mitochondrial dysfunction in various pathological conditions, including cancer (Wallace, 2012), neurodegeneration (Lin and Beal, 2006), diabetes (Giacco and Brownlee, 2010), ischemic injury (Yu et al., 2002) and inflammation (Zhou et al., 2011).

We have accumulated extensive knowledge regarding the importance of mitochondria in energy and substrate metabolism, cell death, as well as ion and redox regulation of the cell. The integrative nature of mitochondria provides an ideal system for the regulation of cell physiology. Recent evidence suggests that different mitochondrial functions share molecular entities. For example, several proteins traditionally implicated in the regulation of mitochondrial cell death have now been linked to mitochondrial energy metabolism and vice versa (Alavian et al., 2014; Alavian et al., 2011; Gimenez-Cassina and Danial, 2015; Gross, 2016; Kruiswijk et al., 2015). Furthermore, alteration of mitochondrial function may play a major role during cellular adaptation under physiological (e.g. development; (Chan, 2006; Hom et al., 2011) and pathological (e.g. cancer; (Wallace, 2012) conditions.

Future challenges include the determination of the regulatory mechanisms that govern mitochondrial metabolism and cell death and how these are integrated into cellular signalling events. Manipulation of these regulatory mechanisms may offer new therapeutic avenues for disorders with mitochondrial malfunction.

1.1.1 Mitochondrial Physiology

Mitochondria are cellular organelles containing an outer (OMM) and inner (IMM) mitochondrial membrane that together enclose the intermembrane space (IMS) (Mannella, 2006) (Figure 1.1). The inner mitochondrial membrane contains numerous invaginations leading to a net increase of membrane surface. Enclosed by the IMM is the mitochondrial matrix. The IMM invaginations give rise to physically constraint structures called cristae (Cogliati, Enriquez et al. 2016). Each of the mitochondrial compartments is functionally specialised and plays a vital role in organelle integrity.

i) The outer mitochondrial membrane

The OMM is a lipid bilayer composed mainly of phosphatidylserine, phosphatidylethanolamine, and phosphatidylinositol (de Kroon et al., 1997). The OMM is considered permeable to most metabolites due to protein channels of the voltage-dependent anion channel (VDAC) family, which allow passive diffusion of molecules up to 6 kDa (Gellerich et al., 2000). Weak substrate specificity and gating of the channels is mainly dependent on membrane voltage and conformational changes of the protein (Villinger et al., 2010). The opening of VDACs is further regulated by ions, small molecules, pro-apoptotic B-cell lymphoma 2 (Bcl-2) proteins (Huang et al., 2013; Shi et al., 2003) and hexokinase I (Azoulay-Zohar et al., 2004). Due to this regulation and its importance in substrate exchange between cytosol and mitochondria VDAC plays an important role in mitochondrial metabolism and cell death (Lemasters and Holmuhamedov, 2006).

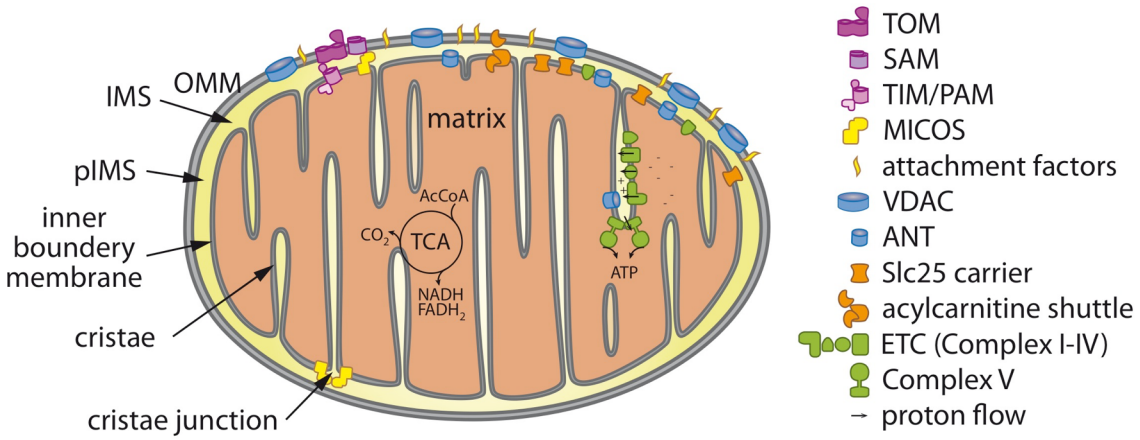


Figure 1.1 – Mitochondrial compartmentalisation. Mitochondria are double membrane-bound organelles that are characterised by typical inner membrane invaginations called cristae. Each mitochondrial compartment is functionally different and contains a specialised set of proteins. Some of the main functions and components are indicated. For more information see text. OMM – outer mitochondrial membrane, (p)IMS – (peripheral) inner membrane space, TCA – tricarboxylic acid cycle, AcCoA – acetyl-Coenzyme A, TOM – translocase of the outer mitochondrial membrane complex, SAM – sorting and assembly machinery, TIM – translocase of the inner mitochondrial membrane, PAM – presequence translocase-associated import motor, MICOS – mitochondrial inner membrane and cristae organising centre, VDAC – voltage-dependent anion channel, ANT – adenine nucleotid translocator, Slc25 – solute carrier 25 family, ETC – electron transfer chain.

In contrast to metabolites VDAC is impermeable to proteins. This is an important feature as the release of IMS proteins, such as cytochrome C and apoptosis-inducing factor (AIF) into the cytosol facilitates the initiation of programmed cell death (Tait and Green, 2010). For the protein transport across the OMM a multi-protein complex called translocase of the outer mitochondrial membrane (TOM) is specialised in protein recognition and translocation into or across the OMM (Chacinska et al., 2009). The TOM complex works in close association with the sorting and assembly machinery (SAM) and the translocase of the inner mitochondrial membrane (TIM) complex, which are located at the OMM and IMM, respectively (Chacinska et al., 2009).

In addition to metabolite and protein transport components, the OMM contains other attachment factors such as anchor proteins for mitochondrial trafficking along the cytoskeleton (Schwarz, 2013; Sheng, 2014) and tethering factors to other membranous compartments of the cell (e.g. the endoplasmic reticulum (ER); (de Brito and Scorrano, 2008). Finally, association of fission and fusion proteins to the OMM are crucial for mitochondrial dynamics (Chen and Chan, 2009), a process linked to mitochondrial integrity and longevity.

Other protein components that are found in or associate with the OMM include acyl-CoA synthetase and carnitine acyl transferase I (both involved in fatty acid transport across the OMM) (Eaton et al., 1996), regulatory proteins of the Bcl-2 family (Gimenez-Cassina and Danial, 2015; Shi et al., 2003), as well as enzymes involved in cell metabolism, namely hexokinase (Danial et al., 2003; Majewski et al., 2004).

Taken together, the mitochondrial outer membrane acts as diffusion barrier for metabolites and mitochondrial IMS proteins. It creates a microenvironment that favours mitochondrial metabolite import (Gellerich et al., 2000), which can alter the kinetics of mitochondrial enzymes. Furthermore, the OMM is implicated in the regulation of mitochondrial activity and dynamics (Liesa and Shirihai, 2013), as well as trafficking and localisation (Sheng, 2014).

ii) The intermembrane space and cristae

The IMS is defined as the lumen between the outer and inner membrane and has been classically considered one single compartment. This view was given up due to our understanding of the structural and functional specialisation of the cristae (Pfanner et al., 2014). Therefore, the intermembrane space can be subdivided into the peripheral intermembrane space (pIMS), where both OMM and IMM (inner boundary membrane) are in close proximity, and the intracristae space (ICS) (Herrmann and Riemer, 2010).

The cristae shape and volume can vary significantly between different cells or during metabolic adaptation. Cristae are physically separated from the pIMS and the inner boundary membrane by a protein complex called MICOS (Pfanner et al., 2014). This multi-subunit complex resides in the IMM and in mammals involves the proteins Mic10/Minos1, Mic19/CHCHD3, Mic25/CHCHD6, Mic26/ApoO, Mic27/ApoO-like, and Mic60/IMMT/mitofilin. The complex may be tethered to the OMM via binding to Sam50, Metaxin (Mtx)1, Mtx2 and DnaJC11 (Zick et al., 2009). Interestingly, the proteins enriched in cristae differ from those in the pIMS. Cytochrome C (cyt C), an integral part of the electron transport chain (ETC), is mainly found in cristae (Scorrano et al., 2002), whereas proteins of the protein import machinery localise to membranes surrounding the peripheral intermembrane space (Zick et al., 2009). In line with cytC enrichment in the ICS, proteins involved in aerobic energy production are abundantly expressed in the cristae membrane and at least one of these complexes, the F_1F_O ATP-Synthase plays an active role in shaping the cristae (Rabl et al., 2009).

Despite the relative permeability of the OMM, the intermembrane space differs from the cytosol in its small molecule composition. In particular, the pH is 0.2 to 0.7 units above the cytosolic pH. This was proposed to be of importance for the kinetics of the ATP producing enzyme F_1F_O ATP-Synthase (Cogliati et al., 2016; Herrmann and Riemer, 2010), which uses the flow of H^+ from the IMS into the matrix for the production of ATP from ADP and organic phosphate (P_i), a biophysical mechanism known as mitochondrial coupling. In addition, the IMS is a more oxidative environment than the cytosol or the mitochondrial matrix as measured by the ratio of oxidised over reduced glutathione (GSH)(Hu et al., 2008). The main release sites of reactive oxygen species (ROS) are complex I and complex III of the ETC, which are mainly found in the cristae membrane. It was proposed that the differences in oxidative capacity of the IMS may be due to differential localisation of GSH and possibly other anti-oxidative molecules (Herrmann and Riemer, 2010). The oxidative environment of the IMS plays a crucial role in protein import and folding and contains specialised enzymes

that catalyse the formation of disulfide bonds (Riemer et al., 2009). Furthermore, the generation of ROS, particularly the membrane-permeable H_2O_2, plays an important role as signalling molecule controlling metabolism and apoptosis at the level of mitochondria, cytosol, plasma membrane and the nucleus (Murphy, 2009).

Alongside the importance of IMS in protein import and redox regulation it plays a role in metal homeostasis (mainly iron, copper and zinc) and the regulation of lipid import or turnover. The IMS contains specific metal binding proteins of the family of metallothioneins (Ye et al., 2001). Metallothioneins are characteristic of a high cysteine (Cys) content and were shown to bind and possibly sequester metal and heavy metal ions (Coyle et al., 2002). Furthermore, several transport and assembly factors of the IMS are proposed to bind metal ions via twin-cysteine motifs (Herrmann and Riemer, 2010). These factors are essential for the targeting and correct assembly of proteins involved in electron transfer and energy production. For example, Cox17 is responsible for the transport of copper to the Cu_A and Cu_B sites of cytochrome oxidase (Horng et al., 2004). A tight control of metal availability is therefore important for the correct functioning of mitochondria (Herrmann and Riemer, 2010).

The role of the IMS in mitochondrial lipid regulation is not well understood. IMS proteins of the Ups family were found to regulate the content of phospholipids in the inner membrane, specifically phosphatidylserine and cardiolipin, in yeast (Tamura et al., 2009). Importantly, the lipid content between inner and outer membrane is not identical, arguing for a compartment-specific lipid transport or conversion system (Herrmann and Riemer, 2010). More research is required to understand the regulation of phospholipid content in the mitochondrial membranes.

iii) The inner mitochondrial membrane and matrix

The inner membrane and the matrix are the core of the mitochondrion. They contain the majority of mitochondrial-targeted proteins as well as the mitochondrial DNA and translation

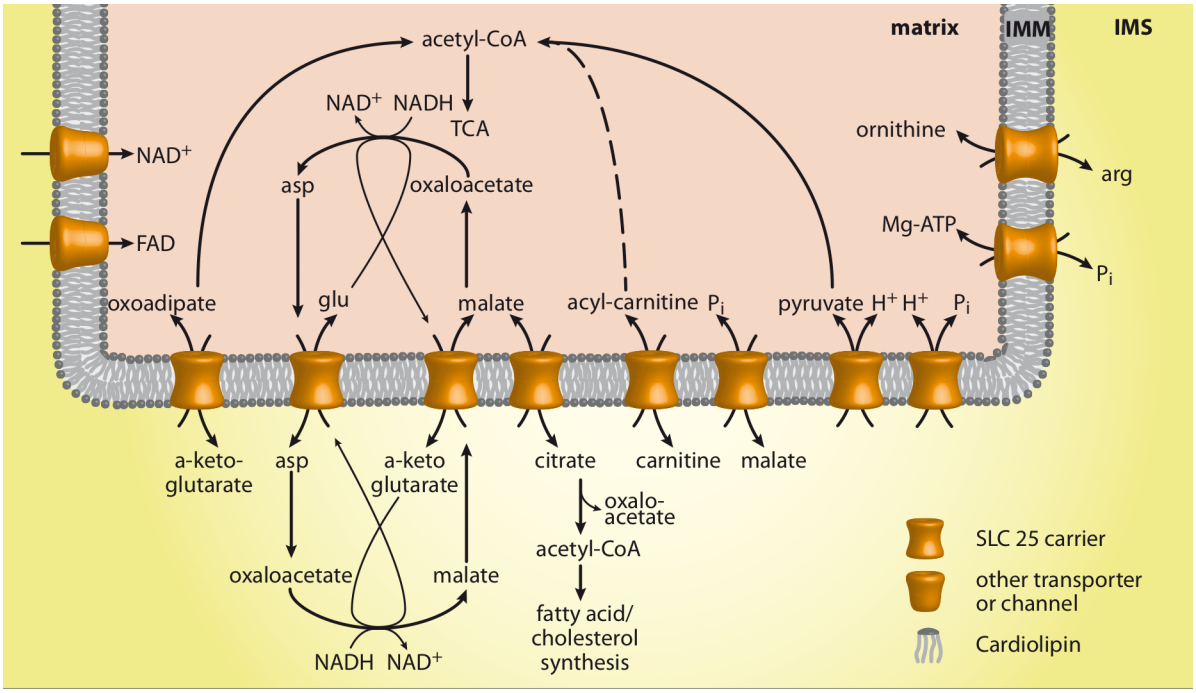


Figure 1.2 – Transport of selected mitochondrial metabolites across the IMM. The IMM is a tightly sealed membrane. Transporters of the Slc25 family of solute carriers regulate the import of most mitochondrial metabolites. Many transport pathways are linked with each other. Some metabolite, such as pyruvate, P_i and Mg-ATP depend on the mitochondrial membrane potential for their import. Other metabolites are transported along a concentration gradient between matrix and IMS/cytosol. Glutamine is known to be imported into mitochondria but the molecular component of the mitochondrial glutamine transporter has not been identified yet. IMM – inner mitochondrial membrane, IMS – intermembrane space, TCA – tricarboxylic acid cycle.

machinery, which are all crucial for mitochondrial energy production and metabolic conversion of amino acids and nucleotide precursors.

In sharp contrast to the OMM the inner membrane is a tightly sealed lipid bilayer of special lipid composition and very rich in proteins. To pass this membrane, most molecules are transported through specialised carriers. The majority of substrate carriers belong to the solute carrier-25 (Slc25) family. These monomeric transporters are almost exclusively expressed in the inner mitochondrial membrane and consist of 6 transmembrane α-helices. The characteristic of Slc25 family members is the tripartite sequence: three tandemly repeated sequences each containing two hydrophobic regions that make up the

transmembrane segments. This sequence homology allowed the identification of 53 genes of the Slc25 family, all encoded in the nucleus (Gutierrez-Aguilar and Baines, 2013).

The majority of metabolites crossing the IMM are substrates for mitochondrial energy metabolism, a process that can be divided into the tricarboxylic acid (TCA) cycle (also known as citric acid or Krebs cycle), β-oxidation, and oxidative phosphorylation (OXPHOS). All proteins that participate in these three pathways are found in the matrix and/or at the IMM. The TCA cycle converts the energy derived from carbohydrates and proteins into the reducing equivalents NADH and $FADH_2$, whereas β-oxidation produces reducing equivalents through the breakdown of fatty acids (Berg et al., 2015).

The electrons bound to NADH and $FADH_2$ are then transferred onto molecular oxygen (O_2) in a stepwise manner by the electron transport chain (ETC). The ETC is the first part of OXPHOS and couples the energy of exothermic redox reactions to the translocation of protons from the matrix into the IMS. This produces an electrochemical gradient (ΔpH) across the IMM. Finally, ΔpH is dissipated by the last component of the OXPHOS, the F_1F_O ATP Synthase (hereafter referred to as ATP Synthase). The enzyme couples the kinetic energy obtained from the backflow of protons into the matrix (via membrane bound F_O) to the production of ATP from ADP and inorganic phosphate (P_i) (at F_1 site) (Berg et al., 2015).

iv) Parameters for the assessment of mitochondrial integrity

The mitochondrial membrane potential ($\Delta\psi_m$) is the key to mitochondrial function. It results mainly from ΔpH across the IMM, although other ion gradients can contribute to the potential. Therefore, both ΔpH and $\Delta\psi_m$ determine the proton motive force (PMF) (Dzbek and Korzeniewski, 2008). From a physical point of view it is the PMF that drives the physical work necessary for the enzymatic reaction of ATP Synthase. However, the direct measurement of PMF is difficult due to its complex nature. In praxis determination of ΔpH and more commonly $\Delta\psi_m$ is the biological determinant used for assessment of mitochondrial function. Because of the practical relevance I will focus this section on the mitochondrial membrane potential.

The importance of $\Delta\psi_m$ is not limited to mitochondrial ATP production. The energy stored in the $\Delta\psi_m$ is used for carrier-driven nutrient import across the IMM (Palmieri, 2004). Furthermore, enzymes of the electron transport chain and the ATP Synthase are voltage-sensitive and $\Delta\psi_m$ has an impact on their activities (Huttemann et al., 2008). Finally, processes that drive mitochondrial fission and fusion, biogenesis, degradation and transport are $\Delta\psi_m$ dependent (Chen and Chan, 2009). Taken together, the mitochondrial membrane potential is used to drive and regulate most, if not all mitochondrial processes.

For most cells, the optimal $\Delta\psi_m$ is maintained between -120 mV and -160 mV (Gerencser et al., 2012). This range is crucial for mitochondrial function but the evaluation of $\Delta\psi_m$ alone has limitations. On the technical side, the $\Delta\psi_m$ is often measured using potentiometric dyes that can only yield relative information. Secondly, at least in theory the $\Delta\psi_m$ could be maintained by virtue of a chemical equilibrium without net flux of protons across the membrane and therefore independent of ATP production. Albeit unlikely in normal cells, this scenario becomes more realistic in some cancer cells. During tumourigenesis many cancer cells are believed to undergo a metabolic shift, which includes production of the majority of ATP by glycolysis at the expense of OXPHOS activity. This process has been known as the Warburg effect (Cairns et al., 2011). It is now recognised, however, that cancer cells maintain their mitochondria even in the absence of OXPHOS activity because these cells rely on mitochondrial enzymes for amino acid, nucleotide and fatty acid production (Ahn and Metallo, 2015). Since non-functional mitochondria are usually degraded, cancer cells have evolved various strategies to circumvent the degradation, including at the level of OXPHOS activity (Chandra and Singh, 2011; Sharp et al., 1992; Wallace, 2012).

To fully understand mitochondrial function, a number of additional parameters beside $\Delta\psi_m$ have to be considered. To assess mitochondrial respiration, oxygen consumption measurements can be undertaken either in single cell experiments (Gleichmann et al., 2009;

Osbourn et al., 2005) or in cell culture (Wagner et al., 2011) and on isolated mitochondria (Lanza and Nair, 2009). Certain conditions can cause oxygen consumption and proton pumping independent of ATP production, a mechanism known as uncoupling. This can be assessed indirectly by measuring mitochondrial ATP production (Fujikawa and Yoshida, 2010) or directly through the electrophysiological assessment of IMM ion permeability (Sacchetti et al., 2013). Metabolite flux can be tested using radiolabelled substrates coupled to mass spectrometry analysis of downstream metabolites containing incorporated radiolabel (Metallo et al., 2012; Wise et al., 2011). Due to the flow equilibrium present in all metabolic processes, only the combined assessment of several mitochondrial parameters can provide the information necessary to understand the mitochondrial function within a specific setting.

1.1.2 Mitochondrial phospholipids

Phospholipids (PL) are the building blocks of biological membranes and fulfil numerous different functions beside their mere structural role. There are a large number of different PLs that exhibit unique physical and functional properties (Dowhan, 1997). Furthermore, every biological membrane has a special function and therefore contains a particular PL composition (Vance and Tasseva, 2013). Phospholipids are composed of a triacylglycerol that contains acyl chains in the sn1 and sn2 position linked via an ester bond, as well as a hydrophilic head group in the sn3 position, linked via a phosphodiester bond. The acyl chains can be saturated or unsaturated. Acyl chain length and saturation are the main determinants of membrane thickness and fluidity. The identity of the hydrophilic head group determines the surface charge of a membrane and can influence membrane shape (Dowhan, 1997). PL head groups often have other functional properties including protein binding and signalling (Posor et al., 2015; Vance and Tasseva, 2013). In addition to phospholipids, different cholesterols can be a main component of some biological membranes. They have a more rigid hydrophobic backbone and a very small hydroxygroup as the hydrophilic component. Cholesterol plays an important role in membrane fluidity and curvature (Grouleff et al., 2015).

i) Composition of the mitochondrial membranes

The main components of mitochondrial membranes are the phospholipids phosphatidylcholine (PC) and phosphatidylethanolamine (PE). Together they represent up to 80% of total mitochondrial PL. In addition, mitochondria of brain, heart, spleen, adrenal cortex and kidney contain up to 5-30% PC and PE plasmalogens (Horvath and Daum, 2013). Plasmalogens contain an ether bond in the sn1 position making them more rigid and lipophilic than conventional phospholipids. They can form membrane microdomains, and are involved in protein interaction as well as membrane fusion events (Braverman and Moser, 2012).

Cardiolipin (CL) is a lipid that can only be found in mitochondria, where it is synthesised in the inner leaflet of the IMM. Under physiological conditions, CL remains in the inner membrane compartment, where it plays an important role in protein-lipid interaction. For example, CL is required for peripheral binding of cytochrome C to the IMM (Ott et al., 2007). Although only present in traces at the OMM, accumulation of CL in the OMM is a marker for induction of apoptosis and is required for Caspase 8 recruitment and pro-apoptotic Bid cleavage at the OMM (Kantari and Walczak, 2011). Truncated Bid facilitates mitochondrial outer membrane permeabilisation in co-operation with Bax (Kuwana et al., 2002), a pre-requisite for the mitochondrial pathway of apoptosis. Other mitochondrial phospholipids are phosphatidylinositol (PI), phosphatidylserine (PS), and cholesterols. PI is a sparse phospholipid with signalling activity (Posor et al., 2015). In mitochondria it is enriched in the OMM, compared to IMM. PS is highly abundant in biological membranes, but present in relatively low amounts in mitochondria compared to plasma membrane (Horvath and Daum, 2013; Osman et al., 2011). Cholesterols are present in mitochondria in varying amounts, depending on the cell type and organism. Levels of cholesterol in mitochondria are usually lower than in other cellular membranes. Sphingolipids are generally absent from mitochondria (Horvath and Daum, 2013; Osman et al., 2011).

ii) Lipid synthesis in mitochondria

The majority of membrane components are synthesised in the ER. However, mitochondria can produce a subset of phospholipids autonomously. Phosphatidic acid (PA), is an intermediate substrate that can be synthesised from glycerol-3-phosphate by addition of one acyl chain by glycerophosphate acyltransferase at the OMM. Addition of another acyl chain leads to formation of diacyl glycerol (DAG), the precursor of all PLs and of CL. At the IMS site of the IMM, addition of ethanolamine from CDP-ethanolamine to DAG is the synthetic pathway for mitochondrially produced PE. Similarly, the addition of glycerol to CDP-DAG results in formation of phophatidylglycerol at the IMM. At the matrix site of the IMM CL synthase catalyses the addition of DAG to phosphorylated PG to form cardiolipin. The characteristic 18:1 acyl chains of CL are added during a final acyl exchange reaction. CL synthase is inhibited by lysophospholipids and activated by the divalent cations, PE and CL. CL levels are changing with developmental stage and metabolic conditions and are regarded as a marker for the development of mitochondrial membranes (Horvath and Daum, 2013; Osman et al., 2011).

iii) Lipid import into mitochondria

Other lipids, such as PC, PS and PI have to be imported into mitochondria. A specialised membrane compartment of the ER, known as the mitochondria-associated membranes (MAM) is enriched in lipid biosynthetic enzymes and is physically tethered to the mitochondrial outer membrane. EM analysis reveals an electron-rich connection of 9-16 nm between smooth ER and mitochondria, suggestive of a proteinaceous bridge (Vance, 2014). In mammalian cells, Mitofusin2 (Mfn2) on mitochondria and ER participates in ER-tethering and knockdown of Mfn2 increases the distance of mitochondria to ER (de Brito and Scorrano, 2008). A role for cholesterol in negative regulation of ER to mitochondria distance has been described as well (Fujimoto et al., 2012). Recently a complex mediating the binding of MAM to mitochondria was identified in yeast. The complex was termed ERMES (ER-mitochondria encounter structure) and consists of the mitochondrial distribution and morphology proteins Mdm10, Mdm12, Mdm34, as well as the ER protein Mmm1. Disruption

of the ERMES complex in yeast leads to impaired mitochondria-ER tethering and impaired mitochondrial PL synthesis (Osman et al., 2011). Importantly, the ERMES components are not conserved in mammalian cells and an essential function for ERMES in mitochondria to ER tethering has therefore been challenged. Rather, a role for ERMES in regulation of mitochondrial morphology has been suggested (Vance, 2014).

A function in phospholipid production and transfer to mitochondria has been proposed for MAM due to the accumulation of phospholipid biosynthetic proteins. Furthermore, increased mitochondria to ER distance caused by depletion of Mfn2 correlates with decreased PS import into mitochondria alongside lowered mitochondrial calcium (Ca^{2+}_{m}) concentration. PE import into mitochondria may be mediated by a direct membrane interaction between MAM and mitochondria whereas mitochondrial import of PC and cholesterol may be attributed to StAR (steroidogenic acute regulatory) protein-dependent transfer between membranes. Taken together, the exact mechanisms of PL transfer from ER to mitochondria require further investigation (Horvath and Daum, 2013; Vance, 2014).

1.1.3 Protein import mechanisms

A majority of mitochondrial proteins are encoded in the nucleus and need to be imported into the mitochondrion. Mitochondria have developed unique import mechanisms that function independently of the endoplasmic reticulum (ER) and Golgi apparatus. Most mitochondrial proteins are translated on ribosomes in the cytoplasm and are targeted to mitochondria post-translationally. Cytosolic chaperones of the heat-shock family, such as Hsp70, Hsp90 and several members of the J-domain containing Hsp40 family bind to mitochondrial precursors to prevent misfolding and aid translocation to the outer mitochondrial membrane (Bhangoo et al., 2007; Young et al., 2003).

With a few exceptions all mitochondrial proteins have to pass through the translocator of the outer mitochondrial membrane (TOM) complex. The TOM complex consists of the receptor

subunits Tom20 and Tom70, the central receptor Tom22, the pore forming subunit Tom40, the auxiliary Tom5 as well as Tom6 and Tom7 that facilitate association and dissociation, respectively (Dudek et al., 2013).

After the TOM-mediated import various anchor and targeting signals define the final destination of each mitochondrial protein. OMM proteins with β-barrel conformation are recognised by intermembrane chaperones Tim9 and Tim10. The Tim9/Tim10 complex guides its substrates to the IMS site of the sorting and assembly machinery (SAM), which is integrated into the outer membrane. The SAM complex then inserts and releases β-barrel proteins into the OMM (Dudek et al., 2013).

The sorting of IMS proteins is mainly driven by the disulfide relay system, which depends on cysteine residues embedded into amphipathic α-helices of the target protein. The oxidative environment of the IMS together with the redox enzyme Mia40 aid the formation of intramolecular disulfide bonds in the target proteins thereby facilitating protein folding. This mechanism traps the now folded proteins in the IMS (Becker et al., 2012).

Finally, IMM and matrix targeted proteins are imported by the translocase of the inner mitochondrial membrane (TIM) complex. Two different TIM complexes, namely TIM22 and TIM23, are being distinguished depending on the presence of Tim22 or Tim23 as the central pore of the complex, respectively. Matrix and IMM proteins with a classical mitochondrial pre-sequence are directly recognised by the TIM23 complex, inserted into the membrane and either released laterally into the IMM or translocated completely into the matrix by means of the presequence translocase-associated import motor complex (PAM) (Chacinska et al., 2009). Alternatively, IMM proteins with an internal targeting sequence, such as those of the Slc25 family of transporters, are guided to the TIM22 complex by the Tim9/Tim10 chaperone complex, followed by insertion and lateral release into the membrane (Becker et al., 2012; Dudek et al., 2013). Importantly, TIM-dependent protein import is driven by the attraction of

the positively charged targeting sequences to the negative matrix and hence depends on an intact mitochondrial electrochemical gradient (Becker et al., 2012; Kovermann et al., 2002; van der Laan et al., 2007).

1.1.4 Mitochondrial genome and evolution

i) Mitochondrial genes

In contrast to all other mammalian organelles, mitochondria contain a separate set of genes that are encoded in the mitochondrial genome. This genome is located on a single plasmid that contains a total of 38 genes. These include 14 protein-coding sequences, 2 rRNA genes and 22 tRNA genes (Gray, 1989). Most of the protein-coding genes are part of the electron-transport chain and all complexes, with the exception of complex II (Succinate dehydrogenase), contain at least one mitochondrial-encoded protein. An exception among the mitochondria encoded genes is the newly discovered peptide humanin, which can be translated either in the matrix or in the cytoplasm. Humanin has pleiotropic functions both inside mitochondria as well as in other compartments of the cell, which generally seem to be cytoprotective (Lee et al., 2013). An interesting feature of the mitochondrial DNA is the presence of various copies of the mitochondrial plasmid within the mitochondrial nucleoid. Due to mutations within single plasmids and subsequent proliferation of the different variants mitochondria can adapt a so-called heteroplasmic state (Solignac et al., 1987).

ii) Mitochondrial inheritance

Mitochondria cannot form de novo within an amitochondrial cell. During cell division mitochondria need to segregate equally into both daughter cells, but very little is known about the mechanism of mitochondrial redistribution. In the dividing yeast *Schizosaccharomyces pombe* mitochondria are first pushed to either cell pole during chromosome division. In a second step mitochondria redistribute equally across the cell before cell division occurs. The later step coincides with microtubule formation and co-localisation with mitochondria, suggesting that it is driven at least in part by the cytoskeleton.

Through these two sequential processes mitochondria segregate in a cell volume dependent manner, which may be important for the metabolic fitness of each daughter cell (Jajoo et al., 2016). Whether a similar mechanism plays a role in mammalian mitosis is unclear.

An even more fascinating process occurs during fertilisation. Most organisms, including mammals, display uniparental inheritance of mitochondria and mtDNA is usually derived from the maternal germ cell. The processes by which paternal mitochondria are eliminated seem to be diverse and can differ even among closely related species. Consequently, several hypotheses exist for exclusion of paternal inheritance, including physical segregation of mitochondria and nuclei in the sperm cell followed by exclusion of the mitochondrial compartment during fertilisation, as well as breakdown of paternal mitochondria via ubiquitination, lysosmal and proteasomal degradation, and autophagy (Sato and Sato, 2013).

During meiosis maternal mitochondria are known to regain a homoplasmic state. This phenomenon, also known as the mitochondrial bottleneck process is thought to prevent the transmission of deleterious mtDNA mutations to the offspring. There is active debate on how exactly the bottleneck process is achieved mechanistically. Different hypothesis include the unequal partitioning of different mtDNA variants before cell division, the segregation of different mitochondrial plasmids into homoplasmic nucleoids or mitochondria prior to cell division, or the replication of a specific subset of mtDNA during oocyte maturation (Stewart and Chinnery, 2015).

1.1.5 Mitochondrial Metabolism

Mitochondria harbour a complex network of metabolic pathways that are linked with each other in uni-, bidirectional and circular fashion. The main energy producing processes are briefly mentioned in chapter 1.1.1, however the metabolic function of some of these pathways, especially the TCA cycle goes beyond a sole energetic purpose. Many cellular components are produced in mitochondria and released into the cytosol, including amino

acids and their precursors, as well as pyrimidine, fatty acid and cholesterol precursors. Co-factors such as heme, Fe-S clusters and glutathione (GSH) critically depend on mitochondria for their biogenesis. Most of these biosynthetic processes require the orchestrated action of cytosolic and mitochondrial enzymes. The description of mitochondria as metabolic hub therefore truly reflects their central role in numerous fundamental metabolic processes (Agathocleous and Harris, 2013; Dolle et al., 2013; Guda et al., 2007).

i) TCA cycle

The TCA cycle is one of the first described metabolic pathways and was proposed by Hans Krebs in 1937 (Krebs and Johnson, 1980). The cycle converts acetate into CO_2, H^+ and electrons (e^-) through a series of isomerisation and redox reactions (Figure 1.3). The highly reactive electrons are stored in form of reduced pyridine or flavin nucleotides, also known as reducing equivalents NADH or $FADH_2$ (derived from NAD^+ or FAD, respectively). The initial step of the TCA cycle is the transfer of acetyl from acetyl-CoA onto oxaloacetate by citrate synthase (CS). The resulting citrate undergoes an isomerisation to isocitrate catalysed by aconitase. This reaction is reversible and is mediated via the hydrated intermediate cis-aconitate. Isocitrate undergoes an irreversible oxidative decarboxylation by isocitrate dehydrogenase (IDH) that transfers the electrons onto NAD^+ and releases one CO_2. The resulting α-ketoglutarate (also 2-oxoglutarate) is further oxidatively decarboxylated into succinyl-CoA. This irreversible reaction is catalysed by α-ketoglutarate dehydrogenase (aKGDH), which uses CoA as additional substrate and releases CO_2 and NADH. Succinyl-CoA synthetase (also succinyl-CoA ligase or thiokinase) reversibly generates succinate thereby releasing CoA. The exothermic nature of this reaction is used to generate one ATP or GTP molecule from ADP/GDP and P_i. The next step is the oxidation of succinate to fumarate generating $FADH_2$. This reaction is performed by the IMM protein complex succinate dehydrogenase, also known as complex II of the electron transport chain.

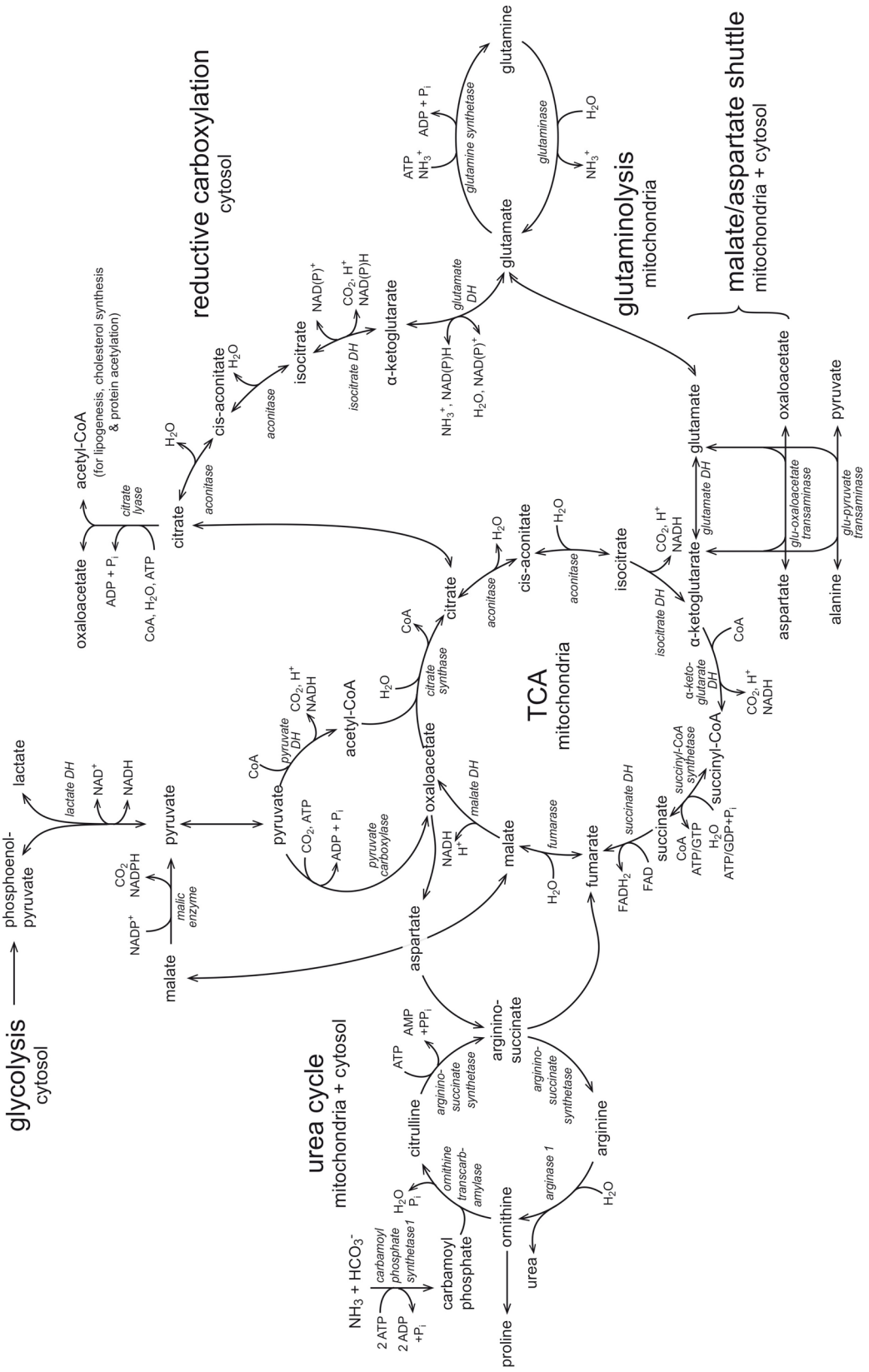


Figure 1.3 – TCA cycle and related metabolic networks. The TCA cycle serves as central metabolic hub for carbohydrate oxidation, amino acid metabolism, nitrogen secretion, fatty acid metabolism, and redox regulation of the cell. DH – dehydrogenase; CoA – acetyl coenzyme A

Fumarate is then reversibly hydrated into malate by fumarase. During the ultimate step of the TCA cycle malate is oxidised into oxaloacetate by the enzyme malate dehydrogenase (MDH). MDH generates NADH and replenishes the pool of oxaloacetate for acetyl assimilation (Kornberg, 2000; Krebs and Johnson, 1980; Nunes-Nesi et al., 2013).

ii) Regulation of the TCA cycle

The TCA cycle is regulated at various levels, including substrate activation, product inhibition, allosteric, post-tanscriptional, transcriptional, and redox regulation (Berg et al., 2015). The first regulatory step is the entry of substrates at the level of pyruvate conversion into acetyl-CoA. This reaction is irreversibly catalysed by the pyruvate dehydrogenate complex (PDC). PDC consists of three enzymes, namely pyruvate dehydrogenase (PDH), dihydrolipoyl acetyltransferase and dihydrolipoyl dehydrogenase. The complex is mainly regulated at the PDH level. The regulatory mechanisms include activation through pyruvate and the co-factor thiamine pyrophosphate and product inhibition by NADH and acetyl-CoA (Williamson and Cooper, 1980). Furthermore, PDH is regulated at the post-translational level by inhibitory PDH kinases and activating phospho-PDH phosphatases (Patel et al., 2014). It was observed that the PDC activity is enhanced upon rising cytosolic Ca^{2+} levels, which is due to enhanced binding of PDH phosphatase 1 to the complex.

High levels of pyruvate conversion into acetyl-CoA stimulate the activity of citrate synthase. CS activity is further determined by the availability of oxaloacetate, which is produced by malate DH. Substrate channelling from malate DH to CS has been proposed to increase the generation of citrate and hence substrate flux through the TCA cycle. CS activity is further positively regulated by ADP, competitively inhibited by its product citrate and negatively regulated by the downstream TCA cycle products NADH and succinyl-CoA (Williamson and Cooper, 1980). The inhibition by succinyl-CoA provides a feedback regulation at the entry of the TCA cycle, thereby avoiding the accumulation of TCA cycle intermediates in mitochondria. In plants, additional Cys residues in CS seem to confer a redox-sensitivity of the enzyme under oxidative conditions (Nunes-Nesi et al., 2013).

Aconitase performs one of the reversible steps in the TCA cycle and plays therefore a minor role for TCA regulation under physiological conditions. However, the protein contains an iron-sulphur (Fe-S) cluster, which is highly sensitive to the mitochondrial redox state (Bulteau et al., 2005) and deletion of mitochondrial anti-oxidant molecule MnSOD/SOD2 results in aconitase dysfunction (Strain et al., 1998). Furthermore, activation of $PKC\beta_2$ in diabetic cardiomyocytes results in phosphorylation of aconitase. This modification favours the reverse reaction from isocitrate to *cis*-aconitate thereby slowing TCA cycle flux (Lin et al., 2009).

Isocitrate dehydrogenase exists in three isoforms, which are differentially targeted to either cytosol or mitochondria. IDH3 is the mitochondrial isoform that participates in the TCA cycle. It forms a heterotetramer ($\alpha_2\beta\gamma$) and requires NAD^+ as co-factor. The other isoforms can be found in either cytosol (IDH1) or mitochondria (IDH2) and are specific for $NADP^+$. IDH3 is mainly regulated by substrate availability (isocitrate and NAD^+). The activation of IDH3 by isocitrate together with the feedback inhibition of CS by citrate are thought to cause an orchestrated flux through the first three steps of the TCA cycle (Williamson and Cooper, 1980). IDH3 can also be activated by ADP (Gabriel and Plaut, 1984), which may result in enhanced TCA cycle flux during cellular activity. The IDH products α-ketoglutarat and NADH exert a negative feedback on enzyme activity (Williamson and Cooper, 1980).

The redox reaction of α-ketoglutarate dehydrogenase (KGDH) is irreversible and is regulated via product inhibition by NADH and succinyl-CoA. The substrate α-ketoglutarate may regulate enzyme kinetics. Furthermore, purified KGDH is inhibited by a high ATP/ADP ratio, providing a regulatory link between energy production and activity. In turn, Ca^{2+} levels in the range of 1 µM have been shown to activate KGDH by limiting the inhibitory effects of NADH and ATP (Williamson and Cooper, 1980). This renders the enzyme insensitive to high NADH and ATP levels at physiological calcium concentrations of the mitochondrial matrix.

The reaction of succinyl-CoA synthetase is reversible and thus mainly dependent on the availability of each of the reactants. The heterodimeric enzyme consists of one α and one β subunit. The latter determines the sensitivity to either ADP or GDP. The ADP-dependent form has a higher Michaelis constant (K_m) for succinate (favouring the forward reaction towards succinate) compared to the GDP-dependent form and is preferentially expressed in muscle and brain. It was proposed that the ADP-dependent enzyme is linked to higher TCA flux and OXPHOS activity in energy demanding cells. In contrast the GDP-dependent form provides succinyl-CoA for heme synthesis in liver or ketone body activation in extra-hepatic tissue during experimentally induced diabetes (see section v of this chapter)(Johnson et al., 1998). Succinyl-CoA synthetase is activated by P_i in substrate depleted mitochondria (Phillips et al., 2009) and inhibited by metabolites of the porphyrin synthesis pathway (Wider and Tigier, 1970).

Succinate dehydrogenase (SDH) is a four-subunit complex in the IMM and as part of the ETC can donate electrons directly to ubiquinone. The catalytic components A and B in the matrix are bound to the IMM via the membrane bound subunits C and D. SDH is the only component of the ETC that does not pump protons across the IMM and contains solely nuclear encoded subunits. The succinate binding site of SDH is competitively inhibited by oxaloacetate. Furthermore, the enzyme is negatively regulated by phosphorylation and acetylation of the catalytic subunits (Rutter et al., 2010).

Fumarase catalyses the reversible hydratation from fumarate to malate. Fumarase regulation plays a minor role for the TCA cycle activity although an inhibitory effect of ATP and NAD+ for the reverse reaction (malate dehydratation) has been shown in parasitic helminths (Payne et al., 1979).

Malate dehydrogenase (MDH) is a homodimer, which oxidises malate to oxaloacetate, the ultimate step in the TCA cycle. This reaction is probably facilitated by a complex formation

between fumarase, MDH and CS resulting in substrate channelling. This mechanism is important because the oxidation of malate to oxaloacetate is thermodynamically unfavourable and substrate channelling could provide the necessary driving force towards oxaloacetate production. Furthermore, MDH is allosterically inhibited by oxaloacetate, which competes with the positive effectors malate and citrate (Minarik et al., 2002).

In addition to intrinsic regulation by its substrates, the TCA cycle is highly sensitive to external stimuli, such as intracellular calcium, usually associated with cellular activity, and the redox state of the cell. Mitochondrial calcium enhances the activity of pyruvate dehydrogenase, isocitrate dehydrogenase and α-ketoglutarate dehydrogenase (Denton, 2009). Furthermore, Ca^{2+} can directly enhance the activity of the ATP Synthase by Ca^{2+}-dependent binding of S100A1 to the F_1 complex (Boerries et al., 2007). Entry of calcium into the mitochondria occurs during cellular activity, such as muscle contraction or neuronal transmission. Hence, this mechanism warrants the concerted regulation of cytosolic energy consuming processes and mitochondrial ATP production. An indirect regulation of the TCA cycle is based on the effect of Ca^{2+} on mitochondrial substrate carriers. Both, the Aspartate/glutamate carrier 1 (AGC1/Aralar) and the ATP-Mg/P_i transporters (APC/SCaMC) reveal faster transport kinetics in presence of enhanced Ca^{2+} concentrations (Llorente-Folch et al., 2015). Since Ca^{2+} binding to both transporters occurs in the IMS, this mechanism depends on cytosolic calcium alterations and is independent of matrix uptake by the mitochondrial calcium uniporter (MCU). Aralar participates in the transport of cytosolic NADH to mitochondria for oxidation via ETC and is important for maintaining the cytosolic NAD^+ pool, an important co-factor for glycolysis. A role for APCs in mitochondrial Ca^{2+} buffering was proposed (Traba et al., 2012) although the mechanism of this effect is incompletely understood.

Redox regulation of cellular processes is gaining interest because a disturbed redox balance was found in many human disorders. Redox regulation is mediated through direct protein

modification at cysteine residues, the side chain of which contains the large, electron-rich sulphur. Cysteine residues can undergo S-oxidation (sulfenylation, sulfinylation), S-glutathionylation and S-nitrosylation (Mailloux et al., 2014). Different enzymes of the TCA cycle display redox sensitive cysteine modifications. Aconitase, NADP-dependent IDH, KGDH and PDH can be reversibly or irreversibly inhibited by oxidation. Interestingly, S-glutathionylation can play a dual role by inhibiting the activity but also preventing further oxidation to an irreversibly oxidised sulfonic acid species (Applegate et al., 2008; Hurd et al., 2008). Inhibition of the carnitine/acyl-carnitine carrier by glutathionylation indirectly inhibits the TCA cycle through decreased acetyl-CoA delivery from fatty acid degradation (Mailloux et al., 2014). Succinate DH is differentially regulated by oxidation compared to the other TCA enzymes. Active SDH is intrinsically glutathionylated and this modification is removed during cardiac ischemia/reperfusion injury. Deglutathionylation results in decreased activity of the enzyme with a concomitant burst in SDH-dependent superoxide (O_2^-) release (Chen et al., 2007). Redox modification not only depends on the global redox state of the cell but also on local production of oxidants and the distribution of anti-oxidants within the cell. In this context, redox signalling is an active and dynamic process that occurs during oxidative stress as well as during normal cellular activity regulating a variety of cellular functions (Hu et al., 2008; Mailloux et al., 2014).

Many of the mitochondrial functions depend on the mitochondrial membrane potential. Most of the TCA cycle enzymes do not have a membrane component and hence do not directly experience changes in $\Delta\Psi_m$. However, the TCA cycle depends on constant supply of nutrients through either pyruvate or glutamine import into mitochondria. Interestingly, many of the mitochondrial transporters use the proton gradient of the IMM to drive import of nutrients into the matrix. For example, the mitochondrial pyruvate carrier (MPC) catalyses the co-transport of pyruvate with H^+ into the matrix (Vanderperre et al., 2015). Furthermore, early studies on glutamine uptake have shown an increased import into energised isolated mitochondria, which is likely to stimulate TCA cycle activity (Kovacevic, 1977). However, the

direct investigation of the transport mechanism of the mitochondrial glutamine transporter is hindered by a lack of knowledge on the molecular components of this carrier (Pochini et al., 2014).

iii) β-oxidation

In peripheral tissue fatty acids (FA) are a major source of energy, especially during prolonged starvation. Heart and muscle cells use fatty acids directly for energy production, whereas the liver produces FA-derived ketone bodies that provide an alternative source of energy for the brain. Fatty acids can be taken up by most cells via plasma membrane transporters and are activated by acyl-CoA synthetases in the cytosol. The resulting acyl-CoA can be used for energy production as well as anabolic processes (Bartlett and Eaton, 2004).

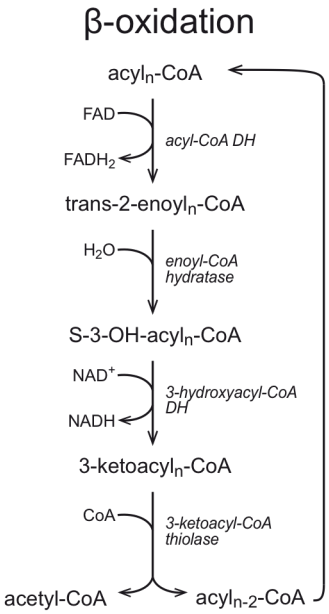


Figure 1.4 – β-oxidation of fatty acids. β-oxidation is the cyclic process of fatty acid breakdown, which is mainly accomplished in mitochondria. For very large chain fatty acids the first cycles are preferentially catalysed in peroxysomes. The shortened acyl chains are subsequently transferred to mitochondrial for final oxidation.

In mammalian cells FAs are metabolised in either the peroxisomes or the mitochondria. For mitochondrial import acyl chains are transferred onto carnitine by the carnitine palmitoyltransferase 1 at the outer mitochondrial membrane. This process is coupled to the translocation of the acyl moiety from the cytosol to the IMS. The carnitine acylcarnitine translocase (Slc25A20) catalyses the anti-port of acylcarnitine into the matrix in exchange of one carnitine. The IMM protein carnitine palmitoyltransferase 2 transfers the acyl chain from acylcarnitine back onto CoA resulting in acyl-CoA, which is the substrate for β-oxidation in the mitochondrial matrix (Houten et al., 2016).

The subsequent degradation of acyl-CoA occurs in a cyclic process that removes 2-carbon moieties per cycle from the acyl backbone in a stepwise fashion (Figure 1.4). In the first step the acyl-CoA is dehydrogenated by acyl-CoA dehydrogenase oxidising the C2 and C3 of the backbone, which produces trans-2-enoyl-CoA. The enzyme transfers the electrons onto the co-factor FAD, which is subsequently reduced by the dimeric electron transfer flavoprotein ETFα/β. This flavoprotein subsequently feeds the electrons into the ubiquinone pool of the ETC via ETF dehydrogenase. The family of acyl-CoA dehydrogenase comprises various proteins with different substrate specificities for acyl chain length, saturation and branching. After this initial oxidation the trans-2-enoyl-CoA is hydrated by Enoyl-CoA hydratase at the C3 position resulting in 3-hydroxyacyl-CoA. This molecule is further oxidised by NAD^+-dependent 3-hydroxyacyl-CoA dehydrogenase forming a 3-ketoacyl-CoA. In the final step the C1 and C2 are cleaved and the remaining acyl chain is transferred onto a new CoA. The reaction is performed by 3-ketoacyl-CoA thiolases. The acyl chain that is now shortened by two carbons can under a further round of oxidation. The last three steps are catalised by the octameric IMM protein mitochondrial trifunctional protein (MTP), which consists of 4 alpha and 4 beta subunits (HADHA and HADHB) and is specialised for long-chain acyl-CoA and to a lesser extend for medium-chain acyl-CoA. The degradation of medium- and short-chain acyl-CoA is catalysed by a subset of matrix enzymes namely crotonase (short-chain enoyl-CoA hydratase), SCHAD (short-chain 3-hydroxyacyl-CoA dehydrogenase) and MCKAT

(medium-chain 3-ketoacyl-CoA thiolase) (Houten et al., 2016). For the degradation of a variety of unsaturated FAs a set of enzymes has evolved that can convert acyl chains with atypical enoyl positions into the conventional trans-2-enoyl-CoA that can re-enter β-oxidation. These enzymes are 2,4-dienoyl-CoA reductase (DECR), Δ3,5-Δ2,4-dienoyl-CoA isomerase, and Δ3,Δ2-enoyl-CoA isomerase (ECI) (Houten et al., 2016).

iv) Electron transport chain and oxidative phosphorylation

Both, TCA and β-oxidation result in an accumulation of reducing equivalents in the form of NADH and $FADH_2$. These molecules serve as storage for the free energy derived from the oxidation of substrates. In order to generate ATP from substrate oxidation, the reducing equivalents feed electrons into the electron transport chain (ETC), which in turn produces a proton (H^+) gradient across the inner mitochondrial membrane. This depletion of protons in the matrix drives an H^+ backflow through the F_1F_O ATP synthase (complex V). The ATP synthase physically couples the H^+ translocation to the production of ATP from ADP and P_i via a rotating mechanism. This mechanism was first proposed in 1961 by Peter Mitchell as the chemiosmotic model (Mitchell, 1961) and is now commonly referred to as oxidative phosphorylation (OXPHOS).

The ETC consists of four complexes, which all reside in the inner mitochondrial membrane. The NADH-Coenzyme Q (CoQ) reductase (complex I) and the succinate-CoQ reductase (complex II) are the major entry points for electrons derived from NADH and $FADH_2$, respectively. Both shuttle electrons onto the lipophilic electron carrier Coenzyme Q, also known as ubiquinone, which resides in the IMM. Ubiquinol-cytochrome c reductase (complex III) transfers the electrons from ubiqinone to cytochrome c. The latter is an iron-sulfur cluster containing hydrophilic IMS protein that is physically tethered to the outer leaflet of the IMM. Finally, the cytochrome c oxidase (complex IV) receives the electrons from cytochrome c and reduces molecular oxygen in a stepwise fashion. Complexes I, III and IV are linked to proton pumping activity and asymmetrical protonation and deprotonation in the matrix and IMS, respectively, which together produce the proton gradient across the IMM.

The conversion of energy into ATP is facilitated by the F_1F_O ATP synthase, which consists of an enzymatic peripheral F_1 and a proton-conducting membrane-bound F_O component. F_O is comprised of a ring of 8 to 12 c-subunits and the associated a-subunit containing a proton hemi-channel. The a-subunit allows for entry of a proton into the membrane. The proton is then believed to bind to the c-subunit and drive the rotation of the c-ring. After one full rotation the proton exits the membrane via a second hemi-channel within the a-subunit resulting in the influx of protons from the IMS into the matrix (Walker, 2013). Further F_O components are the subunits b, d, e, f, g, A6L, and F6 in mammalian mitochondria. The F_1 component protrudes into the matrix and consists of the 3 enzymatic β-subunits that form a ring with 3 alternating α-subunits and the central stalk subunits γ, δ and ε. The central stalk is an asymmetric trimer that is bound to the rotating c-ring. Alternate binding of the long γ subunit to three binding sites within the α-β-hexamer causes the conformational change that drives the enzymatic activity of F_1. A lateral stalk connects F_1 to the membrane bound components and keeps it stationary relative to F_O. The lateral stalk consists of the oligomycin-sensitive protein OSCP as well as the F_O components b, d and F_6 (Baker et al., 2012; Walker, 2013). The F_1F_O ATP synthase has been shown to form dimers and this is thought to be important for the shaping of cristae (Strauss et al., 2008). The F_O subunits e and g extend at the distal end from the c-a axis and ablation of either subunit abrogates ATP synthase dimer formation (Arselin et al., 2004; Baker et al., 2012).

v) Ketone body metabolism

Under conditions of sufficient nutrient supply cells preferentially utilise glucose-derived acetyl-CoA as substrate for OXPHOS. Fatty acids are mainly spared from OXPHOS and instead stored in adipose tissue. However, when blood glucose levels are low, such as during fasting, the release of the hormone glucagon leads to mobilisation of alternative energy sources, mainly fatty acids from adipose tissue. The liver plays a central role in the regulation of whole body nutrient homeostasis. During times of limited blood glucose with the concomitant hormonal changes during fasting the liver produces glucose from glycogen and

other carbon sources, including oxaloacetate and glucogenic amino acids. This results in a decrease of the TCA cycle activity and an accumulation of fatty acid-derived acetyl-CoA. In order to maintain a pool of free CoA for further metabolic reactions liver mitochondria produce a subset of enzymes that catalyse the condensation of two acetyl-CoA into ketone bodies (Morris, 2005) (Figure 1.5). These enzymes include acetoacetyl-CoA thiolase (ACAT), HMG-CoA synthase, HMG-CoA lyase and β-hydroxybutyrate dehydrogenase (BHB-DH). The products of this pathway acetoacetate (ACAC) and β-hydroxybutyrate (BHB) together with acetone, the spontaneous degradation product of acetoacetate, are jointly referred to as ketone bodies. In contrast to fatty acids, ketone bodies can cross the blood brain barrier and are used by neurons as an alternative energy substrate (Morris, 2005; Paoli et al., 2015). In non-liver mitochondria, BHB is taken up into mitochondria and oxidised by BHB-DH. The resulting ACAC is converted into acetoacetyl-CoA by the enzyme succinyl-CoA:3-ketoacid CoA transferase (SCOT) and further lysed into two acetyl-CoA by acetoacetyl-CoA thiolase (ACAT) (Paoli et al., 2015).

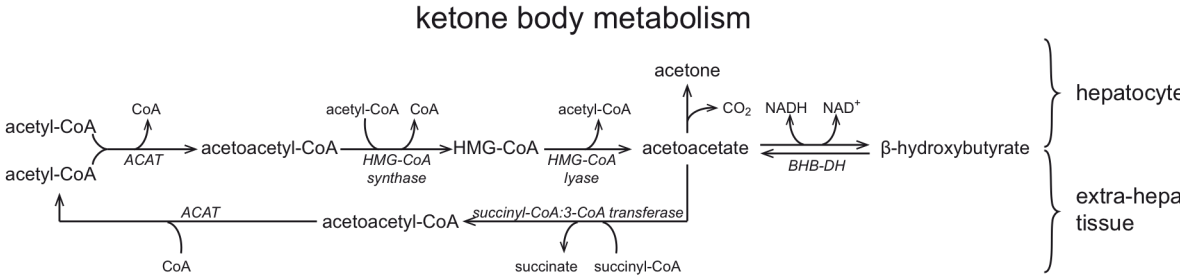


Figure 1.5 – Ketone body metabolism. Ketone bodies are produced in liver during starvation. They are secreted and transported to extra-hepatic tissue, including the brain via the blood. Subsequently, ketone bodies are converted back to acetyl-CoA to be used for mitochondrial energy production. DH – dehydrogenase, ACAT – acetoacetyl-CoA thiolase, CoA – Coenzyme A, HMG – β-hydroxy-β-methylglutaryl, BHB – β-hydroxybutyrate,

vi) Amino acid and pyrimidine synthesis in mitochondria

As mentioned above, the TCA cycle is an important supplier of precursors for amino acid (AA) synthesis (Figure 1.3). Glutamate and downstream amino acids glutamine, proline and arginine are derived from α-ketoglutarate. Oxaloacetate in turn is the precursor for asparate and the downstream amino acids asparagine, methionine, threonine, lysine and isoleucine. All other AAs are produced from the glycolytic metabolites 3-phosphoglycerate, phosphoenolpyruvate and pyruvate. The only exception to this is the synthesis of histidine, which requires ribose-5-phosphate from the pentose phosphate pathway. It is important to mention, however, that the human body cannot produce all proteinogenic amino acids in sufficient amounts and therefore has to take up nutrition-derived essential amino acids, including isoleucine, lysine, methionine and threonine. Furthermore, many of the enzymes necessary for glutamate and aspartate synthesis can also be found in the cytoplasm and can substitute for mitochondrial AA synthesis under certain circumstances (Berg et al., 2015).

Despite the importance of mitochondrial metabolism, certain cells can survive without functional ETC and OXPHOS induced by the depletion of mitochondrial DNA (ρ^0 cells). Respiration is not only required for energy production but also maintains the TCA cycle through oxidation of NADH. Concomitantly, ρ^0 cells show severely impaired TCA cycle activity. However, when supplemented with pyrimidine and high amounts of pyruvate, ρ^0 cells are able to survive and proliferate (King and Attardi, 1989). De novo pyrimidine synthesis requires the reduction of dihydroorotate to orotate, a reaction catalysed by dihydroorotate dehydrogenase, which transfers the released electrons directly into the ETC. A compromised ETC therefore inhibits the production of pyrimidine nucleotides, which explains the auxotrophy of ρ^0 cells for pyrimidine substitution (Gregoire et al., 1984). However, the requirement for supplementation with high levels of pyruvate has long been a mystery, since ρ^0 cell are highly glycolytic and produce excessive amounts of pyruvate. Two groups recently reported that the requirement of ρ^0 cells for pyruvate could be overcome by supplementation with high amounts of aspartate (Birsoy et al., 2015; Sullivan et al., 2015). Aspartate is

required for protein and adenosine nucleotide production. The *de novo* synthesis of aspartate depends on a reductive transamination from oxaloacetate with α-ketoglutarate as the electron acceptor (Figure 1.3, malate/aspartate shuttle). The resulting glutamate in converted back to α-ketoglutarate by glutamate dehydrogenase, which requires NAD^+ as the electron acceptor. Sullivan therefore concluded that in ρ^0 cells pyruvate serves as the final electron acceptor, which is reduced by lactate dehydrogenase to maintain an oxidised pool of NAD^+ for reductive anabolic reactions, especially the synthesis of aspartate.

vii) Urea cycle

In mammals the urea cycle is the sole pathway for nitrogen clearance in form of urea and is mainly performed in hepatic tissue. Genetic mutations have been found for all enzymes of the urea cycle and the subsequent metabolic diseases, collectively termed the urea cycle disorders, are caused by mild to severe dysfunction of the cycle (Ah Mew et al., 1993). The result is a toxic accumulation of nitrogen in form of NH_3 or NH_4^+ in the blood, which is diagnosed as hyperammonemia. Hyperammonemia can cause severe neurologic dysfunction leading to coma and death if not treated adequately. The urea cycle is initiated by the synthesis of carbamoyl phosphate from NH_3 and HCO_3^- and subsequent ligation to ornithine, which gives raise to citrulline in the mitochondrial matrix (Figure 1.3). The enzymes required for this synthesis are carbamoyl phosphate synthetase 1 and ornithine transcarbamylase (see Figure 1.3). The resulting citrulline is then exported into the cytosol by the ornithine-citrulline carrier of the inner mitochondrial matrix. Citrulline is ligated to aspartate by argininosuccinate synthetase to give raise to argininosuccinate. This is lysed in the penultimate step by argininosuccinate lyase to form the amino acid arginine and the TCA cycle intermediate fumarate. Finally, arginine is hydrolysed by arginase 1 releasing two nitrogen atoms in the form of non-toxic urea (CH_4N_2O) and replenishing the pool of ornithine.

viii) NADH-shuttle

NAD^+ is the main electron acceptor for most catabolic reactions, including the reductive synthesis of 1,3-bisphosphoglycerate from glyceraldehyde 3-phosphate during glycolysis in

the cytosol. In contrast, the main NADH consuming process is OXPHOS in the mitochondrial matrix. Two mechanisms have evolved to transfer the electrons to their final acceptors in the mitochondrial matrix. The first one is the malate/aspartate shuttle, which uses NADH and oxaloacetate in the cytosol to produce malate by cytosolic malate dehydrogenase. The malate/α-ketoglutarate antiporter transfers malate into the mitochondrial matrix and exports α-ketoglutarate to the cytosol. The latter is converted into cytosolic oxaloacetate during the transamination reaction of aspartate to glutamate. Finally, the mitochondrial aspartate/glutamate carrier exchanges the more reduced glutamate from the cytosol with oxidised aspartate from mitochondria. Inside the mitochondria, the reverse reactions of those fixing NADH in the cytosol lead to the release of the latter in the matrix and to the recycling of the shuttle components (Berg et al., 2015).

A second system is composed of the cytosolic and mitochondrial glycerol 3-phosphate (G3P) dehydrogenases. The mitochondrial counterpart is found in the IMM, where it oxidises G3P to dihydroxyacetone phosphate. The electrons are first transferred onto the prosthetic group FAD and subsequently fed into the ETC via ubiquinone. The product of this reaction, dihydroxyacetone phosphate is then reduced by the cytosolic G3P dehydrogenase using cytosolic electrons from NADH (Berg et al., 2015).

1.1.6 Other mitochondrial functions

i) Mitochondria as calcium buffering organelles

Intracellular calcium is a versatile regulator of numerous cellular functions, including cell proliferation, neurotransmitter release, muscle contraction, immune response, fertilisation, and apoptosis. Under resting conditions cells maintain a very low cytosolic calcium (Ca^{2+}_c) level through the export of Ca^{2+} via plasma membrane transporters, such as the Ca^{2+}-ATPase or the Na^+/Ca^{2+} exchanger (Guerini et al., 2005). In addition, Ca^{2+}_c clearance can occur through uptake into the ER and the mitochondrial matrix. Both organelles can store large amounts of Ca^{2+} and can potently regulate the calcium response of the cell. There is

intimate crosstalk between ER and mitochondrial Ca^{2+} transients, which is mediated via a specialised ER compartment referred to as the mitochondrial associated membranes (MAM) (Raturi and Simmen, 2013).

Due to its numerous targets inside the cell Ca^{2+}_c levels are highly regulated both temporally and spatially. The uptake of Ca^{2+} in the ER is mediated by sarcoplasmic/endoplasmic reticulum Ca^{2+} ATPases (SERCA). This pump rapidly sequesters Ca^{2+}_c into the lumen of the ER, which is driven by ATP hydrolysis and serves as a global Ca^{2+} sink (Eisner et al., 2013). Mitochondrial Ca^{2+} (Ca^{2+}_m) uptake is somewhat more complex. The ion has to cross two membrane compartments and both, slow and fast uptake kinetics have been observed (Santo-Domingo and Demaurex, 2010). The uptake is driven by the mitochondrial membrane potential. Ca^{2+} crosses the outer membrane via VDAC, a large, unspecific channel that is abundantly expressed in the OMM. However, during fast Ca^{2+}_m uptake VDAC expression levels can be a limiting factor (Rizzuto et al., 2012). A specific Ca^{2+} channel in the IMM has only recently been characterised on the molecular level and is known as the mitochondrial Ca^{2+} uniporter (MCU)(Baughman et al., 2011). The isolated MCU has a rather low affinity for Ca^{2+} and uptake of large quantities seems dependent on the close proximity of the MCU to Ca^{2+} channels at the ER or plasma membrane (Montero et al., 2000; Rizzuto et al., 1993). Mitochondria also release Ca^{2+} back into the cytosol probably via Na^+/Ca^{2+}- and H^+/Ca^{2+}-exchanger. In addition, transient opening of the mitochondrial permeability transition pore (mPTP), a large, unspecific channel in the IMM can rapidly release mitochondrial Ca^{2+} at the expense of the $\Delta\Psi_m$ (Jonas et al., 1999).

Mitochondrial Ca^{2+} uptake results in buffering of high local Ca^{2+}_c levels, while re-release enables a redistribution and a slow and longer lasting increase of total Ca^{2+}_c (Rizzuto et al., 2012). This seems of particular importance during synaptic short term plasticity, where repetitive action potential-triggered Ca^{2+} influx results in enhanced synaptic Ca^{2+} levels thereby facilitating synaptic neurotransmitter release. In pancreatic acinar cells, mitochondria

accumulate between the apical, secretory pole and the basolateral, nucleus-containing pole. This results in compartmentalisation of high Ca^{2+}_c concentrations that are necessary for vesicle secretion on the apical side. Sequestration of Ca^{2+}_c by the mitochondrial belt acts as a firewall that prevents unwanted transcriptional changes triggered by Ca^{2+}_c in the basolateral side (Rizzuto et al., 2012).

ii) ROS and Redox homeostasis

Most cellular compartments, including the cytosol and the mitochondrial matrix are reducing environments. This is crucial for cell viability because uncontrolled oxidative reactions can alter the molecular composition of proteins, lipids and nucleotides. To maintain the reductive potential the cell produces anti-oxidant molecules, such as glutathione (GSH) and thioredoxin (TRX). These molecules can accept electrons from oxidised proteins thereby regenerating their reduced state. In a second step, oxidised glutathione (GSSG) and oxidised TRX are re-generated by GSH reductase and TRX reductase, respectively, with NADPH as electron donor (Holmstrom and Finkel, 2014; Trachootham et al., 2008).

The redox potential of the cell is challenged by reactive oxygen species (ROS). ROS arise through single electron transfer onto molecular oxygen, thereby creating the radical superoxide $^{\bullet}O_2^-$. $^{\bullet}O_2^-$ is highly reactive and needs to be degraded quickly. This is done by the protein superoxide dismutase (SOD), which converts two molecules $^{\bullet}O_2^-$ to hydrogenperoxide (H_2O_2) and molecular oxygen O_2. Subsequently, H_2O_2 can be degraded to H_2O by either catalase, GSH or TRX (Brookes et al., 2004; Trachootham et al., 2008). In contrast to superoxide H_2O_2 can cross biological membranes either by diffusion or through specialised aquaporins, the peroxiporins (Sies, 2014). Interestingly, H_2O_2 has cell-signalling properties and is a potent regulator of cytokine and growth factor signalling thereby regulating diverse processes such as cell metabolism, immune response, cell proliferation and differentiation, and apoptosis (Marinho et al., 2014; Rhee, 2006; Sies, 2014).

ROS generation can be driven by a family of enzymes termed NADPH oxidases (Nox) (Brown and Griendling, 2009). The first member of this family, Nox2 was implicated in the oxidative burst of neutrophils as part of the innate immune response. However, we now know

of at least 7 differentially expressed mammalian isoforms with specialised functions in growth factor and Ca^{2+} signalling, as well as oxygen sensing (Brown and Griendling, 2009).

The second main site of ROS production is located within mitochondria. The transport of highly reactive electrons through the numerous redox reactions in the mitochondrial matrix and the ETC is imperfect and the premature reaction of electrons with O_2 can occur at various stages (Jastroch et al., 2010). The best characterised mitochondrial ROS producing proteins are NADH oxidase (complex I) and Coenzyme Q:cytochrome C oxidoreductase (complex III) of the ETC. Importantly, ROS production by these complexes positively correlates with the electronegativity at each reactive redox centre and therefore is enhanced by low availability of oxygen. On the other side, high oxygen levels increase the unspecific reaction of O_2 with complex I and III, which will also result in enhanced ROS production. Therefore, oxygen availability to mitochondria is regulated at various levels including lung ventilation, capillary blood flow (through vasoconstriction/-dilation) and possibly via partial uncoupling of respiration through bypassing of proton pumping complexes (Papa and Skulachev, 1997). Mitochondrial ROS production is also likely enhanced during increased mitochondrial respiration (Gorlach et al., 2015).

Oxidative damage has been observed in a number of physiological and pathological conditions, including ageing, neurodegeneration and neuroinflammation (Balaban et al., 2005; Dexter and Jenner, 2013; Reynolds et al., 2011). However, direct measurement of ROS *in vivo* is technically challenging (Murphy, 2009). It is important to mention that most of our knowledge on mitochondrial ROS production is derived from experiments on isolated mitochondria. In these experiments mitochondria are exposed to artificial conditions often far from their natural steady-state equilibrium (e.g. high substrate availability, ATP synthase inhibition, atmospheric oxygen levels). Therefore mitochondrial ROS production under natural conditions may be an order of magnitude below those observed in vitro (Murphy, 2009).

The level of cellular ROS is not only dependent on the amount of production but also on its clearance. As mentioned above, several cellular systems are dedicated to the degradation of ROS. These antioxidants can be found ubiquitously throughout the cell. However, the redox potential of different cellular compartments is not equal pointing to differential targeting of antioxidants between compartments (Hu et al., 2008). Most antioxidants require NADPH as final electron donor. There are different pathways for NADPH generation in the cytosol and mitochondria. The main cytosolic route is the pentose phosphate pathway (PPP), which diverts from glycolysis at the level of glucose-6-phosphate. The NADPH producing enzymes are glucose-6-phosphate dehydrogenase and 6-phosphogluconate dehydrogenase. Another important function of the PPP is ribose-5-phosphate production for nucleotide biosynthesis, which requires the enzymes gluconolactonase and ribulose-5-phosphate isomerase. Interestingly, due to a complex set of isomerisation and conversion reactions the carbons that enter the PPP can be diverted back to the glycolytic pathway as fructose 6-phosphate and glyceraldehyde 3-phosphate (Berg et al., 2015). Another mechanism to form cytosolic NADPH is the transport of citrate from the mitochondrial matrix to the cytosol and subsequent conversion and oxidation via cytosolic NADP-dependent IDH1. The resultant α-ketoglutarate can be transferred back to mitochondria to replenish the pool of TCA cycle intermediates (Metallo et al., 2012; Siebert et al., 1957). Mitochondrial NADPH levels can be produced by mitochondrial NADP-dependent IDH2. Thereby electrons are diverted from the energy-producing pathway to the anti-oxidant defence mechanisms. Interestingly, IDH2 can also catalyse the reductive reaction from α-ketoglutarate to isocitrate to replenish the pool of mitochondrial citrate. This was shown to be important for cancer cell proliferation in hypoxia. Under these conditions the entry of pyruvate into the TCA cycle is inhibited due to high NADH levels and the cells switch to glutamine degradation to produce citrate for further anabolic reactions (Wise et al., 2011). Another enzyme that produces NADPH is nicotinamide nucleotide transhydrogenase (NNT). This enzyme transfers electrons between NADH and NADPH. However, NNT activity relies on the translocation of protons across the IMM and is therefore $\Delta\Psi_m$-dependent (Sazanov and Jackson, 1994).

Finally, NADPH-independent ways of redox regulation have been proposed. For example, high levels of α-ketoglutarate were found to scavenge ROS through direct oxidation of this TCA cycle intermediate. In this mechanism α-ketoglutarate reacts with H_2O_2 to undergo a non-enzymatic decarboxylation resulting in water and succinate (Fedotcheva et al., 2006).

iii) Mitochondria and cell death

Regulated cell death is an important function for the development and survival of multi-cellular organisms. During development, tissue size and shape are controlled by cell proliferation and programmed cell death, also called apoptosis (Jacobson et al., 1997). Disrupted or infected cells are often eliminated through necrotic cell death to prevent further damage to neighbouring cells (Vanden Berghe et al., 2014). There are many different pathways that induce cell death and in fact most of them involve mitochondria at an early or later stage (Green and Reed, 1998; Nikoletopoulou et al., 2013; Skulachev, 2006; Vanden Berghe et al., 2014). I will therefore only briefly mention the main modes of cell death and then focus on those aspects that involve mitochondria.

Apoptotic cell death can be initiated by extrinsic stimuli acting through plasma membrane receptors, such as tumour necrosis factor (TNF) receptor (TNFR), Fas receptor and TNF-related apoptosis-inducing ligand (TRAIL) receptor. Binding of ligands causes the association of TNFR- or Fas-associated death domain containing protein (TRADD or FADD) with these receptors. Subsequently, pro-caspases (e.g. pro-caspase 2, 8 and 10) are recruited to the receptor bound death domain containing proteins leading to pro-caspase cleavage. The activated caspases cleave downstream executioner caspases 3, 6 and 7, a process known as the caspase cascade (Green and Kroemer, 1998; Tait and Green, 2010). Caspase activation leads to protein degradation, DNA fragmentation and ultimately cell demise (Thornberry and Lazebnik, 1998).

The intrinsic pathway of apoptosis is often referred to as the mitochondrial pathway. It is triggered for example by DNA damage and ER stress, and particularly in neurons by ROS or Ca^{2+} overload, which causes activation of Bcl-2 homology 3 (BH3)-only proteins Bad, Bim and PUMA. BH3-only proteins inhibit anti-apoptotic Bcl-2 family members thereby activating the pro-apoptotic Bcl-2 proteins Bax and Bak. Bax and Bak can oligomerise in the OMM permeabilising the membrane and releasing apoptotic IMS proteins, most importantly cytochrome c (cytC). Binding of cytosolic cytC to apoptotic protease-activating factor 1 (Apaf1) causes a conformational change and oligomerisation of seven Apaf1 monomers into the active apoptosome complex. Activated Apaf1 binds to pro-caspase 9 via its caspase recruitment domain (CARD). Proteolytic maturation of caspase 9 results in the caspase cascade already mentioned above (Tait and Green, 2010). It is important to mention that apoptotic cell death requires ATP from either glycolysis or mitochondrial respiration for the final execution of death involving DNA fragmentation (Leist et al., 1997).

Interestingly, the initiator caspase 8 of the extrinsic pathway also cleaves pro-apoptotic Bid and the resulting tBid (truncated Bid) can act in a similar way to Bad. By this means both extrinsic and intrinsic pathways crosstalk at the level of OMM permeabilisation (Nikoletopoulou et al., 2013). There are additional mechanisms that keep apoptosis under control in case of accidental caspase activation. The X-linked inhibitor of apoptosis (XIAP) protein binds to and inhibits active caspases. The release of SMAC/DIABLO and Omi/HtrA2 from the IMS into the cytosol inhibits XIAP activity and facilitates induction of apoptosis. Other important IMS proteins are apoptosis inducing factor (AIF) and endonuclease G, the release and nuclear translocation of both can induce caspase-independent nuclear condensation and DNA fragmentation (Tait and Green, 2010).

The classic necrosis is viewed as uncontrolled cell lysis through membrane rupture with concomitant inflammation due to the release of inflammatory molecules from the cytosol. This stands in sharp contrast to recent research, which has unravelled a complex regulatory

network of necrotic cell death. Necrosis can be triggered by many different stimuli, similar to apoptosis. Importantly, cross talk and feedback mechanisms exist both within the range of necrotic pathways but also between necrosis and apoptosis (Vanden Berghe et al., 2014). The term necroptosis has evolved to distinguish regulated necrosis from unregulated cell death. The best-studied mediators of regulated necrosis are receptor-interacting protein kinase (RIPK) 1 and RIPK3. Upon activation, the kinases form fibrillar heterooligomers (Li et al., 2012) that phosphorylate mixed lineage kinase domain-like (MLKL) protein. MLKL can form oligomers and disrupt membranes, thereby leading to the release of lysosomal proteases into the cytosol and cytosolic pro-inflammatory components into the extracellular space, which ultimately leads to necrotic cell death (Vanden Berghe et al., 2014). Interestingly, RIPK1 and RIPK3 induction can occur downstream of TNF receptor, especially when initiator caspase 8 is deleted or inhibited. In addition, low levels of ATP may lead to preferential initiation of necrosis over apoptosis at the level of death receptor signal transduction (Los et al., 2002). In this scenario, caspase-mediated inhibition versus ROS-mediated activation of poly-(ADP ribose) (PAR) polymerase 1 (PARP1) was proposed as a molecular switch between apoptosis and necrosis. PARP1 inhibits neuronal energy metabolism through PAR-mediated inhibition of hexokinase, the initial enzyme of glucose breakdown (Andrabi et al., 2014).

Although cell death can occur independently of mitochondria, this organelle is intimately linked to various pathways of cellular demise. Its close relation to apoptosis has become clear from the first paragraph. However, mitochondria can induce cell death independently of pro-apoptotic Bcl-2 family members and OMM permeabilisation. Mitochondrial stress factors such as high levels of ROS or mitochondrial Ca^{2+} can induce the opening of a large channel that permeabilises the IMM for solutes, such as ions and small metabolites. This process is known as the mitochondrial permeability transition (mPT) and is facilitated by the mPT pore (mPTP) (Ichas and Mazat, 1998). Opening of the mPTP also uncouples electron transfer from production of ATP. The transient opening of the mPTP was proposed to have

physiological functions such as protection from mitochondrial ROS or Ca^{2+} release from the matrix (Jonas et al., 2015; Mnatsakanyan et al., 2016). However, prolonged opening of the mPTP results in irreversible loss of $\Delta\psi_m$ and loss of mitochondrial integrity. Irreversible mPTP opening has two detrimental consequences, which cause cell death independent of each other. The first is the lack of production of ATP and other mitochondrial products important for cell viability. The second is the release of IMS localised mediators of cell death that have already been described above. The latter results from the mPTP induced swelling of the mitochondrial matrix, which causes the rupture of the OMM due to the larger area of IMM compared to OMM (Ichas and Mazat, 1998). Owing to these two consequences mPT has been implicated in both apoptotic and necrotic types of cell death. The molecular identity of the mPTP has been discovered recently as the c-subunit ring of the F_1F_O-ATP Synthase (Alavian et al., 2014). Interestingly, the ATP Synthase has previously been shown to exhibit a proton leak that reduces the efficiency of the enzyme to produce ATP (Alavian et al., 2011; Chen et al., 2011). These findings implicate a tight relation between cell death and the metabolic state of a cell .

1.1.7 Mitochondrial dynamics, biogenesis, and degradation

Mitochondria form a highly dynamic ATP generating network within most cells of our body (Chen and Chan, 2009). The generation and degradation of mitochondria are part of an adaptive process to ensure metabolic homeostasis of the cell, as well as to replace dysfunctional mitochondria (Liesa and Shirihai, 2013; Suen et al., 2008). The movement of mitochondria provides a mechanism to fine-tune energy provision and calcium sequestration in highly compartmentalised cells (Rizzuto et al., 2012), such as neurons (Chen and Chan, 2009). Finally, mitochondrial fission and fusion events are important for various functions such as movement, some forms of apoptosis, as well as complementation or segregation of mildly or severely impaired mitochondria, respectively (Chen and Chan, 2009; Liesa and Shirihai, 2013; Suen et al., 2008).

i) Mitochondrial biogenesis

Mitochondrial biogenesis is mainly controlled at the level of expression of mitochondrial proteins. These are made up of both, nuclear and mitochondrially encoded genes, which are transcribed upon binding of specific sets of transcription factors. Tfam and TFB2M induce mitochondrial gene expression, whereas different transcription factors control the nuclear expression of mitochondrial genes. Among those are the nuclear respiratory factor (Nrf) 1 and Nrf2, peroxisome proliferator-activated receptors (PPAR) α/β/γ, estrogen-related receptors (ERR) α/β/γ, as well as YY1, MEF2, c-myc and CREB. However, the most important factors for mitochondrial proliferation are the master regulators of the PPARγ coactivator-1 (PGC-1) family, consisting of PGC-1α/β and PGC-1 related coactivator (PRC) (Jornayvaz and Shulman, 2010; Scarpulla et al., 2012). PGC-1α, the best-characterised member of the family directly activates Nrfs, PPARs and ERRs, thereby regulating synthesis of most, if not all mitochondrial proteins. Importantly, PGC-1α also induces the expression of Tfam and TFB2M via Nrf1 and Nrf2 providing an orchestrated expression of nuclear- and mitochondrially-encoded proteins of the respiratory chain. The second important finding in the field of mitochondrial biogenesis was that PGC-1α responds to a variety of metabolic signals through transcriptional and post-transcriptional regulatory mechanisms. PGC-1α transcription is upregulated by nutrient deprivation and exercise in a CREB-dependent manner. Furthermore, the nutrient sensor mammalian target of rapamycin (mTOR) is likely to positively regulate the interaction between YY1 and PGC-1α, resulting in enhanced PGC-1α expression in a feed forward manner. mTOR activation thereby facilitates both mitophagy (degradation of non-functional mitochondria), as well as biogenesis of new mitochondria (Wenz, 2011). On the post-translational level, energy depletion results in phosphorylation and activation of PGC-1α by AMPK. Furthermore, the sirtuins Sirt1 and Sirt3 can facilitate activation through deacetylation of PGC-1α as response to nutrient deprivation and oxidative stress, respectively (Jornayvaz and Shulman, 2010; Scarpulla et al., 2012).

ii) Degradation/mitophagy

The primary function of mitochondrial degradation is to exclude dysfunctional mitochondria that would be harmful to the cell upon accumulation. Dysfunction in mitochondria is characterised by low energetic output and high production of ROS, which enhances the probability of mitochondria to undergo permeability transition. The process of mitochondrial degradation was termed mitophagy because it relies on functional autophagosomes and receptors on these double membrane vacuoles, which can recognise mitochondria that are targeted for degradation (Kim et al., 2007). Several autophagosomal proteins are involved in mitophagy of mammalian cells, including autophagy related protein (Atg) 7, unc51-like kinase1 (ULK1) and p62/sequestosome-1, as well as the membrane-bound MAP1LC3 (microtubule associated protein 1 light chain 3) (Youle and Narendra, 2011).

The function of mitochondria is intimately linked to the mitochondrial membrane potential $\Delta\Psi_m$. Loss of $\Delta\Psi_m$ has a variety of consequences including the accumulation of markers for mitophagy on the OMM. In various cell types the accumulation of proteins containing an LC3-interacting region (LIR), such as NIX/BNIP3L, BNIP3 and FUNDC1, at the OMM is induced upon loss of $\Delta\Psi_m$. Interestingly, these proteins also respond to hypoxia with enhanced expression on the OMM. LIR-containing proteins induce the binding of mitochondria to autophagosomal membranes, which leads to the engulfment of the organelle. Subsequent fusion of the autophagosome with lysosomes leads to the hydrolytic degradation of proteins, lipids and mitochondrial DNA (Melser et al., 2015; Youle and Narendra, 2011). A second mechanism to remove damaged mitochondria relies on the PTEN-inducible putative kinase 1 (PINK1) and the E3 ubiquitin ligase parkin. In healthy mitochondria PINK1 is imported into the matrix but has a relatively short half-life due to degradation through matrix proteases. However, protein import relies on the mitochondrial membrane potential and when $\Delta\Psi_m$ is low, PINK1 transport across OMM and IMM is diminished. This results in PINK1 accumulation at the OMM where it phosphorylates a number of proteins, such as Mfn1, Mfn2 and VDAC1 (Geisler et al., 2010; Narendra et al., 2010). PINK1 also recruits cytosolic Parkin

to the OMM via phosphorylation. Parkin-mediated ubiquitination of OMM proteins, such as VDAC and Mfn2 results in binding of sequestosome-1 and recruitment of MAP1LC3 containing membranes (Geisler et al., 2010; Narendra et al., 2008). Interestingly, NIX/BNIP3L can also recruit Parkin to depolarised mitochondria thereby reinforcing the mitopaghic process (Ding et al., 2010). Both, PINK1 and Parkin are recessive Parkinson's disease proteins and were suggested to play an important role during neuronal mitochondrial quality control (Trempe and Fon, 2013; Youle and Narendra, 2011).

Recently, post-translational regulatory mechanisms of mitophagy proteins have been identified. For example, phosphorylation of creatine kinase 2 (CK2) antagonises the activity of FUNDC1. This is reversed by the phosphatase activity of phosphoglycerate mutase 5 (PGAM5) (Chen et al., 2014). PGAM5 activity was also implicated in stabilisation of PINK1 and PGAM5 knock out mice reveal a parkinsonian phenotype (Lu et al., 2014). Interestingly, PGAM5 can be inhibited by the anti-apoptotic Bcl-x_L (Wu et al., 2014), which in addition to its inhibitory effects on pro-apoptotic Bax and Bak also increases mitochondrial energy production by enhancing ATP synthase efficiency (Alavian et al., 2011). This indicates an inhibitory effect of mitochondrial metabolism on degradation at the level of a single mitochondrion.

An interesting aspect of mitochondrial degradation was summarised recently by Lemasters, who pointed out that different physiological conditions may trigger mechanistically and cell biologically distinct types of mitophagy (Lemasters, 2014). He differentiated between 3 types of mitophagy. Type 1 is a nutrient starvation-induced mitophagy, which depends on the classic autophagy proteins Beclin-1 and class III phosphatidyl inositol 3 kinase (PI3K)(Sinha and Levine, 2008) and is accompanied by the engulfment of pre-autophagic structures and mitochondrial fission. Type 2 is caused by mitochondrial damage and induced loss of $\Delta\Psi_m$, which triggers the enclosure of whole mitochondria by LC3-positive membranes. This is mechanistically independent of Beclin-1 and PI3K but requires PINK1 and Parkin activity.

Finally, a newly characterised form of micro-autophagy was assigned as type 3 mitophagy or micro-mitophagy. This is characterised by the budding of small mitochondrial vesicles enriched in oxidised proteins and subsequent engulfment by multivesicular bodies. Type 3 is independent of the mitochondrial fission machinery but requires PINK1 and Parkin (Lemasters, 2014). Finally, the expression of ceramide on the OMM of mitochondria was shown to directly bind autophagic MAP1LC3 thereby directing mitochondria for destruction (Sentelle et al., 2012).

iii) Fission and fusion

Mitochondria are highly dynamic organelles that can form networks of different morphologies depending on the tissue and metabolic state of the cell. This aspect of mitochondrial biology depends on membrane fission and fusion processes. Mitochondrial fission serves primarily two functions, which are the generation of new mitochondria and the segregation of dysfunctional mitochondrial particles for subsequent degradation. Mitochondrial fusion in turn is thought to complement partially damaged mitochondria with material from intact mitochondria resulting in a constant exchange of proteins, lipids and DNA (Westermann, 2012; Youle and van der Bliek, 2012). Furthermore, extended mitochondrial networks created through fusion may facilitate efficient distribution of energy throughout the cell (Skulachev, 2001).

In mammals the core proteins for both fission and fusion constitute large GTPases of the dynamin family. The cytosolic dynamin-related protein 1 (Drp1) can be recruited to mitochondrial fission sites by each of the OMM adaptors Mid49, Mid51, Mff or Fis1. There is evidence for a differential preference of each adaptor and/or different regulatory mechanism depending on the cell type and fission-inducing stimulus (Loson et al., 2013). The mechanism of membrane fission for Drp1 is thought to be very similar to its close family member dynamin. Upon binding to constricted membranes dynamin forms rings of homo-dimers around the surface of the lipid bilayer. The hydrolysis of GTP to GDP by the dynamin GTPase domain causes a conformational change that leads to a constriction and twist of the

Drp1 rings into spirals and subsequent membrane fission (Ferguson and De Camilli, 2012). It is not clear to date whether fission of the IMM proceeds independently of OMM fission or is caused simultaneously through the action of Drp1 at the OMM.

Mitochondrial fusion occurs individually at the outer and inner membrane. The fusion proteins Mitofusin (Mfn) 1 and Mfn2 are OMM transmembrane proteins that can form homo- and heterodimers. The dimer formation between Mfn proteins from opposing mitochondrial membranes facilitates membrane tethering and subsequent fusion after a major conformational change induced by GTP hydrolysis (Koshiba et al., 2004). The fusion of the inner membrane is mainly catalysed by the dynamin-like GTPase family member optic atrophy 1 (Opa1), which is localised at the IMM through a transmembrane domain. IMM fusion only occurs in presence of the mitochondrial membrane potential and ATP. Mitochondrial depolarisation results in stabilisation of the IMM protease Oma1/HtrA2, which catalyses the proteolytic digestion of Opa1 thereby preventing the fusion of functional with non-functional mitochondria (Belenguer and Pellegrini, 2013). The exact molecular mechanism for IMM fusion is not yet clear but it appears that it requires both, a long membrane-bound (Opa1-l) and a smaller IMS soluble (Opa1-s) form (Belenguer and Pellegrini, 2013).

iv) Transport

The transport of mitochondria is extremely important for the efficient supply of energy at distal parts of highly active cells. Mitochondrial transport mechanisms have been studied extensively in neurons. Both, mitochondrial biogenesis and degradation are constraint to the neuronal cell body, hence synaptic mitochondria rely on active transport mechanisms to reach their destination. As a result, disruption of mitochondrial transport impairs axonal outgrowth, synaptic transmission, and ultimately neuronal viability (Sheng and Cai, 2012). The regulated movement of mitochondria can occur along all types of cytoskeletal networks with varying kinetics and usually in a bidirectional manner. Long-distance transport of mitochondria in axons is facilitated by uniformly polarised microtubules that extend in

anterograde direction towards the synapse. The anterograde motors kinesin-like proteins, especially KIF5, KIF1B and KLP6, and the retrograde motor dynein have been shown to attach to mitochondria via mitochondrial Rho-GTPase (Miro1) and VDAC1, respectively. Other mitochondrial adaptors for KIF5 have been reported, including Syntabulin, FEZ1 and RANBP2 (Sheng and Cai, 2012). In dendrites microtubules have mixed polarity and kinesin-mediated anterograde transport can direct mitochondria either towards dendritic spines or the soma. Association of mitochondria with actin filaments and the actin motor protein myosin-XIX mediates short-range transport of mitochondria near synapses, as well as in dendritic spines (Sheng and Cai, 2012).

The velocity and direction of mitochondrial movement is regulated by a variety of mechanisms whereby the different cytoskeletal elements can synergise by passing on mitochondria to one another or antagonise in a competitive manner (Sheng and Cai, 2012). Interestingly, mitochondrial movement is highly sensitive to Ca^{2+} and ADP levels. Elevated Ca^{2+} concentrations typically found in active synapses cause an arrest of mitochondria via Miro, which contains two Ca^{2+} binding domains (Macaskill et al., 2009; Wang and Schwarz, 2009). The ADP-sensitive mechanism is less understood. It was shown, however that mitochondria move rapidly in areas with high intracellular ATP concentration and slow down in response to a rise in ADP. The latter could be triggered through synaptic activity, hypoxia, or direct injection of ADP (Mironov, 2007). Other regulatory mechanisms depend on post-translational modifications and include signalling via different pathways including neuronal growth factor mediated activation of PI3K, serotonergic 5-HT1A receptor activation of Akt kinase, and dopamine D2 receptor mediated inhibition of Akt kinase (Sheng and Cai, 2012).

Although neuronal mitochondria are highly mobile, a large fraction of these organelles appears to be static. These so-called stationary or docked mitochondria are usually found close to synapses where they provide a stable source of energy (Sheng and Cai, 2012). Docking mechanisms include the attachment to microtubule anchor protein syntaphilin, the

displacement of microtubule-associated motors by actin-based myosin or attachment to neurofilaments via the neurofilament heavy chain (Sheng and Cai, 2012). The latter is dependent on the $\Delta\Psi_m$, loss of which results in the release of mitochondria and transport to the soma for the degradation by proteasomal and autophgosomal processes (Wagner et al., 2003).

1.1.8 Role of mitochondria in neuronal metabolism

The neuronal metabolism is very special in many ways. Firstly, nutrient supply to the brain is limited through the transport characteristics of the blood-brain barrier (BBB), which mainly facilitates uptake of glucose into the brain. Secondly, the brain is among the most energy-expensive organs of the human body consuming approximately 20% of glucose at rest while accounting for only about 2% of the body weight (Gobel et al., 2013). In addition, the different functional compartments of a neuron have very distinct energetic demands that need to be regulated both locally and globally (Sheng and Cai, 2012). Finally, the most active cells of the brain, the neurons are extremely sensitive to deprivation of oxygen or nutrients (Mergenthaler et al., 2013).

i) Substrates for neuronal metabolism

The blood vessels of the brain are highly impermeable to the diffusion of molecules into and out of the central nervous system, a property attributed to the formation of tight junctions between brain endothelial cells. In addition, pericytes in the basement membrane and astrocytic endfeet also regulate the permeability of brain capillaries. A small number of hydrophobic molecules can cross the BBB but most substrates including those for energy metabolism are actively transported across the neural endothelium. The uptake of glucose occurs via glucose transporter 1 (GLUT1), which is highly expressed in brain endothelial cells and on astrocytes. The majority of brain glucose is thought to diffuse freely in the extracellular fluid. However, astrocytic glucose uptake and transport between astrocytic gap junctions can facilitate the glucose distribution to distal areas of the brain. In contrast to

astrocytes, neurons express the GLUT3 isoform of the glucose transporter. GLUT3 has a higher rate of glucose uptake than GLUT1 and this is thought to prioritise glucose for neuronal metabolism (Mergenthaler et al., 2013).

In addition to glucose monocarboxylates can also cross the BBB. The main species to be mentioned are lactate and β-hydroxybutyrate (BHB). Pyruvate and acetoacetate can also cross the BBB but their biological significance is much lower due to low blood concentrations. The transport of monocarboxylates can occur in both a non-saturable, diffusion-based mechanism (LaManna et al., 1993) and a saturable, transporter-mediated mechanism. The latter is facilitated by the monocarboxylate transporters (MCT), which catalyse an antiport of monocarboxylate with either monocarboxylate or a proton (Halestrap and Wilson, 2012). Both transport mechanisms make a considerable contribution at physiological monocarboxylate concentratios in the blood (LaManna et al., 1993). Neural metabolism can produce and metabolise lactate and under resting conditions lactate is transported across the BBB in a bidirectional manner (Knudsen et al., 1991). However, under conditions of decreased plasma pH or increased plasma lactate levels, such as during physical activity, the net import of lactate into the brain is enhanced, thereby triggering increase in neuronal lactate oxidation (Dienel, 2012; Knudsen et al., 1991). Ketone bodies are another major neuronal energy source mainly produced in the liver during fasting or metabolic acidosis. Ketone bodies can substitute glucose when blood glucose levels are very low, such as during starvation or diabetic ketoacidosis (Ruderman et al., 1974). Ketone bodies can be taken up by cells and are converted into acetyl-CoA for breakdown via OXPHOS. Finally, glutamine, the most abundant amino acid in the blood, and can be taken up via the BBB through scarcely characterised Na^+-dependent transporters (Ennis et al., 1998). Glutamine conversion to α-ketoglutarate can enhance the pool of TCA intermediates and serve as precursor for further anabolic reactions that require TCA cycle activity.

ii) Neurons generate most ATP via OXPHOS

Positron emission tomography (PET) and functional magnetic resonance imaging (fMRI) have established techniques to assess *in vivo* glucose and oxygen consumption in the human brain. Using the oxygen glucose index (ODI: moles O_2 consumed per mole of glucose up-take; ODI of 6 represents complete combustion of glucose to CO_2 and H_2O under the assumption that all metabolised O_2 is used for glucose oxidation) PET experiments have confirmed the notion that the brain metabolises the majority of glucose to CO_2 (Hyder et al., 2016; Vaishnavi et al., 2010). In line with this, neurons exhibit a large number of mitochondria distributed throughout their different compartments and inhibition of OXPHOS or oxygen depletion renders neurons particularly sensitive to cell death (Mergenthaler et al., 2013). Futhermore, mitochondrial dysfunction is known as one of the main culprits of degeneration in neurodegenerative conditions, including Parkinson's disease (PD) (Dexter and Jenner, 2013; Schapira et al., 1989). Mitochondrial inhibitors, including 1-Methyl-4-phenyl-1,2,3,6-tetrahydropyridin (MPTP), 6-hydroxydopamine (6OHDA), and rotenone can mimic PD both in animal models and in humans (Bove and Perier, 2012; Jackson-Lewis and Przedborski, 2007; Langston et al., 1983).

In addition to the high numbers of neuronal mitochondria, neurons seem to have a very low expression of the key glycolytic enzyme 6-phosphofructo-2-kinase (PFK), which catalyses the rate limiting step in glycolysis. Accumulation of the PFK substrate glucose 6-phosphate facilitates entry of carbohydrates into the pentose phosphate pathway for generation of NADPH, which is crucial for the anti-oxidative response mechanisms of the cell. Diversion of glucose into the glycolytic pathway by overexpression of PFK is detrimental to neuronal survival, likely through the diminished cytosolic redox potential (Belanger et al., 2011; Mergenthaler et al., 2013).

iii) Neuron-astrocyte interplay

Research in the last two decades revealed major functional implications of astrocytes in various aspects of brain physiology. Astrocytes are intimately linked to neuronal metabolism through the regulation of the blood brain barrier and nutrient supply, as well as through a

dynamic exchange of metabolites, such as lactate (Ames, 2000; Sofroniew and Vinters, 2010). Two major hypotheses are currently being discussed of how astrocytic and neuronal metabolism communicates. Both are based on the observation that production of lactate, the anaerobic end product of glycolysis, is enhanced during brain activity in vivo, which is accompanied by a decreased ODI (Ames, 2000; Dienel, 2012). This points towards an important function of glycolysis during enhanced neuronal activity. Both hypotheses assume the partial compartmentalisation of non-oxidative versus oxidative energy metabolism between neurons and astrocytes and assume an active transport mechanism of lactate between neurons and astrocytes. However, they hypothesise a different lactate origin and are based on different experimental findings (Lundgaard et al., 2015; Pellerin and Magistretti, 1994; Simpson et al., 2007).

The astrocyte to neuron lactate shuttle (ANLS) hypothesis is based on the observation that astrocytes under particular culture conditions enhance lactate production when stimulated with the neurotransmitter glutamate, whereas neuronal glucose uptake in culture is inhibited under these conditions. Neurons instead preferentially take up astrocyte-derived lactate as energy substrate (Belanger et al., 2011; Pellerin and Magistretti, 1994).

The neuron to astrocyte lactate shuttle (NALS) hypothesis is based on the kinetics of different glucose transporters. The neuronal isoform GLUT3 has a higher rate of glucose transport than the astrocytic GLUT1, arguing for a preferential glucose uptake by neurons. In addition, lactate uptake and clearance by astrocytes is faster compared to lactate export from astrocytes or import into neurons. The hypothesis assumes that astrocytes primarily facilitate lactate secretion during brain activity (Mergenthaler et al., 2013; Simpson et al., 2007).

1.2 Parkinson's disease

Parkinson's disease (PD) is the second most common neurodegenerative disorder after Alzheimer's disease and is clinically characterised by unilateral onset of motor dysfunctions, which slowly progresses to a bilateral syndrome. At later stages PD affects both voluntary and autonomic motor functions. The prevalence of PD is 0.5% in people over the age of 65 and rises up to 4% at 85. Ageing remains the biggest risk factor for PD (Berg et al., 2015). The median age for the onset of PD is 60, with an average duration of 15 years after diagnosis. Current treatment options are aimed at ameliorating the symptoms but fail to slow the degenerative process.

Despite the traditional classification of PD as a sporadic disorder, 5-10% of patients carry familial mutations (Dexter and Jenner, 2013; Poewe et al., 2017). In addition, genome-wide association studies have confirmed several PD genes and identified new PD susceptibility loci that are associated with enhanced risk for disease development (Nalls et al., 2014). In the early stages PD neurodegeneration is mostly limited to a subset of midbrain dopaminergic neurons located in the substantia nigra pars compacta. The demise of these cells causes lowered levels of dopamine in the striatum, a subcortical nucleus of the brain that is involved in the co-ordination of movement among other functions. Although recent research has broadened our understanding of the pathologic mechanisms, there is no general agreement regarding the etiology of PD (Chan et al., 2010; Dexter and Jenner, 2013; Lees et al., 2009; Poewe et al., 2017; Schapira, 2011).

1.2.1 Clinical diagnosis of PD

Parkinson's disease is diagnosed based on the clinical assessment of a variety of symptoms. Although being described originally as a movement disorder, non-motor symptoms are now recognised as typical PD features, some of which may precede motor-based clinical diagnosis. The Movement Disorder Society (MDS) has recently revised the diagnostic criteria

for PD to include new diagnostic features and to refine the differential diagnosis between true PD and other parkinsonian disorders (Postuma et al., 2015).

i) Motor symptoms

Parkinson's disease is the most prevalent form among a number of related movement disorders, which all show symptoms collectively referred to as Parkinsonism. The diagnosis of Parkinsonism depends on the presence of the cardinal motor symptoms bradykinesia in combination with resting tremor and/or rigidity. To differentiate PD from other parkinsonian disorders the presence or absence of additional features has to be considered. The diagnosis as true PD, however, needs to be confirmed by post-mortem neuropathologic assessment of the affected brain areas (Postuma et al., 2015).

With the prodromal phase now being officially recognised, PD can be categorised into four stages (Berg et al., 2015; Postuma et al., 2015). The diagnosis usually occurs in the early stage, where the cardinal motor symptoms described above are the main symptoms. As the disease progresses to the mid-stage patients suffer from motor complications induced by long-term treatment with L-DOPA, the gold standard for PD treatment. This can result in freezing (dyskinesia) and hypokinetic fluctuations (daily off-time). Progression to late-stage PD is defined by the development of poorly L-DOPA responsive symptoms such as postural instability, shuffling gait and swallowing disability (dysphagia) (Poewe et al., 2017). These usually result in further complications, such as frequent falls and pneumonia, the latter often being diagnosed as the cause of death (Lees et al., 2009). Additional secondary motor symptoms can be present to a variable degree during the course of PD. These include micrographia, hypomimia, and speech disorder (dysarthria) (Jankovic, 2008; Lees et al., 2009). Importantly, the prevailing occurrence of mid- and late-stage motor symptoms at an early stage of the disease, i.e. within the first 5 years, argues against the diagnosis of true PD (Postuma et al., 2015).

ii) Non-motor symptoms

Non-motor symptoms are frequently present in PD patients and may lead to a severe decrease in the patient's quality of life. In many cases, non-motor symptoms can precede motor-based PD diagnosis by years. This recently led the MDS to recognise prodromal PD as an official disease stage for the use in clinical research (Berg et al., 2015; Mahlknecht et al., 2016).

Among the best-documented prodromal non-motor symptoms is rapid eye movement (REM) sleep behaviour disorder and depression (Berg et al., 2015). The loss of smell (hyposmia), daytime somnolence, constipation and anxiety are also often reported and have been suggested as markers for prodromal PD (Poewe et al., 2017). Early- to mid-stage non-motor symptoms are orthostatic hypotension, fatigue, mild cognitive impairment, as well as urinary and erectile dysfunction (Berg et al., 2015; Poewe et al., 2017). As PD progresses to the late-stage patients often suffer from psychotic symptoms (visual hallucinations) and dementia. In general the non-motor symptoms increase with disease progression to a variable degree depending on each patient (Jankovic, 2008; Poewe et al., 2017; Postuma et al., 2015).

1.2.2 The motor circuits of the basal ganglia in PD

The basal ganglia is a subcortical area of the brain that is implicated in the initiation and co-ordination of voluntary movement. The five nuclei of the basal ganglia that are involved in motor control are the striatum, the internal and external globus pallidus (GPi/e), the subthalamic nucleus (STN) and the substantia nigra (Figure 1.6 A) (Poewe et al., 2017). The motor circuit is set off when the striatum becomes activated through the motor cortex. The striatum projects medium spiny neurons, which are inhibitory GABAergic neurons, to the GPi and GPe thereby initiating the direct and the indirect pathway, respectively (Figure 1.6 B). Both pathways are antagonistic and together modulate the activity of the thalamus, which in turn feeds back to the motor cortex. The role of the substantia nigra is to regulate both direct

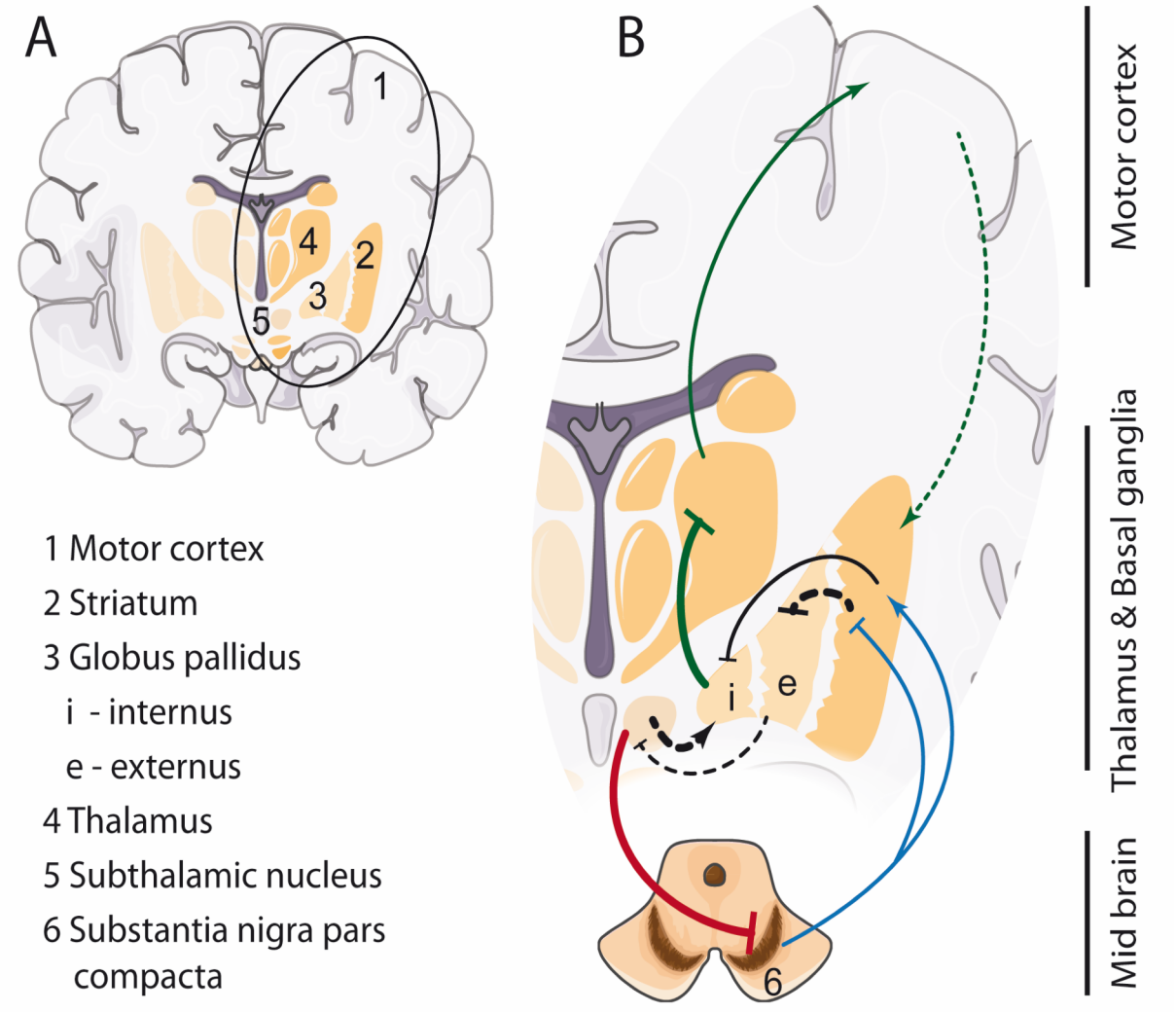


Figure 1.6 – The motor circuit of the basal ganglia. A) Schematic of a human coronal brain section. The areas involved in motor control are encircled. Note that the subthalamic nucleus is superimposed onto this section and is usually located further in the back. B) Close-up of the region encircled in A together with a horizontal section of the mid brain with substantia nigra pars compacta. Upon stimulation of the striatum by the motor cortex (green dotted line) both, the direct (continuous black line) and the indirect (dashed black line) motor circuit of the basal ganglia become activated. Both pathways have antagonistic effects on the activity of the globus pallidus internus, which conveys the output to the motor cortex via the thalamus (green continuous lines). The release of dopamine from the substantia nigra pars compacta into the striatum (blue lines) modulates the activity of both direct and indirect pathway resulting in a net increase of thalamic stimulation. The subthalamic nucleus decreases the activity of the substantia nigra pars compacta (red line). Thick lines represent those pathways that are over-activated in PD due to a lack of striatal dopamine. Images are modified with permission from Servier Medical Art (http://www.servier.com/Powerpoint-image-bank).

and indirect pathways resulting in an overall enhanced thalamic activity. The SNpc projects dopaminergic axons directly to the striatum. The release of dopamine affects both, activating dopamine D1 receptors and inhibiting D2 receptors. These receptors are differentially

expressed on neurons that target the direct pathway (D1) and indirect pathway (D2). Importantly, dopamine is a regulatory neurotransmitter, the activity of which sets the threshold for action potentials in the target neurons (Poewe et al., 2017).

The SNpc neurons are autonomic neurons that fire with regular frequency. The activity of the SNpc is negatively regulated by the STN, which results in an intricate feedback loop between activating and inhibiting circuits (DeLong and Wichmann, 2015; Galvan et al., 2015; Obeso et al., 2008; Yamada et al., 2016). In PD the loss of dopamine in the striatum causes a reduction in D2-mediated inhibition of the indirect pathway resulting in an over-activation of the STN. The inhibitory projections of the STN further downregulate SNpc activity and dopamine release in the striatum thereby disrupting the balance between direct and indirect circuit (Figure 1.6 B).

1.1.3 Treatment of PD

i) Pharmacological treatment

The gold-standard for treatment of PD has changed very little since the discovery of levodopa (L-DOPA) in the early 1960s (Barbeau, 1962; Cotzias et al., 1968), which remains the most effective drug against the motor symptoms of PD. Within its biosynthetic pathway L-DOPA is the direct precursor of dopamine (Hornykiewicz, 2002) and oral administration of L-DOPA was shown to restore the striatal dopamine levels in PD patients (Lloyd et al., 1975). A major drawback is the risk of L-dopa induced dyskinesia, which increases with dose and duration of administration. Dopamine receptor agonists can prove favourable in early disease stages and particularly in young-onset Parkinsonism. Other treatment strategies are aimed at prolonging the half-life of dopamine either in the peripheral blood stream or in the central nervous system. The two important examples are centrally active monoamine oxidase B (MAO B) inhibitors and peripheral catechol-O-methyltransferase (COMT) blockers (Smith et al., 2012). Other pharmacologic strategies for motor-symptoms include beta-blockers that

may be used against L-dopa unresponsive tremor, and anticholinergic drugs, which are probably the oldest treatment for PD but are less popular due to the severe adverse side effects (Connolly and Lang, 2014). Modern PD treatments also include pharmacotherapeutics against non-motor symptoms. However, their management remains challenging due to diagnostic failure, as well as an intricate relationship between the side effects of conventional PD drugs and non-motor symptoms (Smith et al., 2012).

ii) Invasive treatment

Invasive treatments are aimed at interfering with the neuronal network of the basal ganglia, the main effected area of dopaminergic cell loss in PD. They require neurosurgery, which is usually performed at an advanced stage of PD (Deuschl et al., 2006; Williams et al., 2010).

The invasive treatment used as part of the standard of care for PD is deep brain stimulation (DBS) of specific nuclei of the basal ganglia, mainly the subthalamic nucleus (STN) and to a lesser extent the internal segment of the globus pallidus. DBS is achieved by accurate positioning of a neurostimulatory electrode within these subcortical brain structures (Smith et al., 2012). The basis of therapeutic efficacy of DBS is the modulation of neuronal activity in pathologically de-regulated neuronal circuits, such as the motor circuits of the basal ganglia (Lozano and Lipsman, 2013). In order to achieve the appropriate modulation and avoid off-target spreading of the current several parameters of the electrode have to be fine-tuned including frequency, amplitude and pulse width. After correct electrode placement into the STN or GPi, usually aided by stereotactic surgery, immediate amelioration of several PD motor symptoms including tremor, rigidity, akinesia and drug-induced dystonia is often observed resulting in improved quality of life when compared to pharmacologic therapy alone (Lozano and Lipsman, 2013; Williams et al., 2010). Furthermore, DBS-induced improvement of motor functions allows for a lowering of L-DOPA daily doses and has proven beneficial for the development of L-DOPA induced dyskinesia as well as motor fluctuations (Deuschl et al., 2006; Smith et al., 2012). Unfortunately, most patients develop L-DOPA-resistant motor and non-motor symptoms with disease progression, which do not respond to DBS of the STN or

GPi nor to current pharmacologic interventions. These symptoms include gait disability, postural instability, speech disability and dysphagia, as well as the numerous non-motor symptoms, for which other treatment options are urgently needed (Lozano and Lipsman, 2013).

1.2.4 Pathology

i) Neuropathology

Neuropathologically, PD is characterised by the loss of dopaminergic (DA) neurons in the substantia nigra pars compacta (SNpc), which can be visualised by immunostaining with antibodies against tyrosine hydroxylase. Another hallmark of the disorder, present in a majority of cases, is the presence of eosinophilic Lewy bodies (LB) and Lewy neurites (LN) in surviving neurons and other brain areas, which represent protein inclusions in the soma and axons of neurons, respectively (Shulman et al., 2011). These aggregates stain positive for ubiquitin and the core is made up of misfolded α-synuclein (Spillantini et al., 1998). Cytosolic α-synuclein is an intrinsically disordered protein that can spontaneously form aggregation-prone β-stranded sheets (Dikiy and Eliezer, 2012). Importantly, SNpc neuronal demise does not strictly correlate with the presence of LB. For example, young-onset Parkinsonism caused by a genetic mutation of Parkin is clinically very similar to PD and is caused by neuronal loss in the SNpc but does not show α-synuclein pathology. In line with this, 20% of post-mortem brain reveals LB accumulation in absence of clinically diagnosed PD (Shulman et al., 2011). Nevertheless, the presence of non-physiological concentrations of α-synuclein is toxic to cells and a mutation in α-synuclein (*Park1*) was the first evidence for a genetic cause of PD in humans (Shulman et al., 2011).

Because of the prevailing existence of LB pathology in post-mortem PD brain the disease is considered a synucleinopathy. The main effected area in PD is the SNpc but other areas contain protein inclusions as well. After detailed characterisation of the post-mortem LB

pathology, Braak and Braak suggested a neuropathological staging system that was anticipated to correlate with clinical disease progression. They suggested a pattern of LB pathology starting from the enteric and peripheral autonomic nervous system and olfactory bulb in pre-clinical PD. The pathology is present in parts of the lower brain stem, in the SNpc and limbic structures and finally involves increasingly rostral areas such as the neocortex (Braak et al., 2003). However, for a significant number of PD-derived brain samples the Braak staging system does not apply (Jellinger, 2008). It was further suggested, that the staging system for PD would benefit from revision due to the sampling during the original study (Halliday et al., 2006).

ii) Molecular alterations – human studies

Despite the wealth of macroscopic evidence ascribed to parkinsonian neurodegeneration the molecular origin of cell death remains a matter of debate. This is probably due to two main problems: 1) the degenerative process goes along with a rather large number of alterations that were mostly studied in and partially depend on the animal models used and 2) the lack of successful translational strategies that could ameliorate PD-associated alterations and could protect from or slowdown the neuronal decline in humans.

Due to the inaccessibility of neuronal material from humans, studies of cellular alterations in patients are limited to post-mortem analysis and neuroimaging. Among the first observations made in post-mortem brain of PD patients was the presence of Lewy bodies (Goedert et al., 2013). The accumulation of protein-rich aggregates is not unique to PD. A number of other neurodegenerative disorders, most importantly Alzheimer's disease is characterised by such structures, although the location and composition of the aggregates differ (Ross and Poirier, 2004). This observation opened a field of research focussing on the study of protein aggregation properties as well as deregulation of protein degradation and homeostasis in disease.

Another major finding shaping PD research was the discovery of mitochondrial dysfunction, which gained first attention after the discovery that MPP^+, an inhibitor of complex I of the ETC, resulted in a form of induced Parkinsonism (Langston et al., 1983). The identification of complex I deficiency in post-mortem SNpc and patient-derived platelets and muscle cells added further evidence for a mitochondrial implication in the pathogenesis of PD (Bindoff et al., 1989; Parker et al., 1989; Schapira et al., 1989). Pharmacological inhibition of complex I induces the production of reactive oxygen species (ROS). Subsequently, increased oxidative damage of complex I in the form of protein carbonyls was found in post-mortem PD brain when compared to healthy controls (Keeney et al., 2006).

Other post-mortem studies revealed a greater presence of activated microglia in the SNpc of PD cases, which implies a role for these innate immune cells of the brain in higher vulnerability of SNpc neurons and PD pathogenesis (McGeer et al., 1988). Various studies also found differential expression of pro- and anti-apopotic proteins, cell signalling proteins involved in apoptosis and inflammation, as well as proteasome subunits, among others (Hartmann, 2004).

Neuroimaging is a relatively new, non-invasive tool that allows for the assessment of certain parameters of the brain in living subjects. There are two main categories of neuroimaging, which can be divided into structural and functional imaging (Politis, 2014). The former is used to morphologically map different parts of the brain based on tissue-specific physical properties. Functional brain imaging uses particular magnetic or isotopic properties of molecules that fulfil specific functions within the brain. Such molecules include oxygen used for functional MRI (fMRI) and engineered radiolabelled tracers (also called radioligands), such as fludeoxyglucose (FDG). The latter are usually ligands for neuronal receptors or enzymes and have an application in positron emission tomography (PET) imaging and single-photon emission computer tomography (SPECT). Several radioligands are available

that specifically target the dopaminergic system, such as ^{18}F-dopa, ^{11}C-MT, and ^{123}I-FP-CIT among others (Politis, 2014).

The use of dopaminergic tracers in humans revealed that neuronal deficiency precedes the onset of motor symptoms by approximately 6 years in typical PD and more than a decade in early-onset cases of the disease (Politis, 2014). The decline in dopamine activity is very rapid in the early stages and slows at later stages of the disease. The dopamine dysfunction in the putamen may be down to 45-70% of normal uptake at the time of diagnosis and decreases further to 70-80% deficiency at later stages (Politis, 2014). Furthermore, the metabolic activity of the neuronal network as analysed by uptake of FDG is altered early on in the disease probably preceding the onset of motor symptoms (Tang et al., 2010). Consistent with the notion that PD pathology is not limited to SNpc neurons, alterations of activity in other neuronal populations have been observed with functional neuroimaging (Politis, 2014).

iii) Molecular alterations in animal models of PD

The major progress regarding molecular changes associated with PD has been achieved through animal model and cell culture studies. Animal models can be divided into toxin-induced and genetic models. Meanwhile much of the human pathology can be reproduced in these systems there is currently no mouse model that combines all features of Parkinson's disease (Blesa and Przedborski, 2014; Shulman et al., 2011).

Toxin models of PD are based on mitochondrial drugs that inhibit complex I of the ETC (e.g. MPTP/MPP$^+$, rotenone) and/or induction of toxicity through oxidative stress, such as with 6-hydroxydopamine (6OHDA). These toxins recapitulate the mitochondrial damage and oxidative stress that has been associated with the demise of SNpc neurons (Blesa and Przedborski, 2014).

A variety of genetic models of PD have been developed after the identification of genes that cause Parkinsonism in either dominant or recessive forms. The most widely used genetic

model is the overexpression of human mutant α-synuclein in mice, which recapitulates LB pathology and mild synaptic decline but does not show loss of SNpc neurons. Other models include transgenic mice with mutations in the gene for leucine rich repeat kinase 2 (LRRK2), as well as mice deficient for PTEN-induced putative kinase 1 (PINK1), Parkin or DJ-1. These models have been intensively characterised and resemble some characteristic changes, such as mitochondrial deficiencies and varying degrees of neuronal defects. However, they are usually not characteristic for severe SNpc neuron loss and rarely exhibit pronounced motor deficits (Blesa and Przedborski, 2014).

One hypothesis for the incomplete modelling of PD in rodents is the presence of compensatory mechanisms in the basal ganglia network. In such case the slow neurodegeneration and late onset of PD may reflect the collapse of protective compensation. This pathologic cascade would be unlikely to proceed in rodent models due to their short life span (Dawson et al., 2010).

iv) Hypotheses of PD pathogenesis

Several hypotheses regarding the molecular disease mechanism of neuronal demise have evolved, of which the α-synuclein hypothesis (Dauer and Przedborski, 2003), the mitochondrial deficiency hypothesis (Schapira, 2008) and the bioenergetics hypothesis (Surmeier and Schumacker, 2013) are among the best-characterised.

The α-synuclein hypothesis is based on the neurotoxicity of α-synuclein in cell culture and animal models of PD. According to this model, disease is triggered by the accumulation and aggregation of α-synuclein into fibrils and subsequently into Lewy bodies. This can be caused by mutant α-synuclein, which has enhanced aggregation properties over the wildtype protein. Alternatively, aggregation can be the result of a non-physiological rise in α-synuclein concentration caused by a deficiency of the protein degradation machinery or α-synuclein gene multiplication. The aggregated protein has toxic gain-of-function properties that cause neuronal death. In addition, aggregated proteins act as a seed that can induce protein

aggregation and toxic downstream events in neighbouring neurons. The major caveat of this hypothesis is the lack of LB pathology in a subpopulation of parkinsonian patients (Lees et al., 2009; Shulman et al., 2011). The solution for this discrepancy may be the finding that oligomeric α-synuclein rather than LB are the more toxic α-synuclein species (Lansbury and Lashuel, 2006; Winklhofer et al., 2008). The presence of oligomeric α-synuclein in non-LB Parkinsonism remains to be proven.

According to the second hypothesis deficiency of complex I is the origin of the dopaminergic demise. This hypothesis was raised after the discovery that application of the mitochondrial complex I inhibitor MPP^+ was the cause of induced Parkinsonism (Langston et al., 1983). This hypothesis was further strengthened by the finding that post-mortem substantia nigra, as well as muscle cells and platelets from idiopathic PD patients frequently revealed complex I deficiency at the levels of protein quantity and activity (Mizuno et al., 1989; Parker et al., 1989; Schapira et al., 1989). However, complex I deficiency is not uniformly present in all PD cases, which raises the possibility for it to be either a secondary effect or restricted to a subgroup of PD patients (Dexter and Jenner, 2013; Gu et al., 1998; Mizuno et al., 1989).

Another concept regarding the pathogenesis of PD was introduced by Surmeier and his colleagues and is based on the unique physiological properties of the SNpc neurons. These cells are slow autonomic pacemakers with broad action potentials and have relatively high intracellular Ca^{2+} levels due to the activity of the L-type Ca^{2+} channels. Poorly buffered cytosolic calcium in SNpc neurons results in Ca^{2+} uptake by mitochondria, which increases the mitochondrial activity. The Ca^{2+}-induced mitochondrial activity is the source of increased basal levels of ROS, which cause an age-dependent mitochondrial run-down, enhanced mitophagy and subsequent energetic decline. This in turn causes synaptic degeneration and ultimately cell death. Interestingly, the hypothesis is not restricted to SNpc neurons but includes other neuronal populations involved in PD pathology, which have similar physiological properties as the ones outlined above (Surmeier and Schumacker, 2013).

Another study supported the key point of altered mitochondrial bioenergetics but argued against the universal importance of L-type Ca^{2+} channels (Pacelli et al., 2015). Elegant neuroanatomy studies of the SNpc dopaminergic neurons found the formation of large and dense axonal networks (Matsuda et al., 2009). This led to the hypothesis that the activity of the associated large number of synapses imposes a risk for energetic failure, which causes the vulnerability of these neurons to cell death (Pissadaki and Bolam, 2013). A subsequent study revealed more axonal mitochondria specifically in SNpc dopaminergic neurons and a positive correlation between the axonal arborisation and mitochondrial OXPHOS activity. Furthermore, the study provided evidence that inhibition of axonal outgrowth could reduce the vulnerability of SNpc neurons to mitochondrial insult (Pacelli et al., 2015).

Other lines of evidence argue for additional pathogenic factors, such as iron accumulation, disruption of neurotrophic signalling, and inflammation (Dauer and Przedborski, 2003; Exner et al., 2012; Schapira and Jenner, 2011; Shulman et al., 2011). Most of the alterations observed in PD cannot be viewed as singular processes but are highly interrelated. Therefore, it is equally possible that PD may be either a multi-factorial disorder initiated by more than one trigger or an accumulation of pathologically distinct disorders with highly overlapping motor symptoms (Dexter and Jenner, 2013; Shulman et al., 2011).

1.2.5 Genetics of Parkinsonism

The view of Parkinson's disease being a sporadic disorder has changed dramatically since the discovery of several genes that cause familial PD. The first gene that was associated with autosomal dominant familial PD was found in the locus for α-synuclein/Park1 (Polymeropoulos et al., 1997). Subsequently, other familial mutations were linked to the genes for leucine-rich repeat kinase 2 (LRRK2/Park8) (Zimprich et al., 2004), PTEN-induced putative kinase 1 (PINK1) (Valente et al., 2004), Parkin (Kitada et al., 1998), F-box only protein 7 (Fbxo7) (Di Fonzo et al., 2009; Shojaee et al., 2008), glucocerebrosidase (GBA)

(Aharon-Peretz et al., 2004; Sidransky et al., 2009), and DJ-1 (Bonifati et al., 2003). In addition, LRRK2, GBA and α-synuclein mutations have also been found in some sporadic cases of PD. Pathogenic mutations in LRRK2 and GBA confer autosomal dominant PD, whereas dysfunctional PINK1, Parkin, Fbxo7 and DJ-1 cause autosomal recessive Parkinsonism usually associated with early-onset. The latest advances in PD genetics are coming from genome-wide association studies (GWAS). GWAS are based on the genotyping of single nucleotide polymorphisms (SNP) in large cohorts in order to identify correlations between individual SNPs and the disease of interest (Pearson and Manolio, 2008). These studies have confirmed risk alleles that were previously found to cause familial forms of PD, most importantly α-synuclein, and uncovered a number of new alleles that are associated with higher prevalence of PD (Nalls et al., 2014). I will focus here on the established PD related proteins giving a brief overview of their function during neuronal physiology and their role in pathogenesis.

i) α-synuclein

Several pathologic mutations as well as multiplications of the α-synuclein coding gene *SNCA* cause autosomal dominant PD clinically very similar to idiopathic cases. The disorder presents with typical LB pathology and the age-of-onset was proposed to correlate negatively with gene dosage in patients with gene multiplications (Fuchs et al., 2007).

The 140 amino acid (aa) small protein α-synuclein belongs to the family of synucleins further comprised of β- and γ-synuclein. α-synuclein is characterised by an intrinsically disordered secondary structure with a central, aggregation-prone non-amyloid β component (NAC) domain that is thought to mediate Lewy body formation. The N-terminal part of the protein is able to bind to membranes, which induces the formation of an amphipathic α-helix causing partial insertion of the protein into lipid bilayers (Dikiy and Eliezer, 2012; Fusco et al., 2014). α-synuclein is enriched in the presynapse, where it can associate with synaptic vesicle membranes. In various synapses the presence or overexpression of α-synuclein decreases the release of neurotranmitters, possibly by stabilising membrane curvature (Exner et al.,

2012). In addition, α-synuclein was shown to promote the assembly of SNARE complexes, an essential step prior to the fusion of synaptic vesicles with the presynaptic membrane (Burre et al., 2010; Chandra et al., 2005).

The association of α-synuclein with membranes is not limited to synaptic vesicles. The protein has a preference for negatively charged phospholipids. These are abundantly present at the outer mitochondrial membrane (Davidson et al., 1998) and α-synuclein was found to associate with mitochondria in neurons and other cells (Exner et al., 2012; Nakamura et al., 2008). This association drives mitochondrial fragmentation independently of the mitochondrial fission protein Drp1 and may cause mitochondrial dysfunction (Exner et al., 2012).

In addition to mitochondrial and synaptic dysfunction α-synuclein overexpression or mutation causes alterations of the proteasomal and lysosomal pathways of protein homeostasis (Sulzer, 2010). Among the best-characterised properties of α-synuclein is its propensity to form fibrils that aggregate to LB. α-synuclein fibrils and smaller oligomers can act as a seed in neighbouring neurons where they induce the formation of new aggregates. This leads to spreading of α-synuclein both *in vitro* and *in vivo* (Exner et al., 2012). The aggregation of α-synuclein was reduced by the chaperone activity of another PD protein, DJ-1 and PD-causing mutations of DJ-1 were shown to reduce the protective activity against α-synuclein aggregation (Zondler et al., 2014). A family of proteins that is indirectly implicated in PD pathology is the 14-3-3 family of chaperone-like factors. Among the numerous functions of the 14-3-3 proteins is their effect on protein stability and sequestration of protein aggregates (Xu et al., 2013). 14-3-3s can interact with and stabilise α-synuclein oligomers but are sequestered by fibrillating α-synuclein β-sheets (Plotegher et al., 2014). 14-3-3 proteins have a broad range of functions including regulation of metabolism and cell signalling (Berg et al., 2003; Kleppe et al., 2011; Muslin et al., 1996; Shimada et al., 2013). Their sequestration through α-synuclein fibrils may therefore affect numerous cellular activities.

ii) LRRK2

Gene mutations in *LRRK2* are a common genetic cause of familial PD and sometimes occur in sporadic cases as well. Furthermore, LRRK2 variants with smaller effect sizes have been established as risk factors. Pathogenic LRRK2 mutations cause an autosomal dominant form of late-onset Parkinsonism usually with typical LB pathology. The disease mechanism has been proposed to rely on a toxic gain-of-function mutation of LRRK2. The pathogenic process, however, is not well understood nor is the role of LRRK2 in normal physiology (Wallings et al., 2015).

LRRK2 is a large protein of 2257 aa that belongs to the ROCO family of proteins. It contains various functionally distinct domains, including a ROC domain with GTPase activity, the C-terminal to ROC (COR) domain, a kinase domain with homology to the receptor-interacting Ser/Thr protein kinases (RIPK) and mixed lineage kinases (MLK). All three domains form the central enzymatic core of LRRK2 and are flanked by different protein-protein interaction domains, namely the WD40, leucine-rich repeat (LRR) and ankyrin domain (Cookson, 2010). The functional form of LRRK2 is a dimer, which may be important for protein autophosphorylation (Greggio et al., 2008). More than 20 residues mainly within the ROC domain, as well as in the COR and kinase domain have been found to be auto-phosphorylated. However, it is not well understood to what degree those different sites affect protein activity (Wallings et al., 2015). Interestingly, all mendelian LRRK2 mutations lay within the central core of the protein. ROC and COR mutants decrease GTPase activity whereas kinase mutants increase the kinase activity. Both of the LRRK2-intrinsic enzymes interact with each other either directly (Cookson, 2010; Wallings et al., 2015) or indirectly through the GTPase activating protein ArfGAP1 (Stafa et al., 2012), possibly in an antagonistic fashion. LRRK2 is modified by protein phosphatase 1A (PP1A), inhibitor of nuclear κB (IκB) family kinases and casein kinase 1α, as well as by yet unidentified kinases and phosphatases that affect residues distinct from the autophosphorylation sites (Wallings et al., 2015).

Kinase and GTPase activities as well as protein-protein interaction modules are very common in cell signalling pathways. In addition, LRRK2 was found to interact with numerous proteins that are implicated in a variety of signal transduction processes. As a result, LRRK2 was proposed to affect proliferation, inflammation, apoptosis, autophagy, protein expression and trafficking, synaptogenesis and synaptic vesicle recycling (Wallings et al., 2015). In line with an implication of mitochondria in PD pathogenesis, mutant LRRK2 led to impaired mitochondrial function, including OXPHOS deficits, fragmentation, morphological defects and impaired trafficking (Wallings et al., 2015). LRRK2 can associate with mitochondrial membranes and mutant $LRRK2^{G2019S}$ overexpression lowers mitochondrial membrane potential possibly through binding to and phosphorylation of one of the major mitochondrial anti-apoptotic proteins, Bcl-2 (Su et al., 2015).

Among the numerous interaction partners of LRRK2 are those of the 14-3-3 family of phospho-Ser/Thr-binding proteins (Li et al., 2011). 14-3-3 proteins regulate a variety of cellular functions through their effects on signalling molecules (see chapter 1.3). Four out of the five most common familial mutations of LRRK2 showed reduced phosphorylation of Ser^{910} and Ser^{935} and concomitant reduction of 14-3-3 binding (Nichols et al., 2010). This further correlated with redistribution of the mutant protein from diffuse cytosolic expression pattern into punctate cluster. The 5^{th} most common familial mutation, G2019S was shown to exhibit enhanced kinase activity but has otherwise a normal phosphorylation state and 14-3-3-binding capacity. Overexpression of this mutant leads to kinase-dependent decrease of neuronal outgrowth capacities in primary cultures. Interestingly, overexpression of 14-3-3θ ameliorates this effect through reduction of $LRRK2^{G2019S}$ kinase activity (Lavalley et al., 2016).

iii) PINK1

Mutations in the gene for PINK1 cause autosomal recessive Parkinsonism with early disease onset but otherwise indistinguishable from PD. Gene mutations are found in both familial and sporadic cases (Bonifati et al., 2005).

PINK1 is a 581 aa-long kinase with a typical N-terminal mitochondrial targeting sequence. It is imported via the TOM/TIM23 pathway and released laterally into the IMM with its kinase domain facing the intermembrane space. Upon TIM import the mitochondrial targeting sequence is cleaved by MPP (mitochondrial processing peptidase). In addition, the transmembrane helix of PINK1 is sensitive to cleavage by presinilin-associated rhomboid-like protein (PARL), which cuts PINK1 inside the membrane domain (Pickrell and Youle, 2015). This allows for retro-translocation of the cleaved PINK1 into the cytosol, where it is degraded by N-degron type 2 E3 ubiquitin ligases (Yamano and Youle, 2013). Alternatively, in *Drosophila melanogaster* PINK1 levels were found to be sensitive to the matrix protease Lon. Lon knock out selectively led to increased matrix levels of PINK1, which may reflect an alternative translocation pathway for PINK1 (Thomas et al., 2014).

PINK1 translocation across the mitochondrial membranes is driven by the mitochondrial membrane potential. Upon depolarisation of $\Delta\Psi_m$ PINK1 accumulates at the outer mitochondrial membrane where it is inaccessible to degradation by mitochondrial proteases (Narendra et al., 2010). This leads to the stabilisation and subsequent activation of PINK1 (Geisler et al., 2010; Vives-Bauza et al., 2010). A major substrate for PINK1 is ubiquitin. Phosphorylated ubiquitin recruits Parkin, a cytosolic E3 ubiquitin ligase, to mitochondria and activates its ubiquitin ligase activity (Kazlauskaite et al., 2014). PINK1-mediated phosphorylation of the ubiquitin-like domain of Parkin further enhances Parkin activity (Kondapalli et al., 2012). In addition, PINK1-phosphorylation of the outer membrane protein Mitofusin2 (Mfn2) can recruit Parkin to mitochondria in absence of ubiquitinated proteins (Chen and Dorn, 2013), which was suggested to trigger a feed forward loop of PINK1-Parkin

activation. The ubiquitination of proteins by Parkin increases the substrate pool for PINK1, resulting in an amplification of the degradation signal ultimately leading to the removal of damaged mitochondria via mitophagy (Pickrell and Youle, 2015). Of note, ubiquitin phosphorylation by PINK1 is sufficient to induce mitophagy in a Parkin-independent manner (Lazarou et al., 2015) but Parkin seems to facilitates the process of mitochondrial degradation.

Other substrates for PINK1 include the trafficking adaptor Miro1 at the OMM, the mitochondrial IMM protease HtrA2 and the mitochondrial chaperone TNF receptor associated protein 1 TRAP1/Hsp75. PINK1 phosphorylation of HtrA2 and Hsp75 was suggested to increase the resistance to mitochondrial stress (Plun-Favreau et al., 2007; Pridgeon et al., 2007). These findings argue for a role of PINK1 upstream of mitophagy (Voigt et al., 2016), which was recently reinforced by two independent publications. Both groups identified an activating effect of PINK1 on complex I of the ETC through interaction with the subunit NdufA10 (Morais et al., 2014; Pogson et al., 2014).

iv) Parkin

Mutations in the gene locus for Parkin are the most frequent cause of autosomal-recessive early-onset Parkinsonism. Parkin-induced Parkinsonism is clinically very similar to PD although non-motor symptoms are usually absent (Shulman et al., 2011). Mutant Parkin-carriers do not develop LB pathology, which is an interesting observation regarding the development of etiologic hypotheses.

Parkin is a 465 aa protein of a small E3 ubiquitin ligase family termed the ring-between-ring (RBR) family. Parkin consists of 3 zinc-binding RING (really interesting new gene) domains assigned RING0, RING1, and RING2, and a zinc-binding in between RING (IBR) domain between RING1 and RING2 (Pickrell and Youle, 2015). Parkin binds ubiquitin covalently via the RING2 domain after associating to an E2 ubiquitin-conjugating enzyme via RING1. In non-activating conditions, Parkin is autoinhibited through the occlusion of the ubiquitin

binding site by RING0 and the E2 binding site by an α-helix from a linker region between IBR and RING2 (Pickrell and Youle, 2015; Riley et al., 2013; Trempe et al., 2013).

The RBR domains harbour many cysteine residues, which renders Parkin sensitive to oxidative inactivation (Wong et al., 2007) and oxidative modification of Parkin may have pathologic relevance for sporadic PD (LaVoie et al., 2005). Parkin further contains an N-terminal ubiquitin like domain, which plays an important role in enzyme activation through phosphorylation by PINK1 at Ser^{65} (Kondapalli et al., 2012). In addition, phosphorylation of ubiquitin by PINK1 is involved in Parkin activation and accumulation at the outer mitochondrial membrane (Kazlauskaite et al., 2014).

Parkin regulates mitochondrial dynamics in a PINK1-dependent manner via interaction and degradation of the mitochondrial fusion proteins Mfn1 and Opa1, the mitochondrial fission protein Drp1 (Gegg et al., 2010; Yu et al., 2011), as well as the mobility adaptor protein Miro1 (Wang et al., 2011). Furthermore, Parkin regulates mitochondrial biogenesis through degradation of parkin interacting substrate (PARIS), a repressor of PGC1α transcriptional activity (Shin et al., 2011). All of these Parkin substrates are key factors for the different aspects of mitochondrial dynamics.

Other ubiquitination substrates for Parkin have been described including Septin5, Parkin-associated endothelin receptor-like receptor (Pael-R) (Dawson and Dawson, 2010) heat shock protein 70 (Moore et al., 2008), Bax (Johnson et al., 2012), the tyrosine phosphatase $STEP_{61}$ (Kurup et al., 2015), and the α-synuclein interaction partner synphilin (Chung et al., 2001). Parkin was also proposed to play a role in clearance of both α-synuclein (Shimura et al., 2001) and misfolded DJ-1 (Olzmann et al., 2007). Interestingly, Parkin may have ubiquitin-independent functions, such as a role in DNA binding and repression of p53 transcription (da Costa et al., 2009).

Parkin seems to be regulated by various cell signalling pathways at the transcriptional level. The tumour suppressor p53 transcriptionally activates Parkin expression and Parkin deficiency mediated by p53 knockdown was associated with a metabolic shift from mitochondrial OXPHOS to aerobic glycolysis, a hallmark for most cancer cells known as the Warburg effect (Zhang et al., 2011). In contrast, cytosolic p53 could directly interact with Parkin and inhibit Parkin-mediated mitophagy, which was associated with cardiac dysfunction in mice (Hoshino et al., 2013). Both examples showcase the importance of Parkin, as well as a balanced mitochondrial activity and dynamics for correct function of the cell. In addition to p53, the transcription factor ATF4, mediating the unfolded protein response activates Parkin expression, whereas the transcription factors N-myc and c-Jun downregulate Parkin levels (Bouman et al., 2011; West et al., 2004). Parkin activity is further negatively regulated through phosphorylation and binding of 14-3-3η (Sato et al., 2006). The same study also demonstrated that wildtype but not mutant α-synuclein could bind to 14-3-3η and sequester it from Parkin, thereby enhancing Parkin activity.

v) DJ-1

Homozygous gene disruption of the Park7 locus coding for the protein DJ-1 causes early onset Parkinsonism with clinical features similar to those observed in Pink1 and Parkin mutant carriers. DJ-1 mutations are the least common cause of familial PD (Ibanez et al., 2003).

DJ-1 is a 189 aa small protein with homology to bacterial chaperones of the DnaJ family. It has a broad cell protective role and was implicated in numerous pathways from transcriptional regulation to direct regulation of enzyme activity (Trempe and Fon, 2013). More detail on the structure and function of DJ-1 is provided in chapter 1.4.

vi) Other genes

A number of other genes have been implicated in the development of hereditary PD, including F-box only protein 7 (Fbxo7) (Di Fonzo et al., 2009), glucocerebrosidase (GBA)

(Aharon-Peretz et al., 2004; Sidransky et al., 2009) and the lysosomal ATPase ATP13A2 (Park et al., 2015), or were proposed as risk factors in sporadic PD, such as GBA, the genomic region spanning the three genes for Cyclin-G-associated kinase (GAK), the endosomal/lysomomal potassium channel TREM75, and the diacylglycerol kinase theta (DGKQ), as well as the MHC class II histocompatibility antigen HLA-DQB1 (Nalls et al., 2014). The role of most of these genes in pathogenesis has received little or no attention. Fbxo7 and both, GBA and ATP13A2 are implicated in protein degradation and lysosomal function, respectively. Fbxo7 interacts with Parkin to facilitate mitophagy (Burchell et al., 2013). GBA is a lysosomal protein, the activity of which is inversely related to α-synuclein levels (Schapira, 2015) and ATP13A2 is important for lysosomal function and the degradation of autophagosomes (Bento et al., 2016; Park et al., 2015). Thus, the function of these three proteins strengthens a role for protein homeostasis and quality control in the pathogenic process of PD.

1.3 14-3-3β and its implication in Parkinson's disease

The family of 14-3-3 proteins consists of 7 isoforms in humans with structural and functional homology (Berg et al., 2003a; Fu et al., 2000). The range of pathways that employ 14-3-3 proteins covers nearly all aspects of normal cellular activity, including proliferation (DeYoung et al., 2008; Gardino and Yaffe, 2011; Pozuelo Rubio et al., 2004), metabolic regulation (Kleppe et al., 2011; Pozuelo Rubio et al., 2004; Pozuelo Rubio et al., 2003; Weerasekara et al., 2014), excitability and secretion (Beguin et al., 2006; Berg et al., 2003a; Li et al., 2006), as well as regulated cell death (Gardino and Yaffe, 2011; Jang et al., 2009; Zha et al., 1996). 14-3-3 proteins have phospho-serine (pSer) and phospho-threonine (pThr) binding activity and have therefore been studied intensively in kinase- and phosphatase-dependent cell signalling pathways (Kosaki et al., 1998; Pozuelo-Rubio, 2011; Ramakrishnan et al., 2015; Rezabkova et al., 2011; Sato et al., 2002; Zha et al., 1996). The different isoforms of 14-3-3 are partially redundant while isoform-specific functions have also been reported (Pozuelo-Rubio, 2011; Sato et al., 2006; Schoenwaelder et al., 2016; Shumway et al., 2003; Sluchanko et al., 2012; Toyo-oka et al., 2003; Yano et al., 2006). Given their high expression levels in the brain and their broad spectrum of activities, it is not surprising that proteins of the 14-3-3 family have been implicated in various neurological disorders, including Parkinson's disease (Dzamko et al., 2010; Lavalley et al., 2016; Nichols et al., 2010; Ostrerova et al., 1999; Slone et al., 2015; Yacoubian et al., 2010).

1.3.1 Structure and function of the family of 14-3-3 proteins

i) Structural determinants of 14-3-3 binding modes

14-3-3 proteins form a conserved family among eukaryotes and mammalian paralogs often share nearly identical primary protein sequences. In human the family comprises seven isoforms: beta/alpha (β/α), gamma (γ), zeta/delta (ζ/δ), sigma (σ), epsilon (ε), eta (η), and theta/tau (θ/τ). The human isoforms share 80% similarity along the whole protein sequence

and have highly conserved functional regions (Figure 1.7) (Berg et al., 2003a; Fu et al., 2000).

14-3-3s are relatively small (app. 240 aa) acidic proteins with an antiparallel α-helical secondary structure. Although enhanced chaperone-activity of monomeric 14-3-3ζ has been described (Sluchanko et al., 2012), 14-3-3s are thought to act primarily as homo- or heterodimers with other 14-3-3 proteins (Fu et al., 2000; Johnson et al., 2010; Rezabkova et al., 2011; Sluchanko and Gusev, 2012; Tzivion et al., 2001; Yaffe et al., 1997; Yang et al., 2006). The crystal structure of dimeric 14-3-3 adopts a cup-like shape (Figure 1.8, PDB accession number 2c63) (Yang et al., 2006) with a highly conserved inner surface formed by helices 3, 5, 7, and 9, as well as a more variable outer surface (Obsil and Obsilova, 2011). Dimer formation crucially depends on a salt bridge between Arg^{18} and Glu^{89} of the two opposing 14-3-3 entities. The ability to form homodimers may further depend on the presence of Asp^{21} and Lys^{85}. The latter is replaced by a methionine in the 14-3-3ε isoform, which is the only isoform known to favour heterodimer formation, probably due to an incompatibility of the homodimer interface. Instead Glu^{22} of 14-3-3ε preferentially participates in a hydrogen bond with Lys^{85} of other 14-3-3 molecules, which may provide the necessary stabilising effect for dimer formation (Yang et al., 2006).

The most important property of 14-3-3 proteins is the ability to bind phosphorylated serine or threonine (pSer/Thr) containing proteins. The interaction occurs in a highly conserved binding cleft, which coordinates the phosphorylated side chain at (residues relative to β isoform) Lys^{51}, Arg^{58} and Arg^{62} on α-helix 3, as well as Arg^{129} and Tyr^{130} on α-helix 5 (Yaffe et al., 1997). Furthermore, Asp^{127}, Asn^{176} and Asn^{227}, as well as a hydrophobic patch made up of Leu^{175}, Leu^{219} and Ile^{220} are involved in stabilising the backbone surrounding pSer/pThr (Yang et al., 2006). Importantly, the interaction relies mainly on the phosphorylated residue and the conformation of the backbone (Yaffe et al., 1997; Yang et al., 2006), which explains the large number of substrates that were found to interact with 14-3-3 proteins.

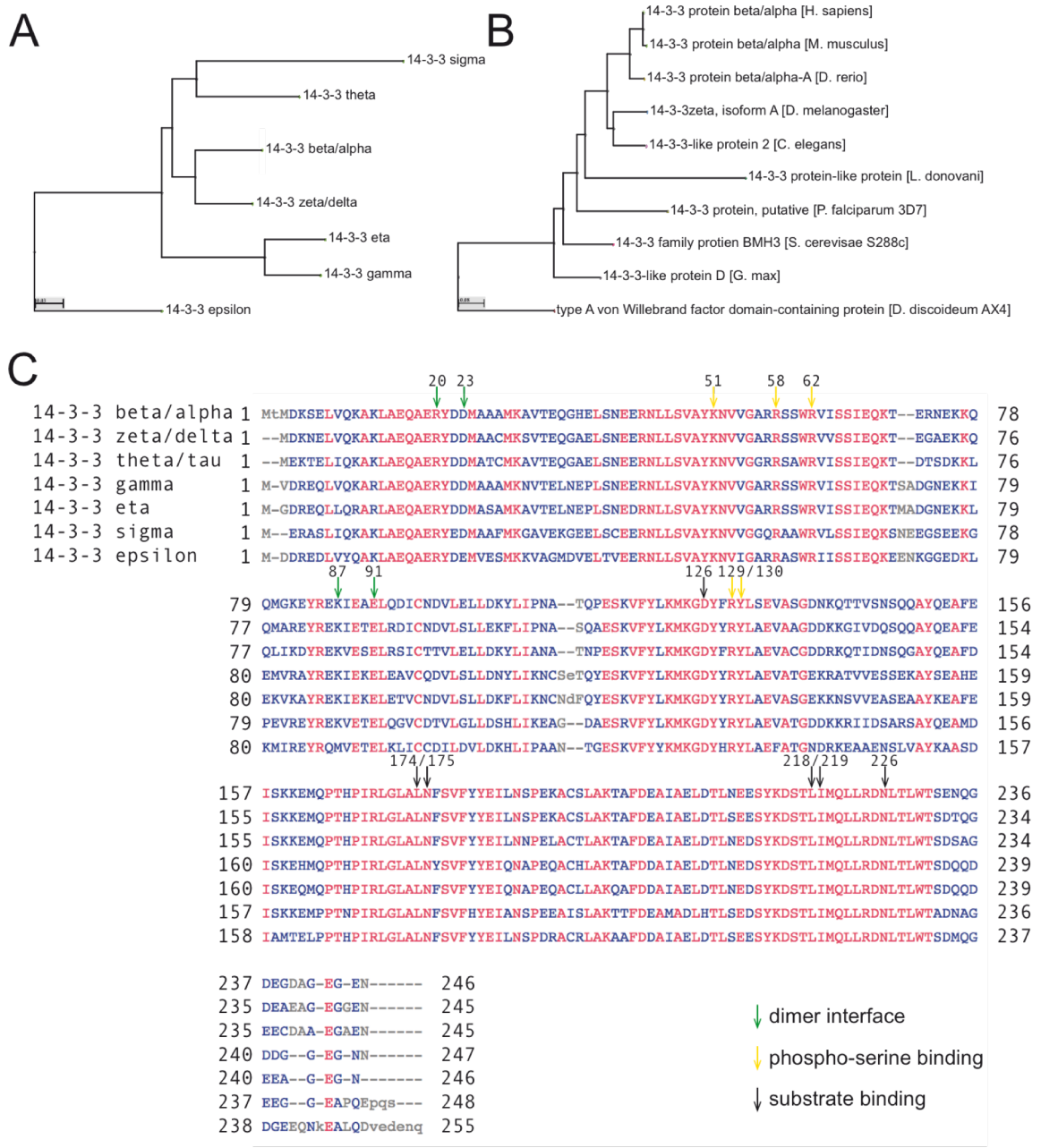


Figure 1.7 – 14-3-3 sequence homology. A,B Phylogenetic tree of human 14-3-3 isoforms (A) and paralogs of 14-3-3β in model organisms (B). C Alignment of the amino acid sequence of all human 14-3-3 isoforms with identical residues in red and conserved substitutions in blue. The arrows highlight selected functional residues. The numbering relates to the position in human 14-3-3β.

To date three distinct phospho-binding motifs were identified as 14-3-3 targets. Mode 1 and 2 are usually situated in internal, often unstructured regions. The consensus sequences are depicted below starting from the N-terminus (Ar = aromatic, b = basic, X = any amino acid) (Fu et al., 2000; Yaffe et al., 1997).

Mode 1: R - S/Ar - b/Ar- pS/T - L/E/A/M -P

Mode 2: R - X - Ar - b - pS/T - L/E/A/M -P

The proline in the +2 position breaks the helix and is important to accommodate the substrate along the binding cleft. The third mode of 14-3-3 binding was identified later and involves the substrate C-terminus (Coblitz et al., 2006; Wurtele et al., 2003). The minimal consensus sequence is:

Mode 3: pS/T - X_{1-2} - COOH

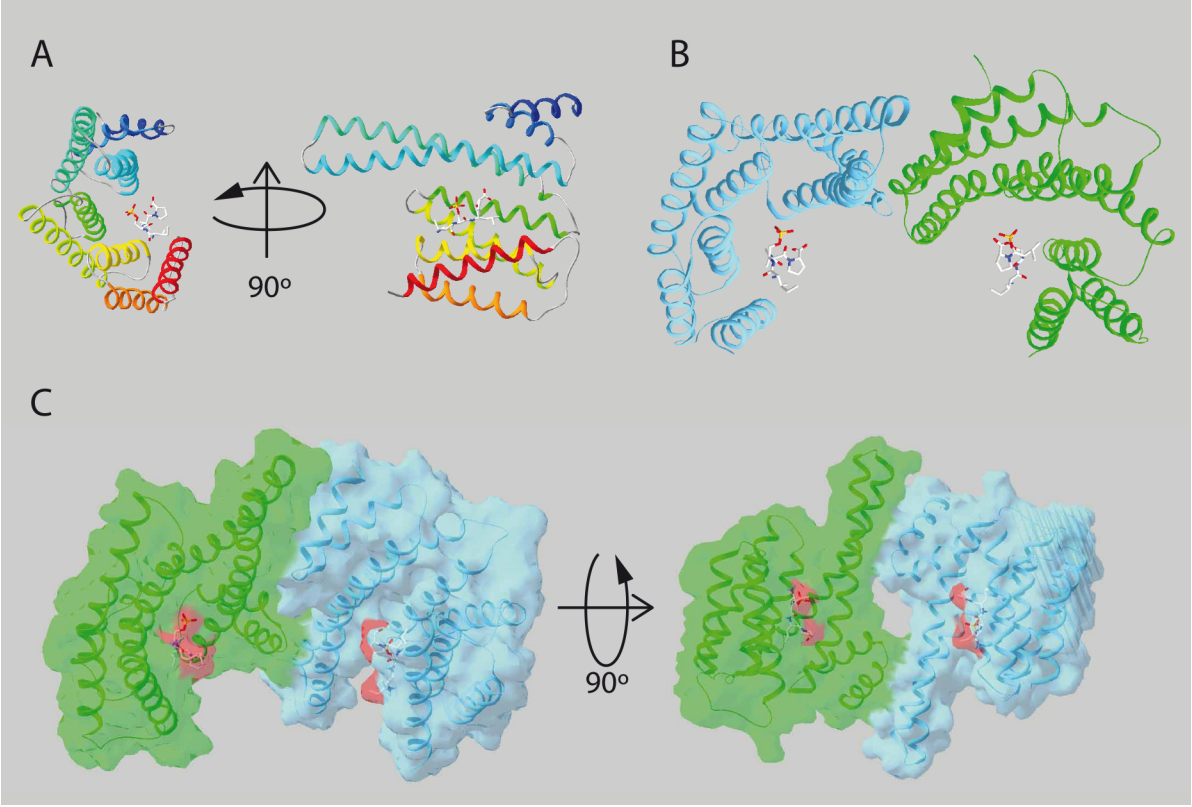


Figure 1.8 – Structure of 14-3-3. The crystal structure of 14-3-3η in complex with a phospho-peptide (PDB accession number: 2c63). A) The ribbon diagram of the monomer. The colour code reflects the 9 helices of the protein from N-terminus (dark blue) to C-terminus (red). The phospho-peptide is shown as stick model. The image on the right is horizontally turned 90° counter clockwise relative to the image on the left. B) 14-3-3η dimer with the typical cup-like shape. Each monomer is bound to the phospho-peptide. The two subunits are differentially colour-coded. The blue subunit is in a similar orientation as in the left image of A with a small turn clockwise. C) The 14-3-3η dimer with the ribbon representation superimposed onto the surface-rendered structure. The red surface corresponds to the phospho-peptide. All images were created using the software SPDBV as described in material and methods.

In addition, arginine residues in upstream positions have been observed frequently in mammalian mode 3 binding studies, which reflects some similarity to mode 1 and 2 (Coblitz et al., 2006). These consensus motifs have been valuable tools to predict new 14-3-3 interaction sites. However, substrates with less conserved motifs can be accommodated as well, largely due to a high conformational flexibility of the tertiary structure of 14-3-3 (Yang et al., 2006). In addition, a few proteins were reported to bind to the central cleft of several 14-3-3 proteins, including the β-isoform, in a phospho-peptide-independent manner (Ottmann et al., 2007; Yang et al., 2006).

The C-terminal domain of 14-3-3 proteins is not resolved in most crystal structures. Nuclear magnetic resonance has shown a highly flexible C-terminus, which shares structural and functional similarity to the C-terminal extensions in heat-shock protein-like chaperones (Williams et al., 2011). Various studies have reported a function for 14-3-3s in resolving protein aggregation and to aid in protein targeting to subcellular compartments (Hachiya et al., 1994; Plotegher et al., 2014; Sluchanko et al., 2012; Williams et al., 2011; Xu et al., 2013; Yano et al., 2006). The chaperone activity of 14-3-3 proteins seems to involve regions outside the conserved binding cleft in addition to the c-terminal flexible extension (Williams et al., 2011). This is in line with an earlier hypothesis, according to which the non-conserved outer surface of 14-3-3 was likely implicated in protein-protein interactions independently of and maybe prior to the phospho-residue binding by the central conserved cleft (Yang et al., 2006). This hypothesis was confirmed by the low-resolution solution structure of 14-3-3ζ in association with regulator of G protein signaling 3 (RGS3) (Rezabkova et al., 2011), which showed the docking of RGS3 at the C-terminal helices 6 and 8 of 14-3-3 in addition to the conserved phospho-binding of an unstructured region around Ser^{264} of human RGS3 isoform 1.

ii) Expression

Although extensive knowledge has been accumulated on the structure and mechanism of 14-3-3 proteins, little is known regarding isoform-specific expression levels or the regulation of 14-3-3 gene expression. 14-3-3s were first identified in brain extracts as a highly abundant protein component. Now we know that these proteins are ubiquitously present in all eukaryotic cells (Fu et al., 2000; Takahashi, 2003).

14-3-3 is expressed throughout all of the central nervous system, with highest levels in the hippocampal pyramidal cells, cerebral cortex, the olfactory bulb, and Purkinje cells of the cerebellum, as well as in peripheral tissue with high levels found in the liver, the intestine and the adrenal gland (Takahashi, 2003). An isoform specific expression pattern has been observed, which may be important for cell-specific functions of different 14-3-3 homologs. For example, whereas the ζ isoform is mainly expressed in the rat grey matter, θ is only found in glial cells of the white matter (Takahashi, 2003).

A function for 14-3-3 in development was supported by some older studies that showed expression of 14-3-3 β, γ, and ε early on in the developing brain and of isoform γ in the whole body (McConnell et al., 1995; Watanabe et al., 1993). Both studies revealed a dynamic regulation of expression throughout development.

With respect to the subcellular distribution, 14-3-3 proteins are found in cytosol and nucleus, in cytosolic organelles such as the Golgi and ER, as well as in association with the cytoskeleton and membranous structures, including the plasma membrane and synaptic membranes with little isoform-specific differences (Fu et al., 2000; Martin et al., 1994; Takahashi, 2003). Furthermore, an interaction between 14-3-3 and the F_1F_O ATP Synthase, which was identified in a mass spectrometry screen, suggests that 14-3-3 proteins may also be present in mitochondria (Pozuelo Rubio et al., 2004).

iii) 14-3-3 – Mechanisms of action

The activity of 14-3-3 proteins can be differentiated into three distinct, phosphorylation-dependent mechanisms with distinct effects on the target proteins (Obsil and Obsilova, 2011). Binding of a 14-3-3 dimer to its substrate can induce a conformational change within the substrate and alter its activity. This is exemplified by the binding of 14-3-3 to tyrosine hydroxylase, the rate-limiting enzyme in the synthesis of the catecholaminergic neurotransmitters dopamine, norepinephrine and adrenalin (Halskau et al., 2009).

Another mechanism is the simultaneous binding of 14-3-3 dimers to two different phosphorylated target proteins, whereby 14-3-3 acts as a scaffold. The resulting proximity of both target proteins may facilitate activation or inhibition of either binding partner. Simultaneous binding of 14-3-3β to the kinase Raf-1 and the cell cycle phosphatase Cdc25 was shown to activate Cdc25 through phosphorylation, thereby mediating Ras/Raf-1 induced cell cycle progression (Conklin et al., 1995).

A third mechanism of 14-3-3 activity is the occlusion of functional sites on target proteins. This may cause subcellular retention of the binding partner if the blocked site contains a targeting sequence, or inhibition of protein interaction if the site contains a protein interaction motif. In addition, protection of the phospho-residue from dephosphorylation was also observed, whereby 14-3-3 could alter the duration of substrate activity. The occlusion of functional sites has been observed in the binding of 14-3-3 to Bad, which was shown to sequester the pro-apoptotic Bad from the anti-apoptotic Bcl-2 and Bcl-x_L resulting in protection from cell death (Zha et al., 1996). In a different anti-apoptotic mechanism 14-3-3ζ was found to bind to and retain the pro-apoptotic transcription factor c-Abl in the cytoplasm. Interestingly, the release of c-Abl was mediated by JNK-dependent phosphorylation of Ser^{184} on 14-3-3ζ, rather then by dephosphorylation of c-Abl (Yoshida et al., 2005). Hence, Ser^{184} has a regulatory function on the binding activity of 14-3-3ζ, although this residue is not conserved among all human 14-3-3 isoforms.

1.3.2 Functions of 14-3-3 proteins

i) Metabolic regulation

Since their discovery, many different functions have been associated with the 14-3-3 family of proteins. A large screen for 14-3-3 interacting phospho-proteins has identified novel interaction partners involved in metabolism, including key enzymes such as phospho-fructokinase-2 (PFK2), glucose-6-phosphate dehydrogenase, glyceraldehyde-3-phosphate (GAPDH), pyruvate kinase muscle-type (PKM), and the α and β subunit of F_1F_O ATP synthase (Pozuelo Rubio et al., 2004). The large number of interaction partners indicates that 14-3-3-dependent direct modulation of energy metabolism can occur at various levels, although the precise function of these interactions has not been investigated for most of the proteins mentioned above.

A complex regulation of metabolism occurs upstream of metabolic enzyme activity. Several signalling pathways have been linked to 14-3-3 activity, including the insulin-receptor/phosphoinositol-3-kinase(PI3K)/Akt pathway, the AMP-activated protein kinase (AMPK) pathway, the autophagy pathway at the level of class III PI3K/Beclin1 complex and the mammalian target of rapamycin (mTOR) pathway. The latter integrates signals from all three aforementioned pathways (Kleppe et al., 2011).

Stimulation of the insulin receptor causes tyrosine phosphorylation of the insulin receptor substrates 1 (IRS1), which in turn activates the pro-glycolytic PI3K/PI3-dependent kinase1(PDK1)/Akt kinase cascade. Various 14-3-3 isoforms, namely β, ε, and ζ can interact with IRS1, thereby reducing its tyrosine phosphorylation and insulin sensitivity (Kosaki et al., 1998; Ogihara et al., 1997).

One of the effectors of Akt is the glycogen synthase kinase 3 (GSK3), which is negatively regulated by Akt phosphorylation at Ser^9 of GSK3β. GSK3 inhibits the activity of glycogen synthase but has many other upstream functions including the regulation of protein

expression, microtubule stability and apoptosis (Beurel et al., 2015). Interestingly, GSK3β has a positive effect on mitochondrial Ca^{2+} uptake through the activation of InsP3-Receptor Ca^{2+} channels at the ER to mitochondria contact sites (Gomez et al., 2016). Given the stimulating effect of mitochondrial Ca^{2+}, GSK3β could act as a positive regulator of mitochondrial metabolism. Consistent with the negative effect of 14-3-3 on IRS1 is the finding that a 14-3-3 peptide inhibitor enhances PI3K activity, thereby exacerbating GSK3β inhibition downstream of Akt in mouse cardiomyocytes (Liao et al., 2005). 14-3-3 can also bind directly to phosphorylated Ser^9 of GSK3β. Interestingly, instead of promoting the inhibitory effect of $pSer^9$ the binding of 14-3-3ζ to this residue increased the activity of GSK3β towards its substrate microtubule-associate protein tau (MAPT) (Yuan et al., 2004). Tau is implicated in microtubule stabilisation and mitochondrial trafficking in neurons (Stamer et al., 2002). Abnormally phosphorylated tau is found in neurodegenerative tauopathies. It is not clear weather the positive effect of 14-3-3 binding to GSK3β is specific for tau or can be expanded to other GSK3β substrates.

14-3-3 proteins also bind to other Akt phosphorylated substrates, such as the Akt substrate 160 (AS160) and proline-rich Akt substrate 40 (PRAS40). The interaction with AS160 releases its inhibitory activity on glucose transporter 4 (GLUT4) trafficking and induces an insulin-dependent relocation of GLUT4 from internal stores to the plasma membrane (Kleppe et al., 2011) thereby promoting glycolysis. Binding of 14-3-3 to PRAS40 is important for activation of the mTOR complex. The binding of PRAS40 to regulatory-associated protein of mTOR (Raptor) suppresses mTOR activation. The inhibition is released upon binding of 14-3-3 to Akt-phosphorylated PRAS40 (Kleppe et al., 2011). The mTOR pathway has many downstream effectors, which in conjunction activate protein synthesis, glucose metabolism and cell growth. The mTOR complex is therefore regulated at various levels. In addition to PRAS40, a second complex consisting of tuberous sclerosis complex 1 and 2 (TSC1/2) inhibits mTOR activity. TSC1/2 has GTPase activating function towards the Ras homologue-enriched in brain (RHEB) protein, the GTP bound form of which is necessary for mTOR

activation. Phosphorylation of TSC1/2 and subsequent inhibition through 14-3-3β binding enhances the level of GTP-RHEB in an extracellular-regulated kinase (ERK)-dependent manner (Kleppe et al., 2011; Shumway et al., 2003).

The activity of the mTOR pathway stands in contrast to the function of the AMPK pathway. AMPK is a sensor for energy shortage in the form of increased AMP/ATP ratio. As such, AMPK directly inhibits the mTOR pathway through phosphorylation of TSC2 as well as Raptor, causing an inhibitory association with 14-3-3 (Gwinn et al., 2008). AMPK, as well as the related kinases SIK2 and MARK2 are activated by the liver kinase 1 (LKB1). Phosphorylation of SIK2 and MARK2 results in binding of 14-3-3 and activation. The activated kinases in turn inhibit their target cAMP-regulated transcriptional coactivator (CRTC), the phosphorylation of which results in 14-3-3-dependent sequestration in the cytosol (Kleppe et al., 2011). Interestingly, the ζ isoform of 14-3-3 seems to negatively regulate LKB1 upon autophosphorylation (Bai et al., 2012). One direct output of the AMPK pathway is the activation of autophagy, which has a protective function during short-term depletion of nutrients. However, interaction of 14-3-3ζ with a key autophagic kinase, the class III PI3K results in inhibition of autophagy, likely mediated by protein kinase C (PKC) phosphorylation (Pozuelo-Rubio, 2011). These and many other studies exemplify the intricate relationship between 14-3-3 proteins and the regulation of cell metabolism. Of note, the binding of 14-3-3 to substrates is regulated dynamically in response to metabolic alterations. For example, during starvation 14-3-3ζ substrate binding was increased with respect to the autophagy factor Atg9a but decreased for the negative GLUT4 regulator AS160 (Weerasekara et al., 2014). Therefore, it is likely that 14-3-3 proteins are multifunctional players in the regulation of metabolism and more generally cell signalling. This may also explain why the role of 14-3-3s in pathological conditions is not always coherent. An example is the function of 14-3-3 in cancer. These proteins are usually considered oncogenic factors owing to their anti-apoptotic and pro-proliferative functions (Morrison, 2009). Nevertheless, tumour suppressor activity has been described especially for

the 14-3-3σ isoform regarding cell cycle control and the suppression of metabolic reprogramming, a phenomenon intrinsically linked to tumour formation and progression (Phan et al., 2015).

In summery, 14-3-3 proteins are potent regulators of energy metabolism both through upstream key signalling pathways and at the level of metabolic enzyme activity. In addition, these multifunctional proteins act in a highly dynamic manner to accommodate a large range of cellular activity.

ii) Mitochondrial functions

In fact, little is known about the direct effect of 14-3-3 proteins on mitochondria. Early studies identified a protein complex called the mitochondrial import stimulating factor (MSF) that could bind to and unfold mitochondrial precursor proteins. MSF further facilitates the association of mitochondrial precursor with the import complex TOM, probably via the Tom37/Tom70 receptors (Mihara and Omura, 1996). cDNA isolation from rat liver identified 14-3-3 isoforms ζ, γ, and ε as the large and small components of the MSF. Purified 14-3-3ζ and ε were able to stimulate the import of the precursor of ferredoxin (also known as adrenodoxin) into isolated mitochondria (Alam et al., 1994), suggesting a positive effect of 14-3-3 proteins on mitochondrial protein import and biogenesis.

Later an interaction between the mitochondrial and chloroplast ATP Synthase β-subunit and plant 14-3-3B was identified. Interestingly, this interaction was associated with inhibition of the ATP Synthase during dark adaptation of barley chloroplasts (Bunney et al., 2001). The barley 14-3-3B protein sequence is to 74% identical to ε and 63% identical to the β isoform of human 14-3-3 (NCBI protein blast using accession number Q43470 for barley 14-3-3B against reference protein data base limited to human protein sequences).

In line with this a publication recently revealed a positive effect of 14-3-3ζ knock out on mitochondrial ATP generation in platelets. In this study the knock out had a negative effect on thrombus formation, which was linked to a decrease of phosphatidylserine at the platelet

surface. It was shown that 14-3-3ζ deficiency led to increased ATP levels and reserve respiratory capacity in activated platelets (Schoenwaelder et al., 2016). The authors argued that thrombus formation is initiated through cell death pathways and in particular, by metabolism-dependent necrotic cell death. The increased mitochondrial capacity observed in 14-3-3 knock down cells may ameliorate the metabolic decline during platelet activation and hence protect from necrotic cell death. Taken together, this suggests a pro-necrotic role for 14-3-3ζ in mouse platelets. This finding is somewhat in contrast to the well-established role of 14-3-3 proteins in the inhibition of the mitochondrial pathway of apoptosis. 14-3-3 proteins bind to and negatively regulate the activity of Bad to induce mitochondrial outer membrane permeabilisation and apoptosis (Zha et al., 1996). These seemingly opposing effects on mitochondrial function demonstrate one more time the flexibility of 14-3-3 proteins to participate in very distinct regulatory processes.

iii) Neuronal functions of 14-3-3 and the implications in PD

Neurons are highly specialised signal transducing entities and as such 14-3-3 proteins are likely to fulfil a subset of functions that may be unique to these cells (Berg et al., 2003a). The most important property of neurons is their electrochemical excitability. In order to transmit action potentials, neurons maintain a sodium ion gradient across the axonal membrane thereby creating an inward negative membrane potential. The activation of voltage-gated sodium channels causes Na^+ influx, which decreases the negative potential thereby driving action potential propagation. Potassium ion efflux plays an important role during the re-polarisation of the membrane and Na^+/K^+-pumps are required to restore the ionic gradient during the refractory period of an action potential (Bean, 2007).

Another ion that is important for neuronal and synaptic transmission is calcium. Ca^{2+} is not only the main ion that induces synaptic vesicle secretion at the axonal endpoints, but can also change the excitability of the axon itself through inward-rectifying voltage-gated Ca^{2+} channels (Surmeier and Schumacker, 2013). Interestingly, 14-3-3 proteins were found to regulate the activity and inactivation properties of Ca^{2+} channel activity. 14-3-3 binds to the

C-terminal region of the pore forming α_{1B} subunit of $Ca_v2.2$ channels, which are implicated in synaptic short-term plasticity (Li et al., 2006). Binding of 14-3-3 slows the inactivation of $Ca_v2.2$ channel opening thereby enhancing Ca^{2+} influx and facilitating synaptic short-term potentiation. The interaction of 14-3-3 with ion channels of the CNS is not limited to $Ca_v2.2$. Other channels including the pH-sensitive potassium channels TASK1 and 3, and the chloride channel Clic4 were found to interact with 14-3-3 proteins (Berg et al., 2003a).

Recently, 14-3-3 functional knock out has been established in a mouse transgenic line. In this model, the overexpression of the dimeric 14-3-3 peptide inhibitor (difopein), which targets the phospho-binding activity of 14-3-3, induces a variety of neurologic defects. 14-3-3 deficit in the hippocampus for example was associated with impaired memory and decreased long-term potentiation (Qiao et al., 2014). In addition, cortical neurotransmission was also disturbed, which was associated with schizophrenia-related behaviour and increased dopamine release in the striatum of these animals (Foote et al., 2015).

These studies demonstrate the importance of the 14-3-3 proteins during physiologic activity of the nervous system. Interestingly, deletion of the 14-3-3ε gene was found in patients with the neurodevelopmental Miller-Dieker syndrome (Toyo-oka et al., 2003). Deregulation of 14-3-3 activity has also been reported in other neurologic disorders, although a causal role has not been established. For example, abnormal secretion of 14-3-3 into the cerebrospinal fluid has been observed in various brain disorders, including multiple sclerosis, stroke, vascular dementia, frontotemporal dementia, brain tumours and metastasis, various types of encephalopathy, tuberous sclerosis and epilepsy (Berg et al., 2003a). 14-3-3 expression is also altered in astrocytes after ischemic injury (Kawamoto et al., 2006) and in certain brain regions in Alzheimer's disease (AD) patients (Berg et al., 2003a). The neurophathology of AD is characterised by intra- and extracellular deposits of misfolded amyloid beta protein, as well as by intracellular aggregates of hyper-phosphorylated tau. Pathologic analysis revealed the presence of 14-3-3 in the intracellular aggregates but not in extracellular amyloid

plaques. Furthermore, 14-3-3ζ binding to tau enhances tau phosphorylation by protein kinase A and GSK3β and impairs tau function in microtubule stabilisation (Agarwal-Mawal et al., 2003; Berg et al., 2003a).

Several 14-3-3 isoforms are also present in PD-associated Lewy bodies. LB stain positive for a majority of 14-3-3 isoforms (Berg et al., 2003b). In fact, there is a long-standing relation between PD and 14-3-3. One of the first identified functions of 14-3-3 was their effect as tyrosine (Y) and tryptophane (W) hydroxylase activators (hence their gene ID YWHA) (Isobe et al., 1991; Itagaki et al., 1999). The loss of dopamine in the striatum is the main effect of neurodegeneration in PD. The spontaneous degradation of dopamine and subsequent production of reactive oxygen species (ROS) is at the core of the ROS hypothesis for the pathogenesis of PD neurodegeneration (Dauer and Przedborski, 2003).

Another implication of 14-3-3 in PD comes from several studies that showed an interaction between 14-3-3 and α-synuclein (Ostrerova et al., 1999; Plotegher et al., 2014). The two proteins share limited regional homology in their amino acid sequence and show some overlap in their interaction partners, including tyrosine hydroxylase (Halskau et al., 2009; Perez et al., 2002). Whereas 14-3-3 proteins activate TH upon Ser^{19} phosphorylation (Halskau et al., 2009), both WT and mutant A53T α-synuclein inhibit TH and reduce dopamine secretion in a dopaminergic cell line (Perez et al., 2002). The authors speculated that sequestration of α-synuclein into Lewy bodies, a pathologic hallmark of PD, may result in TH over-activation, which could increase ROS levels through formation of dopamine quinones.

Another interesting relationship between 14-3-3 and α-synuclein involves the chaperone activity of 14-3-3η, which could inhibit fibril formation of oligomeric α-synuclein during the early aggregation process. However, as α-synuclein levels increased and the aggregation process continued 14-3-3η was effectively sequestered from the cytoplasm into insoluble

inclusions suggesting a role for deregulated 14-3-3η protein expression to play a role in PD (Plotegher et al., 2014).

14-3-3 was found to interact with two other PD gene products, LRRK2 and Parkin. In the case of LRRK2, binding promotes a soluble, cytoplasmic localisation of LRRK2, which is disrupted by several PD-causing mutations (Nichols et al., 2010). Furthermore, 14-3-3θ reduces the kinase activity of $LRRK2^{G2019S}$ (Lavalley et al., 2016), a mutant that has previously been associated with enhanced kinase activity. In the case of Parkin, 14-3-3η was shown to bind to and inhibit the activity of wildtype but not mutant Parkin. Furthermore, this interaction was disrupted by wildtype α-synuclein. In contrast mutant α-synuclein could not sequester 14-3-3η, which led to prolonged inhibition of Parkin (Sato et al., 2006). Interestingly, a screen for novel interaction partners using the *Saccharomyces cerevisiae* 14-3-3 isoforms as bait identified DJ-1/Park7 as a putative binding partner (Pozuelo Rubio et al., 2004). This finding has not been confirmed to date and a functional significance for an interaction between DJ-1 and 14-3-3 remains to be elucidated.

Recently, the expression and phosphorylation status of 14-3-3 proteins were examined in two PD model systems and patients. Out of three regulatory phosphorylation sites Ser^{232} phosphorylation was increased in 14-3-3θ in PD models and PD post-mortem brain. The phosphorylation was likely mediated by casein kinase and had a negative effect on the ability of 14-3-3θ to inhibit Bax (Slone et al., 2015).

Taken together, many different lines of evidence support a role for 14-3-3 proteins in the pathologic alterations observed in neurodegenerative conditions and PD. Furthermore, 14-3-3 proteins have a neuroprotective effect in several models of Parkinsonism (Slone et al., 2015; Yacoubian et al., 2010), which is in line with their negative effect on cell death and protein aggregation (Gardino and Yaffe, 2011; Plotegher et al., 2014). A detailed

understanding of the role of 14-3-3 proteins in PD-associated molecular alterations may aid the development of novel neuro-protective therapies.

1.4 DJ-1/Park7

Among one of the best-characterised PD loci is *PARK7*, which harbours the gene for DJ-1. Homozygous mutation or deletion of *PARK7* causes autosomal recessive, early-onset Parkinsonism (Bonifati et al., 2003). Due to the low frequency of *PARK7* mutations, very little is known about the clinical picture but it seems to present with a phenotype similar to PD caused by mutant PINK1 and Parkin (Shulman et al., 2011). A large body of evidence supports a cell-protective effect of DJ-1 against various factors including oxidative and metabolic stress (Aleyasin et al., 2010; Guzman et al., 2010; McNally et al., 2011; Ren et al.,

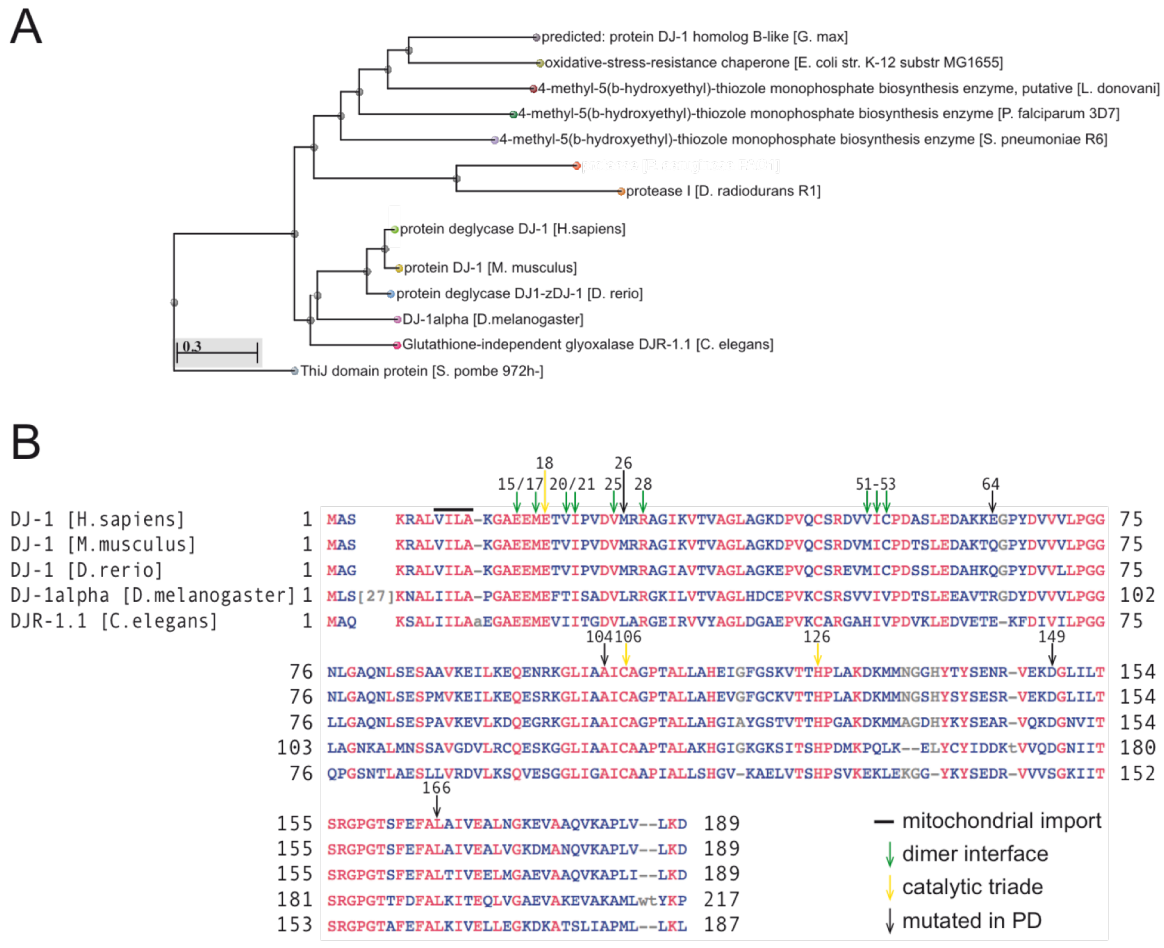


Figure 1.9 – Sequence homology of different DJ-1 paralogues. A) The phylogenetic tree of DJ-1 among model organisms, including mouse, *D.melanogaster*, *C.elegans* and various unicellular organisms. B) Alignment of the amino acid sequence of human DJ-1 and the closest relatives in higher eukaryotes with identical residues in red and conserved substitutions in blue. The arrows highlight selected functional residues (green and yellow) and sites of pathologic mutations (black). The numbers relate to the position in DJ-1.

2011; Richarme et al., 2015; Shi et al., 2015; Taira et al., 2004b; Vasseur et al., 2009).

1.4.1 Structure of DJ-1

DJ-1 is a small, soluble protein of 189 aa length that can form homodimers both *in vitro* and *in vivo*. The protein is conserved from mammals to bacteria (Figure 1.9) and the crystal structure revealed similarity to bacterial proteases and glyoxalases (Honbou et al., 2003). The tertiary structure of DJ-1 is comprised of a central β-sheet that is surrounded by α-helices. DJ-1 acquires a conformation known as a Rossmann-fold that usually binds to dinucleotides, such as FAD and $NAD(P)^+$ (Honbou et al., 2003) (Figure 1.10). However, no dinucleotides are known to bind to DJ-1 and no canonical binding motifs (Hanukoglu and Gutfinger, 1989) are found within the primary sequence. DJ-1 has an active site with a catalytic triad consisting of the reactive cysteine Cys^{106} as well as auxiliary histidine His^{126} and glutamate Glu^{18}. Catalytic triads are present in proteases where they hydrolyse amino acid chains (Carter and Wells, 1988; McGrath, 1999). However, in contrast to the active proteases in bacteria, the DJ-1 triad is spatially distorted, which is likely to render the protein catalytically inactive (Lee et al., 2003). Furthermore, dimer formation as well as the C-terminal helix of DJ-1 blocks the active site for substrate entry (Honbou et al., 2003). It was proposed that conformational changes in DJ-1 resulting from dimer disruption or protein modification may cause an activation of the proteolytic activity (Chen et al., 2010; Honbou et al., 2003). One such modification may occur at residue Cys^{53}, which is situated within the dimer interface. DJ-1 can exist in two forms that differ in their isoelectric point (pI=6.2 and pI=5.8). It was proposed that the more electronegative protein contains oxidative modifications (Mitsumoto et al., 2001). The electronegative form could be blocked by mutation of Cys^{53} to Ala (Taira et al., 2004b). However, other mutations also blocked the pI=5.8 species, including mutation of the active site Cys^{106} and the pathologic mutant DJ-1^{L166P}. Later studies suggested that Cys^{106} is more susceptible to oxidative modification (Canet-Aviles et al., 2004), probably due to the electrostatic environment surrounding this residue (Witt et al., 2008). In support of this, mutation of Cys^{106} to Ala abrogated the

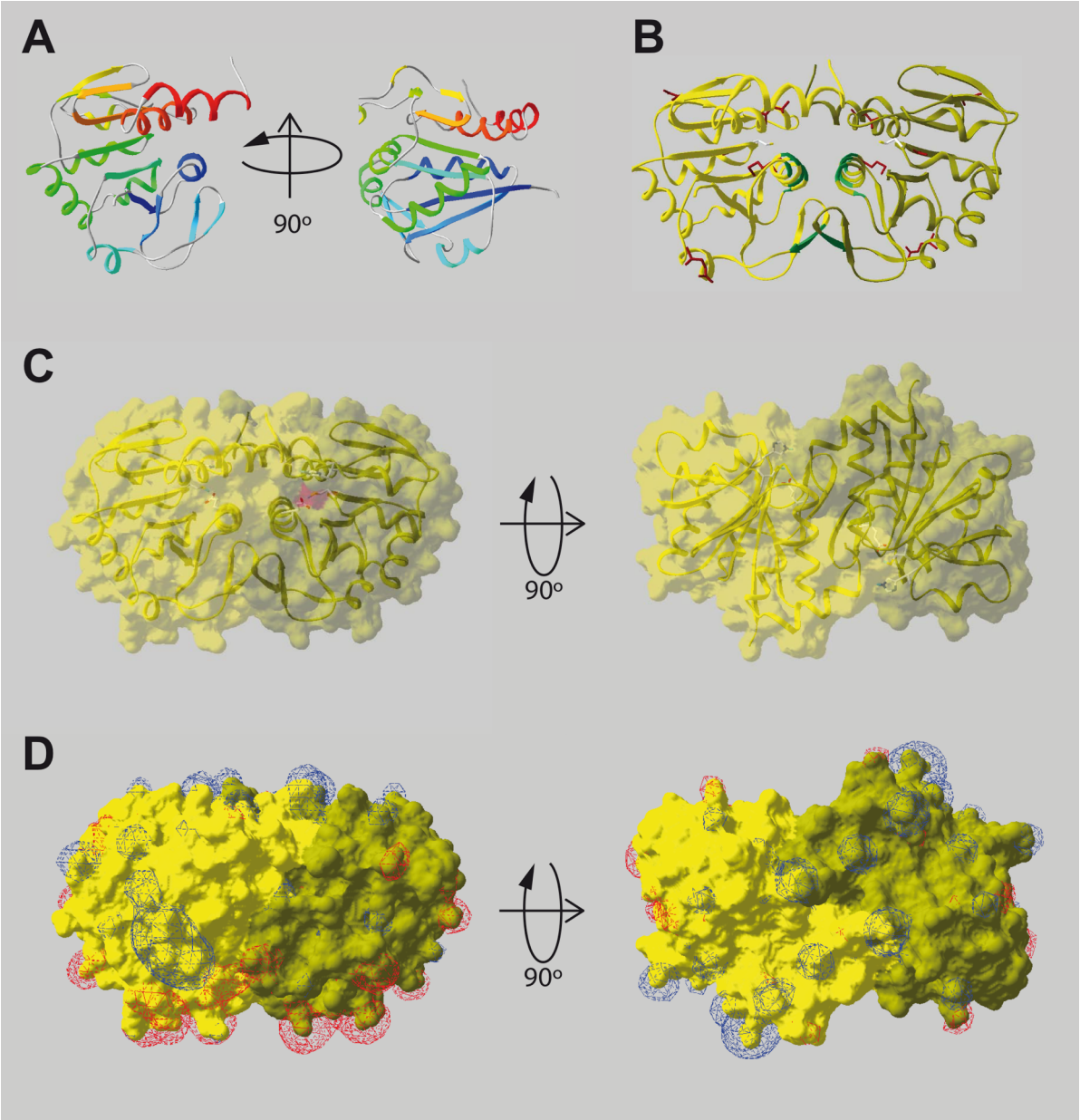


Figure 1.10 – The crystal structure of human DJ-1 (PDB accession number 2OR3). A) The ribbon diagram of the monomer. The colour code indicates the individual secondary structural elements of the protein from N-terminus (dark blue) to C-terminus (red). The image on the right is horizontally turned 90° counter clockwise relative to the image on the left. B) DJ-1 dimer as ribbon representation with differently coloured yellow and golden subunits. The green ribbon indicates dimer interaction and the red side chains indicate the sites of pathologic mutations. The side chain of the active Cys106 is depicted in white and yellow. The yellow subunit is in the same orientation as in A (left). C) The DJ-1 dimer surface-rendered with the ribbon representation superimposed. The red surface marks the small cavity in vicinity of the active Cys106. The right image is turned 90° vertically to visualise the top of the left image. D) Images are depicted as in C (only surface representation). In addition, the computed electrostatic potential at the surface of DJ-1 is visualised. Red indicates negative potentials and blue indicates positive potentials. All images were created using the free software SPDBV as described in material and methods.

protective effect of DJ-1 against oxidative stress in cells (Canet-Aviles et al., 2004; Martinat et al., 2004; Taira et al., 2004b).

1.4.2 Expression and translocation

DJ-1 is ubiquitously expressed throughout the body. The intracellular location of DJ-1 has been reported to be both, cytoplasmic and mitochondrial. Mitochondrial levels of DJ-1 are enhanced during oxidative stress. It was first proposed that oxidation of Cys^{106} triggers the translocation (Canet-Aviles et al., 2004). However, mutation experiments revealed that Cys^{106} is dispensable for the accumulation of DJ-1 in mitochondria and rather disruption of the DJ-1 dimer interface and the presence of an N-terminal hydrophobic sequence $L^{7}VIL^{10}$ were necessary and sufficient for mitochondrial targeting (Maita et al., 2013). The same study also provided evidence for a preferential mitochondrial localisation of PD-associated mutant forms of DJ-1 (M26I, L166P mutations). This was later reinforced by a study that used a targeted GFP-construct, which became fluorescent upon complementation with a DJ-1-tagged moiety. This study further revealed that DJ-1 is located both at the OMM and matrix of mitochondria and that it not only translocates during oxidative stress but also upon nutrient deprivation (Cali et al., 2015).

The subcellular location of DJ-1 is not limited to the cytosol and mitochondria. In neuroblastoma cells exposed to oxidative stress DJ-1 first accumulated in mitochondria at an early phase (3h) and in the nucleus at a later stage (12-24h) (Junn et al., 2009). Another study identified a complex between DJ-1, striatin-3 and Akt, which was suggested to target DJ-1 to the plasma membrane in a striatin-3-dependent manner (Tanti and Goswami, 2014). Furthermore, in neurons, DJ-1 was co-purified with synaptic membranes and was found to be associated with synaptic vesicles (Usami et al., 2011).

1.4.3 Function of DJ-1

The localisation of DJ-1 to many subcellular compartments (Kim et al., 2013; Kim et al., 2012; Usami et al., 2011; Zhang et al., 2005) suggests that the protein participates in a variety of cellular processes and research over the last decade supports this view. Deregulation of DJ-1 plays a role in various disorders, including cancer (Cao et al., 2015; Kim et al., 2005a; Miyajima et al., 2010; Nagakubo et al., 1997), male infertility (Klinefelter et al., 1997; Taira et al., 2004a; Wagenfeld et al., 1998), ageing-related type 2 diabetes mellitus (Jain et al., 2012), and a causative role in early-onset Parkinson's disease (Bonifati et al., 2003; Hague et al., 2003; Ibanez et al., 2003). In line with this, DJ-1 is implicated in numerous different processes including protein homeostasis (Fan et al., 2008; Im et al., 2012; Moscovitz et al., 2015), cell proliferation (Kim et al., 2005a; Nagakubo et al., 1997), anti-oxidant metabolism (Kim et al., 2005b; Meiser et al., 2016; Taira et al., 2004b; Zhou and Freed, 2005), transcriptional and translational regulation (Blackinton et al., 2009; Fan et al., 2008; Taira et al., 2004a; van der Brug et al., 2008), as well as metabolism (Hayashi et al., 2009; Meiser et al., 2016; Shi et al., 2015). DJ-1 is generally cell protective. The fact that DJ-1 functions in so many diverse cellular activities suggests a role as master regulator.

i) DJ-1 in cancer and cell proliferation

The first function of DJ-1 was related to its transforming effect on mouse embryonic fibroblasts. Overexpression of DJ-1 had a similar effect on cell proliferation like c-myc and a strong cooperative effect when co-transfected with the oncogenic kinase Ras (Nagakubo et al., 1997). Ras is upstream of two major pro-survival and proliferative signalling cascades, namely the PI3K/Akt cascade and the mitogen-activated protein kinase (MAPK) cascade. Akt is directly activated by the phosphatidylinositol-3,4,5-trisphosphate (PIP_3)-dependent protein kinase (PDK) on Thr^{308} (Stephens et al., 1998) and its activity is suppressed by PIP_3 dephosphorylation through phosphatase and tensin homolog (PTEN) (Maehama and Dixon, 1998; Stambolic et al., 1998). There is an intricate relation between DJ-1 and the Akt signalling pathway. DJ-1 activates Akt via direct inhibition of PTEN as well as transcriptional repression of p53 (Kim et al., 2005a; Kim et al., 2009). p53 and PTEN positively cooperate

on the transcriptional level (Freeman et al., 2003). Consistently, DJ-1 overexpression enhances Thr^{308} phosphorylation and activation of Akt (Wang et al., 2013; Zhang et al., 2016). Akt on the other hand represses p53 activity, thereby enhancing DJ-1 expression and activating a positive feed forward loop (Duplan et al., 2013). In summary, PTEN and DJ-1 are upstream regulators of the survival and proliferation kinase Akt. Although it is clear that the activity of the two proteins needs to be under stringent control, it is not known to date, which factors are responsible for this regulation. Interestingly, DJ-1 and Akt were found in a ternary complex with striatin-3, a scaffolding protein which localised to both mitochondria and the plasma membrane (Tanti and Goswami, 2014). The study further showed that H_2O_2 treatment could alter the subcellular localisation not only of DJ-1, but also Akt probably through increased complex formation with striatin-3. This suggests that the subcellular localisation of DJ-1 and Akt could play a major role in the regulation of their downstream signalling activities.

ii) DJ-1 in PD and protein homeostasis

Soon after the discovery of DJ-1 as a putative oncogene its causative role in several familial cases of PD became evident (Bonifati et al., 2003; Hague et al., 2003). This led to the discovery of the function of DJ-1 in the oxidative stress response, mitochondrial integrity, as well as protein and mitochondrial quality control. DJ-1 was shown to physically and functionally interact with several PD proteins. For example, DJ-1 expression protects from α-synuclein-induced toxicity by reducing protein aggregation (Batelli et al., 2015; Shendelman et al., 2004; Zondler et al., 2014). DJ-1 was also shown to associate with synaptic vesicles and has a role in regulation of tyrosine hydroxylase activity (Ishikawa et al., 2009), similarly to α-synuclein. Consistent with a synaptic function, DJ-1 was shown to be important for long-term synaptic plasticity in hippocampal synapses (Wang et al., 2008).

A second line of evidence connects DJ-1 to the PINK1/Parkin pathway of protein degradation and mitochondrial quality control. All three proteins were found in a ternary complex that was

proposed to function as an E3 ligase in protein degradation (Xiong et al., 2009). In line with this, DJ-1 was recently shown to regulate the activity of the 20S proteasome in a redox dependent manner (Moscovitz et al., 2015). Although the E3 complex formation could not be confirmed in a later study (Thomas et al., 2011), a functional link between DJ-1 and PINK1/Parkin was established in maintaining mitochondrial integrity. The study further demonstrated that Parkin could rescue the mitochondrial deficits induced by DJ-1 knockdown. In Drosophila overexpression of DJ-1 rescued muscle degeneration caused by PINK1 KO, but not Parkin KO (Hao et al., 2010). Finally, a p53-dependent and ubiquitin-independent, positive effect of Parkin on DJ-1 expression was shown in cell culture and mouse brain (Duplan et al., 2013), arguing for a protective mechanism of Parkin upstream of mitophagy. These studies reveal an intricate relationship between the early-onset PD-related proteins, which has been suggested to reflect parallel mitochondrial salvage pathways (Thomas et al., 2011).

iii) The role of DJ-1 in the regulation of peripheral metabolism

In mouse pancreatic β-cells, DJ-1 protects against an age-related increase in ROS production and preserves normal mitochondrial function, which is required for insulin secretion (Jain et al., 2012). The loss of DJ-1 results in an age- and weight-dependent glucose intolerance, which correlates with the loss of β-cells and suggests a role for DJ-1 in peripheral glucose regulation.

In another study the loss of DJ-1 was found beneficial in a rodent model of obesity. When kept on a high-fat diet (HFD), DJ-1-deficient mice had reduced weight gain compared to their wild type littermates and were protected from the HFD-associated increase in pro-inflammatory cytokines (Kim et al., 2014). The authors suggested a role for DJ-1 in the proliferation of adipocytes, thereby contributing to adipocyte-derived pro-inflammatory signalling.

iv) DJ-1, reactive intermediates and the redox state

The implication of DJ-1 in the oxidative stress response was among one of the first findings due to its isoelectric shift after oxidative stress (Mitsumoto and Nakagawa, 2001; Mitsumoto et al., 2001). DJ-1 expression levels are enhanced upon H_2O_2 administration (Taira et al., 2004b). To date several mechanisms have been described for the role of DJ-1 in regulation of the cellular redox state. Initial studies found that DJ-1 can directly react with and reduce H_2O_2 in vitro and protect cells from oxidative damage in cell culture (Taira et al., 2004b). These results were confirmed in DJ-1-deficient mouse neurons (Andres-Mateos et al., 2007). The authors came to the conclusion that DJ-1 is an atypical ROS scavenger, since no effect of thioredoxin or glutathione on DJ-1 oxidation state was found. Other studies have suggested a role for oxidation as a modulator of DJ-1 activity rather than direct ROS scavenging (Canet-Aviles et al., 2004). This view was encouraged after the identification of other redox-dependent activities of DJ-1 (Ishikawa et al., 2009; Moscovitz et al., 2015; Shendelman et al., 2004).

Interestingly, DJ-1 could not only protect cells from reactive oxygen species but also from reactive glyoxal species (Lee et al., 2012). Glyoxals are reactive intermediates that contain two adjacent carbonyl groups, which render the α-carbon susceptible to spontaneous reactions with electrophiles, such as the amine groups of the protein side chain lysine or cytosine and guanine bases of the DNA. DJ-1 directly functions as glyoxalase that catalyses the hydration of glyoxal and methylglyoxal into glycolic and latic acid, respectively (Lee et al., 2012).

Further evidence for a protective role in the anti-oxidant response of the cell came from the identification of a stabilising effect of DJ-1 towards nuclear factor erythroid 2-related factor (Nrf2). Nrf2 is a transcriptional co-activator and master regulator of the expression of anti-oxidant proteins, such as thioredoxins, superoxide dismutases (SOD) and NAD(P)H quinone oxidoreductase1. DJ-1 binding to Nrf-2 inhibits the association with inhibitory Keap and

subsequent protein degradation of Nrf2 (Clements et al., 2006). In a similar manner DJ-1 seems to activate peroxisome proliferator-activated receptor-gamma co-activator 1α (PGC-1α) via inactivation of pyrimidine tract-binding protein-associated splicing factor (PSF), a repressor of PGC-1α (Zhong and Xu, 2008). PGC-1α is a transcriptional co-activator that induces the expression of most nuclear genes required for mitochondrial biogenesis and further activates expression of Nrf1 and Nrf2 thereby regulating the redox homeostasis of the cell (Scarpulla et al., 2012).

The activity of DJ-1 on transcriptional regulation is not limited to Nrf-2 and PGC-1α. A positive indirect (Vasseur et al., 2009), as well as direct (Parsanejad et al., 2014) effect of DJ-1 on hypoxia-inducible factor (HIF) 1α was proposed to be important for the cellular adaptation to hypoxia. HIF1α is constitutively degraded in the cytoplasm under normal conditions but becomes stabilised during hypoxia and upon oxidative stress. HIF1α then translocates into the nucleus, where it forms a complex with HIF1β/ARNT to initiate transcription of genes that regulate oxygen levels and glycolysis (Bardos and Ashcroft, 2005). The regulation of HIF1α and PGC-1α by DJ-1 are among the first studies that suggested a role for DJ-1 in energy metabolism (Parsanejad et al., 2014; Vasseur et al., 2009; Zhong and Xu, 2008).

v) Metabolism and DJ-1 in PD

The cellular redox homeostasis has an intimate relation with the metabolic activity of the cell. For example, the redox equivalents NADH and NADPH are essential substrates for OXPHOS and the anti-oxidant system, respectively and both can be converted into one another at the level of mitochondria (Metallo et al., 2012; Siebert et al., 1957). Furthermore, certain metabolic pathways are crucial for the generation of anti-oxidative molecules. The conversion of glucose-6-phosphate from glycolysis into the pentose phosphate pathway (PPP) creates the main pool of cytosolic NADPH (Berg et al., 2015) and production of serine from 3-phosphoglycerate is required for glutathione synthesis (Meiser et al., 2016). These pathways lead to a decrease in cytosolic production of NADH and pyruvate, which are the

main substrates for the TCA cycle and OXPHOS. Recently a role for DJ-1 in metabolic regulation of the redox balance was demonstrated by stable isotope assisted metabolic profiling of a DJ-1 deficient neuronal cell line. These experiments revealed reduced glutamine uptake and utilisation by the TCA cycle, as well as reduced serine production in DJ-1 knockdown cells (Meiser et al., 2016). Furthermore, expression levels of several key enzymes of NADPH generating pathways were reduced in DJ-1-deficient cells. Serine-derived glycine and cysteine as well as glutamine-derived glutamate are the essential amino acids for glutathione synthesis, which together with reduced NADPH production led to anti-oxidant deficiency in these cells (Meiser et al., 2016). Importantly, enhanced oxidative stress has been implicated in the pathogenesis of PD.

Another putative role for impaired metabolism in PD came from the finding that cytosolic acidification, usually associated with metabolic adaptation during mitochondrial inefficiency, facilitated accumulation of mitochondrial α-synuclein (Cole et al., 2008). Furthermore, mitochondria where shown to be essential mediators of α-synuclein toxicity in yeast (Buttner et al., 2008). In mammals, mitochondrial α-synuclein has various sinister effects. Accumulation of α-synuclein at the OMM results in blockage of protein import via occlusion of the Tom20 receptor (Di Maio et al., 2016), whereas internalised accumulated α-synuclein was shown to inhibit complex I activity both in human primary dopaminergic cells and in post-mortem brain of PD patients (Devi et al., 2008). Interestingly, DJ-1 is protective against α-synuclein toxicity by reducing its aggregation capacity (Batelli et al., 2015; Shendelman et al., 2004). These findings indicate a complex relation between metabolic deregulation, protein aggregation and mitochondrial dysfunction, which might contribute to the vulnerability of neurons at risk of Parkinson's disease.

In line with this, several studies suggested an effect of DJ-1 on the energy metabolism of the cell. Translocation of wildtype DJ-1, but not PD-associated mutant forms, into the mitochondrial matrix was associated with enhanced ATP production through oxidative

phosphorylation (Cali et al., 2015). In muscle cells, DJ-1 deficiency was associated with ROS-dependent mitochondrial uncoupling and metabolic reprogramming via upregulation of AMP-activated protein kinase. The authors concluded that DJ-1 was involved in efficient substrate utilisation and metabolic adaptation (Shi et al., 2015). Interestingly, DJ-1 was shown to interact with Bcl-x_L and prevent the degradation of the latter after UV irradiation (Ren et al., 2011). Knock down of DJ-1 increased sensitivity to apoptosis in this scenario, consistent with the anti-apoptotic function of Bcl-x_L. However, Bcl-x_L has another direct effect on energy metabolism through regulation of the efficiency of the F_1F_O ATP synthase (Alavian et al., 2011). The mitochondrial ATP generating enzyme was found to harbour a non-productive, $\Delta\Psi_m$-depleting proton leak in the inner mitochondrial membrane, which was inhibited by Bcl-x_L. By closing this leak, Bcl-x_L increased neuronal ATP production by ATP synthase without affecting the electron flux through the ETC. Taken together, these studies provide another line of evidence for a role of DJ-1 in substrate metabolism, and more precisely energy metabolism of the cell.

In summary, recent studies suggest a role of DJ-1 in cell metabolism via transcriptional regulation of mitochondrial biogenesis, regulation of mitochondrial turnover, as well as the regulation of metabolic enzymes and key metabolic pathways, possibly mediated by oxidative protein modifications.

1.5 Hypothesis and aims

Despite the wealth of knowledge with respect to the function of DJ-1, very little is known regarding the regulation of this protein. It is clear, however, that subcellular localisation (Junn et al., 2009), dimer formation (Maita et al., 2013), and oxidative modification (Canet-Aviles et al., 2004; Ishikawa et al., 2009; Ren et al., 2011) have an effect on the function of DJ-1. Hence, studying the molecular mechanisms that regulate DJ-1 may help to understand the activity of this protein during normal cell physiology as well as in PD-associated cell demise.

1.5.1 DJ-1 preliminary screen for novel interaction partners

In order to identify novel binding partners implicated in the regulation of DJ-1, our group used liquid-chromatography assisted mass spectrometry to screen for proteins that co-immunoprecipitate with overexpressed Flag-tagged DJ-1 in HEK293T cells. We discovered 14-3-3β as a putative interaction partner (unpublished data). This interaction was further supported by the identification of DJ-1 in a screen for new phosphoprotein binding partners of 14-3-3s in an earlier study (Pozuelo Rubio et al., 2004). The fact that 14-3-3β was absent in the immunoprecipitate of the PD-associated mutant DJ-1^{L166P} suggested that the interaction is specific to the wildtype and might have functional implications for PD. Interestingly, 14-3-3 proteins have been found to bind to and modulate the activity of at least three of the well-characterised PD proteins, α-synuclein (Plotegher et al., 2014), LRRK2 (Nichols et al., 2010) and Parkin (Sato et al., 2006). 14-3-3 proteins are versatile signal regulators affecting, among others, metabolism and apoptosis (Kleppe et al., 2011). Binding of 14-3-3 to phosphorylated proteins can alter the activity, affinity or subcellular localisation of its target (Obsil and Obsilova, 2011). Of note, the binding of 14-3-3 proteins to their substrates is highly dynamic and changes in response to metabolic alteration (Weerasekara et al., 2014), a pre-requisite for a regulator of metabolic adaptation. Taken together, 14-3-3β provides an ideal candidate for a putative regulator of DJ-1 activity.

1.5.2 Hypothesis

14-3-3β and DJ-1 physically and functionally interact in a phosphorylation-dependent manner, which is regulated by the metabolic state of the cell. We hypothesise that 14-3-3β effects the localisation and/or activity of DJ-1 and disruption of the interaction results in altered energy metabolism.

1.5.3 Aims

Aim 1

To verify the interaction between DJ-1 and 14-3-3β. Immunoprecipitation (IP) of DJ-1 from cell lines and rodent brain will be performed and 14-3-3β specific antibodies will be used to detect 14-3-3β co-immunoprecipitate. The effect of metabolic alterations such as serum, glucose and oxygen concentrations on the complex formation will be tested. The dependence of complex formation on phosphorylation will be tested first by applying phosphatase treatment prior to the IP. In addition, putative phosphorylation and 14-3-3 binding sites in DJ-1 will be determined using the freeware ScanSite3. Several putative phosphorylation sites will be mutated in the DJ-1 overexpression plasmid to be tested in cells for their ability to bind 14-3-3β.

Aim 2

To test the effect of 14-3-3β on DJ-1 protein level and subcellular localisation. 14-3-3 knockdown and overexpressing cell lines will be submitted to subcellular fractionation experiments. The levels of DJ-1 protein will be determined both in total lysates and in the subcellular fractions using western blot analysis.

Aim 3

To determine the effect of 14-3-3β and DJ-1 on cellular metabolism. The proteins will be targeted with shRNA-mediated knockdown. Metabolic experiments will be performed on the knock down cells, including the quantification of cellular ATP levels, mitochondrial membrane

potential and lactate secretion. The assessment of cell proliferation and viability will further complete the functional studies.

2 Material and Methods

2.1 Tissue culture

2.1.1 General considerations

All cell culture experiments were performed in a designated cell culture laboratory equipped with vertical laminar flow cabinets (ScanLaf Mars, LaboGene, Lynge, Denmark), cell culture incubator (Galaxy 170S, New Brunswick, Eppendorf, Hamburg, Germany), a bright field cell-culture microscope (Leica DMIL) and a water bath (Grant W28). Cabinets were surface-cleaned with 70% ethanol before and after use and deep cleaned monthly. The incubator maintained a temperature of 37ºC and a CO_2 concentration of 5%. A water bath supplied with autoclaved, deionised H_2O at the bottom of the incubator provided a humidified atmosphere. The water tray was cleaned and re-filled regularly. The incubator was calibrated at the beginning of the research that is presented in this thesis. All cell culture media and supplements were purchased from Sigma Aldrich (Sigma Aldrich Co Ltd, Dorset, UK), if not mentioned otherwise. Cell culture dishes and plates were purchased from Corning (Corning, US). Cells in culture were handled under aseptic conditions at all times and only came in contact with sterile lab ware. All media, Dulbecco's phosphate buffered saline (DPBS), and trypsin protease were pre-warmed to 37ºC in a water bath before use and otherwise stored at 4ºC in a designated cell culture shelf. Cell dilutions and culture duration were chosen to avoid acidification of the medium during the period of each cell culture cycle. Table 2.1 contains the approximate growth area and the amount of medium used for each cell culture vessel.

Table 2.1 – Cell culture vessels. Approximate growth area and amount of medium used for the different cell culture vessels in this study.

Vessel	Growth area	V (medium)
150 mm round dish	152 cm^2	20 ml
100 mm round dish	55 cm^2	10 ml
6-well plate	9.5 cm^2	2 ml
12-well plate	3.8 cm^2	1 ml
24-well plate	1.9 cm^2	0.5 ml
96-well plate	0.32 cm^2	0.1 ml

2.1.2 Coating of coverslips and culture dishes

Where indicated cells were grown on poly-D-lysine (PDL) to provide better adherence. 13 mm round coverslips No.1 (VWR International Ltd, Lutterworth, UK) were washed in 70% nitric acid (Sigma Aldrich) for one day with gentle swirling from time to time. The coverslips were washed 4 to 5 times with H_2O and sterilised in 70% ethanol. Then they were placed into 24-well plates and irradiated with UV light for a minimum of 20 min. PDL was diluted in borate buffer (see 2.8 Material) to the desired concentration and 400 µl were added to each well. The coverslips were incubated over night at room temperature and washed 3 times the next day with sterile DPBS. The coverslips were kept in DPBS until plating. If plates were to be coated, PDL was added without pre-treatment and volume was adjusted to cover the surface of the plate.

2.1.3 Culture maintenance

i) Culture conditions

HEK293T cells were a kind gift from Dr Amin Hajitou from Imperial College London. The cells were maintained in sterile, cell-culture treated 100 mm or 150 mm round dishes in DMEM-AQ medium containing 4.5 g/l glucose (25 mM), 2 mM alanyl-glutamine dipeptide and supplemented with 10% fetal bovine serum (FBS), 100 U/l penicillin and 100 µg/ml streptomycin (hereafter referred to as complete DMEM). HEK293T cells were routinely sub-cultured every 3 days by diluting the trypsinised cells 1:12 in fresh complete DMEM. For some experiments glucose was substituted with galactose. For these experiments DMEM without glucose (Gibco, # 11966-025) was used and supplemented with either glucose or galactose at 25 mM.

ii) Sub-culturing

For sub-culturing the cells were washed once with 5 ml or 10 ml DPBS per 100 mm dish or 150 mm dish, respectively and incubated with 500 µl or 2 ml of 0.05% Trypsin containing 0.02% ethylene diamine tetra acetic acid (EDTA) per 100 mm or 150 mm dish, respectively.

The cells were incubated for 2 min at 37ºC before fresh complete medium was added up to the original volume. Cells were further diluted in fresh complete medium for maintenance or centrifuged for 4 min at 400 relative centrifugal force (rcf) for cell seeding. The supernatant was aspirated and the cell pellet was resuspended to the original volume in complete medium.

iii) Counting cells

The cell numbers were determined using a Neubauer chamber (Marienfeld, Lauda-Königshofen, Germany). To distinguish viable from non-viable cells, the trypan blue dye exclusion method was used. An aliquot of 10 to 15 µl of a single cell suspension prepared as above was diluted 1:2 with trypan blue (Sigma Aldrich) and 10 µl were placed into the Neubauer chamber. The cell numbers from two big squares of the Neubauer grid (each containing a volume of 0.1 µl) were counted and averaged. The cell density of the single cell suspension was calculated as follows:

$$c = n(s) * \frac{D}{V(s)}$$

c – cell concentration; n(s) – cells/square; D – dilution factor; V(s) – volume/square

The cell dilutions were adjusted to the desired concentration using the following equation:

$$V = c(f) * \frac{V(f)}{c}$$

V – volume cells; c – concentration of cells; c(f) – final concentration; V(f) – final volume

iv) Cryopreservation and reviving of cell lines

Cell stocks were obtained from the first passages that were grown in our laboratory. These were as early as passage 23 for HEK293T cells and passage 8 for N27 cells. For stable cell lines the first confluent 150 mm round cell culture dish after the clonal expansion (see below) was cryopreserved as passage 1. 2 ml cryopreservation vials (Fisher Scientific, Loughborough, UK) with screw caps were filled with 100 µl dimethyl sulfoxide (DMSO)(Sigma Aldrich). The cells for cryopreservation were grown to confluence in a 100 mm and 150 mm round cell culture dish yielding typically 3 and 10 stock vials, respectively. The cells were trypsinised and pelleted as described under section 2.1.2(ii). The pellet was

resuspended in fresh, chilled freezing medium (DMEM for HEK293T and RPMI-1640 for N27) supplemented with 30% FBS. 900 µl cell suspension was added per vial and pipetted once. The cells were placed quickly into an isopropanol-based freezing container (Thermo Fisher Scientific, Waltham, MA, USA), frozen down over night at -80ºC and transferred for long-term storage in a liquid nitrogen tank.

To revive frozen stocks, cells were thawed quickly in a 37ºC water bath and immediately placed into a 15 ml conical tube containing 10 ml pre-warmed complete medium. The cells were spun at 400 rcf for 4 min at room temperature and supernatant was aspirated. The cells were resuspended in 10 ml complete medium and placed into a 10 cm dish. Cells usually started to proliferate within 12 h.

2.1.4 Genetic manipulation of cell lines

i) $CaPO_4$ transfection

HEK293T or HEK293 cells were seeded at $2.3x10^4$ cells/cm^2 two days prior to transfection or at $4.6x10^4$ cells/cm^2 one day prior to transfection. On the day of transfection the cells would typically achieve a confluence of approximately 50%. For transfection a fresh aliquot of 2xHBS (see 2.8 Material) was thawed slowly. All reagents were allowed to achieve room temperature. The amount of reagents that were used for each format is listed in table 2.2 . Separate tubes were prepared to contain either 2xHBS or the DNA diluted in sterile H_2O. Sterile 2M $CaCl_2$ (see 2.8 Material) was added slowly to the DNA and pipetted twice to mix. After one minute the DNA/$CaCl_2$ solution was added very slowly to the 2xHBS. The mix was incubated for one to five minutes at room temperature for DNA precipitation. The transfection mix was added dropwise to the cells covering the entire culture vessel. The cells were placed into the cell culture incubator for 12 to 16 h and the medium was replaced with fresh complete DMEM. Transfected cells were left to recover for 2 days prior to the experiment.

Table 2.2 – $CaPO_4$ transfection. Quantities of transfection reagents required for $CaPO_4$ transfection depending on the size of the cell culture vessel

Reagent	24-well plate*	6-well plate*	100 mm dish	150 mm dish
DNA	0.5 µg	2.5 µg	14 µg	40 µg
H_2O	ad 18.8 µl **	ad 94 µl **	ad 0.5 ml **	ad 1.5 ml **
$CaCl_2$	2.3 µl	11.5	61 µl	183 µl
2xHBS	18.8 µl	94 µl	0.5 ml	1.5 ml
Total volume	37.6 µl	188 µl	1.0 ml	3.0 ml

* All quantities are given per well, ** including DNA and $CaCl_2$.

ii) Plasmids

The plasmids that were used in this study are listed in table 2.3.

Table 2.3 – DNA plasmids.

ID	plasmid	Company	Type	Insert	Promoter	Information
1	pCMV6-Entry	Origene	OE	-	CMV	G418 resistance
2	pCMV6-DJ1	Origene	OE	Human DJ-1 myc-flag tag (C-term)	CMV	Derived from #1 G418 resistance
3	pcDNA3.1	Thermo Scientific	OE	-	CMV	G418 resistance
4	pcDNA3-flag-HA-h1433b	William Sellers (Addgene #8999)	OE	Human 14-3-3β flag-HA tag (N-term)	CMV	G418 resistance
5	pGIPZ-hScr	Thermo Scientific	LV KD	non-targeting shRNA	CMV	Puromycin
6	pGIPZ-shRNA hDJ-1	Thermo Scientific	LV KD	shRNA against human DJ-1	CMV	Puromycin
7	pGIPZ-shRNA hYWHAB	Thermo Scientific	LV KD	shRNA against human 14-3-3β	CMV	Puromycin
8	pCMV6-DJ1-T125A	Derived from plasmid 2	OE	Human DJ1-T125A myc-flag tag (C-term)	CMV	Generated by mutagenesis
9	pCMV6-DJ1-T125D	Derived from plasmid 2	OE	Human DJ1-T125D myc-flag tag (C-term)	CMV	Generated by mutagenesis
10	pCMV6-DJ1-S161A	Derived from plasmid 2	OE	Human DJ1-S161A myc-flag tag (C-term)	CMV	Generated by mutagenesis
11	pCMV6-DJ1-S161D	Derived from plasmid 2	OE	Human DJ1-S161D myc-flag tag (C-term)	CMV	Generated by mutagenesis

* OE - overexpression; KD - knockdown; LV - lentiviral; YWHAB is the gene ID for 14-3-3β.

2.1.5 Production of stable cell lines

Several stable overexpression and knockdown cell lines for the proteins DJ-1 and 14-3-3β where produced during the course of this project. We took this decision because the transient transfection method resulted in low and variable knockdown efficiencies and inconsistent results; meanwhile more drastic transfection conditions were incompatible with cell viability.

i) Selection with puromycin – stable knockdown cell lines

The pGIPZ knockdown plasmids carry shRNA sequences either directed against human DJ-1, human YWHAB (the gene ID of 14-3-3β), or non-targeting shRNA (see table 2.3, plasmid ID 5-7). The pGIPZ plasmid carries a resistance gene for the antibiotic puromycin. In order to determine the appropriate concentration of puromycin (Sigma Aldrich) a dose response was performed in naïv HEK293T. Cells were seeded in a 24-well plate at $1x10^4$ cells/cm^2. On the next day the cells were treated with puromycin concentrations from 0.1 to 1.5 µg/ml with medium change every two days. 0.8 µg/ml puromycin was effective at killing all cells within one week (determined by observation).

ii) Selection with G418 – stable overexpression cell lines

Stable overexpression cell lines were generated carrying either the pcDNA3.1 backbone or pcDNA3-flag-HA-h1433b plasmid (Table 2.3, plasmid ID 3 and 4). The plasmids carry the neomycin resistance gene that targets the mammalian ribosome inhibitor G418. Importantly, HEK293T cells cannot be selected with G418 because they already carry a transgene coding for the large T-antigen as well as the neomycin resistance gene. We therefore used the alternative HEK293 cells (kindly provided by Dr Amin Hajitou) for the generation of stable overexpression cell lines. HEK293 cells were maintained as described for HEK293T in section 2.1.2. The effective dose for G418 (Sigma Aldrich) for HEK293 cells was determined as described in the section above for puromycin using a range from 100 µg/ml to 600 µg/ml. 300 µg/ml G418 was the lowest effective dose killing all HEK293 cells within one week.

iii) Transfection and selection of stably transfected cells

HEK293T or HEK293 cells were seeded in 6-well plates and transfected according to 2.1.4 using the knockdown or overexpression plasmids mentioned above. Two days after transfection the cells were subcultured in a 1:10 dilution into a fresh 6-well plate and allowed to proliferate. Two days after subculturing the medium was changed and replaced with complete DMEM containing 0.8 µg/ml puromycin (hereafter referred as complete DMEM/puro) or complete DMEM containing 300 µg/ml G418 (hereafter referred as complete DMEM/G418). The cells were further maintained in the presence of antibiotic for three weeks with medium changes every 2 to 3 days to allow efficient selection of stable clones. A mock-transfected sample was treated simultaneously to monitor efficient selection. The cells were subcultures upon confluence or formation of large cell clusters.

iv) Single clone isolation and expansion

After three weeks of selection each heterogenous cell line was trypsinised, the cells were diluted to a concentration of 5 cells/ml and seeded into 96-well plates at 100 µl per well. The next day each well was screened for the presence of single cells. Those wells that contained a single cell were marked and the proliferation of these cells was monitored. Several clones formed proliferative colonies. The clonal cell lines were amplified over the next two to three weeks. The first confluent 150 mm dish was used for cryopreservation and designated with passage 1 of the new clonal cell line.

v) Verification of knock down and overexpression

The knock down or overexpression of the gene of interest was examined by Western blotting (WB, see section 2.6 Biochemistry). Four to six proliferative clones per construct were tested for knockdown efficiency or expression of the transgene (see 4.2 Results). When the clonal cell line was large enough to yield a confluent 100 mm dish the cells were trypsinised and the resuspended cells were divided. 3 quarter of the cells were further propagated, whereas one quarter was used for WB analysis. The cells for WB analysis were pelleted at 600 rcf for 5 min at 4ºC, washed once with cold PBS and spun again. The pellet was lysed with cold TBS

lysis buffer (see 2.8 Material) for 30 min on ice and vortexed occasionally. The lysate was cleared at 1000 rcf for 5 min at 4ºC and stored at -80ºC until protein quantification and WB was performed.

2.2 Interaction studies

2.2.1 Co-immunoprecepitation (IP) from HEK293T cells

i) Transfection and co-IP

HEK293T cells were seeded on 150 mm round dishes and transfected 2 days post-seeding with either pCMV6-Entry plasmid or pCMV6-hDJ1 plasmid. The latter expresses human DJ-1 C-terminally tagged with the myc and flag epitopes. Transfection was performed as described in 2.1.3(i). Two days after transfection the cells were either directly harvested or treated as described in 2.2.1(iii).

For cell lysis, cell culture medium was removed and the culture dish was placed on ice. Cells were scraped in 2 ml ice-cold IP lysis buffer (see section 2.8), placed in a conical tube and rotated for 2h at 4ºC. The samples were cleared from cell debris by centrifugation for 5 min at 1000 rcf and 4ºC. Approximately 2 ml of the supernatant was recovered and placed into a fresh conical tube. Typical protein concentration was 3 to 4 mg/ml.

Per 2 ml-lysate from a 150 mm dish 50 µl slurry EZView anti-Flag beads (Sigma Aldrich) were equilibrated by washing 3 times with 0.5 to 1.0 ml cold TBS and centrifuged at 2000xg for 2 min. Equilibrated beads were added to cleared lysate and incubated over night at 4ºC rotating. Lysate and beads were spun at 1000xg for 2 min at 4ºC and supernatant was discarded. The bead pellets were washed with 0.5 to 1.0 ml ice-cold TBS three times briefly on ice and twice for 30 min at 4ºC in a rotating wheel. The beads were spun as above after each wash and supernatant was discarded. After the last wash supernatant was carefully removed until no more liquid remained above the pellet. The proteins bound to the beads were eluted in 50 µl of 300 µg/ml 3xFlag peptide (Sigma Aldrich) for 1 h at 4ºC under rotation

followed by centrifugation at 10000xg for 5 min at 4ºC and the supernatant was recovered. The centrifugation was repeated with the supernatant to ensure that no beads remained. The final supernatant was placed in a 1.5 ml tube and stored at -80ºC until analysis.

For IP analysis, first the amount of precipitated DJ-1-myc-Flag was determined for each sample. 5 µl sample was diluted in 5 µl 2xLaemmli sample buffer (see Material – 2.8) and analysed by WB using anti-myc-HRP antibody (9B11, Cell Signalling, # 2040). After myc quantification all sample volumes were adjusted relative to the sample with the lowest myc quantity to obtain equal concentrations of immunoprecipitate. The samples were prepared for SDS-PAGE and WB according to section 2.6 using a total volume of 50 µl per well. DJ-1$^{myc-Flag}$ lysate was diluted 1:50 and 10 µl diluted lysate (0.6 to 0.8 µg protein) was loaded as input sample. After WB the membranes were first probed with anti-14-3-3β antibody (C-20, Santa Cruz, # sc-628) for detection of 14-3-3β co-immunoprecipitation and then with anti-myc-HRP for quantification of the immunoprecipitated myc-flag tagged DJ-1.

ii) Phosphatase treatment of HEK293T lysate

HEK293T cells lysates were prepared as described under (i) of this section using AP lysis buffer (see Materials – 2.8). After clearing by centrifuation the lysate was diluted 1:10 in AP lysis buffer and the diluted DJ-1-myc-flag lysate was divided into 10 ml samples. The samples were treated with or without 50 U of alkaline phosphatase (FastAP, Thermo Scientific) for 30 min at 37ºC in a water bath. The cells were placed back on ice and the IP was performed as above using 50 µl slurry EZView anti-flag beads per 10 ml treated lysate.

iii) Interaction screen

HEK293T cells were seeded and transfected as described in 2.2.1(i). 2 days post-transfection the medium was changed and the cells were treated as follows.

EGF: Cells were incubated in complete DMEM for 24h. 1h prior to harvesting cells were treated with 1 µg/ml epidermal growth factor.

Serum deprivation: Cells were incubated in DMEM containing 1% FBS for 24 h.

Glucose substitution: Cells were incubated in glucose-free DMEM containing 10% FBS and 25 mM galactose for 24 h.

Hypoxia: Cells were incubated in complete DMEM at 1% O_2 for 24 h.

γ-irradiation: Cells were incubated in complete DMEM for 24 h. 1 h prior to harvesting cells were treated with 10 Gy in an biological irradiator

H_2O_2: Cells were incubated in complete DMEM for 24 h. 1 h prior to harvesting cells were treated with 100 µM for 1h H_2O_2.

Ionomycin: Cells were incubated in complete DMEM for 24 h. 1 h prior to harvesting cells were treated with 20 µM ionomycin for 1 h.

Tunicamycin: Cells were incubated in complete DMEM for 24 h. 1 h prior to harvesting cells were treated with 1 µM tunicamycin for 1 h;

Oligomycin: Cells were incubated in complete DMEM for 24 h. 1 h prior to harvesting cells were treated with 1 µM oligomycin for 1 h.

Cyclosporin A: Cells were incubated in complete DMEM for 24 h. 1 h prior to harvesting cells were treated with 2 µM cyclosporine A for 1 h.

2.2.2 co-immunoprecipitation (IP) from rat brain lysate

A female Sprague-Dawley rat was euthanized according to the regulations of the Central Biological Service at Imperial College London. The skull was opened and the whole brain was removed quickly using a spatula. The brain was rinsed twice in PBS and placed into a clean petri dish on ice containing ice-cold RIPA lysis buffer (see section 2.8). The tissue was minced with clean scissors and transferred into a chilled 10 ml glass homogeniser fitted tightly to a Teflon pestle. The tissue was homogenised on ice with 40 strokes in 10 ml RIPA lysis buffer, whereby the pestle was rotated electrically at 500 rounds per minute (rpm). The lysate was incubated for 3 h at 4ºC under agitation and spun at 1000 rcf for 5 min at 4ºC. The supernatant was diluted 1:20 in RIPA buffer containing PPI, mixed thoroughly and spun as above. The final concentration of the lysate was approximately 1 mg/ml.

20 µl slurry agarose beads coupled to protein A/G (Santa Cruz) were used per reaction. Beads were pre-blocked and directly added to 900 µl of cleared rat brain lysate per reaction. 2 µg per reaction of antibody against DJ-1 (FL-189) (rabbit polyclonal, Santa Cruz, sc-32874) or unspecific rabbit IgG (rabbit polyclonal, Santa Cruz, sc 66931) were added to the reaction tubes followed by an over night incubation at 4ºC in a rotating wheel. The beads were pelleted at 1000 rcf for 2 min at 4ºC and washed 3 times briefly and once for 30 min with 1 ml PBS. After the last wash the supernatant was removed carefully until no more liquid remained above the pellet. The proteins were eluted in 40 µl 2xLaemmli sample buffer by boiling the samples for 10 min at 95ºC. Finally, the samples were spun at 10000 rfc for 5 min at room temperature and the supernatant was recovered and placed into a new 1.5 ml tube. The supernatant was stored at -80ºC. For analysis 25 µl of the eluted samples were loaded and analysed by SDS-PAGE and WB as described in section 2.6. 14-3-3β co-precipitate was identified with 14-3-3β (J2E9) mouse monoclonal antibody and DJ-1 precipitate was identified with DJ-1 (D-4) mouse monoclonal antibody.

2.3 Subcellular fractionation of stable cell lines

Stable HEK293T (knockdown cell lines) or stable HEK293 (overexpression cell lines) cells were seeded at $2.3x10^4$ or $3.3x10^4$ cells/cm^2, respectively into 150 mm dishes 3 days prior to the subcellular fractionation. 24h before fractionation the medium was changed and the cells were either kept in the cell culture incubator (Normoxia) or subjected to hypoxic conditions (1% O_2, 5% CO_2, 94% N_2, 75% humidity). The hypoxic environment was established by a Don Whitley hypoxia workstation (Don Whitley Scientific, Shipley, UK). Due to instrumental limitations the humidity inside the workstation did not exceed 75%.

For fractionation the cells were scraped on ice and placed into a 50 ml conical tube. The dish was rinsed with 5 ml ice-cold PBS and the wash was pooled with the scraped cells. All samples and buffers were kept on ice. The cells were spun at 600xg for 5 min at 4ºC in a

swing-out rotor. Supernatant was then removed and the cells were washed once with PBS and spun as above. Next, the cells were resuspended in 2 ml mannitol isolation buffer (see 2.8 Material) and homogenised in a Teflon Dounce homogeniser with 50 strokes at 520 rpm. Subcellular fractionation was carried out by sequential centrifugation in mannitol isolation buffer as depicted in figure 2.1. The homogenised cells (H) were spun at 600xg for 5 min at 4ºC yielding the supernatant S1.1 (mitochondria and cytosol) and the pellet P1.1. The pellet P1.1 was resuspended in 10 ml mannitol isolation buffer and homogenised (only 20 strokes) and spun as above to yield the pellet P1.2 (nuclear fraction), as well as supernatant S1.2 (more mitochondria, very little cytosol). S1.1 and S1.2 were treated the same but kept separate to isolate the more concentrated cytosol from S1.1. Both, S1.1 and S1.2 were spun at 1000xg for 10 min at 4ºC. The pellets were discarded and the supernatants S2.1 and S2.2 were centrifuged at 10000xg for 15 min at 4ºC. The supernatant derived from S2.1 was referred as S3 (cytosolic fraction). The supernatant of S2.2 was discarded. The pellets of both S2.1 and S2.2 were pooled and referred to as P3 (mitochondrial fraction). P3 was washed 3x with 1 ml isolation buffer and spun as above. The weight of the mitochondrial pellet was measured. P1.2 was washed twice with 5 ml isolation buffer and once with 1 ml isolation buffer and spun at 600xg for 10 min at 4ºC. The weight of the final nuclear pellet was measured. Homogenate, cytosol, mitochondria, and nuclei were either lysed directly or frozen at -80ºC. For lysis of the homogenate 10% Triton-X100 stock (see 2.8 Material) was added to a final concentration of 1%. The mitochondrial and nuclear pellets were lysed in 5x volume/weight (mitochondria) and 10xvolume/weight (nuclei) of mitochondrial lysis buffer (see 2.8 Material). All samples were thoroughly resuspended and incubated for 30 min on ice. Mitochondria and homogenates were vortexed occasionally. The nuclear fraction was turned up-side down occasionally but not vortexed to avoid clumping of DNA. All samples were sonicated for 30 sec in a water bath and then centrifuged for 5 min and 1000 rcf at 4ºC. The supernatants were transferred into a new 1.5 ml tube and stored at -80ºC.

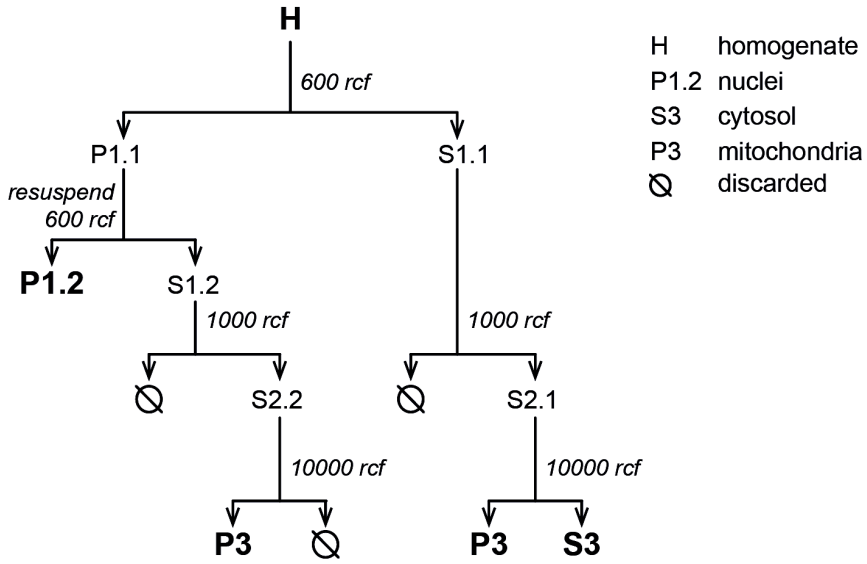


Figure 2.1 – Cell fractionation. Schematic of sequential centrifugation protocol for the isolation of subcellular fractions from HEK cells

2.4 Functional assays

i) Live cell imaging of mitochondrial potential

Stable knockdown HEK293T cells were seeded on 0.1mg/ml PDL-coated 13 mm round coverslips (see section 2.1.1) in 24-well plates at a density of $3.2x10^5$ cells/cm^2 in complete DMEM/puro. 24h after seeding the cells were loaded with freshly prepared 10 nM tetramethylrhodamine ethyl ester (TMRE) (Sigma Aldrich) in complete medium. The final DMSO concentration in solution did not exceed 0.1%. The cells were incubated for 30 min in the cell culture incubator. The coverslip was quickly mounted into an open diamond bath imaging chamber (size RC-25, Warner Instruments, Hamden, US), which was sealed with high vacuum grease (Dow Corning, Midland, US). 1 ml pre-warmed (37ºC) extracellular solution (ECS, see 2.8 Material) containing freshly added 10 nM TMRE was quickly added to the cells through a side well of the chamber.

Cells were imaged immediately on a Leica TSC SP5 II confocal microscope for a maximum of 25 min. Acquisition was performed with a 63x oil immersion objective using the following

parameters for excitation and emission. The sample was excited using both an argon 514 nm laser beam and a 20 mW diode pumped solid state 561 nm laser beam both at 20% intensity. The argon laser power was set to 20% corresponding to 13 mW. The emission was detected between 570 and 610 nm at a line scan speed of 200 Hz. The image was acquired using the Leica LAS AF software at a resolution of 16-bit with a frame size of 1024x1024 pixels and a scan zoom of 2. The scanner smart gain was adjusted to detect at a sub-maximal intensity for TMRE and typically was between 600 and 700 V. After initial adjustment the gain was kept identical throughout an experimental session. The scanner offset was set to -0.1% and the pinhole size was 40.79 µm. All images were focused to approximately 5 µm above the base of the cell, which corresponds roughly to the centre of the cell. Images analysis was performed using the free software FIJI (Schindelin et al., 2012) with a customised automated image analysis macro (see supplementary).

ii) Luciferase assay for ATP determination

The whole cell ATP levels where measured using the luciferine-based luminescence assay ATPlite (Perkin Elmers, Waltham, Ma, USA) performed in 96-well format. For each condition the ATP levels were assessed at least in duplicate and ATP levels were normalised to protein levels, which were measured on a duplicate plate using the SRB assay (see part (v) of this section). The cells were seeded in a 96-well plate at $12.5x10^3$ cells/cm^2 in complete DMEM/puro. 24 h after seeding the medium was replaced with fresh complete DMEM/puro and the cells were treated for 48 h as indicated in the results.

The ATP assay was performed essentially according to the manufacturer's protocol with several amendments. The cell lysis buffer was diluted 1:3 in H_2O. The medium was removed carefully and the cells were lysed in 150 µl diluted lysis buffer for 5 min at room temperature in an orbital shaker at 200 rpm. Then 100 µl of the lysate or 100 µl of lysis buffer (for the ATP standard and background, 8 wells) was transferred into white 96-well plates (Corning). 10 µl H_2O or 10 µl ATP standard diluted in H_2O at concentrations of (in µM) 0.3125, 0.625, 1.25, 2.5, 5, 10 were added to separate wells containing lysis buffer. Then 35 µl substrate was

added to all wells and the plate was incubated for 5 min at room temperature at 200 rpm in an orbital shaker. The plate was incubated for another 10 min in the dark and the luminescence was read in a Promega GloMax® Multi+ plate reader (Promega, Southhampton, UK).

iii) AnnexinV-PI cell death assay for flow cytometer

The cell viability was assessed using the AnnexinV-PI (BioLegend, San Diego, US) co-staining of cells and single cell detection of the resulting fluorescence by flow cytometry on a FACSCalibur (BD Bioscience, Franklin Lakes, NJ, US). The flow cytometer is equipped with a 15 mW 488 nm argon laser coupled to detectors for three fluorescent parameters (FL1-3), and a 635 nm diode laser with an additional detector (FL4). The co-staining with AnnexinV-FITC and PI coupled to the simultaneous detection of both dyes determines between viable (double negative), early apoptotic (AnnexinV positive/PI negative), necrotic (PI positive, AnnexinV negative) and dead cells (double positive).

Stable HEK293T cells were seeded in triplicates in 12-well plates at $1.6x10^3$ cells/cm^2 in complete DMEM/puro. 24 h post-seeding the medium was replaced and the cells were treated as indicated in the results for 48 h. On the day of analysis the cells were trypsinised, the single cell suspension was kept on ice, spun at 400 rcf for 4 min at 4 ºC, washed once with cold PBS and spun as before. The staining was essentially performed as described in the manufacturer's protocol with minor amendments. The cell pellet was re-suspended in 1 ml cold cell staining buffer, spun as above and the supernatant was discarded. The cell pellet was re-suspended in 100 µl cold Annexin V binding buffer and transferred to a 5 ml round bottom polystyrene tube on ice. Sequentially 5 µl AnnexinV solution and 10 µl PI solution was added. The samples were briefly vortexed and incubated in the dark for 15 min at room temperature. After incubation, 400 µl cold AnnexinV binding buffer was added. The cells were placed on ice, covered to avoid light exposure and analysed immediately by flow cytometry. Before acquiring each sample was briefly vortexed. Flow rates were adjusted between 100 and 500 cells per second.

Acquisition was performed using the acquisition software CellQuest (BD Bioscience). Before the first run, the fluorescence settings were adjusted using unstained and single stained samples. Fluorescence intensities and channel compensation was then kept for all of the following experiments. For acquisition the total cell population was selected using the forward and side scatters and the FL3 and FL4 fluorescent intensities were detected and visualised as scatter plot. Analysis was performed using FlowJo software (FlowJo LLC, Ashland, OR, US). The population was plotted against the AnnexinV-FITC fluorescence (FL3 detector) and the PI (FL4 detector) fluorescence. The FL3-FL4 scatter plot was gated on the control cells to obtain individual populations representative of double negative, $FL3^{+}/FL4^{-}$, $FL3^{-}/FL4^{+}$ and double positive cells. The gate was applied to all other samples.

iv) Lactate dehydrogenase assay

Stable HEK293T knockdown cells were seeded in a 96-well plate at $12.5x10^{3}$ cells/cm^{2} in complete DMEM/puro (6 wells per condition). 24 h after seeding the medium was replaced with fresh complete DMEM/puro and the cells were treated for 48 h as indicated in the results section. For the lactate assay, 50 µl medium was removed carefully and transferred into a new 96-well plate on ice. The cells in the original plate were fixed by adding 25 µl of 15% TCA to perform protein quantification by SRB assay (see (v) of this section). The medium was spun at 1000 rcf for 5 min at 4ºC and the supernatant was recovered in a new 96-well plate on ice. In a second 96-well assay plate 150 µl glycine/hydrazine buffer (see 2.8 Material) is added to each well (1 well/sample, 8 wells for the standard and 1 well/condition for the blank). To the sample and blank wells 19 µl H_2O and 1 µl medium was added (corresponding to a 1:20 dilution of medium). For the standard, lactate (Sigma Aldrich) was diluted in H_2O to the following concentrations (mM): 0, 0.0625, 0.125, 0.25, 0.5, 1.0, 2.0, 4.0 and 20 µl of standard was added per well. 25 µl NAD^{+} (see 2.8 Material) was added to all wells including standard and blank. 1 µl LDH enzyme (type II from rabbit muscle, Sigma) was added to all wells except the blank wells. The samples were incubated for 1 h at room temperature in an orbital shaker at 200 rpm. The optical density at 340 nM was measured

using a Tekan Infinite 200 plate reader (Tecan Group Ltd, Männedorf, Switzerland). The conditions were optimised to obtain an OD below 1.

v) SRB proliferation assay

In order to assess cell proliferation, protein quantification was performed using the sulforhodamine B (SRB) (Sigma Aldrich) colorimetric assay in 96-well plates. The proliferation was followed over a period of 6 days. The cells were seeded at a density of $12.5x10^3$ cells/cm^2 in 100 µl complete medium in 96-well plates. 6 or 8 wells per cell line and condition were quantified. 24 h after seeding the first samples were fixed and used as seeding value for normalisation. On all other plates the medium was replaced with fresh complete medium and the cells were treated as indicated in the results chapter.

Prior to the SRB stain cells were fixed by adding 15% cold trichloroacetic acid (TCA) directly to each well to obtain a final concentration of TCA of 5%. The cells were incubated at 4ºC for a minimum of 2 h or over night to precipitate all protein. The plates were washed under slowly running tap water and dried at room temperature over night. After all conditions were collected the proteins were stained by adding 50 µl 0.4% SRB (see 2.8 Material) for 1 to 2 h at room temperature. Excess SRB was decanted and plates were washed 3 to 4 times with 1% acetic acid (Sigma Aldrich) until no more dye came off. The plates were dried over night at room temperature or for 2 h at 37ºC. For detection the SRB was dissolved in 100 µl 10 mM Tris (Sigma Aldrich), pH 10.5 for 30 min and absorbance was measured at 490 nM in a BioTek EL800 plate reader (BioTek Instruments Ltd, Swindon, UK).

For the proliferation assay it is essential that cells be seeded at equal densities. To correct for small seeding variations all values of day x after treatment $A_{490}(x)$ were normalised against the mean of A_{490} at the day 0 (seeding value) $A_{490}(0)$. The proliferation P on day x (P(x)) is displayed as percentage of normalised A_{490}.

$$P(x) = \frac{A490(x)}{A490(0)} * 100\%$$

The variation of $A_{490}(0)$ between different cell lines and experiments was typically less than 10%. Experiments with a variation above 10% were excluded.

2.5 Molecular biology

2.5.1 Propagation and purification of plasmid DNA

Plasmid preparation and purification was performed according to standard procedures. All plasmid were propagated in *Escherichia coli* strains Top10, Stbl3 or DH5α. Bacterial glycerol stocks for all plasmids were prepared and kept at -80ºC to be used for propagation and purification of plasmid DNA. Bacterial broth and labware that came in contact with the bacterial cultures or purified plasmids were sterile.

i) Preparation of LB-Agar plates

LB-Agar was prepared as described in Materials (see 2.8) and kept sterile. All LB-agar plates were prepared fresh on the same day or one day prior to use. The LB-agar was heated in a microwave at low power until it was completely liquid. The LB-agar was cooled down to approximately 50ºC with regular swirling. If kanamycin (Fisher Brand) or ampicillin (Fisher Brand) was used, antibiotic was added in a 1:1000 dilution (see 2.8 Material) to obtain a final concentration of 100 µg/ml. LB-agar was poured into 100 mm sterile petri dishes with a volume of 20 ml to 25 ml per dish and allowed to cool down. After polymerisation the plates were stored up side down at room temperature or at 4ºC in a dedicated refrigerator for next-day use.

ii) Preparation of $CaCl_2$ competent E.colis

5 µl of an *E.coli* stock was streaked on LB-agar and incubated over night at 37°C in a dedicated bacterial incubator. A single colony was used to inoculate 3 ml LB broth (see 2.8

Material). The pre-culture was grown over night at 37°C with vigorous shaking at 250 rpm. On the next morning 50 ml LB agar was inoculated with 1 ml of the pre-culture and grown at 37ºC with shaking at 250 rpm. The culture was grown until the optical density at 600 nm was approximately 0.4. The culture was cooled on ice and centrifuged for 10 min at 4°C and 4000 rcf. The supernatant was discarded and the pellet was resuspended in 10 ml ice-cold sterile 0.1 M $CaCl_2$ (see 2.8 Material). The bacteria were incubated for 3 to 4 h on ice and spun as before. The supernatant was discarded and the competent bacteria were resuspended in 2 ml ice-cold 0.1M $CaCl_2$ using wide pipette tips and mixed carefully with 500 µl sterile 50% glycerol (see 2.8 Material, Sigma Aldrich). The competent bacteria were aliquoted into pre-chilled 1.5 ml tubes at a volume of 100 µl per tube, snap-frozen in liquid nitrogen and stored at -80ºC.

iii) Bacterial transformation

For transformation of plasmid DNA into *E.coli* competent bacteria from -80ºC store (see part (ii) of this section) were thawed slowly on ice. One vial of competent bacteria was used per construct to be transformed plus one extra vial as negative control to test for efficient bacterial selection by the antibiotic-containing LB-agar. A maximum of 10 µl cold DNA (max 1/10 of bacterial volume) was added to 100 µl competent bacteria on ice. For the transformation of purified high quality plasmid DNA usually 1 µl (or 0.5 µg of DNA) was sufficient for good transformation results. The bacteria were incubated on ice for 30 min, placed into 42ºC water bath for 45 s and placed back on ice for 2 min. 500 µl pre-warmed LB broth was added and the bacteria were allowed to recover for 1 h at 37ºC shaking at 250 rpm. The bacteria were pelleted at 3000 rcf for 5 min and 500 µl of the supernatant was removed. The pellet was resuspended in the remaining supernatant and streaked out on LB-agar plates containing the corresponding antibiotic at a final concentration of 100 µg/ml. The plates were incubated at 37ºC in a dedicated bacterial incubator over night.

iv) Preparation of bacterial glycerol stock

Bacterial glycerol stocks were prepared from single colonies freshly grown on LB-agar plates over night at 37ºC. 3 to 5 ml LB broth was inoculated with a single colony and grown over night at 37ºC in a shaking incubator at 250 rpm. The pre-cultures were grown for no longer than 16 h for glycerol stock preparation. Cryogenic 2ml stock vials with screw cap were labelled with the plasmid name, the bacterial strain, the antibiotic resistance and the date of stock preparation. In a dedicated bacterial sterile cabinet 1 ml 50% sterile glycerol was added to a 2 ml cryogenic stock vial with screw cap. 1 ml of the freshly grown over night culture was added to the respective vial and mixed by pipetting. The glycerol stocks were frozen down at -20ºC over night and stored at -80ºC on the next day.

v) Plasmid propagation and purification

All plasmid DNA used for transfection was purified with the GenElute Plasmid Midi kit (Sigma Aldrich, # NA0200). Two days before plasmid purification a bacterial pre-culture of 5 ml LB broth including 100 µg/ml antibiotic was inoculated from the bacterial glycerol stock. The culture was grown over night at 37ºC in a shaking incubator at 250 rpm. 120 ml of LB broth containing 100 µg/ml antibiotic was inoculated with 1 ml pre-culture and grown at 37ºC in a shaking incubator at 250 rpm for 12 to 14 h. The bacteria were pelleted at 6000 rcf at 4ºC for 15 min. The supernatant was discarded and the pellet was resuspended in 6 ml RNase H containing resuspension buffer. 6 ml lysis buffer was added to the bacterial suspension and mixed by turning and swirling of the tube for several times during an incubation time of 5 min. The lysis was stopped by adding 6 ml cold neutralisation buffer and immediate mixing by turning and swirling of the tube until all of the liquid phase became clear and the proteinaceous phase formed a white precipitate. 4.5 ml of the binding buffer was added, mixed by turning the tube up side down and the whole content of the tube was immediately transferred into the filter syringe. The liquid phase and precipitate where allowed to separate for 5 min. 5 ml equilibration solution was added to the DNA column and spun for 2 min at 3000 rcf. The flow through was discarded and the filtered bacterial lysate was added to the column. The column was spun as above and the flow through was discarded. This step was

repeated until all lysate was loaded onto the column. The column was washed twice with 5 ml wash buffer 1 and once with wash buffer 2 containing ethanol (Sigma Aldrich). After the last wash step the column was spun once for 5 min at 3000 rcf to completely remove all traces of ethanol. The column was placed into a clean collection tube and the DNA was eluted with 1 ml elution buffer and spun at 2 min for 3000 rcf. The eluate was placed onto the column again and the elution was repeated by spinning at 3000 rcf for 5 min. The DNA was placed into a sterile 1.5 ml and stored at -20ºC. The DNA concentration was determined using a NanoDrop with the elution buffer as blank. DNA concentrations usually ranged from 400 to 700 ng/µl.

2.5.2 Plasmid generation

i) Site directed mutagenesis

Site specific mutations were introduced into the plasmid of DJ-1 using the QuikChange Lightning Site-Directed Mutagenesis Kit (Agilent Technologies LDA UK Ltd, Stockport, UK) according to the manufacturers protocol. The primers were directed against human DJ-1 coding sequence (NCBI Consensus CDS (CCDS) database, ID CCDS93.1) and purchased from Sigma Aldrich. Primer design was performed using the Agilent QuikChange primer design online tool (http://www.genomics.agilent.com/primerDesignProgram.jsp), optimised for the QuikChange Lightning polymerase chain reaction (PCR). The primer sequences are listed in table 2.4.

The mutagenesis is based on a two-step reaction and does not require agarose gel purification of the PCR or restriction products. First, the high fidelity Pfu polymerase amplifies both strands of the plasmid starting from the mutated primers. Thereby two complementary mutated single-strands of the plasmid are created. After hybridisation of the DNA strands the *Dpn I* restriction enzyme degrades the parental plasmids in a second step. The enzyme

recognises 5'-G^{m6}ATC-3' methylated and hemimethylated dsDNA sequences that are present in the *E.coli* derived parental DNA only.

Table 2.4 – Primers for DJ-1 functional mutations. The mutated codon is marked in green with the mutated base(s) in capital letter. The melting temperature T_m of each primer pair should be above 78ºC. Values are as provided by the agilent primer design tool and do account for mismatch relative to the parental DNA.

Mutation	Forward primer	Reverse primer	T_m
T125A	taggttttggaagtaaagttacaGcacaccctc ttgctaaag	atccaaaaccttcatttcaatgtcgtgtgggag aacgatttc	78.7
T125D	catgaaataggttttggaagtaaagttacaGAT caccctcttgctaaagacaaaatgat	gtactttatccaaaaccttcatttcaatgtcta gtgggagaacgatttctgttttacta	78.2
S161A	ggggcctgggaccGCCttcgagtttgcg	ccccggaccctggcggaagctcaaacgc	78.1
S161D	gggggcctgggaccGActtcgagtttgcgc	cccccggaccctggctgaagctcaaacgcg	79.7

The PCR was set up in 100 µl reaction tubes in a total volume of 50 µl in sterile H_2O on ice by mixing 5µl 10x reaction buffer, 50 ng pCMV6-hDJ1 plasmid DNA, 125 ng of forward and reverse primer, 1 µl dNTPs, 1.5 µl QuikSolution reagent (all components included in the kit except DNA and H_2O). 1 µl of QuikChange Lightning polymerase was added and the PCR was performed using the program outlined in table 2.5. 2 µl Dpn I enzyme (provided) was added to each PCR product and incubated for 5 min at 37ºC. 45 µl ultracompetent *E.coli* strain XL10 GOLD (provided) were directly transformed with 2 µl of the restriction product as described above (see section (iii)).

Table 2.5 – PCR program for QuikChange Lightning

Site directed mutagenesis of pCMV6-hDJ-1.

Step	# Cycles	Temperature	Time
1	1	95ºC	2 min
2	18	95ºC	20 s
		60ºC	10 s
		68ºC	2.5 min
3	1	68ºC	5 min

ii) Plasmid sequencing

For each mutated plasmid three colonies were picked from freshly plated transformed *E.coli* and 5 ml pre-cultures were grown over night as described above. 3 ml of these pre-cultures were used to purify DNA using a GenElute Plasmid Mini kit (Sigma Aldrich) according to the manufacturers protocol. 500 ng plasmid DNA was mixed with 3.2 pmole T7 sequencing primer (5´- TAATACGACTCACTATAGGG- 3´, Thermo Scientific) in a total volume of 10 µl. Sequencing was performed by the MRC Genomic facility (Imperial College London, Hammersmith Campus, ICTEM, London, W12 0NN). The sequencing results were blasted against the NCBI nucleotide collection database for human sequences (nucleotide blast) and against the non-redundant protein sequences database for human sequences (nucleotide to protein blast).

2.6 Biochemistry

2.6.1 Bradford assay

The Bradford assay was used to determine protein concentrations in cell lysates. The Bradford reagent working dilution was prepared from the stock (BioRad) by diluting 1 part of stock in 4 parts H_2O. The working dilution was kept for maximum 1 month at 4ºC. BSA (Sigma Aldrich) was used as protein standard by dissolving the lyophilised reagent in H_2O to a concentration of 1mg/ml. The stock was serially diluted to achieve standard concentrations of (mg/ml) 0.5, 0.25, 0.125 and 0.05 in H_2O. 10 µl H_2O or standard was added per well of a 96-well plate to determine the standard curve. Lysates were directly diluted in the wells of the same 96-well in PBS to a final volume of 10 µl. The background was determined by diluting the lysis buffer in PBS (dilution factor as for samples). All samples were measured at least in triplicates. 100 µl Bradford working dilution was added and the plate was incubated in the dark for 10 to 30 min on an orbital shaker at 200 rpm. The absorbance was detected at 600 nm in a Glomax Plus plate reader (Promega UK Ltd, Southampton, UK).

The protein concentration was determined relative to the BSA standard. To obtain a standard curve the absorbance at 600 nm (A_{600}) of the BSA background (only H_2O) was subtracted from the A_{600} of each BSA standard. The linear equation of the standard curve therefore had the following form, whereby A600(x) is A_{600} at the BSA concentration of x mg/ml and m is the slope of the linear equation.

$$A600(x) = m * x$$

To determine the protein concentrations of the sample, background absorption was subtracted from A_{600} of each sample. The background corrected A_{600} was used to determine protein concentration using the following equation, whereby c is the protein concentration of the original sample, m is the slope of the standard curve, A_{600} is the absorption of the diluted sample, and D is the dilution factor.

$$c = \frac{A600}{m} * D$$

2.6.2 SDS-PAGE and Western blotting

Sodium dodecyl sulphate (SDS) polyacrylamide gel electrophoreses (PAGE) and Western Blotting (WB) was performed to quantify specific proteins. The SDS-PAGE was performed using 10-20% gradient midi-size Tris-glycine gels. During WB proteins were transferred onto PVDF membranes using the tank blotting technique. All equipment and reagents for SDS-PAGE and WB were purchased from Bio-Rad Laboratories Ltd. (Hertfordshire, UK) if not mentioned otherwise.

10 µg of protein samples were diluted with freashly prepared 4x Laemmli sample buffer (SB)(see Materials -2.8) to a final concentration 25% SB. 5 µl of Dual Colour protein standard was used as molecular weight marker. Electrophoresis was carried out at 90 V for 2 to 2.5 h. The gel was placed onto an activated PVDF membrane (methanol soaked) and assembled between Whatman paper and a sponge. Proteins were transferred for 2 h at 90 V in cooled WB transfer buffer (see Materials - 2.8). The membrane was blocked for 30 min in

Table 2.6 – Antibodies.

Antibody (reactivity)	epitope	Origin	Dilution for WB	Reference	Manufacturer Order #
14-3-3β (h, rt, m, etc.)		rabbit (pAb)	1:1000 (IP) 1:2000 (lysates)	C-20	Santa Cruz sc-628
14-3-3β (h)		mouse (mAb)	1:1000 (IP)	J2E9	Atgen A1211201
DJ-1 (h, rt, m, etc)		rabbit (pAb)	1:1000	FL-189	Santa Cruz sc-32874
DJ-1 (h, rt, m)		mouse (mAb)	1:1000 (IP)	D-4	Santa Cruz sc-55572
ATP5B (h)		rabbit (pAb)	1:3000	Centre	Abgent AP2973c-ev
ATP5B (h, rt)		rabbit	1:3000	-	Aviva system biology ARP48185_T100
Tom40 (h, m, rt)		rabbit (pAb)	1:1000	H-300	Santa Cruz sc-11414
GAPDH (h, rt)		rabbit (pAb)	1:1000-1:2000	FL-335 HRP coupled	Santa Cruz sc-25778 HRP
Hsp60 (h, rt, m)		rabbit (pAb)	1:3000-1:5000	-	GeneTex GTX110089
Calnexin (h, m)		rabbit (pAb)	1:1000-1:2000	-	GeneTex GTX112886
α-tubulin (h, rt, m)		mouse (mAb)	1:3000	10D8	BioLegend 627902
Histone H3 (h, rt, m)		rabbit (pAb)	1:3000	N-term	Merck 06-755
PSD-95 (h, rt, m)		mouse (mAb)	1:1000	K28/43	Biolegend MMS5182-100
myc (tag, exogenous)		mouse (mAb)	1:10000-1:20000	9B11 HRP coupled	Cell Signalling 2040
mouse IgG-HRP (m)		horse (pAb)	1:10000	HRP coupled	Cell Signalling 7076
rabbit IgG-HRP (rabbit)		goat (pAb)	1:10000	HRP coupled	Cell Signalling 7074

h - human; rt - rat; m - mouse; pAb - polyclonal antibody; mAb - monoclonal antibody

blocking buffer (see Materials - 2.8) and incubated with primary antibodies in blocking buffer over night at 4ºC on an orbital shaker (for dilutions see table 2.6). The membranes were washed 4 times for a total of 2 h on an orbital shaker in PBS-T (see Material – 2.8) and incubated for 1 h at room temperature shaking with secondary antibodies coupled to horseradish peroxidase (HRP) diluted in PBS-T. The membranes were washed 4 times for a total of 30 min to 1 h on an orbital shaker in PBS-T.

For HRP-based detection the membranes were incubated for 5 min with freshly prepared enhanced chemi-luminescence (ECL) reagent. Chemi-luminescence was detected in darkness on autoradiography films (Santa Cruz) for various lengths of time. The films were developed in a Konika SRX-101A film processor (Konika, Tokyo, Japan) using RG Universal X-ray developer, RG Universal X-ray fixer (both Champion photochemistry, Kuala Lumpur, Malaysia) and H_2O. The films were scanned using an HP Scanjet 300 and the protein quantity was determined by densitometry with the free software Fiji (Schindelin et al., 2012).

2.7 Statistical analysis

Unless otherwise stated all data are presented as mean ± SEM. All experiments were performed at least in three independent replicates. For individual comparisons, two-tailed unpaired Student t-test was used. For multiple comparisons either one-way or two-way (repeated measures) analysis of variance (ANOVA) was applied. For multiple comparisons to a single control group a one-way ANOVA was used with Dunnet's post-hoc test. For multiple comparisons between groups one-way ANOVA with Sidak's post-hoc test was used. Individual tests conducted on each dataset are detailed in the corresponding figure legend. Statistical significance refers to: * $p<0.05$, ** $p<0.01$, *** $p<0.001$, **** $p<0.0001$. All statistical tests were performed using GraphPad Prism 6.0 for Mac OS (GraphPad Software, San Diego, CA, USA).

2.8 Material

All reagents were purchased from Sigma Aldrich (Sigma Aldrich Co Ltd, Dorset, UK) if not stated otherwise. All solutions were prepared using distilled and deionised water prepared by a Barnstead system and filtered through an irradiated 0.2 µm hollow fibre filter (Barnstead D3750).

Reagents

2M $CaCl_2$: 2 M $CaCl_2$*$6H_2O$ in H_2O, sterile filtered through 0.22 µm PES membrane, stored at 4°C

2xHBS (pH 7.05 ± 0.01): 274 mM NaCl, 1.5 mM Na_2HPO_4, 54.5 mM HEPES in H_2O, sterile filtered through 0.22 µm PES membrane (Corning, Corning, US), stored at -20ºC in aliquots, thawed slowly at room temperature before use, stable at 4ºC for one week, not suitable for freeze-thaw cycling

2xLaemmli Sample buffer: 5% (v/v) β-mercaptoethanol (Bio-Rad Laboratories Ltd., Hertfordshire, UK) in 2xLaemmli buffer (Bio-Rad)

3xFlag peptide: 300 µg/ml 3xFlag peptide in TBS, stored at -20ºC in aliquots

4xLaemmli Sample buffer: 10% (v/v) β-mercaptoethanol (Bio-Rad Laboratories Ltd., Hertfordshire, UK) in 4xLaemmli buffer (Bio-Rad)

Acetic acid: 1% (v/v) acetic acid in H_2O

Ampicillin stock: 100 mg/ml ampicillin (Fisher Brand) in H_2O, aliquoted and frozen at -20ºC

AP lysis buffer (pH 7.9): 50 mM Tris-HCl, 100 mM NaCl, 10 mM $MgCl_2$, 1% (v/v) Triton-X100 in H_2O, protease inhibitor (Sigma Aldrich, #P8340) freshly added

Borate buffer (pH 8.5): 0.1 M borate in H_2O, sterile filtered through 0.22 µm PES, stored at 4°C

$CaCl_2$ transformation solution: 0.1 M $CaCl_2$ in H_2O, sterile filtered through 0.22 µm polyethersulfone (PES) membrane (Corning, Corning, US), store at 4°C

EC solution (pH 7.3): 125 mM NaCl, 3 mM KCl, 10 mM HEPES, 5 mM D-Glucose, 2 mM $CaCl_2$, 1 mM $MgCl_2$, sterile filtered through 0.22 µm PES, store at 4°C

FCCP stock: 20 mM FCCP in ethanol, stored in aliquots at -20ºC

G418 stock: 50 mg/ml G418 in H2O, sterile filtered through 0.22 µm PES, stored at 4°C

Glycine/hydrazine buffer (pH 9.0): 0.5 M glycine, 0.4 M hydrazine in H_2O

IP lysis buffer (pH 7.5): 10 mM Tris, 150 mM NaCl, 1% (v/v) Triton-X100 in H_2O, protease and phosphatase inhibitor (Thermo Scientific, # 88669) freshly added

Kanamycin stock: 100 mg/ml kanamycin (Fisher Brand) in H_2O, aliquoted and frozen at -20ºC

LB-Agar: 35 g LB-agar (AppliChem, Darmstadt, Germany) in 1 l H_2O, sterilised by autoclaving

LB broth: 25 g LB broth (Merck, Darmstadt, Germany) in 1 l H_2O, sterilised by autoclaving

Mannitol isolation buffer (pH 7.5): 210 mM mannitol, 70 mM sucrose, 10 mM HEPES, 1 mM EDTA in H_2O

Mitochondrial lysis buffer (pH 7.5): 50 mM Tris, 250 mM NaCl, 10 mM EDTA, 1% (v/v) Triton-X100 in H_2O

NAD^+: 17 mg/ml β-Nicotinamide adenine dinucleotide hydrate in H_2O

PBS (pH 7.5): 137 mM NaCl, 2.7 mM KCl, 10 mM $Na_2HPO_4*2H_2O$, 1.8 mM NaH_2PO_4 in H_2O

TBS (pH 7.5): 50 mM Tris-HCl, 150 mM NaCl in H_2O

Sterile glycerol solution: 50% glycerol (w/v) in H_2O, autoclaved

SDS-Page running buffer: 100 ml 10xTris-glycine-SDS buffer (Bio-Rad), 900 ml H_2O

WB transfer buffer: 100 ml 10xTris-glycine buffer (Bio-Rad), 200 ml methanol, 700 ml H_2O

PBS-T: 0.1% (v/v) Tween-20 in PBS

WB blocking buffer: 5% (w/v) BSA in PBS-T

Triton-X100 diluted stock: 10% (v/v) Triton-X100 in H_2O, stored at 4ºC

Oligomycin stock: 10 mM oligomycin in ethanol

PDL stock: 1 mg/ml poly-D-lysine (MW 70000-150000) in borate buffer, sterile filtered through 0.22 µm PES, stored at 4°C

PDL working dilution: diluted as required in borate buffer

Puromycin stock: 1 mg/ml puromycin in H_2O, sterile filtered through 0.22 µm PES, stored at -20°C

RIPA lysis buffer: 10% (v/v) 10xRIPA buffer (Cell Signalling) in H_2O, protease and phosphatase inhibitor (Thermo Scientific, # 88669) freshly added

SRB Tris buffer (pH 10.5): 10 mM Tris in H_2O

SRB: 0.4% (w/v) Sulforhodamine, 1% (v/v) acetic acid in H_2O

TBS lysis buffer (pH 7.5): 50 mM Tris-Hcl, 150 mM NaCl, 1% (v/v) Triton-X100 in H_2O, protease and phosphatase inhibitor (Thermo Scientific, # 88669) freshly added

TMRE stock: 50 mM TMRE in DMSO, stored in small aliquots at -20ºC

TMRE working solution: 10 µM TMRE in DMSO freshly prepared from TMRE stock

Trichloracetic acid (TCA): 15% (w/v) TCA in H_2O, stored at 4ºC

Kits

ATPlite (Perkin Elmers, # 6016943)

AnnexinV-PI cell viability assay kit (BioLegend, San Diego, US)

GenElute Plasmid Midi kit (Sigma Aldrich, # NA0200)

QuikChange Lightning (Agilent Technologies, # 210518)

3 Results

–

Interaction studies of DJ-1 and 14-3-3β

3.1 Introduction and Aims

In order to identify new interaction partners of the Parkinson's disease linked protein DJ-1 our group performed a mass spectrometry screen for interaction partners of overexpressed and immunoprecipitated DJ-1^{mycFlag} in collaboration with Elizabeth Jonas (Yale University). Among the interaction partners was 14-3-3β. Interestingly, 14-3-3β co-precipitated with wildtype, but not the PD-associated mutant (L166P) DJ-1. Another study also had identified an interaction between DJ-1 and 14-3-3 proteins in a mass spectrometry screen, confirming our result. In this study, yeast BMH1/2 (14-3-3 orthologs of *S. cerevisae*) coupled to sepharose were used to pull down proteins from a HeLa cell extract (Pozuelo Rubio et al., 2004). A phospho-peptide corresponding to the minimal 14-3-3-binding motif was subsequently used to elute interactors that bound to BMH1/2 in a phosphorylation-dependent manner. Although several of the proteins that have been identified with MS were validated by WB, the interaction between 14-3-3 and DJ-1 had not received further attention. My first aim therefore was to validate the interaction between 14-3-3, specifically the β-isoform and DJ-1 by immunoprecipitation (IP) from human cell extracts and rodent brain and to identify putative phosphorylation sites on DJ-1 that may mediate the interaction. Furthermore, to identify the cellular pathways that regulate binding of the two proteins, several metabolic and stress conditions will be tested for their effect on the interaction between DJ-1 and 14-3-3β.

3.2 In vitro and in vivo interaction between DJ-1 and 14-3-3β

In order to validate the binding between DJ-1 and 14-3-3β found in our mass spectrometry screen, I performed IP experiments. Exogenous DJ-1 C-terminally tagged with myc and Flag epitopes (hereafter referred to DJ-1^{mycFlag}) was expressed in human embryonic kidney (HEK293T) cells. The overexpressed protein was precipitated from the cell extracts using anti-Flag agarose beads (Sigma Aldrich) and 14-3-3β co-precipitation was identified by Western blot (WB) analysis (Figure 3.1 A). To determine whether this interaction also exists between endogenous proteins, DJ-1 was immunoprecipitated from rat brain lysate using a

specific antibody (Santa Cruz, FL-189). The endogenous protein-protein interaction between DJ-1 and 14-3-3β was confirmed by WB (Figure 3.1 B). Note that the mouse antibody against DJ-1 used for WB in Figure 3.1 B only detected a band at app. 50 kDa, which is corresponding to the size of a DJ-1 dimer.

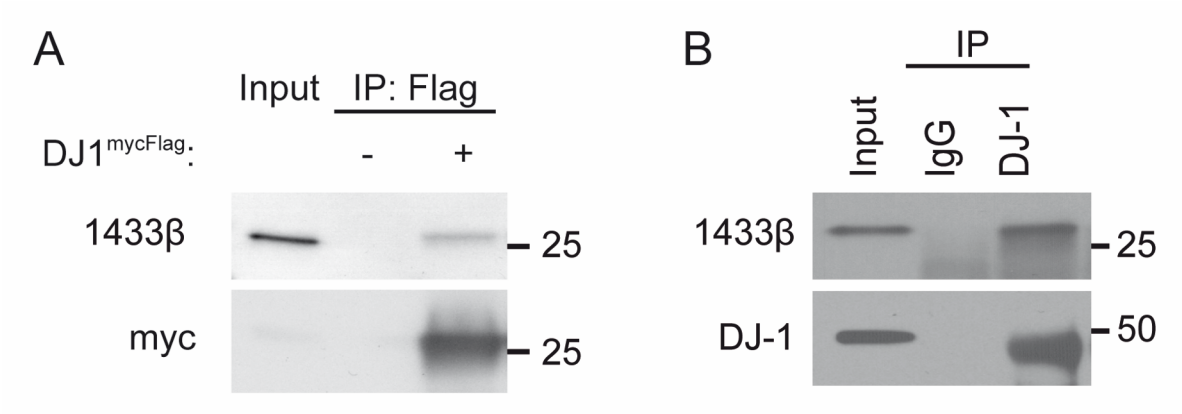


Figure 3.1 – Interaction between DJ-1 and 14-3-3β was tested by immunoprecipitation (IP) using anti-Flag antibodies against overexpressed DJ-1^{mycFlag} from HEK293T cells (A) and in vivo using specific antibodies against endogenous DJ-1 from rat brain lysate. Total lysate (input) and IP eluate was analysed by Western Blot (WB) and the interaction was identified using specific antibodies against 14-3-3β. Antibodies against myc (A) or DJ-1 (B) were used to verify the IP. The data is representative of at least three independent experiments.

3.3 The interaction of DJ-1 and 14-3-3β is mediated by phosphorylation of DJ-1

3.3.1 Phosphorylation-dependence

With very few exceptions, binding of 14-3-3 proteins depends on the presence of a phosphorylated serine or threonine of the target. To determine whether the interaction of DJ-1 with 14-3-3 was dependent on phosphorylation, I tested the effect of phosphatase treatment on the interaction between DJ-1^{mycFlag} and 14-3-3β. DJ-1^{mycFlag} overexpressing cell lysates were treated with or without alkaline phosphatase (AP). The treated lysates were subjected to IP and the 14-3-3β co-IP was analysed by WB (Figure 3.2). The protein levels were quantified by densitometry and 14-3-3β was plotted relative to the myc levels. In line with the 14-3-3β phospho-binding mechanism, AP treatment reduced the 14-3-3β levels to 57.3 ± 5.5% (mean ± SEM) of the untreated control samples (Figure 3.2).

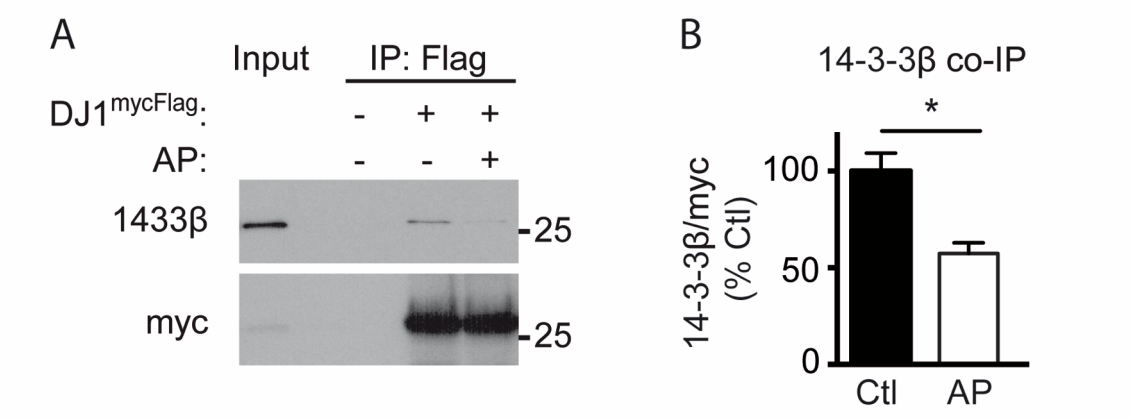


Figure 3.2 – Phospho-dependence of DJ-1 interaction with 14-3-3β was tested in HEK293T lysates containing overexpressed DJ-1$^{myc\text{-}Flag}$. Lysates were treated without (Ctl) or with alkaline phosphatase (AP) prior to Flag IP and total lysate (input) and IP eluate was analysed by WB using antibodies against 14-3-3β and myc (A). Quantification of three independent experiments revealed reduced interaction of 14-3-3β with DJ-1 after AP treatment (57.3 ± 5.5% relative to Ctl). 14-3-3β protein levels were normalised against myc. Data represented as mean ± SEM, unpaired two-tailed t-test, n = 3, *p = 0.0164).

3.3.2 Prediction of phosphorylation sites on DJ-1

To date no kinase has been identified to phosphorylate DJ-1. I therefore performed an *in silico* study for predicted phosphorylation sites using the online motif search tool Scansite 2.0 (Obenauer et al., 2003)(http://scansite.mit.edu/). This tool identifies phosphorylation sites based on known consensus motifs for most known serine/threonine and tyrosine kinases as well as protein-protein and protein-phospholipid interaction motifs. The Scansite search was performed using the SwissProt identifier for human DJ-1 (Q99497). Using high and medium stringency, motif search did not yield any predicted phosphorylation sites but identified several kinase-binding domains (Table 3.1). At low stringency conditions the motif search resulted in three predicted N-terminal phosphorylation sites (Thr^{34}, Ser^{57}, Tyr^{67}) and three phosphorylation sites near the C-terminus (Tyr^{141}, Ser^{142}, Ser^{161}). In addition, a 14-3-3 mode 1 consensus motif was identified with Thr^{125} as the central phosphorylated residue. Although Thr^{140} was not predicted to be a phosphorylation site, the corresponding residue Ser^{140} was found phosphorylated in a mass spectrometry screen of phospho-proteins from mouse

Table 3.1 – Scansite 2.0 motif search performed on human DJ-1 protein sequence at low stringency revealed several putative phosphorylation sites as well as a 14-3-3 binding site at Thr^{125}. Medium stringency did not reveal any phosphorylation sites but several kinase-binding motifs (marked with #). Bold letter marks active/phosphorylated site. Asterisks indicate several phosphorylation sites that were previously identified in mass spectrometry screens and are deposited in PhosphoSite Plus. SA: surface accessibility.

Site	Specficity Scansite group	Gene	Sequence	SA	Score	Percentile
V33#	Erk D-domain Kinase binding site	MAPK1	MRRAGIK**V**TVAGLAG	0.258	0.6359	0.46%
T34	PKC zeta Basophil. serine/threonine kinase	PRKCZ	RRAGIKV**T**VAGLAGK	0.364	0.6075	3.84%
S57	DNA PK DNA damage kinase	PRKDC	VVICPDA**S**LEDAKKE	1.236	0.616	3.19%
Y67*	Lck Kinase Tyrosine kinase	LCK	DAKKEGP**Y**DVVVLPG	0.505	0.5202	1.23%
Y67*	Insulin Receptor Kinase Tyrosine kinase	INSR	DAKKEGP**Y**DVVVLPG	0.505	0.7354	4.83%
Y67*	Fgr SH2 Src homology 2	FGR	DAKKEGP**Y**DVVVLPG	0.505	0.5586	3.31%
Y67*	Nck SH2 Src homology 2	NCK1	DAKKEGP**Y**DVVVLPG	0.505	0.5806	3.96%
Y67*	Crk SH2 Src homology 2	CRK	DAKKEGP**Y**DVVVLPG	0.505	0.6078	4.64%
V69#	Erk D-domain Kinase binding site	MAPK1	KKEGPYD**V**VVLPGGN	0.202	0.5973	0.24%
I105#	Erk D-domain Kinase binding site	MAPK1	RKGLIAA**I**CAGPTAL	0.088	0.4851	0.03%
T125	14-3-3 Mode 1 Phosphoserine/threonine binding	YWHAZ	GFGSKVT**T**HPLAKDK	0.615	0.573	2.70%
T140#*	PDK1 Binding Kinase binding site	PDPK1	MMNGGHY**T**YSENRVE	2.564	0.6048	0.73%
Y141*	Src Kinase Tyrosine kinase	SRC	MNGGHYT**Y**SENRVEK	3.147	0.6257	4.64%
S142*	DNA PK DNA damage kinase	PRKDC	NGGHYTY**S**ENRVEKD	3.934	0.6382	4.30%
L151	Erk D-domain Kinase binding site	MAPK1	NRVEKDG**L**ILTSRGP	0.261	0.7549	2.59%
S161	Akt Kinase Basophil. serine/threonine kinase	AKT1	TSRGPGT**S**FEFALAI	0.57	0.6694	2.42%
E163#	PDK1 Binding Kinase binding site	PDPK1	RGPGTSF**E**FALAIVE	0.332	0.6206	0.93%

adipocytes (Humphrey et al., 2013). Furthermore, the predicted phospho-residues Tyr^{67}, Tyr^{141} and Ser^{142} were identified as phosphorylated sites in mass spectrometric experiments according to Phosphosite Plus (www.phosphosite.org/)(Hornbeck et al., 2012). However, no studies had been conducted to test the effect of any of these phosphorylation sites on the activity of DJ-1.

Interestingly, most of the predicted phosphorylation sites cluster into two distinct regions within the tertiary structure of DJ-1 (Figure 3.3). Thr^{34}, Ser^{57} and Tyr^{67} form cluster 1 found in two pockets adjacent to the dimer interface (Figure 3.3 B). All three residues are surface accessible as shown in figure 3.3 C. The residues Thr^{125}, Thr^{140}, Tyr^{141} and Ser^{142} form cluster 2, which is located on the C-terminal domain on the opposite side relative to cluster 1 (Figure 3.3 E). The C-terminal domain harbours a small parallel β-sheet containing β7 and β8 linked by α6 (β-helix-β motif), the helix-kink-helix motif made of the C-terminal α7/8, as well as the antiparallel β-sheet formed by β9/10. The latter extends from the large central β-sheet and is located next to β6, which contains the active Cys^{106}. All residues of phospho-cluster 2 are located on the β-helix-β motif, with Thr^{125} in the loop between β7 and α6 and Thr^{140}, Tyr^{141} and Ser^{142} on β8. Furthermore, the predicted 14-3-3 binding site Thr^{125} and Tyr^{141} interact through a hydrogen bond (calculated by Swiss PdbViewer, based on a minimum distance of 1.2 Å and a maximum distance of 2.76 Å between hydrogens and nucleophils). Ser^{161} (the putative Akt phosphorylation site) is located in the C-terminal domain just before the helix-kink-helix motif. It was demonstrated that mutations within this motif have a destabilising effect on dimer formation (Cali et al., 2015; Gorner et al., 2007; Hulleman et al., 2007). Furthermore, the pathologic mutant $DJ\text{-}1^{L166P}$ that was used in our initial mass spectrometry screen localises to the helix7 adjacent to Ser^{161}. Interestingly, cleavage of the C-terminal helix has been proposed as an activating post-translational modification that enhances DJ-1 protective activity towards oxidative stress (Chen et al., 2010).

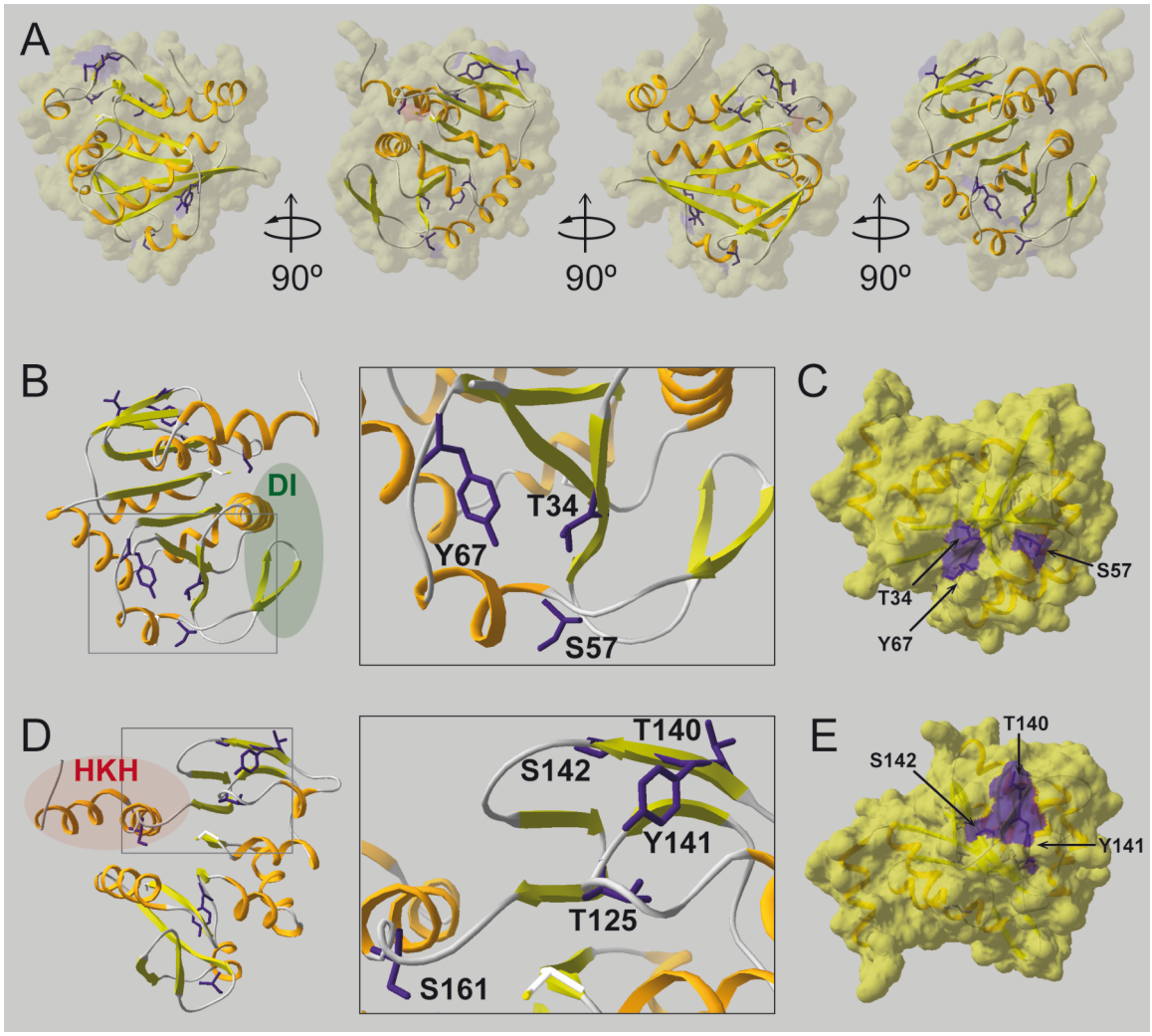


Figure 3.3 – Putative DJ-1 phosphorylation sites are clustered at two sites of the crystal structure of DJ-1 (PDB ID: 2OR3), which is depicted as monomer with the putative 14-3-3 binding site Thr^{125}, the predicted phosphorylation sites (all shown as purple sticks) and the active Cys^{106} (white/yellow stick, red surface patch) (A). The N-terminal cluster near the dimerization interface (DI) (B,C) and the C-terminal cluster adjacent to the helix-kink-helix motif (HKH) (D,E) become apparent. Most phosphorylation sites are surface accessible as indicated by the corresponding purple patches (A,C,E). Image reproduction as follows: A - Ribbon diagram superimposed on the transparent surface. The molecule is turned anti-clockwise in sequential 90º steps around the vertical axis. B,D - DJ-1 ribbon diagram (left) and close-up of the boxed area (right). C,E - Surface rendered DJ-1 with superimposed transparent ribbon diagram showing DJ-1 from the bottom (C) and top (E) relative to the representation in A. Images are produced using SwissProt PDviewer.

3.3.3 Interaction of 14-3-3β with functional mutants of DJ-1

Because binding requires serine or threonine phosphorylation, the putative 14-3-3β target sites are restricted to Thr^{34}, Ser^{57}, Thr^{140}, Ser^{142} and Ser^{161} in addition to Thr^{125}. A study of the

binding sequence of known interaction partners revealed that 14-3-3 proteins have a preference for motifs that are phosphorylated by basophilic protein kinases, such as PKA, PKB/Akt and PKC (Johnson et al., 2010). Among those, Akt is known to phosphorylate several 14-3-3 binding partners, including Bad (Datta et al., 2000), GSK3β (Yuan et al., 2004), PRAS40 (Vander Haar et al., 2007), Notch4 (Ramakrishnan et al., 2015), and SRPK2 (Jang et al., 2009). I therefore generated phosphorylation-resistant and phospho-mimicking mutants of DJ-1^{mycFlag} targeting the predicted 14-3-3 binding site Thr^{125} and the putative Akt-phosphorylation site Ser^{161}. Both residues were substituted with either alanine (phosphorylation-deficient) or aspartate (phosphorylation mimic) resulting in DJ1-T125A^{mycFlag}, DJ1-T125D^{mycFlag}, DJ1-S161A^{mycFlag}, and DJ1-S161D^{mycFlag}. HEK293T lysates containing wildtype (wt) DJ-1^{mycFlag} or the mutants were subjected to IP and the binding to 14-3-3β was analysed by WB (Fig 3.4). Mutation of Thr^{125} to alanine did not disrupt the interaction between DJ-1 and 14-3-3β (Fig 3.4 B). In contrast, DJ1-S161A^{mycFlag} revealed significantly lower levels of 14-3-3β co-IP compared to wildtype DJ1 (mean ± SEM: 30.1 ± 1.7%; Figure 3.4C). Surprisingly, three out of four mutants (T125A, T125D, S161D) co-immunoprecipitated with a second higher molecular weight species that was recognised by the 14-3-3β antibody. The molecular weight for this band corresponded to the size of a 14-3-3β dimer. Furthermore, a double band at the size of monomeric 14-3-3β was also frequently observed indicating the presence of a post-translational modification on 14-3-3β. Meanwhile the level of monomeric 14-3-3β was unchanged in the S161D IP samples, the total levels showed a significant increase relative to wt (mean ± SEM: 433 ± 133%; Figure 3.4C). These data suggest that the putative Akt phosphorylation site Ser^{161} may be required for the phosphorylation-dependent binding of DJ-1 to 14-3-3β. Surprisingly, compared to the wildtype DJ-1, the T125A and T125D mutants showed increased interaction with both, monomeric and dimeric 14-3-3β (total 14-3-3β as mean ± SEM for T125A: 841 ± 99% and for T125D: 881 ± 251%; Figure 3.4C). This argues against a role of Thr^{125} as phosphorylation-dependent binding site. However, the increased binding of 14-3-3β to either phospho-mimicking or phospho-resistant mutant of Thr^{125} suggests a different effect of this residue,

possibly involving structural changes of DJ-1. This idea is supported by the presence of a hydrogen bond between Thr^{125} and Tyr^{141}, which may play a structural role within the β-helix-β conformation in the C-terminal domain.

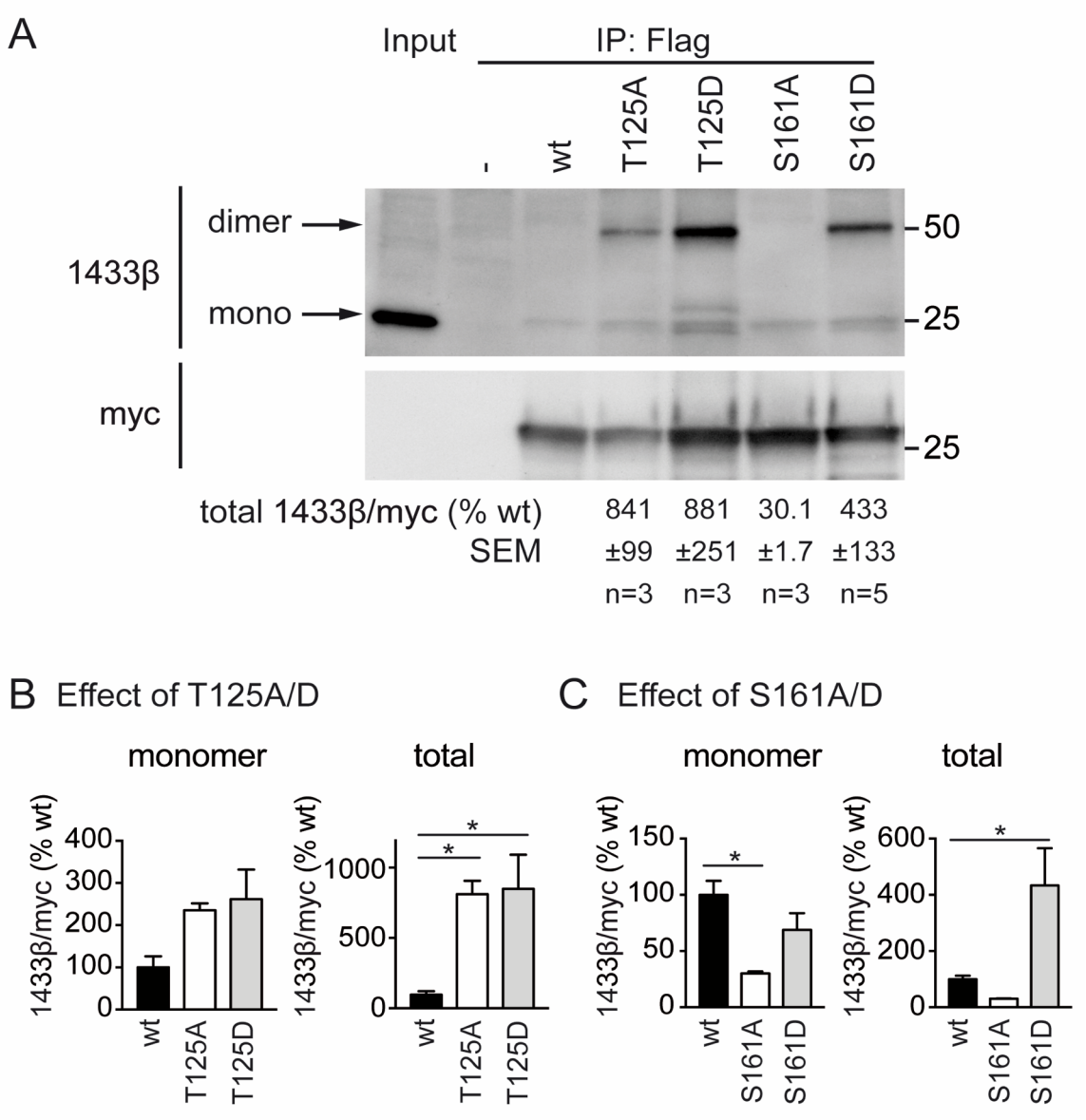


Figure 3.4 – Interaction of 14-3-3β with functional mutants of DJ-1 was tested by IP using HEK293T cells overexpressing either DJ-1^{mycFlag} wildtype (wt) or DJ-1^{mycFlag} carrying the point mutations T125A, T125D, S161A or S161D. Lysate (Input) and IP eluate was analysed by WB (A) as in figure 3.2 and 14-3-3β co-IP was quantified relative to myc (B,C). Note that two or more bands for 14-3-3β appear in IPs of three out of four DJ-1^{mycFlag} mutants, of which the single or double band at 25 kDa was referred to the monomer and the band at 50 kDa was referred to the dimer. T125A mutant fails to disrupt 14-3-3β interaction with DJ-1^{mycFlag}. In contrast, 14-3-3β interaction is diminished in IP samples of S161A and increased with S161D mutant of DJ-1^{mycFlag} (C). The data is represented as mean ± SEM in % wt (one-way ANOVA with Dunnett's test for multiple comparisons, n=3 for T125A/T125D/S161A, n=5 for S161D, *p<0.05).

3.3.4 Summary of phosphorylation studies

Our results showed a phosphorylation-dependent interaction between DJ-1 and 14-3-3β. Mutation of the Akt phosphorylation site Ser^{161} of DJ-1 to the phospho-resistant Ala^{161} disrupted the interaction between DJ-1 and 14-3-3β. In addition, the phospho-mimicking mutation S161D did not disrupt the binding of DJ-1 to 14-3-3β, but caused a significant increase of interaction, due to the co-immuoprecipitation of a higher molecular weight species of 14-3-3β. These findings indicate a role for Ser^{161} as phosphorylation-dependent binding site for 14-3-3β. In contrast, mutation of Thr^{125} to Ala did not abrogate the association between DJ-1 and 14-3-3β arguing against a role of this residue as phosphorylation-dependent binding site. Surprisingly, both T125A as well as T125D resulted in increased immunoprecipitation of the higher molecular weight species of 14-3-3β. This indicates a structural role of this residue possibly effecting the conformation of DJ-1 and thereby altering the binding to 14-3-3β.

3.4 Regulation of the interaction between DJ-1 and 14-3-3β by hypoxia

In order to investigate the functional significance of the binding between 14-3-3β and DJ-1, I aimed to decipher the physiologic conditions that may alter or enhance this interaction. Both proteins functionally overlap in their ability to regulate energy metabolism as well as the sensitivity of cells to stress conditions (Cao et al., 2015; Gardino and Yaffe, 2011; Kleppe et al., 2011). Several metabolic and stress-inducing treatments were chosen to screen for their ability to alter the interaction between DJ-1 and 14-3-3β.

3.4.1 Conditions that alter cellular metabolism

In order to modulate the cellular metabolism, two strategies were chosen. The first is based on upstream regulation of cell metabolism through growth factors. Growth factors such as epidermal growth factor (EGF) and insulin modulate metabolism alongside other cellular activities such as cell survival and proliferation (Mendoza et al., 2011). The second strategy is to directly modulate the substrate supply by glucose and oxygen deprivation, interfering with glycolysis and OXPHOS. Both are also potent activators of cell signalling mediated by,

for example, the AMP-activated protein kinase, the hypoxia-inducible factor 1α, and the mTOR pathway (Kleppe et al., 2011).

Serum deprivation (SD)

The addition of serum to cell culture medium supplies the cells with growth and survival factors. Serum starvation is therefore used to reduce the basal activity of growth factor receptor-mediated signalling and simultaneously increases the sensitivity of the cell to growth factors. Therefore, a preceding period of serum starvation is often used to enhance the effect of receptor ligands on growth factor signalling.

Epidermal growth factor (EGF)

EGF was chosen because it was shown to have broad signalling effects by inducing both the MAPK and Akt kinase cascade (Mendoza et al., 2011). Both kinase cascades positively regulate cell proliferation and metabolism and have been shown to crosstalk at various levels (Mendoza et al., 2011). The effect of EGF on the ability of DJ-1 to interact with 14-3-3β was tested alone and in combination with serum starvation. Starvation is used to sensitize the cells to EGF because receptor activation by growth factors present in the serum decreases the plasma membrane expression of EGF receptor (Tomas et al., 2014). In the combined treatment cells were starved for 24h prior to addition of EGF for 1 h.

Hypoxia and glucose substitution

Hypoxia is a potent antagonist of the mitochondrial pathway of energy production in favour of glycolysis (Bunn and Poyton, 1996; Metallo et al., 2012). Glucose substitution (GS) with galactose in turn was shown to decrease glycolysis. Under these conditions glutamine becomes the major energy substrate through aerobic oxidation via the TCA cycle (Gohil et al., 2010; Reitzer et al., 1979). Glutamine is provided at 2 mM in our cell culture medium (compared to 25 mM glucose or galactose). Finally, combined treatment with GS and hypoxia severely interferes with energy metabolism since both glycolysis and OXPHOS are inhibited.

3.4.2 Stress-inducing treatments

In a second set of experiments the following treatments were used to alter cellular and mitochondrial stress.

γ-irradiation (γ-IR)

γ-IR induces stress through DNA double strand breaks as well as ROS. The latter also provokes DNA double strand breaks independently of ionizing radiation (Jeggo and Lobrich, 2007). A deficiency in DNA-repair mechanisms has recently been implicated in Parkinson's disease (Sepe et al., 2016).

Hydrogen peroxide (H_2O_2)

H_2O_2 induces oxidative stress and causes an up-regulation of expression and oxidative modulation of DJ-1 (Taira et al., 2004b). Enhanced oxidative damage is found in neuronal mitochondria of PD patients (Keeney et al., 2006).

Ca^{2+} overload

At high concentrations ionomycin acts as a plasma membrane Ca^{2+} ionophore (10 µM and above) that facilitates the diffusion of Ca^{2+} into the cytosol. At lower concentrations ionomycin may cause Ca^{2+} release through Ca^{2+} channels from internal stores, such as the ER (Dedkova et al., 2000). Both results in an increase of cytosolic Ca^{2+} levels, which alters mitochondrial function alongside other physiological changes (Ichas and Mazat, 1998). Deficiency in neuronal Ca^{2+} buffering has been implicated in PD (Surmeier et al., 2011).

Tunicamycin

Tunicamycin is an inhibitor of a family of N-acetylhexosamine phosphotransferases, essential enzymes for the post-translational modification of glycoproteins in the ER and Golgi. Treatment with tunicamycin inhibits the glycosylation process and subsequent folding and transport of glycoproteins. This in turn triggers the induction of the unfolded protein response (Heifetz et al., 1979). ER-stress and activation of the unfolded protein response has been associated with PD (Celardo et al., 2016).

Oligomycin

Oligomycin inhibits the mitochondrial ATP synthase and thereby the mitochondrial pathway of energy production via OXPHOS (Penefsky, 1985). Mitochondrial deficiency is one of the hallmarks of PD (Bender et al., 2006; Lu et al., 2014; Schapira et al., 1989; Subramaniam and Chesselet, 2013).

Cyclosporin A (CsA)

CsA was chosen due to its protective function in mitochondria. By binding to cyclophilin D, CsA inhibits the opening of the mitochondrial permeability transition pore (mPTP). mPTP is a mega-channel within the mitochondrial inner membrane that decreases $\Delta\Psi_m$ during short-term opening but causes cell death when irreversibly activated (Bonora et al., 2015).

3.4.3 Interaction screen

HEK293T cells overexpressing DJ-1^{mycFlag} were subjected to either metabolic or stress-altering treatments (Figure 3.5). The cells were then lysed and IP was performed using an anti-Flag antibody. As outlined in chapter 3.3, I speculate that altered metabolism or stress-conditions will have structural effects on DJ-1, which could alter the interaction with 14-3-3β. Metabolic stress induced by hypoxia and hypoxia with glucose substitution (GS) had the strongest effect on the interaction between DJ-1 and 14-3-3β (Figure 3.5). The IP of DJ-1^{mycFlag} under hypoxia caused a 45% reduction of monomeric 14-3-3β interaction and the simultaneous treatment of hypoxia with GS resulted in a 32% reduction of monomeric 14-3-3β relative to untreated. EGF and serum concentration had no prominent effect on the interaction between DJ-1 and 14-3-3β (Figure 3.5). Unfortunately, due to a faulty WB membrane the results for combined treatment of serum starvation and EGF could not be quantified. The experiment was repeated in a separate run and is shown in the supplementary figure S1. The combined treatment did not alter the interaction between DJ-1 and 14-3-3β (14-3-3β/myc (%ctl): 95.4).

None of the stress-inducing treatments showed a prominent change in 14-3-3β co-precipitate (Figure 3.6) and treatment with CsA slightly reduced the co-IP of 14-3-3β to 75.7% of untreated.

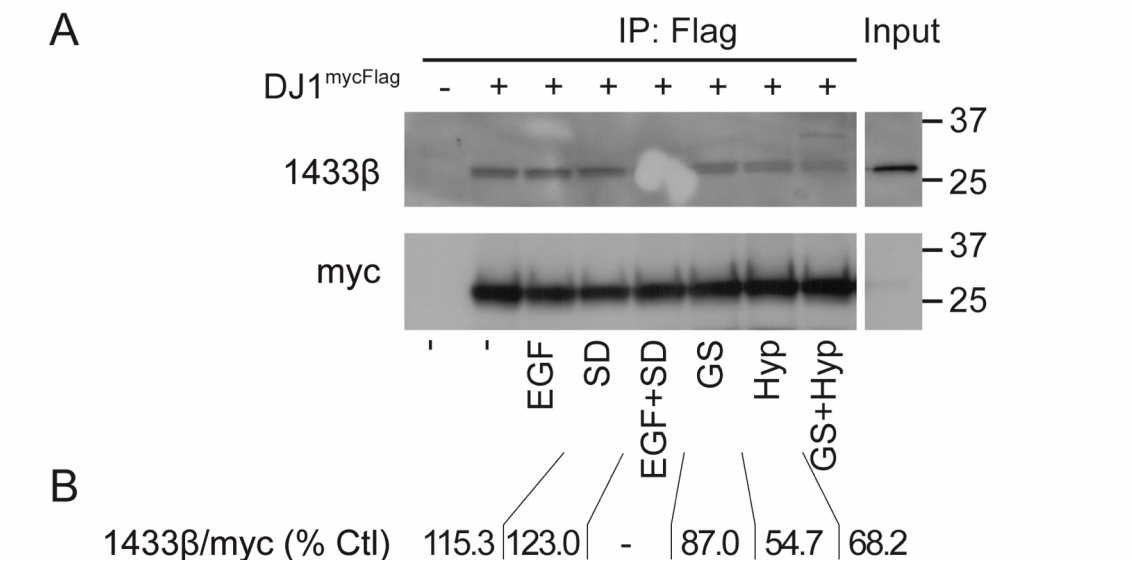


Figure 3.5 – Screen for metabolic modulators of interaction indicates a selective negative effect of hypoxia (Hyp) and hypoxia with glucose substitution (GS) on the interaction between DJ-1 and 14-3-3β. IP of overexpressed DJ1^{mycFlag} was performed as in Figure 3.1A after treatment of HEK293T cells with epidermal growth factor (EGF), serum starvation (SD), GS, Hyp and a combination of the first two and the latter two. The screen was performed only once. The details of each treatment are specified in Material and Methods. WB (A) and quantification (B) of 14-3-3β/myc as in Figure 3.2. Values are displayed as % of untreated DJ1^{mycFlag} (Ctl). 14-3-3β refers to the single or double band at 25 kDa.

3.4.4 Hypoxia is a modulator of 14-3-3 and DJ-1 interaction

In order to validate the effect of hypoxia and hypoxia with glucose substitution on the interaction between DJ-1 and 14-3-3β additional IP experiments were performed, which confirmed a significant decrease of binding of 14-3-3β to DJ-1 upon hypoxia (mean ± SEM in % ctl: 52.9 ± 12.1%, Figure 3.7). A band corresponding to 14-3-3β dimer was not consistently present throughout all experiments and was therefore excluded from the analysis. The results of combined treatment of hypoxia with glucose substitution were inconsistent and failed to reach significance. Taken together, the data confirms that hypoxia partially disrupts the interaction between 14-3-3β and DJ-1.

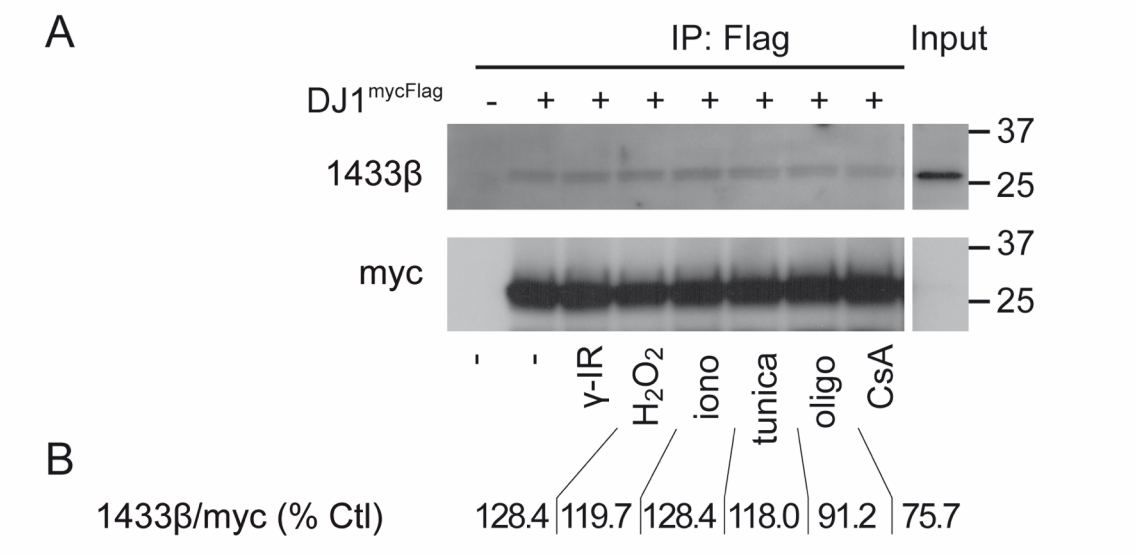


Figure 3.6 – Screen for stress-induced modulators of interaction shows little or no effect on the interaction between DJ-1 and 14-3-3β under the conditions used for the screen. IP of overexpressed DJ1^{mycFlag} was performed as in Figure 3.1A after treatment of HEK293T cells with γ-irradiation (γ-IR), H_2O_2, ionomycin (iono), tunicamycin (tunica), oligomycin (oligo) and cyclosporin A (CsA). The screen was performed only once. Concentrations and timing are detailed in Material and Methods. WB (A) and quantification (B) of 14-3-3β/myc as in Figure 3.2. Values are displayed as % of untreated DJ1^{mycFlag} (Ctl). 14-3-3β refers to the single or double band at 25 kDa.

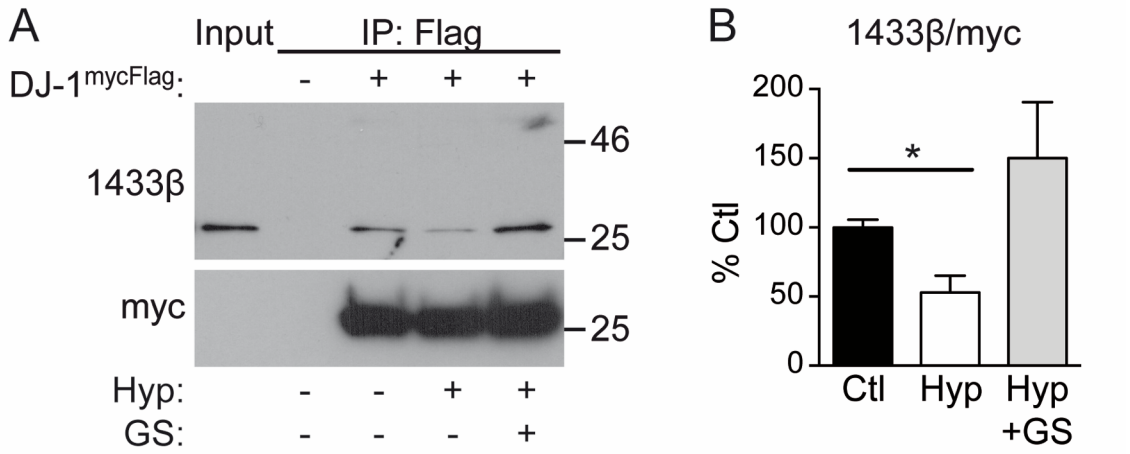


Figure 3.5 – Effect of hypoxia on the interaction between DJ-1 and 14-3-3β. HEK293T cells overexpressing DJ-1^{mycFlag} were incubated for 24h in normoxic (Ctl) or hypoxic (Hyp) conditions without or with glucose substitution (GS). IP was performed as in Figure 3.1A and total lysate (input) and IP eluate was analysed by WB (A) and quantified as 14-3-3β relative to myc (B). Hyp, but not Hyp+GS, consistently decreases the interaction between DJ-1^{mycFlag} and 14-3-3β to 52.9 ± 12.1% of Ctl. Data is represented as mean ± SEM in % Ctl of three independent experiments (n=3, two-tailed student's t-test, *p=0.0244).

3.4.5 Summary of the regulation studies

During a screen of factors that could regulate the interaction between DJ-1 and 14-3-3β, hypoxia was identified as a physiologic condition that reduces the protein interaction between DJ-1 and 14-3-3β to 53% of control levels. Surprisingly, I could not confirm an effect of hypoxia with glucose substitution on the binding of DJ-1 to 14-3-3β. It is likely, that low oxygen levels do not act autonomously to regulate the interaction. For example, the acidification of the cell culture medium during hypoxia in presence of glucose may provide important metabolic clues to adapt to the hypoxic environment (Khacho et al., 2014). Cells grown in medium containing galactose in substitution for glucose do not experience the acidic pH shift since their glycolytic rate is markedly decreased (Gohil et al., 2010; Reitzer et al., 1979).

3.5 Discussion

Here I provide evidence for a phosphorylation-dependent interaction between DJ-1 and 14-3-3β. The reduced binding of the S161A mutant of DJ-1 argues for a role of this site as mediator of the interaction with 14-3-3β. However, it is likely that binding to the dimeric 14-3-3β is mediated by at least two sites, since the S161A mutation in DJ-1 does not fully abrogate the interaction. Furthermore, the binding site does not conform to the canonical 14-3-3β binding motif, which predicts low efficiency of unilateral binding (Johnson et al., 2010). A second phosphorylation site may be present on the same molecule or, alternatively could be provided through dimerization of DJ-1. The location of Ser^{161} is opposite to the dimerization interface and hence accessible both in monomeric and dimeric DJ-1. Both, DJ-1 and 14-3-3 proteins were shown to provide conformational flexibility (Girotto et al., 2012; Yang et al., 2006). In particular, flexibility of the 14-3-3β dimer in the hinge region (between both subunits) can account for large structural changes, leading to an open and exposed conformation of the otherwise closed binding cleft (Yang et al., 2006). This allows for accommodation of larger entities by 14-3-3β. In addition, both proteins adopt mirror

symmetry in the dimeric state as revealed by their crystal structures (Figure 1.8 and 1.10), which would facilitate dimer-dimer interaction. Dimer formation of DJ-1 may also account for the incomplete disruption of the interaction of DJ1-S161A^{mycFlag}, since HEK293T cells express endogenous DJ-1. In order to address this possibility, further structural studies are required. Several key residues at the dimerization interface of DJ-1 have been identified to mediate intermolecular interactions, most importantly Met17 and Phe162 (Honbou et al., 2003), as well as Arg28 (Herrera et al., 2007). Site-directed mutagenesis of these residues could be used to test the effect of DJ-1 dimerization on the binding of 14-3-3β. This is particularly valuable because many of the pathologic mutants of DJ-1 were shown to be deficient in homo-dimer formation (Cali et al., 2015; Repici et al., 2013).

The increased binding of 14-3-3β to the mutant T125A of DJ-1 argues against the role of this residue as phosphorylation-dependent binding site of 14-3-3β. Interestingly, Thr^{125} forms a hydrogen bond with Tyr^{141} (Figure 3.3), which is absent in the T125A mutant and is probably disrupted by the T125D mutation. Therefore, it is possible that the Thr^{125} mutations have an impact on the folding of the C-terminal β-helix-β motif. Interestingly, phosphorylation of Tyr^{141} is also likely to alter the conformation of the β-helix-β motif and has been reported in mass spectrometry analysis (Table 3.1) suggesting a physiological function of the interaction between Thr^{125} and Tyr^{141}. If these assumptions are correct then conformational changes of the β-helix-β motif may enhance binding between DJ-1 and 14-3-3β in a phosphorylation independent-manner, which could explain the altered interaction observed with both Thr^{125} mutants. It is noteworthy that additional structural components of 14-3-3 targets, which are distinct from the conserved consensus sequences, have recently been implicated in binding of 14-3-3 proteins (Obsilova et al., 2014). For example, binding of the Regulator of G-protein signalling 3 (RGS3) was mediated by both, the central phospho-residue binding cleft, as well as the C-terminal helices α6 and α8 of 14-3-3ζ (Rezabkova et al., 2011).

Interestingly, nuclear magnetic resonance (NMR)-spectroscopy, the gold standard to determine molecular flexibility, has been used to examine structural changes of DJ-1 induced by dopamine-derived quinones (DAQ). DAQ was found to covalently bind to DJ-1 at Cys^{53} and Cys^{106} (Girotto et al., 2012). Cys^{53} was more prone to DAQ-modification, which induced structural changes in parts of the dimer interface as well as the pocket that harbours Ser^{57} of the phosphorylation cluster 1. DAQ binding to Cys^{106} in turn had wide-range effects on the structure of DJ-1 including the dimer interface, the active site surrounding Cys^{106}, as well as the C-terminal helix-kink-helix and β-helix-β motifs. Notably, dopamine-conjugation of DJ-1 has been shown to occur *in vitro* and *in vivo* using mass spectrometry analysis of a neuroblastoma cell line and rat brain mitochondria, respectively (Van Laar et al., 2009). These findings in conjunction with our mutation experiments point towards an intricate relation between DJ-1 phosphorylation, oxidation, and conformational changes. Although to this point I cannot reliably confirm that the 50 kDa band in our IP experiments represents dimeric 14-3-3β, it seems likely that both, phosphorylation and structural re-arrangements of DJ-1 are implicated in binding to this 14-3-3β species. Furthermore, I speculate that oxidative modification and phosphorylation of DJ-1 structurally co-operate to facilitate binding to 14-3-3β.

With respect to the physiological function, the perturbation of the interaction by hypoxia argues for a role of 14-3-3β in regulating the function of DJ-1 in a metabolic context, possibly mediated by hypoxia-dependent post-translational modification or oxidation of DJ-1 by hypoxia-induced ROS (Solaini et al., 2010) formation. The finding that H_2O_2 treatment did not alter the interaction between DJ-1 and 14-3-3β during the screen (Figure 3.5, Table 3.3) argues against a role for ROS. However, higher doses or longer treatment with H_2O_2 can possibly have a different effect. Furthermore, broad H_2O_2 application may not adequately mimic the mitochondrial ROS production (Schaar et al., 2015) that is observed during hypoxia. A third possibility of hypoxia-dependent release of DJ-1 from 14-3-3β could be mediated by phosphorylation of 14-3-3 itself. It was shown that phosphorylation of Ser^{184} in

14-3-3ζ (corresponding to Ser^{182} in the β isoform) by c-Jun N-terminal kinase resulted in c-Abl dissociation and translocation into the nucleus (Yoshida et al., 2005). Although this mechanism was found to regulate 14-3-3ζ activity during DNA-damage response, it may be applicable to other cellular stress situations.

Hypoxia initiates a cascade of cellular responses on the transcriptional and post-transcriptional level leading to metabolic adaptation among other things (Majmundar et al., 2010; Semenza, 2014; Solaini et al., 2010). As a result mitochondrial bioenergetics is thought to be down-regulated, meanwhile substrate flux through the glycolytic pathway and consequently lactate production are enhanced (Solaini et al., 2010). Interestingly, DJ-1 was shown to translocate to mitochondria during hypoxic/ischemic conditions, thereby protecting the cells from ischemic cell death (Kaneko et al., 2014a; Kaneko et al., 2014b). Furthermore, DJ-1 has been implicated in the cellular response to hypoxia as an upstream regulator of several metabolic key proteins, including HIF1α, AMPK and mTOR (Vasseur et al., 2009). For example, DJ-1 physically interacts with Von Hippel Lindau protein (VHL) and inhibits the ubiquitin-ligase activity of VHL towards HIF1α in a redox-dependent manner (Parsanejad et al., 2014). In another study it was shown that DJ-1 deficiency led to an increase in AMPK activity in myocytes due to ROS production and OXPHOS-deficiency (Shi et al., 2015). Hypoxia also alters the function of 14-3-3 family proteins. It was shown that the binding partners of 14-3-3ζ change both qualitatively and quantitatively during hypoxia. The study thereby demonstrated the remarkable flexibility by which 14-3-3 proteins regulate different cellular processes (Weerasekara et al., 2014). In support of this, binding of 14-3-3 proteins to TSC1/2 was inhibited during hypoxia or overexpression of REDD1, which led to reduced mTOR signalling and down-regulation of protein synthesis and cell proliferation (DeYoung et al., 2008). Taken together, our findings suggest that reduced interaction between DJ-1 and 14-3-3β may play a role in the cellular adaptation to hypoxia. I further speculate that the release of DJ-1 from 14-3-3β is involved in the regulation of cellular metabolism due to the

effect of DJ-1 on key metabolic regulators as well as its direct effect on mitochondrial function.

4 Results

–

The effect of 14-3-3β on the localisation of DJ-1

4.1 Introduction and Aims

After establishing the interaction between both proteins and its regulation through hypoxia, we aimed to elucidate the functional implications of an interaction between DJ-1 and 14-3-3β. A well-established activity of 14-3-3 proteins is to regulate the subcellular localisation of its binding partners (Zha et al., 1996) (Yoshida et al., 2005) (Jang et al., 2009). DJ-1 is present in various subcellular compartments including the cytosol and mitochondria (Bjorkblom et al., 2014; Cali et al., 2015; Canet-Aviles et al., 2004; Kato et al., 2013; Maita et al., 2013). Although the targeting mechanism for DJ-1 is not clear, mitochondrial localisation was found to be enhanced upon oxidative stress (Canet-Aviles et al., 2004) or ischemic insult (Kaneko et al., 2014a), suggesting a regulatory mechanism for the translocation of DJ-1 into mitochondria. We therefore decided to examine whether 14-3-3β is implicated in the regulation of the localisation of DJ-1 to mitochondria. Interestingly, mitochondrial DJ-1 provided enhanced cytoprotection against H_2O_2-induced cell death when compared to untargeted DJ-1 (Junn et al., 2009). Thus targeting of endogenous DJ-1 to mitochondria may offer a new strategy for a neuroprotective treatment.

To determine whether 14-3-3β plays a role in the intracellular localisation of DJ-1, we generated stable cell lines with reduced or increased expression of 14-3-3β and studied them under normoxic or hypoxic conditions. The knockdown of 14-3-3β will be mediated by RNA interference using stable expression of shRNA, and the overexpression will be achieved through stable expression of a 14-3-3β transgene (see table 2.4). To determine the localisation of DJ-1, we performed subcellular fractionation to separate the mitochondrial and cytosolic compartments, in the stable cell lines.

4.2 Generation of stable cell lines

In order to test the effect of 14-3-3β on the localisation of DJ-1 we established cell lines that stably express either shRNA against human 14-3-3β (sh14-3-3β) or a scrambled, non-targeting shRNA (Scr). For downstream functional analysis, a DJ-1 knockdown cell line was

also generated. For each cell line four to six single colonies were expanded to test for stable transgene expression.

4.2.1 Verification of knockdown and overexpression of stable cell lines

The knockdown of the sh1433β and shDJ1 cell lines was assessed in an initial screen using WB analysis (Figure 4.1). Clones number 1 and 2 of the sh1433β cell lines and all clones of the shDJ1 cell lines revealed prominent knockdown compared to the control cell lines. Scr clone 3, sh1433β clone 1, and shDJ1 clone 3 were quantified for knockdown efficiency and used in further experiments. The quantification confirmed 14-3-3β levels of 35.7 ± 8.6% (mean ± SEM in % Scr, Figure 4.2A) for sh1433β, as well as DJ-1 levels of 2.3 ± 1.3% (mean ± SEM in % Scr, Figure 4.2B) for shDJ1.

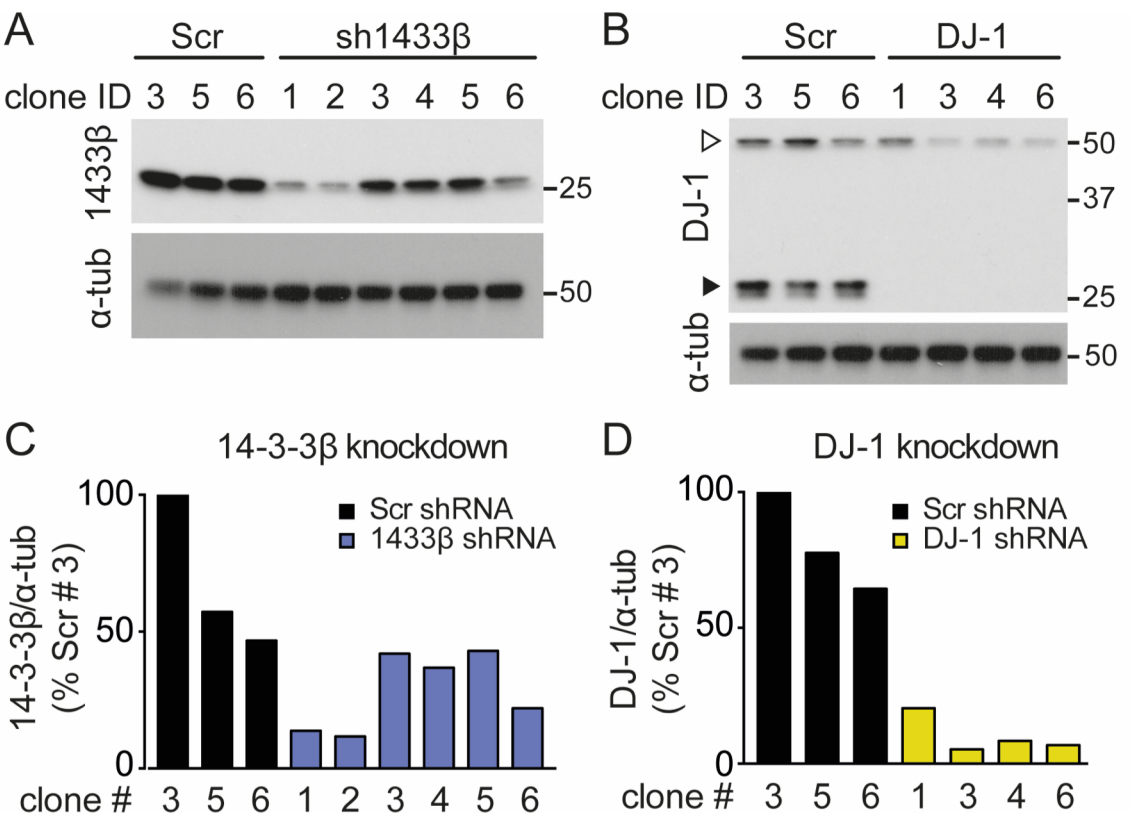


Figure 4.1 – Generation of stable knockdown cell lines. HEK293T cells were transfected with pGIPZ-hScr (Scr), pGIPZ-shRNA-sh1433β (sh1433β) or pGIPZ-shRNA-hDJ1 plasmids. Cells were selected with puromycin and single cell clones were amplified and tested for the expression level of 14-3-3β (A, C) and total DJ-1 (B,D). The data is derived from a single experiment and clone 3 of the Scr cell line, clone 1 of the 14-3-3β shRNA cell line and clone 3 of the DJ-1 shRNA cell line were further assessed for knockdown efficiency and used in all subsequent experiments. Total DJ-1 refers to monomer (black arrowhead) and dimer (transparent arrowhead).

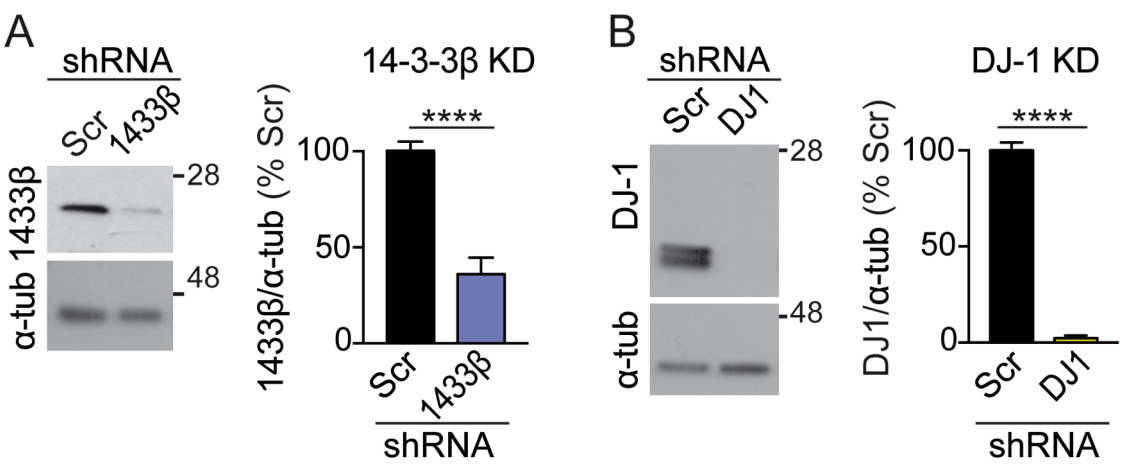


Figure 4.2 – Quantification of knockdown efficiency. The knockdown efficiency of clone 1 of the 14-3-3β shRNA cell line (A) and clone 3 of the DJ-1 shRNA cell line (B) was analysed relative to clone 3 of the Scr cell line. Expression level of 14-3-3β is reduced to 35.7 ± 8.6% (A) and of DJ-1 is reduced to 2.3 ± 1.3% (B) relative to Scr. Protein levels were quantified relative to α-tubulin (α-tub). The data represents six (A) and three (B) independent experiments (displayed as mean ± SEM, unpaired two-tailed t-test, ****p<0.0001).

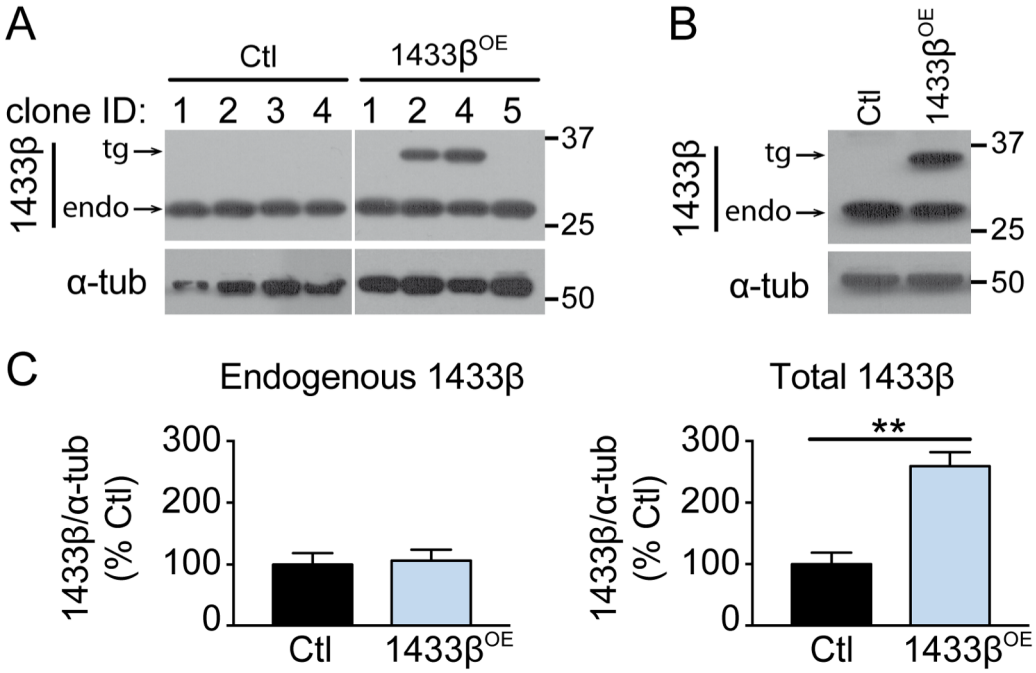


Figure 4.3 – Generation and verification of stable 14-3-3β overexpression cell lines. HEK293 cells were transfected with pcDNA3-flag-HA-h1433b (14-3-3β^{OE}) or pcDNA3.1 vector (Ctl). Cells were selected with G418 and single cell clones were amplified and tested for overexpression of 14-3-3β (A). Clone 1 of the Ctl cell lines and clone 4 of the 14-3-3β^{OE} cell lines were quantified for 14-3-3β expression levels (B,C) and used for all subsequent experiments. A) The data is derived from a single experiment. B,C) The data represents three independent experiments. Endogenous 14-3-3β (C, left panel) expression is unaltered in 14-3-3β^{OE} relative to Ctl meanwhile total 14-3-3β levels are 259 ± 22% of Ctl (C, right panel) (mean ± SEM, n=3, unpaired t-test, **p<0.01), tg: transgene, endo: endogenous.

The overexpression levels of 14-3-3β in the stable cell lines were assessed in 4 clones by WB, of which clones 2 and 4 revealed prominent overexpression of the transgene (Figure 4.3 A). Clone 4 of the 14-3-3β^{OE} cell line and clone 1 of the control (Ctl) cell line were quantified for 14-3-3β expression levels and used in further experiments. The total amount of 14-3-3β was increased to 259 ± 22% (represented as mean ± SEM relative to Ctl, Figure 4.3 B,C) in 14-3-3β^{OE}. No change was found in the expression level of endogenous 14-3-3β between 14-3-3β^{OE} and Ctl cell lines.

4.3 Translocation studies

4.3.1 Knockdown of 14-3-3β increases mitochondrial levels of DJ-1

To test the effect of 14-3-3β on the cellular localisation of DJ-1, we performed subcellular fractionation using the stable Scr and sh1433β cell lines. We further tested the effect of hypoxia on the mitochondrial translocation of DJ-1 in both cell lines. In line with previous results (Kaneko et al., 2014a), mitochondrial levels of DJ-1 in the Scr cell line were significantly increased under hypoxia (mean ± SEM in % Scr Nor: 328 ± 27%, Figure 4.4). More importantly, under normoxia the knockdown of 14-3-3β caused a significant increase of mitochondrial DJ-1 relative to Scr (mean ± SEM in % Scr Nor: 434 ± 54%, Figure 4.4). In contrast, under hypoxic conditions no difference was found in the mitochondrial levels of DJ-1 between Scr and sh1433β cell lines, indicating that the effect of 14-3-3β on mitochondrial localisation of DJ-1 is regulated in a hypoxia-sensitive manner. In addition, hypoxia did not result in further increase of mitochondrial levels of DJ-1 in sh1433β cell lines (Figure 4.4), suggesting that the remaining pool of cytosolic DJ-1 is maintained by 14-3-3β-independent mechanisms. The total levels of DJ-1 were unchanged between both cell lines although there was a small but not significant increase of DJ-1 expression under hypoxia (Figure 4.4). The cytosolic levels of DJ-1 were slightly reduced in the sh1433β cell line but the difference was not significant (Figure 4.4). The expression of the mitochondrial marker Tom40 relative to α-tubulin was unchanged between the cell lines and conditions although we noted a different

Tom40 band pattern between normoxia and hypoxia, as well as Ctl and 1433β KD in the mitochondrial fraction indicating differences in post-translational modifications (Figure 4.4).

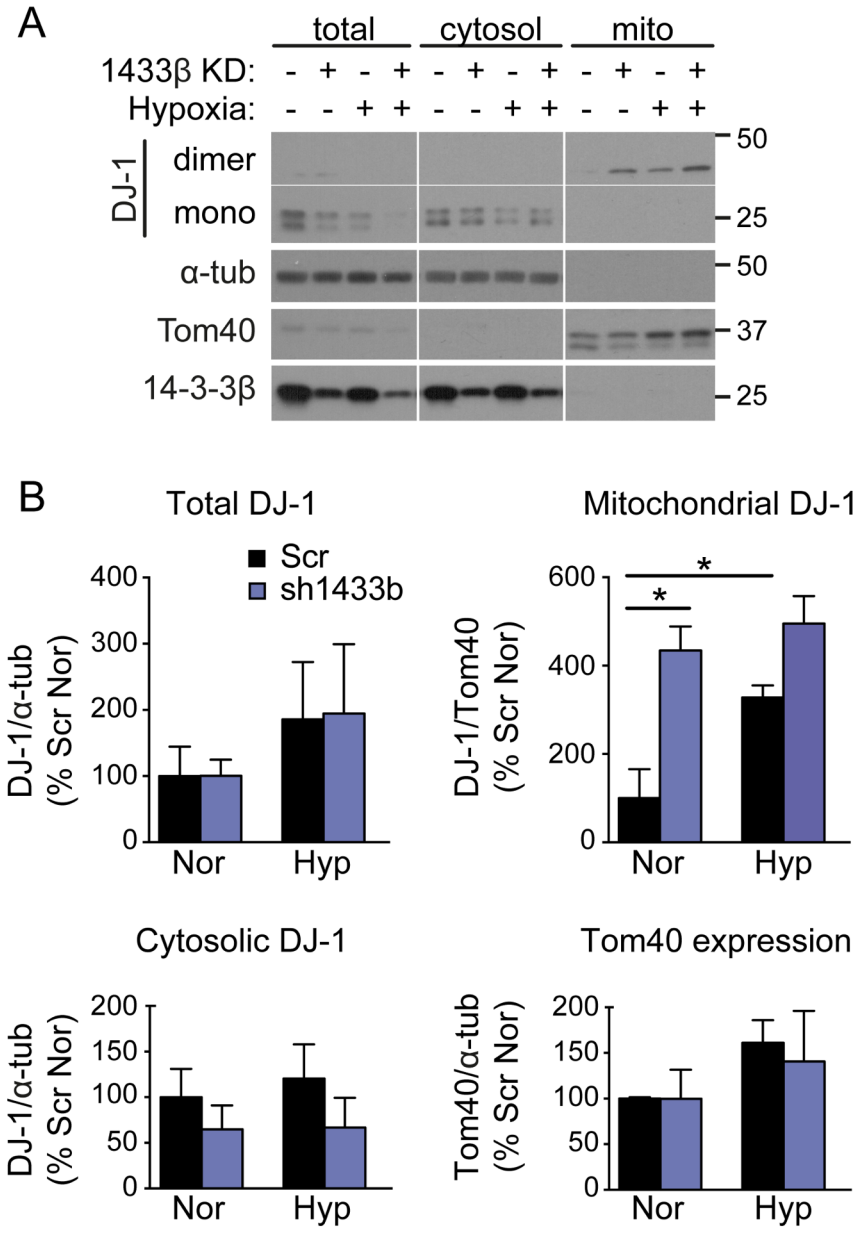


Figure 4.4 – 14-3-3β knockdown enhances the mitochondrial levels of DJ-1. Stable 14-3-3β knockdown (sh1433b) and scrambled shRNA (Scr) cell lines were exposed to 24 h normoxia (Nor) or hypoxia (Hyp) and the effect on the localisation of DJ-1 was tested by subcellular fractionation. Total cell lysate, cytosolic and mitochondrial fractions were analysed by WB (A) and DJ-1 levels were quantified relative to α-tubulin for total DJ-1 (monomer and dimer) and cytosolic DJ-1 or Tom40 for mitochondrial DJ-1 (B). 14-3-3β knockdown increases mitochondrial levels of DJ-1 to 434 ± 54% relative to Scr. This effect is mitigated by hypoxia, which increases mitochondrial DJ-1 to 328 ± 27% relative to Norm in Scr, but not in sh1433b cells. Total DJ-1, total Tom40 and cytosolic DJ-1 levels are not significantly different between Scr and 14-3-3β knockdown cell lines. The data is representative of three independent experiments (mean ± SEM, n=3, one-way ANOVA with Sidak's post hoc test, *p<0.05), KD: knockdown; α-tub: α-tubulin.

4.3.2 Overexpression of 14-3-3β decreases mitochondrial levels of DJ-1

To confirm the effect of 14-3-3β on the mitochondrial localization of DJ-1, we next tested the effect of 14-3-3β overexpression. We performed the subcellular localization experiments (described above) using 14-3-3β^{OE} and Ctl cell lines. Overexpression of 14-3-3β significantly inhibited the accumulation of DJ-1 in mitochondria compared to Ctl (mean ± SEM in % Ctl Normoxia: 40.4 ± 6.4%, Figure 4.5). These results suggest enhanced sequestration of DJ-1 by 14-3-3β in the overexpressing cells. Furthermore, 14-3-3β-dependent differences in mitochondrial levels of DJ-1 were abolished by hypoxia (Figure 4.5), indicating that hypoxia abrogated the inhibitory effect of 14-3-3β on DJ-1 accumulation in mitochondria. No 14-3-3β-dependent changes were found for total levels of DJ-1, cytosolic levels of DJ-1, or the expression of the mitochondrial marker ATP5B (Figure 4.5). Importantly, in the Ctl cell lines a substantial amount of DJ-1 was localised to mitochondria in normoxia as opposed to the Scr cell line, where DJ-1 was mostly absent in normoxic mitochondria (compare WB Figure 4.4 and 4.5) indicating cell-specific differences in mitochondrial enrichment of DJ-1. Importantly, while both sets of stable cell lines were made in human embryonic kidney (HEK) cells, they were derived from different strains (HEK293T for knockdown, HEK293 for overexpression). The presence of DJ-1 in normoxic mitochondria in the HEK293 Ctl cell line may also explain the lack of enrichment of mitochondrial DJ-1 under hypoxia in these cells (Figure 4.5). In fact, the quantification of mitochondrial DJ-1 relative to the mitochondrial marker ATP5B shows a downregulation of DJ-1 in hypoxic Ctl cells relative to normoxia. However, we also noticed that hypoxia consistently increased the levels of ATP5B in mitochondria and therefore the apparent decrease of mitochondrial DJ-1 in hypoxic Ctl cells is likely an artefact of normalisation. Taken together, the results suggest that 14-3-3β overexpression inhibits the translocation or accumulation of DJ-1 in mitochondria and that this effect is abolished by hypoxia. Of note, Tom40 could not be employed for mitochondrial normalisation as the mitochondrial levels of this marker were effected both by 14-3-3β overexpression as well as hypoxia (Figure 4.5).

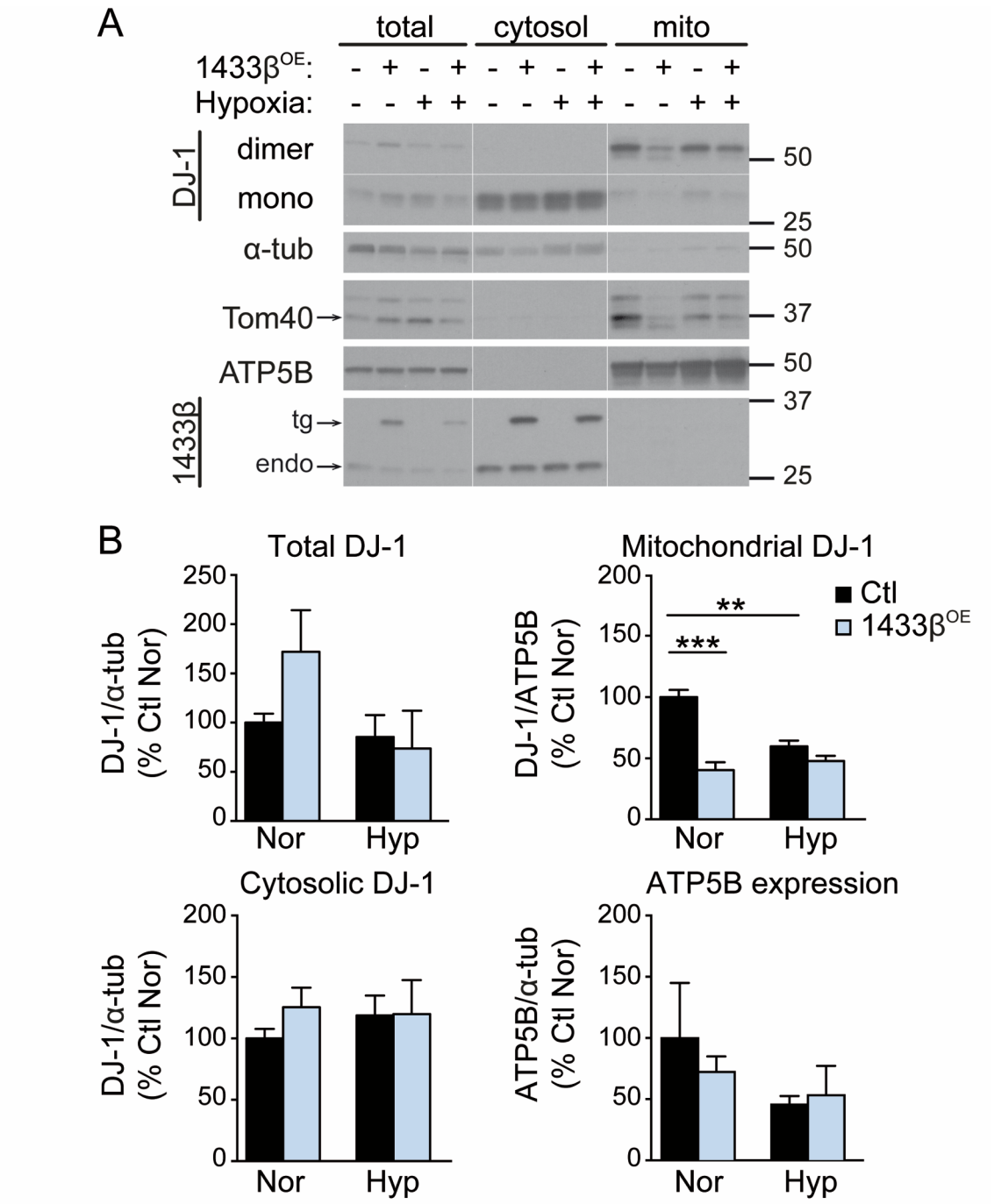


Figure 4.5 – 14-3-3β overexpression decreases the mitochondrial levels of DJ-1. Stable control cells (Ctl) or 14-3-3β^{FlagHA} overexpressing cells (1433β^{OE}) were exposed to 24 h normoxia (Nor) or hypoxia (Hyp) and the effect on the localisation of DJ-1 was tested by subcellular fractionation. Total cell lysate, cytosolic and mitochondrial fractions were analysed by WB (A) and DJ-1 levels were quantified relative to α-tubulin for total DJ-1 and cytosolic DJ-1 or ATP5B for mitochondrial DJ-1 (B). Where present, monomer (mono) and dimer DJ-1 were included in the quantification. 14-3-3β overexpression decreases mitochondrial levels of DJ-1 to 40.4 ± 6.4% of Ctl. This effect is abolished by hypoxia, which reduces mitochondrial DJ-1 normalised to ATP5B to 59.7 ± 4.8% relative to normoxia in Ctl, but not in 1433β^{OE} cells. No effect of 14-3-3β overexpression was found on levels of total DJ-1, total ATP5B or cytosolic DJ-1 (B). The data represents three independent experiments (mean ± SEM, n=3, one-way ANOVA with Sidak's post hoc test, **p<0.01, ***p<0.001). α-tub: α-tubulin; ATP5B: beta subunit of mitochondrial ATP synthase; tg: transgene; endo: endogenous.

4.4 Summary and discussion

Several groups have studied the trafficking of DJ-1 under various stress conditions (Bjorkblom et al., 2014; Canet-Aviles et al., 2004; Joselin et al., 2012; Kaneko et al., 2014b). Albeit a number of structural elements on DJ-1 have been identified to be important for mitochondrial translocation (Maita et al., 2013), no mechanism is reported to date that could explain the preferential localisation of DJ-1 in different subcellular compartments. Our results show that 14-3-3β negatively regulates the levels of mitochondrial DJ-1. 14-3-3β is a member of the 14-3-3 phospho-protein binding family that is known to regulate protein translocation for a subset of its interaction partners (Beguin et al., 2006; Gardino and Yaffe, 2011; Jang et al., 2009; Zha et al., 1996). Release of 14-3-3-sequestered proteins may be caused by dephosphorylation of the binding partner or by phosphorylation of a regulatory residue on 14-3-3 (Yoshida et al., 2005). Our binding studies using phospho-mimicking and phospho-deficient mutants revealed that Ser^{161} on DJ-1 might be implicated in phosphorylation-dependent binding to 14-3-3β. Importantly, the binding studies also revealed that hypoxia abrogated the binding of DJ-1 to 14-3-3β. This is in line with the finding that hypoxia alleviated the repressive effect of 14-3-3β on the mitochondrial levels of DJ-1, indicating that hypoxia-driven signalling events are causative for the translocation of DJ-1 into mitochondria. In summary, our data argues for a direct role of 14-3-3β binding and sequestration of DJ-1 in the cytosol of HEK cells.

Future studies are required to identify the kinases and phosphatases that regulate the binding and release, respectively of DJ-1 from 14-3-3β. Our binding studies showed that phosphorylation of Ser^{161} of DJ-1, a putative target site for Akt, can mediate enhanced binding to 14-3-3β. While phosphorylation of DJ-1 by Akt has not been reported to date, Akt and DJ-1 were shown to interact via the adaptor protein striatin-3 (Tanti and Goswami, 2014). These studies, however found that the complex formation was facilitated by oxidative

stress, correlated with an enhanced localisation of DJ-1 and Akt in mitochondria and membranes. This argues against an Akt-mediated binding of DJ-1 to 14-3-3β. Of note, these studies were performed in mouse neuroblastoma cell lines and we cannot exclude cell specific differences in signalling mechanisms.

In order to be released from 14-3-3β during hypoxia, dephosphorylation of DJ-1 is the most likely mechanism. It was shown that expression of the protein phosphatase 2A (PP2A) is induced in neurons upon intermittent hypoxia (Chen et al., 2014). Interestingly, the scaffold protein striatin-3, which facilitates interaction between DJ-1 and Akt, has also been implicated in regulation of the activity and substrate selectivity of PP2A (Moreno et al., 2000). PP2A is therefore a promising target for the regulated release of DJ-1 from 14-3-3β during hypoxia.

Mechanistically, 14-3-3β may inhibit DJ-1 translocation into mitochondria by stabilising dimer formation. This hypothesis is supported by several reports that found enhanced mitochondrial import of DJ-1 upon disruption of the dimer (Bjorkblom et al., 2014; Maita et al., 2013). Interestingly, PD-associated mutant forms of DJ-1 that display decreased dimer formation properties (Repici et al., 2013) were also found constitutively targeted to mitochondria (Bjorkblom et al., 2014; Cali et al., 2015; Maita et al., 2013). In this regard, it is important to mention that the PD-associated mutations of DJ-1 are believed to be loss of function mutations. Accordingly, meanwhile the presence of mitochondrial-targeted wild-type DJ-1 was shown to be most protective compared to nuclear or untargeted DJ-1, the pathologic mutants of DJ-1 do not exhibit cell protective effects (Junn et al., 2009).

The mitochondrial marker Tom40 revealed similar changes in mitochondrial expression as DJ-1 in all our translocation experiments. Tom40 is the central channel of the mitochondrial outer membrane protein translocation complex, which appears as a double band on WB (see Figure 4.4 and 4.5) suggesting the presence of post-translational modifications. In

mitochondrial fractions of hypoxic and 14-3-3β knockdown cells Tom40 expression was shifted towards the slower migrating species (see Figure 4.4), possibly representing a dephosphorylated form. On the other hand, overexpression of 14-3-3β decreased the expression of Tom40 in mitochondria (see Figure 4.5), particularly of the slower migrating species. These findings implicate that the expression of Tom40 may be regulated by similar or the same signalling mechanisms that regulate DJ-1 translocation into mitochondria. Importantly, decreased expression of Tom40 did not generally inhibit import of mitochondrial proteins. For example, the levels of mitochondrial ATP5B, the β subunit of the mitochondrial ATP Synthase, were unaffected by the reduced expression of Tom40 in the 14-3-3β^{OE} cells. Unfortunately, very little is known regarding the regulation of Tom40 during hypoxia. However, several phosphorylation sites have been identified on Tom40 (Schmidt et al., 2011). Phosphorylation of Ser^{54} by PKA was shown to disrupt Tom40 integration into the outer mitochondrial membrane albeit Tom40 precursor can still bind to the OMM (Rao et al., 2012). Another phosphorylation site, Thr^{220} was found to impair pre-sequence binding to and translocation through the central pore of Tom40, although the kinase mediating this phosphorylation is still unknown (Melin et al., 2014).

Finally, although our results strongly suggest a role for 14-3-3β and hypoxia in regulation of mitochondrial levels of DJ-1, neither 14-3-3β deficiency nor hypoxia resulted in ablation of cytosolic DJ-1. Of note, DJ-1 is a protein that is implicated in numerous cellular functions and many different binding partners have been identified that are located in various cellular compartments, including mitochondria, cytosol and the nucleus (Clements et al., 2006; Kim et al., 2009; McNally et al., 2011; van der Brug et al., 2008; Vasseur et al., 2009). It is therefore plausible that a fraction of DJ-1 may reside in the cytosol as part of other complexes. At the same time a pool of freely diffusible DJ-1 can translocate between different subcellular compartments functioning as a stress surveillance factor. In light of this, we propose that 14-3-3β binds to the free pool of cytosolic DJ-1, thereby changing the equilibrium between its cytosolic and mitochondrial levels. This activity, and therefore the

mitochondrial levels of DJ-1, is regulated by as yet undefined cell signalling mechanisms. We further hypothesise that the release of DJ-1 from 14-3-3β, resulting in mitochondrial accumulation of DJ-1, would affect the efficiency of mitochondrial energy metabolism.

5 Results

–

Metabolic co-operation of DJ-1 and 14-3-3β

5.1 Introduction

We have established a novel interaction between DJ-1 and 14-3-3β and found that a complex is formed between the two proteins in a phosphorylation-dependent and hypoxia-sensitive manner. Furthermore, hypoxia-mediated disruption of this interaction or depletion of 14-3-3β enhances the accumulation of DJ-1 in mitochondria (see chapter 4). These findings point towards a role of this interaction in mitochondrial function through the regulation of mitochondrial levels of DJ-1. Several reports support the idea that DJ-1 increases the mitochondrial membrane potential $\Delta\Psi_m$ (Hao et al., 2010; Thomas et al., 2011), possibly by decreasing the opening of the mitochondrial permeability transition pore (mPTP)(Giaime et al., 2012). The mPTP is a mega-channel in the inner mitochondrial membrane, which can be activated by mitochondrial stress, such as ROS or high $Ca2^+$ levels, and allows for unselective exchange of molecules across the IMM (Jonas et al., 2015). A major component of the mPTP is the c-subunit ring of the mitochondrial ATP synthase (Alavian et al., 2014). The ATP synthase is also the main consumer of the proton gradient across the IMM either due to physiologic ATP production (Walker, 2013), or by enzyme-independent (patho)physiologic dissipation of the $\Delta\Psi_m$ in the form of mitochondrial uncoupling (Alavian et al., 2014; Ichas and Mazat, 1998; Jonas et al., 2015; Mnatsakanyan et al., 2016). Because of its positive effect on mitochondrial Ca^{2+} accumulation (Ottolini et al., 2013) and the role as a negative regulator of mitochondrial ROS and mPTP (Giaime et al., 2012), the accumulation of DJ-1 in mitochondria likely results in enhanced production of ATP via mitochondrial OXPHOS. We hypothesised that the mitochondrial accumulation of DJ-1 observed upon 14-3-3β knockdown positively regulates mitochondrial energy production. In contrast, knockdown of DJ-1 would negatively affect OXPHOS, resulting in decreased ATP levels. These changes may subsequently lead to enhanced glycolytic activity.

5.2 Effect of DJ-1 and 14-3-3β on cellular energy metabolism

In order to test the metabolic effect of DJ-1 and 14-3-3β, we assessed $\Delta\Psi_m$ in knockdown cell lines using the fluorescent dye TMRE, which accumulates in mitochondria in a

membrane potential-dependent manner. Furthermore, the effect of DJ-1 and 14-3-3β on cellular ATP was quantified in a chemiluminescent assay. For this assay we used the enzymatic activity of luciferase, which converts non-luminescent luciferin into the luminescent oxyluciferin. For this biochemical reaction the enzyme requires ATP, which is provided by the metabolism of the cells. The assay conditions maintain luciferase and luciferin in excess and therefore, the luminescent signal is directly proportional to the cellular ATP (Crouch et al., 1993). As an alternative source of energy, aerobic glycolysis was assessed based on the levels of the glycolytic end product, lactate. Lactate formation from pyruvate is enhanced in cells with dysfunctional mitochondria or decreased mitochondrial metabolism (Gladden, 2004; Vander Heiden et al., 2009). Secreted lactate levels were tested enzymatically using lactate dehydrogenase (Cahn et al., 1962; Markert, 1984) and the product NADH was quantified spectrophotometrically at 340 nm.

5.2.1 Effect of DJ-1 and 14-3-3β on mitochondrial membrane potential

In order to test, whether DJ-1 and 14-3-3β have an effect on the mitochondrial membrane potential, we compared the fluorescence intensity of TMRE in the stable HEK293T knockdown cell lines by confocal live cell imaging. Scr, shDJ1 and sh1433β cells were loaded with 10 nM TMRE. The DJ-1 deficient mitochondria showed a significantly lower TMRE fluorescence intensity relative to Scr (Figure 5.1), as previously shown by others (Giaime et al., 2012; Hao et al., 2010; Thomas et al., 2011). More interestingly, the mitochondria of sh1433β cells reveal a significant increase of TMRE intensity (Figure 5.1), indicating mitochondrial hyperpolarisation in 14-3-3β-deficient cells compared to Scr. As shown in chapter 4, 14-3-3β knockdown enhances the accumulation of DJ-1 in mitochondria. The alteration of $\Delta\Psi_m$ supports our hypothesis that enhanced levels of mitochondrial DJ-1 caused by 14-3-3β KD increases mitochondrial energy production. The magnitude of the proton gradient, the main determinant of $\Delta\Psi_m$, is defined by a steady-state equilibrium. This equilibrium is maintained by the constant formation of the proton gradient through the electron transport chain and its dissipation mainly through the ATP synthase. Therefore, a change of the equilibrium may be caused by altering the activity of either ETC or ATP

synthase. Although unlikely, an inhibition of $\Delta\Psi_m$ dissipation by the ATP synthase could in principle provoke an increase in $\Delta\Psi_m$. If this were the case, ATP levels would be decreased or glycolysis would be upregulated in sh1433β cells compared to Scr. On the other hand, enhanced $\Delta\Psi_m$ could be caused by increased ETC activity or decreased mitochondrial uncoupling in the form of IMM proton leaks. In this case enhanced $\Delta\Psi_m$ would facilitate OXPHOS and likely enhance the activity of the ATP synthase, which would increase cellular ATP levels and may decrease glycolytic lactate production.

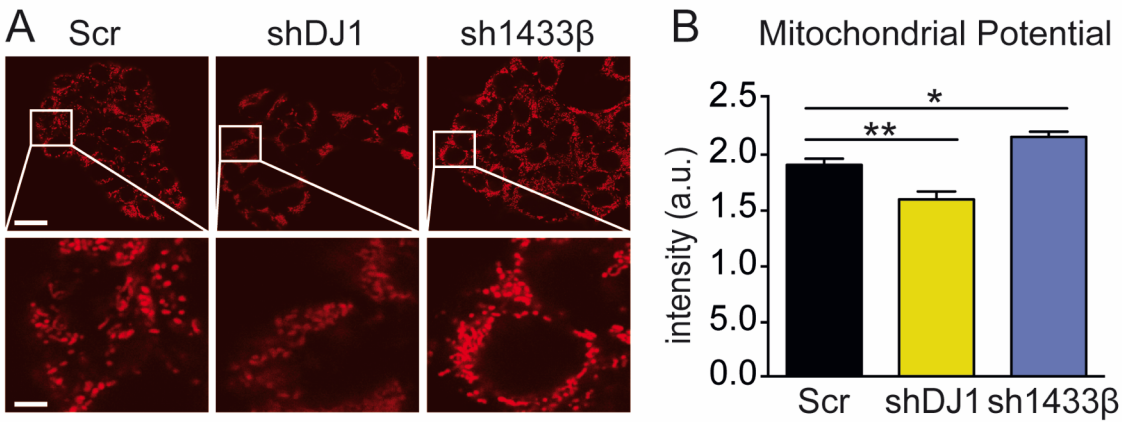


Figure 5.1 – DJ-1 and 14-3-3β knockdown have opposing effects on mitochondrial membrane potential. The mitochondrial membrane potential ($\Delta\Psi_m$) of stable HEK cells expressing either scrambled shRNA (Scr) or shRNA against DJ-1 (shDJ1) and 14-3-3β (sh1433β) was assessed using the dye TMRE. The fluorescence intensity was acquired by confocal microscopy and representative images are depicted in A top panel, with a higher magnification of the boxed area in the bottom panel. Quantification of the peak fluorescence intensity of each mitochondrion, which was averaged for each image, reveals that $\Delta\Psi_m$ is reduced in shDJ1 and increased in sh1433β relative to Scr (B) (mean ± SEM in arbitrary units, Scr: 1.89±0.06, shDJ1: 1.58±0.07, sh1433β: 2.14±0.05). The data is derived from three independent experiments where the total number of pictures for Scr is n=23, shDJ1 is n=30, and sh1433β is n=25 (one-way ANOVA with Dunnett's test for multiple comparison, *p<0.05, **p<0.01). Scale bar top: 100 µm; scale bar bottom: 20 µm. a.u.: arbitrary units.

5.2.2 $\Delta\Psi_m$ differences do not effect ATP levels or glycolytic activity

In order to characterise the effect of altered $\Delta\Psi_m$ in sh1433β cells on cellular energy metabolism and to understand the origin of these differences, we performed ATP measurements after incubation of the cells for 48 h in normoxic or hypoxic conditions. Hypoxia inhibits mitochondrial energy production (Solaini et al., 2010). Therefore, if sh1433β cells perform a higher rate of OXPHOS, we expect hypoxia to mitigate the effect of 14-3-3β

knockdown on ATP levels. In turn, if shDJ1 cells are deficient in mitochondrial energy production, their ATP levels should be less affected by hypoxia. To our surprise, we found no differences in whole-cell ATP levels relative to protein between any of the cell lines or conditions tested. This suggests that adaptive mechanisms are involved in maintaining the cellular energy balance during hypoxia and possibly as well in the knockdown cell lines. The most likely adaptive mechanism that would explain maintained ATP levels is altered glycolytic activity. We therefore tested the levels of lactate. As expected, hypoxia significantly enhanced lactate production in all cell lines (Figure 5.2B), which explains why ATP levels are maintained relative to normoxia. Interestingly, hypoxic lactate production was exacerbated by DJ-1 knockdown relative to Scr, indicating that shDJ1 cells show enhanced glycolytic upregulation under metabolic stress conditions. The increase of lactate under hypoxia was slightly less pronounced in sh1433β cells than in Scr. However, there were no differences in lactate production between Scr and sh1433β or shDJ1 under normoxia. This argues against a role of glycolysis in metabolic adaptation when cells are deficient for DJ-1 or 14-3-3β.

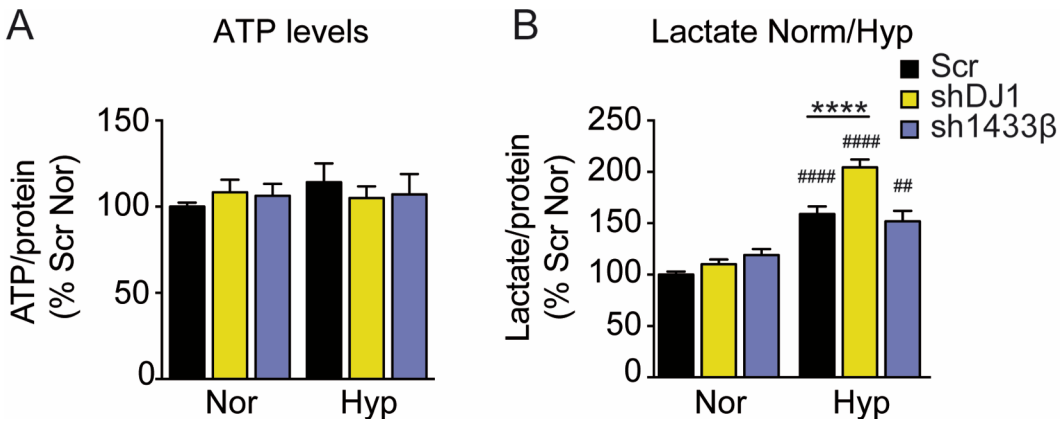


Figure 5.2 – Metabolic analysis of DJ-1 and 14-3-3β knockdown. Stable cell lines were incubated for 48 h in normoxia (Nor) or hypoxia (Hyp). Analysis of whole cell ATP levels relative to total protein revealed no differences between Scr, shDJ1 and sh1433β cell lines (A). Lactate levels of cell supernatant was determined relative to total protein as a surrogate of glycolytic activity (B). Knockdown of DJ-1 or 14-3-3β had no effect on secreted lactate under normoxia. 48h hypoxia significantly increased lactate secretion in all cell lines when compared to normoxia. Hypoxic lactate secretion was exacerbated in shDJ-1 compared to Scr. The data represents 3 independent experiments (mean ± SEM; A: one-way ANOVA, n=8; B: One-way ANOVA with Sidak's test for multiple comparison, Scr: n=17(Nor)/n=18(Hyp), shDJ1: n=19, sh1433β: n=19; ****p<0.0001, $^{\#\#}$p<0.01 relative to Nor, $^{\#\#\#\#}$p<0.0001 relative to Nor).

In summary, sh1433β cell lines show increased $\Delta\Psi_m$ while no change in cellular ATP or lactate production was apparent under normoxic conditions. On the other hand, shDJ1 cells reveal decreased $\Delta\Psi_m$ in absence of ATP and lactate alterations. These results may be explained by two alternative scenarios. The differences of the mitochondrial membrane potential observed with TMRE may not affect the enzymatic activity of the ATP synthase in our stable HEK293T knockdown cell lines. The second possibility is that enhanced production of ATP may be used directly for energy-consuming cellular activities and therefore no change in the steady-state level of ATP can be observed. To address this question, we next aimed at characterising other cell-specific activities.

5.3 Proliferation and cell death

The assessment of cell proliferation may be used as an indirect read-out for the energetic status of the cell. To determine the effects of energetic changes on cellular proliferation, we measured the proliferation using the colorimetric SRB assay. Furthermore, the effect of OXPHOS on cell proliferation was assessed using an inhibitor of the ATP synthase, oligomycin. Using low concentrations, we would be able to assess the sensitivity of the knockdown cell lines to oligomycin-mediated inhibition of mitochondrial ATP production. Finally, the cell death of Scr, shDJ1 and sh1433β was analysed in normoxia and hypoxia. This was necessary because differences in cell death would effect the rate of proliferation and therefore would have to be taken into account when drawing conclusion. The cell viability was assessed using AnnexinV-PI staining and single-cell acquisition by flow cytometry. This allowed for determination of the percentage of viable, early apoptotic, early necrotic and dead cells as outlined in Material and Methods.

5.3.1 $\Delta\Psi_m$ differences alter cell proliferation

We first tested whether the alterations of mitochondrial membrane potential observed in the knockdown cell lines have an effect on cell proliferation. Scr, shDJ1 and sh1433β cell lines

were tested over a period of four days, during which replicate plates were fixed each day after seeding starting with day 0. All values were normalised against the protein amount obtained after seeding (day 0)(Figure 5.3A). As evident from the proliferation curve, sh1433β cells were proliferating faster in both normoxia and hypoxia (blue continuous and interrupted line, respectively) compared to Scr. In contrast, the shDJ1 cells (yellow line) proliferated slightly slower compared to Scr during the first three days. After day three hypoxic cells stopped proliferating, which may be due to either adaptive mechanisms induced by chronic hypoxia or nutrient deprivation caused by enhanced glucose utilisation (see Figure 5.2B). To exclude these adverse effects, we statistically analysed the proliferation at day 3 (Figure 5.3B). The graph shows that 14-3-3β knockdown resulted in a significant increase in proliferation compared to Scr indicating an energetic advantage. Previous lactate analysis showed no difference between both cell lines in aerobic glycolysis (Figure 5.2B). However, the enhanced mitochondrial membrane potential of sh1433β cells suggests enhanced

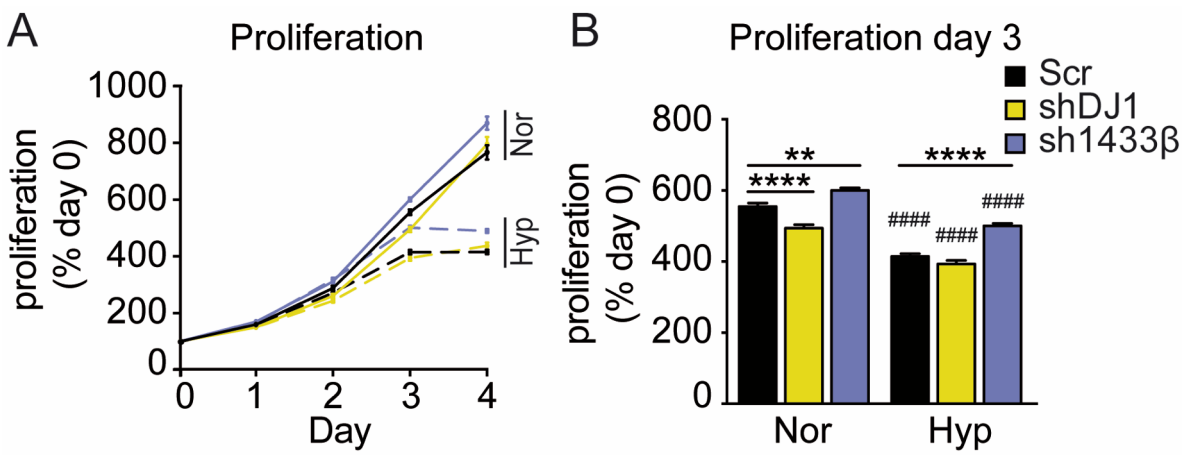


Figure 5.3 – Effect of DJ-1 and 14-3-3β knockdown on cell proliferation. The proliferation of stable Scr and knockdown cell lines was assessed over 4 days under normoxia (Nor) and hypoxia (Hyp). Proliferation curves were generated relative to the cell numbers on day 0 (A). After 3 days the cells are still growing exponentially. After 4 days in culture proliferation rate slows down under most conditions. The proliferation on day 3, plotted as bar graph (B), reveals slower proliferation of shDJ1 cells and faster proliferation of sh1433β cells relative to Scr (mean ± SEM as % day 0; Scr: 534±9.8, shDJ1: 474±9.8, sh1433β: 600±7.1). Hypoxia significantly slows the growth of all cell lines relative to normoxia (mean ± SEM as % day 0; Scr: 414±7.9, shDJ1: 393±9.9, sh1433β: 501±6.8). sh1433β cells maintain a significantly higher proliferation rate in hypoxia compared to Scr. The data is representative of 3 independent experiments. (One-way ANOVA with Sidak's test for multiple comparison, n = 22; **p<0.01, ****p<0.0001, $^{\#\#\#\#}$p<0.0001 relative to normoxia).

OXPHOS activity (Figure 5.1). This result therefore supports the hypothesis that 14-3-3β knockdown enhances mitochondrial ATP production. On the other hand, shDJ1 cells showed a significant decrease of proliferation under normoxia relative to Scr (Figure 5.3B), arguing for a deficiency of OXPHOS. Interestingly, the negative effect of DJ-1 knockdown on cell proliferation relative to Scr was mitigated by hypoxia. This effect is likely mediated by enhanced up-regulation of glycolysis, as evident by exacerbated lactate production of hypoxic shDJ1 cells (Figure 5.2B). Therefor, glycolytic activity may compensate for increased energy deficiency in DJ-1 knockdown cells under energetic stress conditions. Importantly, all cell lines proliferated significantly slower under hypoxia indicating that the fast proliferation of HEK cells generally depends on mitochondrial metabolism. Surprisingly, hypoxia was not sufficient to inhibit the proliferative advantage of 14-3-3β knockdown cells relative to Scr. The lactate results exclude a role of glycolysis as additional energy source for the growth of hypoxic sh1433β cells (see Figure 5.2B). Therefore, we conclude that decreasing the oxygen level to 1% is not effective at reducing the enhanced rate of OXPHOS provoked by 14-3-3β deficiency. This points towards an oxygen independent effect of 14-3-3β knockdown, such as for example decreasing the leak channel activity in the inner mitochondrial membrane.

5.3.2 Oligomycin sensitivity

To confirm that the enhanced growth of sh1433β cells is indeed dependent on mitochondrial energy production, we tested the effect of oligomycin on cell proliferation. Oligomycin is an inhibitor of the F_1F_O ATP synthase that interferes directly with mitochondrial energy production. Stable HEK cells were treated without (untr.) or with 2.5 nM oligomycin (oligo) for 2 days in normoxia or hypoxia and proliferation, ATP levels and lactate were assessed. The proliferation after 2 days was plotted as % day 0 for each condition (Figure 5.4A). ΔP refers to the difference of proliferation between untreated and treated cells under normoxia (ΔP_{Nor}) or hypoxia (ΔP_{Hyp}). The arrow indicates the effect of oligomycin on proliferation. As expected from the TMRE experiment, the negative effect of oligomycin on proliferation is more pronounced in 14-3-3β knockdown cells and less pronounced in DJ-1 knockdown cells compared to Scr in both normoxia and hypoxia. In order to quantify this effect, we plotted ΔP

relative to the proliferation of untreated cells for each condition (Figure 5.4B). The analysis revealed that 14-3-3β knockdown sensitises the cells to oligomycin both under normoxia and hypoxia when compared to Scr. This is in line with our hypothesis that enhanced OXPHOS

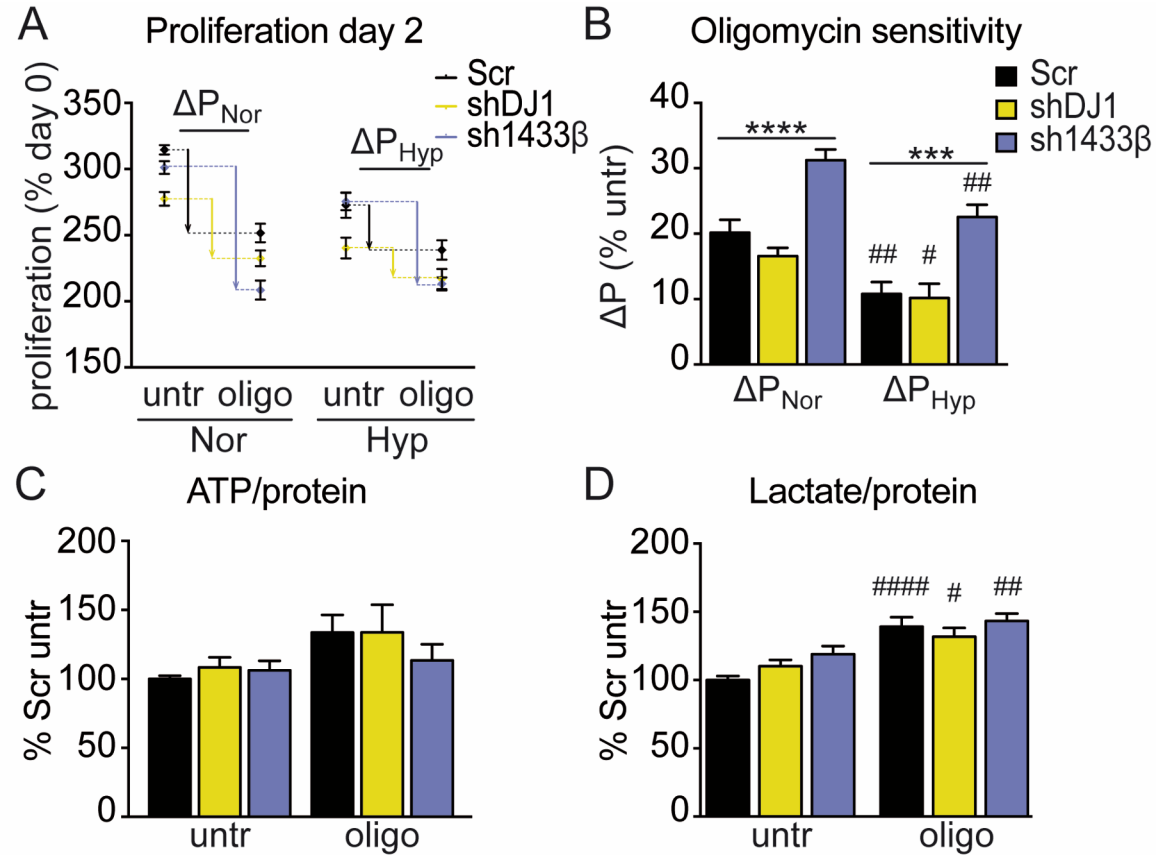


Figure 5.4 – Oligomycin sensitivity of DJ-1 and 14-3-3β knockdown cell lines. To test the role of OXPHOS in proliferation, stable Scr and knockdown cell lines were treated for 2 days without (untr) or with 2.5 nM oligomycin (oligo) in normoxia (Nor) or hypoxia (Hyp). The proliferation was assessed as in figure 5.3 (A) and the difference in proliferation between oligo treated and untreated cells (ΔP) was plotted as % of untreated proliferation (B). sh1433β cells are significantly more inhibited by oligomycin compared to Scr in Nor (mean ± SEM; n=32; Scr: 20.2±1.97, shDJ1: 16.6±1.62, sh1433β: 31.3±1.64). Hypoxia reduces the negative effect of oligomycin in all cell lines (mean ± SEM; Scr: 10.8±1.8, n=23; shDJ1: 10.2±2.18, n=24; sh1433β: 22.6±1.88, n=24). However, sh1433β cells remain significantly more inhibited compared to Scr. Treatment with oligomycin under the same conditions as above has no effect on whole cell ATP levels (C) but enhances the rate of lactate production (D, mean ± SEM as % Scr untr; Scr untr: 100.0±3.0, n=17; shDJ1 untr: 110.1±4.6, n=19; sh1433β untr: 119.0±5.9, n=19; Scr oligo: 139.1±7.0, n=19; shDJ1 oligo: 131.7±6.5, n=19; sh1433β oligo: 143.2±5.4, n=19). However, no significant differences were found between the cell lines. The data represents at least three independent experiments (One-way ANOVA with Sidak's test for multiple comparison; ***p<0.001, ****p<0.0001, $^{\#}$p<0.05 relative to untr, $^{\#\#}$p<0.01 relative to untr, $^{\#\#\#\#}$p<0.0001 relative to untr).

due to 14-3-3β knockdown and accumulation of mitochondrial DJ-1 fuels the proliferation of these cells under normoxia, as well as hypoxia compared to Scr. Furthermore, it consolidates the idea that the positive effect of 14-3-3β knockdown on OXPHOS is likely O_2-independent but ATP synthase-dependent. Hypoxia significantly decreases the sensitivity to oligomycin in all cell lines when compared to normoxia, indicating that 1% O_2 is partially limiting to mitochondrial ATP production. This is in line with the up-regulation of glycolysis that we observed by increased lactate production. Importantly, oligomycin treatment reduced the growth of sh1433β cells to the same or even below the rate of shDJ1 cells (Figure 5.4A). This clearly argues for OXPHOS as an important energy provider in sh1433β cells and is consistent with the enhanced membrane potential observed in this cell line. We therefore suggest that enhanced mitochondrial ATP production contributes towards faster proliferation of sh1433β cells compared to Scr in the presence of high and low oxygen levels. The effect of 2.5 nM oligomycin on shDJ1 proliferation was not significant compared to Scr under either normoxia or hypoxia. However, preliminary results from the dose response experiments of oligomycin on cell proliferation show that higher doses of oligomycin are more effective at down-regulating the growth of Scr cells compared to shDJ1 cells (Supplement S2). These findings suggest that, although OXPHOS is functional in DJ-1 knockdown cells, it probably contributes less to the energy supply of the cells. Finally, similar to hypoxia oligomycin treatment did not alter the levels of ATP between either cell line or condition (Figure 5.4C). Furthermore, lactate levels were unchanged between the cell lines, although an increase in lactate was observed in the treated relative to untreated cell lines (Figure 5.4D). Taken together, this suggests that the cells adapted to ATP synthase inhibition through increased glycolysis and decreased cell growth in favour of maintained ATP levels. Interestingly, whereas hypoxia exacerbated lactate production in shDJ1 relative to Scr, no difference between DJ-1 knockdown and Scr could be observed when treated with oligomycin (compare Figures 5.2D and 5.4D). This points towards a differential metabolic effect of both treatments in DJ-1-deficient cells.

5.3.3 The effect of DJ-1 and 14-3-3β on cell viability

Finally, we assessed the effect of DJ-1 and 14-3-3β knockdown on cell viability. This was necessary to see whether the differences in proliferation would be due to changes in susceptibility to cell death. We performed the AnnexinV-PI co-staining of Scr and knockdown cell lines after incubation for two days in normoxia or hypoxia. The fluorescence intensity of both dyes was acquired by flow cytometry and double negative cells were considered viable. AnnexinV positive cells are referred to apoptotic, PI positive cells are referred to necrotic and double positive cells are considered dead. To assess the total cell death single positive and

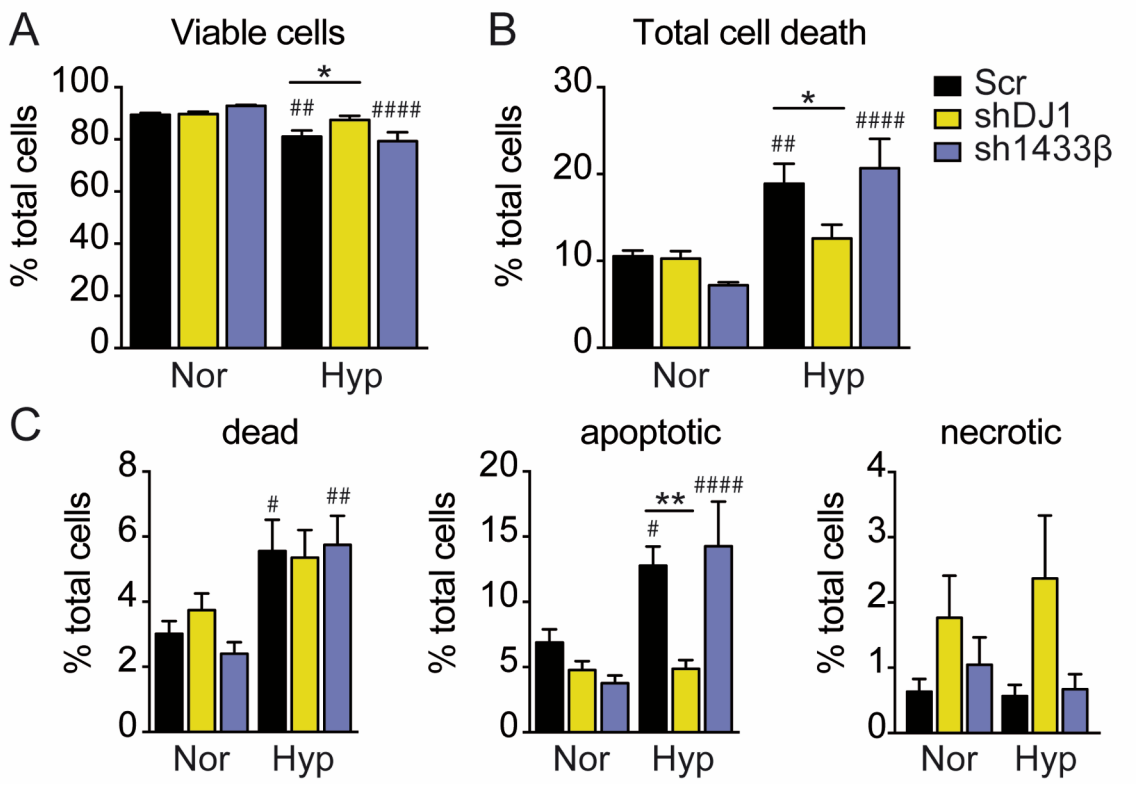


Figure 5.5 – Cell viability of stable cell lines. Viability of stable Scr and knockdown cells was analysed after 2 days in normoxia (Nor) and hypoxia (Hyp) using AnnexinV and PI staining. The double negative populations represent viable cells (A), single and double positive cells were jointly classified as the total cell death (B), with the following subpopulations: double positive are dead, $AnnexinV^+/PI^-$ are apoptotic and $AnnexinV^-/PI^+$ are necrotic (C). No differences were found between the cell lines under normoxia. Hypoxia significantly decreases the viability of Scr and sh1433β cells compared to Nor but not shDJ1 cells (A,B). The higher viability of shDJ1 cells under hypoxia is due to a protection from apoptotic cell death (C). The data represents the mean ± SEM of three (hypoxia) and four (normoxia) independent experiments (One-way ANOVA with Sidak's test for multiple comparison; Nor: n = 12, Hyp: n = 9; *p<0.05, **p<0.01, $^{\#}$p<0.05 relative to Nor, $^{\#\#}$p<0.01 relative to Nor, $^{\#\#\#\#}$p<0.0001 relative to Nor).

double positive populations were combined. All data was presented as % of total cell numbers. The total cell death reflects the inverted percentage of viable cells (Figure 5.5B and A, respectively). We observed no difference in cell death between Scr and either knockdown cell line under normoxia, confirming that the effect of DJ-1 and 14-3-3β knockdown on proliferation is not due to differences in cell viability (Figure 5.5B). Interestingly, hypoxia significantly decreased cell viability of Scr and sh1433β, but not shDJ1 cells relative to normoxia. These findings suggest that under hypoxia both, deficiency of mitochondrial energy production (see Figure 5.4), as well as enhanced cell death (Figure 5.5) contribute to lowered proliferation of Scr and sh1433β cells. In contrast, in DJ-1-deficient cells differences in viability do not contribute to decreased proliferation in hypoxia, suggesting their dependence on non-mitochondrial mechanisms of energy production. We therefore conclude that DJ-1 knockdown has a negative effect on cell proliferation likely through reduced OXPHOS activity or increased mitochondrial uncoupling (Figures 5.1 and S2).

Interestingly, when looking at the sensitivity of shDJ1 and sh1433β cells to apoptotic versus necrotic cell death, we observed a clear tendency of shDJ1 cells towards necrotic cell death with little or no sensitivity for apoptosis. It has been shown that apoptotic cell death is dependent on the availability of ATP, whereas regulated necrosis is favoured when ATP levels are low (Nikoletopoulou et al., 2013; Vanden Berghe et al., 2014). On the other side, mitochondrial hyperpolarisation is often involved in apoptotic cell death (Skulachev, 2006). Hyperpolarisation can also be caused by an accumulation of mitochondrial Ca^{2+}, which is transferred from the ER via ER-mitochondria contact sites (Raturi and Simmen, 2013). Interestingly, DJ-1 was shown to promote these contact sites, thereby increasing the accumulation of Ca^{2+} in mitochondria (Ottolini et al., 2013). It is therefore possible, that the lack of induction of apoptosis in shDJ1 cells is due to a deficiency of Ca^{2+} accumulation in mitochondria. In addition, a link between DJ-1 deficiency and enhanced sensitivity to mitochondrial permeability transition (mPT) was proposed in an earlier study (Giaime et al., 2012). mPT is a form of mitochondrial uncoupling that is often linked to necrotic cell death

(Skulachev, 2006) and increased mPT in DJ-1-deficient cells could explain the tendency of this cell line to undergo necrotic cell death.

5.4 Summary and discussion

Fast proliferating cells need an efficient energy supply to maintain their growth. We have shown that the stable knockdown of 14-3-3β enhances the mitochondrial membrane potential in HEK293T cells and increases the proliferation of these cells in an oligomycin-sensitive manner (see Table 5.1 for overview). In contrast, DJ-1 knockdown cell lines show a reduced membrane potential and decreased proliferation rate. The enhanced proliferation of 14-3-3β knockdown cells was maintained even under hypoxia, indicating an oxygen-independent advantage in proliferation. No differences were observed between the knockdown cell lines and Scr in ATP levels and lactate production except for hypoxia-induced increase of lactate in DJ1-deficient cells relative to Scr.

Table 5.1 – Overview of functional results summarising the differences between knockdown and Ctl cell lines under nomoxia and hypoxia. Increase is indicacted by +, decrease is indicated by -, and = refers to non-significant differences. KD - knockdown

	DJ-1 KD vs Ctl		14-3-3β KD vs Ctl	
Experiment	Nor	Hyp	Nor	Hyp
$\Delta\Psi_m$	-		+	
ATP levels	=	=	=	=
Lactate levels	=	+	=	=
Proliferation	-	= (-)[1]	+	+
Viability	=	+	=	=
Oligomycin sensitivity	= (-)[2]	=	+	+

1 - reduced when considering enhanced viability
2 - at higher concentrations of oligomycin (see Figure S2)

Lactate levels usually rise as a result of enhanced glycolysis or a deficiency of mitochondria to metabolise glycolytic NADH (Solaini et al., 2010). During hypoxia, HIF1 activation is a potent mediator of metabolic adaptation resulting in up-regulation of glycolysis and down-regulation of OXPHOS activity. However, HIF1-dependent gene expression is prevented under normoxia due to HIF1α-hydroxylation by peptidyl prolyl hydroxylases (PHD) and subsequent recognition by the Von Hippel Lindau (VHL) ubiquitin ligase (Solaini et al., 2010; Wheaton and Chandel, 2011; Wise et al., 2011). Interestingly, it was shown that the hypoxia-induced activation of HIF1α and subsequent gene expression is compromised in DJ-1-deficient cells (Vasseur et al., 2009). On the other hand, DJ-1 was shown to directly prevent the interaction of HIF1α to VHL and therefore should mediate protein stability upstream of hypoxia-mediated stabilisation of HIF1α (Parsanejad et al., 2014). Furthermore, aberrant ROS production is a potent inhibitor of HIF1α-destabilising PHDs (Fong and Takeda, 2008). DJ-1 deficiency was shown to result in enhanced mitochondrial ROS production, possibly via incorrect assembly of complex I and decreased formation of respiratory super-complexes (Heo et al., 2012). Therefore, the effect of DJ-1 on HIF1α-mediated gene expression is not entirely resolved. Furthermore, the particular effect of hypoxia on cell signalling is highly dependent on the cellular context and would therefore require a separate investigation (Sermeus and Michiels, 2011).

Interestingly, the response of DJ-1-deficient cells with respect to lactate production was significantly different under hypoxia compared to their responbse to ATP synthase inhibition. Under hypoxia, shDJ1 cells showed significantly higher lactate levels than Scr, whereas under oligomycin treatment, lactate levels were unchanged between both cell lines. Importantly, while both treatments inhibit mitochondrial energy metabolism, hypoxia acts mainly through O_2-mediated inhibition of the ETC whereas oligomycin down-regulates the activity of the ATP synthase. In the context of mitochondria, both treatments have profoundly different effects on the mitochondrial membrane potential. Inhibition of the ETC at complex VI (cytochrome C oxidase) through hypoxia results in a build-up of reduced complexes, which

enhances the chance of pre-mature electron transfer to molecular oxygen and increases the production of mitochondrial ROS (Chandel and Schumacker, 2000; Solaini et al., 2010). Furthermore, the reduced activity of the ETC decreases the $\Delta\Psi_m$. Both, ROS and low $\Delta\Psi_m$ induce the opening of the permeability transition pore, which further dissipates $\Delta\Psi_m$ (Alavian et al., 2014; Jonas et al., 2015; Szabo et al., 1992) and ultimately renders the mitochondria metabolically dysfunctional. The increased lactate production observed in shDJ1 cells suggests that these cells are more sensitive to hypoxia induced $\Delta\Psi_m$ dissipation, which is in line with reports of increased $\Delta\Psi_m$ activity in DJ-1 deficient cells as well as with our unpublished results showing DJ-1-mediated increased mitochondrial coupling. On the other hand, oligomycin inhibition slows the activity of the ATP synthase thereby decreasing the dissipation of the proton gradient across the IMM. Furthermore, oligomycin protects against the opening of the mPTP (Chavez et al., 2005; Shchepina et al., 2002). This suggests that oligomycin treatment, especially at sub-maximal levels, can protect from mitochondrial dysfunction through preventing $\Delta\Psi_m$ dissipation thereby ameliorating the mitochondrial dysfunction caused by DJ-1 knockdown.

Surprisingly, despite the role of OXPHOS in enhancing the proliferation of 14-3-3β knockdown cells, hypoxia did not ameliorate the differences in growth rate. This indicates an oxygen-independent effect of 14-3-3β knockdown on mitochondrial energy metabolism, which could be mediated by enhanced mitochondrial coupling through enrichment of mitochondrial DJ-1. This is supported by the findings indicating a role of DJ-1 in decreasing mitochondrial permeability transition pore opening (Giaime et al., 2012). Furthermore, our own preliminary results suggest decreased leak channel activity and enhanced activity of the ATP synthase in the presence of wildtype DJ-1 but not the PD-associated mutant protein (unpublished data from our lab).

Finally, our experiments show that mitochondrial energy production is not entirely inhibited in the presence of 1% oxygen. Indeed, physiological concentrations of O_2 are below 21%

atmospheric level ranging for example between 1% to 5% in the brain (Erecinska and Silver, 2001). Furthermore, studies in neurons have shown that low oxygen levels (2% to 5%) can promote mitochondrial function, both through cell signalling and possibly through reduced ROS production (Tiede et al., 2011; Zhu et al., 2012). This suggests that future research in cell sciences should aim to better mimic in-vivo oxygen and nutrient supply, especially when investigating mitochondrial pathways and cell metabolism.

6 Conclusions and future directions

6.1 Conclusions

6.1.1 Background and rational

DJ-1 is an important regulator of many cellular activities, including proliferation and metabolism (Im et al., 2012; Kim et al., 2009; Klawitter et al., 2013; Requejo-Aguilar et al., 2015; Shi et al., 2015; Vasseur et al., 2009), regulation of neurotransmitter production (Ishikawa et al., 2009; Ishikawa et al., 2010), maintenance of redox homeostasis (Clements et al., 2006; Cuevas et al., 2015; Im et al., 2012; Malhotra et al., 2008; Vasseur et al., 2009) and mitochondrial function (Giaime et al., 2012; Goldberg et al., 2012; Hao et al., 2010; Heo et al., 2012; Junn et al., 2009; Kaneko et al., 2014a; Kaneko et al., 2014b; Krebiehl et al., 2010; Ottolini et al., 2013; Thomas et al., 2011). The effect of DJ-1 depends on the cellular context resulting in either enhanced proliferation (Kim et al., 2014; Kim et al., 2009; Wang et al., 2014) or protection from cell death (Aleyasin et al., 2010; Canet-Aviles et al., 2004; Dongworth et al., 2014; Fan et al., 2008; Kim et al., 2005b; Martinat et al., 2004; McNally et al., 2011; Sekito et al., 2006; Taira et al., 2004; Waak et al., 2009). Therefore, a role of DJ-1 as an oncogene has been proposed. Furthermore, loss of function mutations in the gene result in early-onset Parkinsonism (Bonifati et al., 2003; Taipa et al., 2016), a disorder known to involve mitochondrial dysfunction as one of the key pathologic processes (Bender et al., 2006; Keeney et al., 2006; Langston et al., 1983; Schapira et al., 1989; Schapira and Jenner, 2011; Subramaniam and Chesselet, 2013; Surmeier et al., 2016). The centrally located Cys^{106} residue of DJ-1 was shown to be prone to oxidative modification (Canet-Aviles et al., 2004; Witt et al., 2008) and is thought to be involved in regulation of the binding of DJ-1 to at least some of its substrates (Cao et al., 2014; Kato et al., 2013; Ren et al., 2011; Zhou et al., 2006). Furthermore, oxidation of Cys^{106} correlates with enhanced levels of DJ-1 in mitochondria and is thought to protect these organelles from dysfunction (Canet-Aviles et al., 2004). On the other hand, mutation of Cys^{106} to serine did not compromise the ability of DJ-1 to accumulate in mitochondria (Junn et al., 2009) indicating that oxidation of Cys^{106} is not critical for mitochondrial translocation. Although oxidative stress enhances mitochondrial

levels of DJ-1 it is not clear whether the oxidation of Cys^{106} occurs in the cytosol prior to translocation to the mitochondria. Importantly, mitochondria naturally produce small amounts of ROS as a by-product of oxidative phosphorylation and ROS may itself regulate the function of DJ-1. Furthermore, the mitochondrial intermembrane space is a highly oxidative environment (Herrmann and Riemer, 2010; Hu et al., 2008) and it seems likely that the translocation of DJ-1 to this compartment would result in oxidative modification of DJ-1 thereby altering its function. On the other hand, DJ-1 regulates the mitochondrial redox state, which was shown to control the balance between oxidative metabolism and glycolysis (Shi et al., 2015). This suggests a role for DJ-1 as a feedback regulator of metabolism.

Interestingly, a study targeting DJ-1 to various subcellular compartments in dopaminergic neuroblastoma cells revealed that mitochondrially targeted DJ-1 is most protective against oxidative insult induced by H_2O_2 (Junn et al., 2009). This indicates that targeting of neuronal DJ-1 to mitochondria may be a new therapeutic strategy for neuroprotection against oxidative stress in neurodegenerative conditions, including Parkinson's disease. Despite extensive knowledge of its functions, very little is known regarding the mechanism, through which DJ-1 is regulated. In particular, besides a requirement for the N-terminus and monomerisation (Maita et al., 2013), no mechanism has been described to date that explains the preferential accumulation of DJ-1 in mitochondria under certain physiologic conditions. A molecular understanding of this mechanism would enable us to directly target DJ-1 to mitochondria, thereby enhancing mitochondrial metabolism and decreasing the sensitivity to mitochondrial pathways of cell-death.

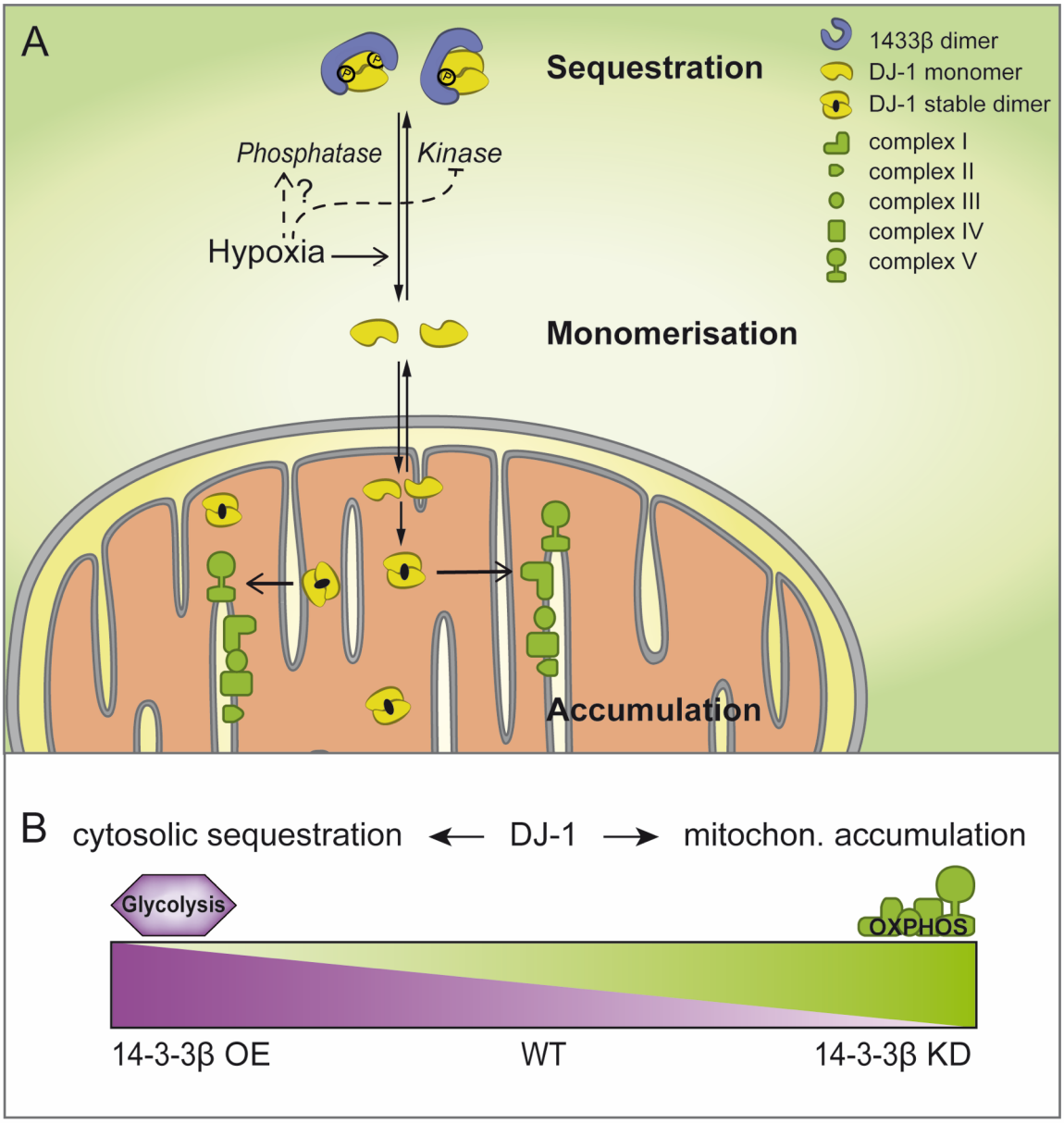


Figure 6. 1 Metabolic regulation by DJ-1 and 14-3-3β. A) Schematic of the effect of 14-3-3β and DJ-1 on mitochondrial energy metabolism during normal cell physiology and the effect of hypoxia on DJ-1 localisation. 14-3-3β stabilises transient cytosolic dimers of DJ-1 in a phosphorylation-dependent manner, which inhibits mitochondrial import. Hypoxia disrupts the interaction between 14-3-3β and DJ-1 thereby triggering cytosolic monomerisation and facilitating mitochondrial import of DJ-1. Inside mitochondria DJ-1 forms stable, SDS-resistant dimers, which contributes to accumulation of DJ-1 in mitochondria in a trapping mechanism. B) The balance of cellular energy metabolism as a function of the localisation of DJ-1.

6.1.2 Results and conclusions

We have established a novel protein-protein interaction between DJ-1 and the β-isoform of the 14-3-3 protein and found that this interaction regulates the accumulation of DJ-1 in mitochondria. Our experiments suggest that 14-3-3β binds to DJ-1 via phosphorylated Ser^{161}. Furthermore, other structural components are likely to be involved in binding because mutation of Ser^{161} to alanine failed to completely abolish the interaction. Interestingly, one of the most severe PD mutations DJ-1^{L166P} resulting in decreased DJ-1 stability (Anderson and Daggett, 2008) is located 5 residues downstream of Ser^{161}. This PD mutation is linked to major structural derangements and would likely effect the binding of interaction partners (Anderson and Daggett, 2008). The phospho-protein binding 14-3-3 proteins are structurally and mechanistically conserved (Fu et al., 2000; Obsil and Obsilova, 2011; Yaffe et al., 1997) but show an enormous functional flexibility (Coblitz et al., 2006; Kleppe et al., 2011; Meek et al., 2004; Shimada et al., 2013) with dynamic re-arrangement, when cellular conditions are changing (Weerasekara et al., 2014). In line with this, we found that the binding between DJ-1 and 14-3-3β is partially disrupted by hypoxia, suggesting that the interaction participates in metabolic adaptation of the cells to hypoxic stress. Indeed, we could show that 14-3-3β inhibits the accumulation of DJ-1 in mitochondria under normal conditions and that this function of 14-3-3β is disrupted by hypoxia. This is consistent with the finding that hypoxia abrogates the binding between both proteins and suggests that 14-3-3β is a regulator of DJ-1 localisation. Interestingly, disruption of the transient DJ-1 dimer in the cytosol was proposed to occur prior to the translocation of DJ-1 into mitochondria (Bjorkblom et al., 2014; Maita et al., 2013) and mutation of key residues within the dimer interface was shown to enhance mitochondrial levels of DJ-1 (Maita et al., 2013). 14-3-3 proteins form dimers with each other (Obsil and Obsilova, 2011; Yaffe et al., 1997; Yang et al., 2006) and can mediate or stabilise dimer formation of phosphorylated proteins. Therefore, we propose that stabilisation of a transient cytosolic DJ-1 dimer by binding to 14-3-3β is the mechanism, through which DJ-1 is sequestered in the cytosol under normal conditions. Most PD mutations of DJ-1 were found to disrupt dimer formation in vitro (Repici et al., 2013) and are

found constitutively localised to mitochondria, including the DJ-1^{L166P} mutant (Cali et al., 2015). We have shown that DJ-1^{L166P} does not bind to 14-3-3β. These findings are consistent with our model that 14-3-3β negatively regulates the levels of mitochondrial DJ-1 in our system. Unfortunately, very little is known about the localisation and dimerisation properties of DJ-1 in vivo. Importantly, 14-3-3 proteins are mediators of cell signalling events through their binding to phosphorylated proteins, thereby conveying signalling events into functional changes (Datta et al., 2000; Gardino and Yaffe, 2011; Jang et al., 2009; Johnson et al., 2010; Kleppe et al., 2011; Kosaki et al., 1998; Muslin et al., 1996; Pozuelo Rubio et al., 2003; Sato et al., 2002; Shinoda et al., 2003; Tzivion et al., 2001). Preliminary studies using inhibitors directed against kinases, including PDK1, an upstream activator of Akt (Li et al., 2013) with binding sites on DJ-1, and GSK3, a hypoxia-sensitive kinase that was shown to regulate mitochondrial Ca^{2+} uptake (Gomez et al., 2016), did not alter the binding between DJ-1 and 14-3-3β (results not shown). Nevertheless, the phosphorylation-dependent interaction that occurs between the two proteins *in vitro* suggests that cell-signalling cues are implicated in the regulation of the subcellular localisation of DJ-1.

Our experiments have shown that the translocation of DJ-1 resulted in accumulation in mitochondria with little or no effect on cytosolic levels of DJ-1. This may be explained by the maintenance of cytosolic levels at a steady state by changes in expression and degradation, while mitochondrial localisation could inhibit degradation of DJ-1. To date, no mitochondrial protease is known to degrade DJ-1, whereas cytosolic levels of DJ-1 are controlled by the ubiquitin-proteasome system (Gorner et al., 2007; Song et al., 2016). Interestingly, the proteasomal degradation of DJ-1 was shown to be promoted by structural changes caused by either oxidation (Song et al., 2016) or destabilising mutations of the C-terminal helix-kink-helix motif (Gorner et al., 2007). Although the 14-3-3-binding residue Ser^{161} of DJ-1 is adjacent to the helix-kink-helix motif, we could not observe a significant effect of 14-3-3β on the stability of DJ-1. However, the negative effect of the helix-kink-helix motif on protein stability may be limited to specific mutants of DJ-1, such as the instable PD-linked mutant

DJ-1^{L166P} (Anderson and Daggett, 2008), since the effect of this motif on protein stability has not been shown with wildtype DJ-1 yet.

Given the role of DJ-1 (Giaime et al., 2012; Kim et al., 2005a; Meiser et al., 2016; Requejo-Aguilar et al., 2015; Shi et al., 2015; Vasseur et al., 2009) and 14-3-3β (Bunney et al., 2001; DeYoung et al., 2008; Gwinn et al., 2008; Kleppe et al., 2011; Kosaki et al., 1998; Liao et al., 2005; Pozuelo Rubio et al., 2004; Pozuelo Rubio et al., 2003; Puri et al., 2008; Schoenwaelder et al., 2016; Shumway et al., 2003; Vander Haar et al., 2007; Weerasekara et al., 2014) in regulation of metabolism we hypothesised that the interaction between these proteins has a metabolic function. This idea was supported by the hyperpolarization of the mitochondrial membrane potential in the 14-3-3β knockdown cells and their enhanced sensitivity to oligomycin. On the other hand, DJ-1 knockdown had a negative effect on $\Delta\Psi_m$, which is consistent with other studies (Giaime et al., 2012). 14-3-3β knockdown causes the translocation of DJ-1 into mitochondria, which suggests that DJ-1 may be the factor that causes the increase of $\Delta\Psi_m$ in the 14-3-3β knockdown cells. Although we cannot exclude additional DJ-1-independent mechanisms, our findings argue for a role of 14-3-3β in down-regulation of mitochondrial energy metabolism through sequestration of DJ-1 in the cytoplasm. DJ-1, on the other hand, enhances mitochondrial energy metabolism possibly through inhibition of mitochondrial ROS (Canet-Aviles et al., 2004; Giaime et al., 2012; Goldberg et al., 2012; Meiser et al., 2016) as well as enhanced ETC activity (Hayashi et al., 2009; Heo et al., 2012). We therefore propose that the binding between DJ-1 and 14-3-3β regulates the balance of cellular energy metabolism at the level of OXPHOS activity.

6.1.3 Impact

The regulation of cellular energy metabolism is important to ensure an adequate response of the cell to nutrient and oxygen supply as well as to growth stimuli and cell activation. In the case of differentiated cells, OXPHOS is the main energy-producing pathway (Agathocleous and Harris, 2013; Hom et al., 2011; McGraw and Mittal, 2010; Wahl et al., 2012). However, when cells enter the cell cycle mitochondrial metabolism is partially diverted at the level of

the TCA cycle, which produces amino acids for cell growth (Ahn and Metallo, 2015; DeBerardinis et al., 2008; Vander Heiden et al., 2009; Wallace, 2012). Under such a condition, glycolysis may become an important supplier of energy for the cell. The prime example of this scenario occurs in cancer cells that usually sustain high glycolytic activity and lowered OXPHOS under aerobic conditions, the so-called Warburg effect (Warburg, 1956). We now know that mitochondria are not generally dysfunctional in cancer cells, but rather serve the role of biosynthetic factories instead of the conventional function as power plants (Ahn and Metallo, 2015; Cairns et al., 2011; Sullivan et al., 2015; Vander Heiden et al., 2009; Wallace, 2012). Interestingly, both DJ-1 (Kim et al., 2005a; Kim et al., 2009; Nagakubo et al., 1997; Wang et al., 2014) and 14-3-3 proteins (Cao et al., 2015; Gardino and Yaffe, 2011; Morrison, 2009; Shumway et al., 2003) are considered oncogenes, due to their positive effect on cell proliferations and resistance to death stimuli. Hence, the finding that 14-3-3β and DJ-1 have opposing effects on metabolism appeared contradictory. However, kinase signalling is often impaired in cancer (Cairns et al., 2011) and it is possible that at least in some tumours, binding of DJ-1 to 14-3-3β is impaired in the absence of cellular stress. If this is the case, the functions of DJ-1 and 14-3-3β become independent of each other to promote different aspects of tumour formation, such as protection from ROS (Clements et al., 2006; Im et al., 2012) and resistance to cell death (Datta et al., 2000; Zha et al., 1996), respectively. According to our data, the dissociation of DJ-1 from 14-3-3β enhances mitochondrial levels of DJ-1, which correlates with increased mitochondrial function and protection against ROS-induced cell death. Because the binding of DJ-1 to 14-3-3β has an inhibitory effect on the mitochondrial function of DJ-1, it seems likely that this interaction is disrupted at least in some types of cancer. If this is the case, restoring the interaction between both proteins through pharmacological intervention of the phosphatase or kinase activity that regulate DJ-1 binding to 14-3-3β may be a suitable strategy to reduce tumour growth and to enhance the sensitivity of cancer cells to radiotherapy.

Energy metabolism is also highly regulated in differentiated cells in order to match ATP production to the energy requirements of the cell as well as to adapt metabolism to varying substrate levels. In general, OXPHOS is thought to meet the basal energetic needs, whereas glycolysis can rapidly and transiently provide the cell with additional ATP. When ATP requirements increase for longer periods, mitochondrial biogenesis is initiated to ameliorate the energy deficiency (Jornayvaz and Shulman, 2010; Scarpulla et al., 2012; Wu et al., 1999). Neurons, however, are believed to depend mainly on mitochondrial energy metabolism, particularly during activation (Pellerin and Magistretti, 2012) and therefore energetic requirements have to be regulated by other means. Importantly, glucose is the main substrate for neuronal energy metabolism but in contrast to astrocytes or muscle cells, neurons do not regulate glucose uptake through the expression level of the glucose transporter at the plasma membrane (Mergenthaler et al., 2013). Furthermore, neurons have little or no capacity to store energy in form of fatty acids or glycogen and rely therefore on a constant supply of glucose from the blood. Therefore, the balance between ATP production and utilisation is met directly at the level of mitochondria. This may occur by various mechanisms including the activity- and calcium-dependent regulation of substrate flux through TCA cycle and ETC (Del Arco et al., 2016; Denton, 2009; Llorente-Folch et al., 2015), the Ca^{2+}- and ROS-sensitive uncoupling of oxidation from phosphorylation (also known as mitochondrial uncoupling) (Gorlach et al., 2015; Jonas et al., 2015), as well as the dynamic movement of mitochondria to hot spots of neuronal activity (Mironov, 2007; Wang and Schwarz, 2009). Meanwhile substrate flux and mitochondrial dynamics are aimed at enhancing ATP levels, mitochondrial uncoupling is a rescue mechanism that protects mitochondria from over-activation at the cost of energy dissipation. Finally, mitochondrial biogenesis and degradation are important for meeting long-term amendments to energetic requirements and to remove dysfunctional mitochondria (Liesa and Shirihai, 2013). The latter is particularly important because dysfunctional mitochondria increase the stress burden of a cell and are vulnerable to the release of apoptotic factors (Suen et al., 2008; Van Laar and Berman, 2013). Due to the formation of ROS as a by-product correlating with mitochondrial

activity, as well as the related mitochondrial uncoupling, mitochondrial energy production can become limiting to neuronal activity. We propose that dynamic translocation of DJ-1 into mitochondria may provide a mechanism, through which neurons regulate their oxidative metabolism. DJ-1 enhances mitochondrial tolerance to high Ca^{2+} levels (Ottolini et al., 2013) and reduces ROS (Shi et al., 2015), thereby increasing both substrate flux (Shi et al., 2015) and mitochondrial coupling (Giaime et al., 2012). On the molecular level DJ-1 was shown to enhances complex I activity (Hayashi et al., 2009; Heo et al., 2012) and studies from our lab have shown binding and activation of the ATP synthase by DJ-1 (data not shown). This simultaneous regulation is beneficial since it stimulates both $\Delta\Psi_m$ formation through enhanced substrate entry into the ETC as well as $\Delta\Psi_m$ dissipation through the final ATP producing mechanism.

However, when energy demands are low, mitochondrial uncoupling may be relevant to dissipate ETC-stimulating high intra-mitochondrial calcium thereby avoiding unwanted substrate depletion. Furthermore, mitochondrial uncoupling decreases high $\Delta\Psi_m$, which otherwise may contribute to excess ROS formation and mitochondrial fatigue. Hence, down-regulation of mitochondrial energy metabolism during low activity is equally important for neuronal health and survival as up-regulation of OXPHOS when energy needs are high. Several other factors have been described to fulfil such a regulatory role on OXPHOS. Bcl-x_L for example, was shown to enhance the efficiency of mitochondrial energy production through the closure of a leak channel at the ATP synthase, thereby enhancing mitochondrial coupling (Alavian et al., 2011; Chen et al., 2011). Interestingly, in plants 14-3-3 proteins where shown to directly inhibit mitochondrial and chloroplast ATP synthase by binding to the β subunit of F_1. This mechanism was proposed to facilitate the adaptation of energy metabolism to changing environmental conditions, such as during dark adaptation of chloroplasts (Bunney et al., 2001). A similar mechanism has not been described for mammalian mitochondria yet. Instead, we have shown that 14-3-3β inhibits mitochondrial metabolism indirectly through sequestration of DJ-1 in the cytoplasm. Importantly, targeting of DJ-1 to mitochondria was shown to enhance the protective effect of DJ-1 against oxidative

stress in a dopaminergic cell line. We therefore propose that mitochondrial targeting of DJ-1 by interfering with the binding to 14-3-3β may be suitable as a new therapeutic strategy for neuroprotection in PD. Dopaminergic neurons affected in PD show increased ROS formation, possibly due to enhanced cytosolic calcium levels and a concomitant over-activation of mitochondrial energy metabolism (Surmeier and Schumacker, 2013; Surmeier et al., 2016). Furthermore, dopaminergic neurons from the substantia nigra pars compacta have a very elaborate axonal network with significantly more synapses then other dopaminergic neurons (Pacelli et al., 2015). These features are likely to pre-dispose these neurons to mitochondrial deficiency and energetic failure. In addition, other Parkinson's disease causative protein variants have been shown to interfere with mitochondrial function (Devi et al., 2008; Morais et al., 2014; Narendra and Youle, 2011; Su et al., 2015; Wang et al., 2012), placing mitochondria in the spotlight of PD pathogenesis. Interestingly, a DJ-1-derived peptide enclosing residues 12 to 24 fused to the HIV tat protein translocation sequence (TAT) was shown to provide neuroprotection in the 6-hydroxydopamine and MPTP mouse models of PD (Lev et al., 2015). Although the intracellular localisation of this peptide was not investigated in this study, the TAT sequence is known to mediate translocation into mitochondria in the absence of a mitochondrial targeting sequence (Rapoport et al., 2008). Hence, it is possible that the protective effects observed with this peptide are at least partially due to a positive effect on mitochondrial function. However, the peptide only comprises α-helix 1 of DJ-1 and it is unlikely that this relatively small sequence can replace all of the protective activities that have been ascribed to DJ-1. Therefore, targeting of the full-length DJ-1 to mitochondria may provide additional and possibly superior protection against neuronal insult.

6.2 Future directions

Our experiments consistently demonstrate that translocation of DJ-1 into mitochondria is regulated by 14-3-3β and hypoxia. Furthermore, our functional experiments have shown that both proteins differentially regulate mitochondrial energy metabolism and we speculate that

this is mediated by mitochondrial localisation of DJ-1. The enhanced mitochondrial energy metabolism under conditions where DJ-1 is enriched in mitochondria is consistent with the literature showing a direct effect of DJ-1 on OXPHOS (Hayashi et al., 2009). However, to this point we cannot exclude a DJ-1-independent effect of 14-3-3β knockdown on mitochondrial metabolism. To answer this question mitochondrial energy metabolism would have to be tested when the cells are deficient for both DJ-1 and 14-3-3β. Meanwhile the shRNA-mediated double knockdown by both transient transfection and viral transduction has been achieved in HEK cells, both methods failed to produce consistent results when using mitochondrial membrane potential assays with TMRE (data not shown). A stable knockdown using bicistronic expression of both shRNAs on the same selectable plasmid could be performed to avoid transfection- or transduction-induced stress.

In order to consider targeting of DJ-1 to mitochondria a rational target for the development of a pharmacologic treatment against Parkinson's disease, several open questions have to be addressed. Firstly, the regulation of the interaction between DJ-1 and 14-3-3β has to be characterised in more detail. Particularly, the kinase and phosphatase that regulate the phosphorylation-dependent binding of DJ-1 to 14-3-3β need to be identified, not only to understand the biological pathway but to be able to modulate the localisation of DJ-1 in vivo. Many kinases are structurally and pharmacologically well characterised, which may be of advantage for the development of new treatments. Secondly, a more detailed analysis of secondary structural components of DJ-1 that induce or inhibit the binding of 14-3-3β may be helpful for structure-guided development of small molecule inhibitors. And finally but most importantly, it is of utter importance to test the sub-cellular localisation of DJ-1 in human brain. Many studies report a mostly cytosolic localisation of DJ-1 with translocation occurring under stress conditions. However, these studies were exclusively performed in cell culture, where cells are grown under a surplus of substrates and oxygen levels that are far above the native situation inside the brain. Furthermore, under physiologic conditions in the brain SNpc dopaminergic neurons are constantly firing, which imposes an increased energy demand on

mitochondria. Therefore, the native localisation of DJ-1 in brain needs to be tested in tissue sections at subcellular resolution. Importantly, it was reported that the levels of DJ-1 in idiopathic PD is decreased compared to healthy control. Although it is not clear to date what causes the decline of DJ-1 in the brain of PD patients, one could speculate that impaired translocation of DJ-1 to mitochondria and a lack of subsequent stabilisation might be responsible for this observation. Furthermore, if translocation of DJ-1 is impaired in idiopathic PD, then this is likely to cause mitochondrial deficiency, one of the hallmarks of PD. The subcellular localisation of DJ-1 in human brain can be determined using immunofluorescent co-labelling of DJ-1 and mitochondria in post-mortem brain of PD patients and healthy controls. To address the question whether DJ-1 turnover is indeed different in mitochondria and the cytosol, stable isotope labelling in cell culture (SILAC) with subsequent cellular fractionation may be a suitable method (Boisvert et al., 2012; Larance et al., 2013).

7 Supplement

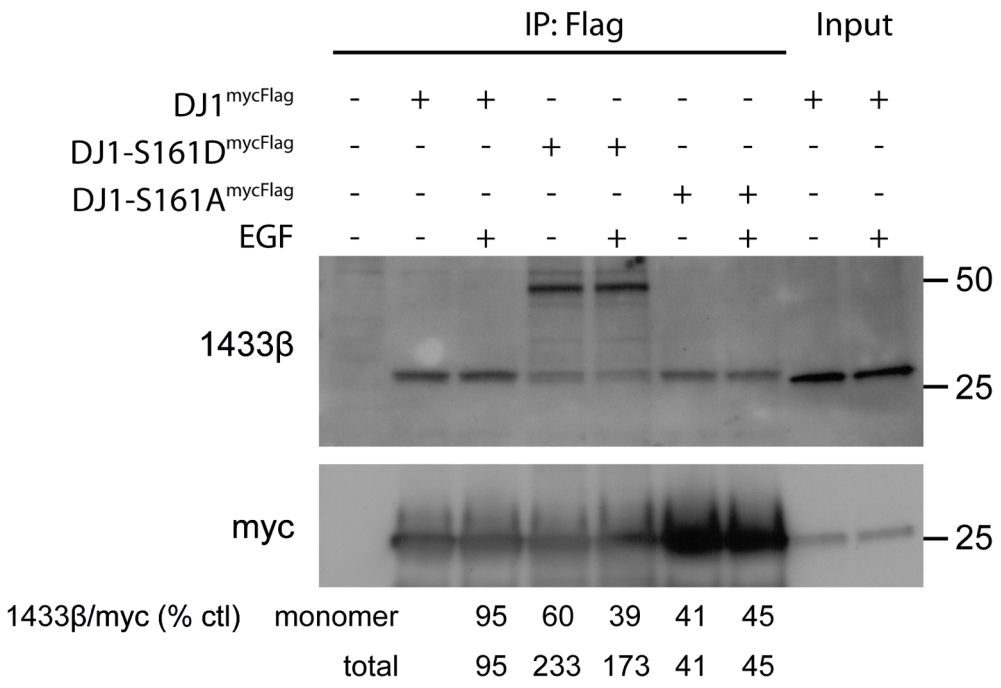


Figure S1 – Effect of EGF on the interaction of DJ-1 with 14-3-3β. Flag immunoprecipitation from DJ-1^{mycFlag} containing HEK293T lysates. Cells were starved for 24h with 1% FBS and treated with 1µg/ml EGF for 1h prior to IP. WB and quantification of 14-3-3β and myc. Values are displayed as % relative to 14-3-3β monomer/myc of Ctl. Monomer refers to the single or double band at 25 kDa and dimer refers to the single band at 50 kDa. EGF: epidermal growth factor.

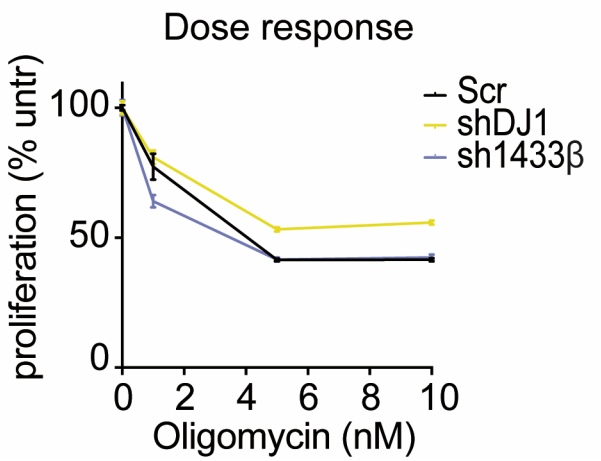


Figure S2 – Oligomycin dose response in stable knockdown cell lines. Stable HEK293T Scr and knockdown cell lines were seeded in 96-well replicate plates. Medium was replaced after 24h (day 0) and the cells were treated for two days with various concentrations of oligomycin. Cells were fixed on day 0 and day 2 after treatment and cell proliferation relative to day 0 was assessed by SRB assay. The data represents 8 replicates of one experiment.

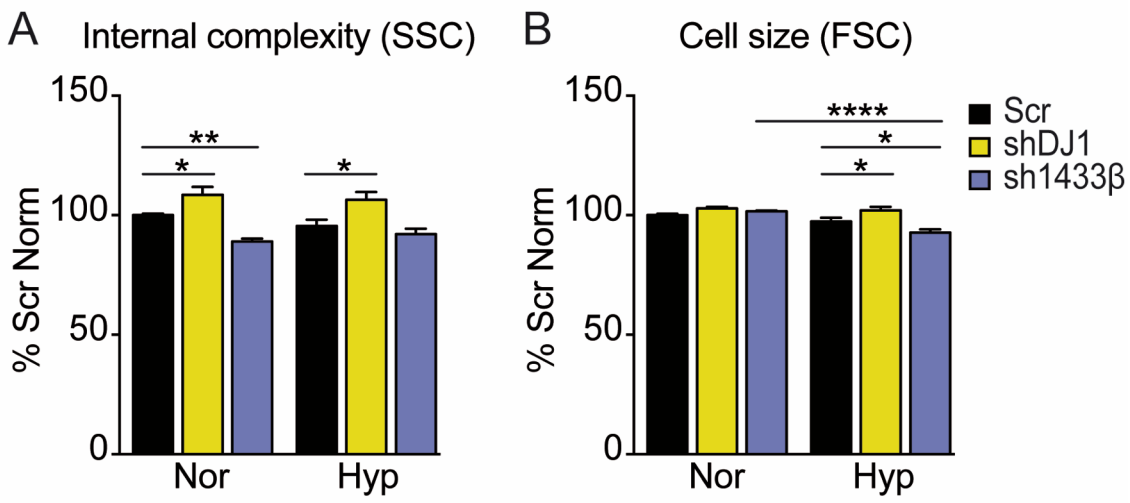


Figure S3 – Cell size and internal complexity of stable knockdown cell lines. Stable HEK293T Scr and knockdown cell lines were kept for 24h in normoxia (Nor) or hypoxia (Hyp) prior to harvesting. Cells were subjected to flow cytometry. Cell size estimated by forward scatter and internal complexity estimated by the side scatter were plotted relative to Scr Nor. The data represents the mean ± SEM of 3 independent experiments (One-way ANOVA with Sidak's test for multiple comparison, Nor: n = 12, Hyp: n = 9, *p<0.05, **p<0.01).

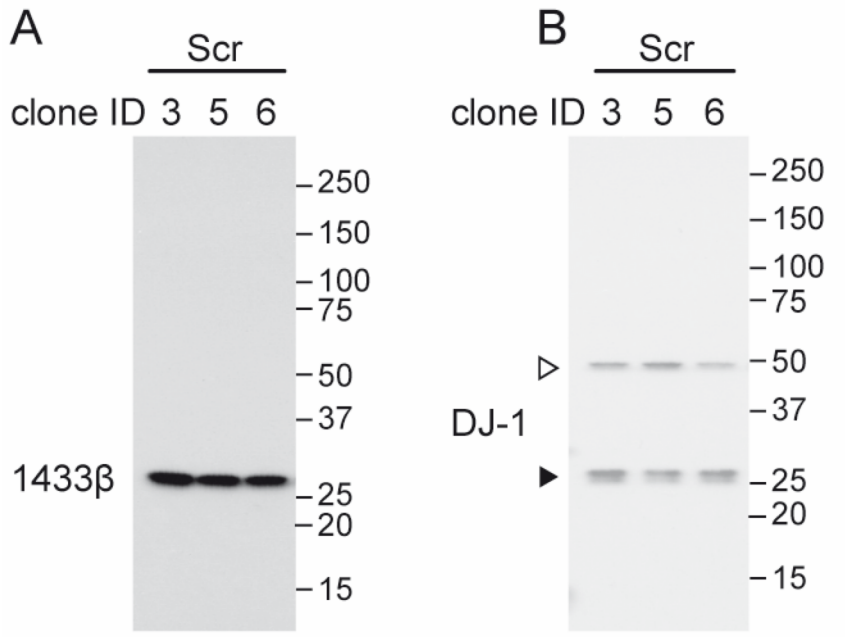


Figure S4 – Antibody specificity. Whole western blot of HEK293T Scr clones were incubated with 14-3-3β (A) and DJ-1 (B) antibody. 14-3-3β antibody shows one specific band with an apparent molecular weight of 27 kDa, corresponding to the size of 14-3-3β protein. DJ-1 antibody shows specific bands at 25 kDa (double band, black arrowhead) corresponding to the size of monomeric DJ-1 and at 50 kDa (transparent arrowhead) corresponding to the size of dimeric DJ-1.

References

Regulation of Cellular Energy Metabolism by DJ-1 and 14-3-3β Implications for Parkinson's Disease.

Agarwal-Mawal, A., Qureshi, H.Y., Cafferty, P.W., Yuan, Z., Han, D., Lin, R., and Paudel, H.K. (2003). 14-3-3 connects glycogen synthase kinase-3 beta to tau within a brain microtubule-associated tau phosphorylation complex. J Biol Chem *278*, 12722-12728.

Agathocleous, M., and Harris, W.A. (2013). Metabolism in physiological cell proliferation and differentiation. Trends Cell Biol *23*, 484-492.

Ah Mew, N., Lanpher, B.C., Gropman, A., Chapman, K.A., Simpson, K.L., Urea Cycle Disorders, C., and Summar, M.L. (1993). Urea Cycle Disorders Overview. In GeneReviews(R), R.A. Pagon, M.P. Adam, H.H. Ardinger, S.E. Wallace, A. Amemiya, L.J.H. Bean, T.D. Bird, C.T. Fong, H.C. Mefford, R.J.H. Smith*, et al.*, eds. (Seattle (WA)).

Aharon-Peretz, J., Rosenbaum, H., and Gershoni-Baruch, R. (2004). Mutations in the glucocerebrosidase gene and Parkinson's disease in Ashkenazi Jews. N Engl J Med *351*, 1972-1977.

Ahn, C.S., and Metallo, C.M. (2015). Mitochondria as biosynthetic factories for cancer proliferation. Cancer Metab *3*, 1.

Alam, R., Hachiya, N., Sakaguchi, M., Kawabata, S., Iwanaga, S., Kitajima, M., Mihara, K., and Omura, T. (1994). cDNA cloning and characterization of mitochondrial import stimulation factor (MSF) purified from rat liver cytosol. J Biochem *116*, 416-425.

Alavian, K.N., Beutner, G., Lazrove, E., Sacchetti, S., Park, H.A., Licznerski, P., Li, H., Nabili, P., Hockensmith, K., Graham, M.*, et al.* (2014). An uncoupling channel within the c-subunit ring of the F1FO ATP synthase is the mitochondrial permeability transition pore. Proc Natl Acad Sci U S A *111*, 10580-10585.

Alavian, K.N., Li, H., Collis, L., Bonanni, L., Zeng, L., Sacchetti, S., Lazrove, E., Nabili, P., Flaherty, B., Graham, M.*, et al.* (2011). Bcl-xL regulates metabolic efficiency of neurons through interaction with the mitochondrial F1FO ATP synthase. Nat Cell Biol *13*, 1224-1233.

Aleyasin, H., Rousseaux, M.W., Marcogliese, P.C., Hewitt, S.J., Irrcher, I., Joselin, A.P., Parsanejad, M., Kim, R.H., Rizzu, P., Callaghan, S.M.*, et al.* (2010). DJ-1 protects the nigrostriatal axis from the neurotoxin MPTP by modulation of the AKT pathway. Proc Natl Acad Sci U S A *107*, 3186-3191.

Ames, A., 3rd (2000). CNS energy metabolism as related to function. Brain Res Brain Res Rev *34*, 42-68.

Anderson, P.C., and Daggett, V. (2008). Molecular basis for the structural instability of human DJ-1 induced by the L166P mutation associated with Parkinson's disease. Biochemistry *47*, 9380-9393.

Andrabi, S.A., Umanah, G.K., Chang, C., Stevens, D.A., Karuppagounder, S.S., Gagne, J.P., Poirier, G.G., Dawson, V.L., and Dawson, T.M. (2014). Poly(ADP-ribose) polymerase-dependent energy depletion occurs through inhibition of glycolysis. Proc Natl Acad Sci U S A *111*, 10209-10214.

Andres-Mateos, E., Perier, C., Zhang, L., Blanchard-Fillion, B., Greco, T.M., Thomas, B., Ko, H.S., Sasaki, M., Ischiropoulos, H., Przedborski, S.*, et al.* (2007). DJ-1 gene deletion reveals that DJ-1 is an atypical peroxiredoxin-like peroxidase. Proc Natl Acad Sci U S A *104*, 14807-14812.

Applegate, M.A., Humphries, K.M., and Szweda, L.I. (2008). Reversible inhibition of alpha-ketoglutarate dehydrogenase by hydrogen peroxide: glutathionylation and protection of lipoic acid. Biochemistry *47*, 473-478.

Arselin, G., Vaillier, J., Salin, B., Schaeffer, J., Giraud, M.F., Dautant, A., Brethes, D., and Velours, J. (2004). The modulation in subunits e and g amounts of yeast ATP synthase modifies mitochondrial cristae morphology. J Biol Chem *279*, 40392-40399.

Azoulay-Zohar, H., Israelson, A., Abu-Hamad, S., and Shoshan-Barmatz, V. (2004). In self-defence: hexokinase promotes voltage-dependent anion channel closure and prevents mitochondria-mediated apoptotic cell death. Biochem J *377*, 347-355.

Bai, Y., Zhou, T., Fu, H., Sun, H., and Huang, B. (2012). 14-3-3 interacts with LKB1 via recognizing phosphorylated threonine 336 residue and suppresses LKB1 kinase function. FEBS Lett *586*, 1111-1119.

Baker, L.A., Watt, I.N., Runswick, M.J., Walker, J.E., and Rubinstein, J.L. (2012). Arrangement of subunits in intact mammalian mitochondrial ATP synthase determined by cryo-EM. Proc Natl Acad Sci U S A *109*, 11675-11680.

Balaban, R.S., Nemoto, S., and Finkel, T. (2005). Mitochondria, oxidants, and aging. Cell *120*, 483-495.

Barbeau, A. (1962). The pathogenesis of Parkinson's disease: a new hypothesis. Can Med Assoc J *87*, 802-807.

Bardos, J.I., and Ashcroft, M. (2005). Negative and positive regulation of HIF-1: a complex network. Biochimica et biophysica acta *1755*, 107-120.

Bartlett, K., and Eaton, S. (2004). Mitochondrial beta-oxidation. European journal of biochemistry / FEBS *271*, 462-469.

Batelli, S., Invernizzi, R.W., Negro, A., Calcagno, E., Rodilossi, S., Forloni, G., and Albani, D. (2015). The Parkinson's disease-related protein DJ-1 protects dopaminergic neurons in vivo and cultured cells from alpha-synuclein and 6-hydroxydopamine toxicity. Neurodegener Dis *15*, 13-23.

Baughman, J.M., Perocchi, F., Girgis, H.S., Plovanich, M., Belcher-Timme, C.A., Sancak, Y., Bao, X.R., Strittmatter, L., Goldberger, O., Bogorad, R.L.*, et al.* (2011). Integrative genomics identifies MCU as an essential component of the mitochondrial calcium uniporter. Nature *476*, 341-345.

Bean, B.P. (2007). The action potential in mammalian central neurons. Nature reviews Neuroscience *8*, 451-465.

Becker, T., Bottinger, L., and Pfanner, N. (2012). Mitochondrial protein import: from transport pathways to an integrated network. Trends Biochem Sci *37*, 85-91.

Beguin, P., Mahalakshmi, R.N., Nagashima, K., Cher, D.H., Ikeda, H., Yamada, Y., Seino, Y., and Hunziker, W. (2006). Nuclear sequestration of beta-subunits by Rad and Rem is controlled by 14-3-3 and calmodulin and reveals a novel mechanism for Ca2+ channel regulation. Journal of molecular biology *355*, 34-46.

Belanger, M., Allaman, I., and Magistretti, P.J. (2011). Brain energy metabolism: focus on astrocyte-neuron metabolic cooperation. Cell Metab *14*, 724-738.

Belenguer, P., and Pellegrini, L. (2013). The dynamin GTPase OPA1: more than mitochondria? Biochimica et biophysica acta *1833*, 176-183.

Bender, A., Krishnan, K.J., Morris, C.M., Taylor, G.A., Reeve, A.K., Perry, R.H., Jaros, E., Hersheson, J.S., Betts, J., Klopstock, T.*, et al.* (2006). High levels of mitochondrial DNA deletions in substantia nigra neurons in aging and Parkinson disease. Nature genetics *38*, 515-517.

Bento, C.F., Ashkenazi, A., Jimenez-Sanchez, M., and Rubinsztein, D.C. (2016). The Parkinson's disease-associated genes ATP13A2 and SYT11 regulate autophagy via a common pathway. Nat Commun *7*, 11803.

Berg, D., Holzmann, C., and Riess, O. (2003a). 14-3-3 proteins in the nervous system. Nature reviews Neuroscience *4*, 752-762.

Berg, D., Postuma, R.B., Adler, C.H., Bloem, B.R., Chan, P., Dubois, B., Gasser, T., Goetz, C.G., Halliday, G., Joseph, L.*, et al.* (2015a). MDS research criteria for prodromal Parkinson's disease. Mov Disord *30*, 1600-1611.

Berg, D., Riess, O., and Bornemann, A. (2003b). Specification of 14-3-3 proteins in Lewy bodies. Annals of neurology *54*, 135.

Berg, J.M., Tymoczko, J.L., Gatto, G.J., and Stryer, L. (2015b). Biochemistry, Eighth edition. edn (New York: W.H. Freeman & Company, a Macmillan Education Imprint).

Beurel, E., Grieco, S.F., and Jope, R.S. (2015). Glycogen synthase kinase-3 (GSK3): regulation, actions, and diseases. Pharmacol Ther *148*, 114-131.

Bhangoo, M.K., Tzankov, S., Fan, A.C., Dejgaard, K., Thomas, D.Y., and Young, J.C. (2007). Multiple 40-kDa heat-shock protein chaperones function in Tom70-dependent mitochondrial import. Molecular biology of the cell *18*, 3414-3428.

Bindoff, L.A., Birch-Machin, M., Cartlidge, N.E., Parker, W.D., Jr., and Turnbull, D.M. (1989). Mitochondrial function in Parkinson's disease. Lancet *2*, 49.

Birsoy, K., Wang, T., Chen, W.W., Freinkman, E., Abu-Remaileh, M., and Sabatini, D.M. (2015). An Essential Role of the Mitochondrial Electron Transport Chain in Cell Proliferation Is to Enable Aspartate Synthesis. Cell *162*, 540-551.

Bjorkblom, B., Maple-Grodem, J., Puno, M.R., Odell, M., Larsen, J.P., and Moller, S.G. (2014). Reactive oxygen species-mediated DJ-1 monomerization modulates intracellular trafficking involving karyopherin beta2. Molecular and cellular biology *34*, 3024-3040.

Blackinton, J., Kumaran, R., van der Brug, M.P., Ahmad, R., Olson, L., Galter, D., Lees, A., Bandopadhyay, R., and Cookson, M.R. (2009). Post-transcriptional regulation of mRNA associated with DJ-1 in sporadic Parkinson disease. Neuroscience letters *452*, 8-11.

Blesa, J., and Przedborski, S. (2014). Parkinson's disease: animal models and dopaminergic cell vulnerability. Front Neuroanat *8*, 155.

Boerries, M., Most, P., Gledhill, J.R., Walker, J.E., Katus, H.A., Koch, W.J., Aebi, U., and Schoenenberger, C.A. (2007). Ca2+ -dependent interaction of S100A1 with F1-ATPase leads to an increased ATP content in cardiomyocytes. Molecular and cellular biology *27*, 4365-4373.

Boisvert, F.M., Ahmad, Y., Gierlinski, M., Charriere, F., Lamont, D., Scott, M., Barton, G., and Lamond, A.I. (2012). A quantitative spatial proteomics analysis of proteome turnover in human cells. Mol Cell Proteomics *11*, M111 011429.

Bonifati, V., Rizzu, P., van Baren, M.J., Schaap, O., Breedveld, G.J., Krieger, E., Dekker, M.C., Squitieri, F., Ibanez, P., Joosse, M.*, et al.* (2003). Mutations in the DJ-1 gene associated with autosomal recessive early-onset parkinsonism. Science *299*, 256-259.

Bonifati, V., Rohe, C.F., Breedveld, G.J., Fabrizio, E., De Mari, M., Tassorelli, C., Tavella, A., Marconi, R., Nicholl, D.J., Chien, H.F.*, et al.* (2005). Early-onset parkinsonism associated with PINK1 mutations: frequency, genotypes, and phenotypes. Neurology *65*, 87-95.

Bonora, M., Wieckowski, M.R., Chinopoulos, C., Kepp, O., Kroemer, G., Galluzzi, L., and Pinton, P. (2015). Molecular mechanisms of cell death: central implication of ATP synthase in mitochondrial permeability transition. Oncogene *34*, 1475-1486.

Bouman, L., Schlierf, A., Lutz, A.K., Shan, J., Deinlein, A., Kast, J., Galehdar, Z., Palmisano, V., Patenge, N., Berg, D.*, et al.* (2011). Parkin is transcriptionally regulated by ATF4: evidence for an interconnection between mitochondrial stress and ER stress. Cell Death Differ *18*, 769-782.

Bove, J., and Perier, C. (2012). Neurotoxin-based models of Parkinson's disease. Neuroscience *211*, 51-76.

Braak, H., Del Tredici, K., Rub, U., de Vos, R.A., Jansen Steur, E.N., and Braak, E. (2003). Staging of brain pathology related to sporadic Parkinson's disease. Neurobiol Aging *24*, 197-211.

Braverman, N.E., and Moser, A.B. (2012). Functions of plasmalogen lipids in health and disease. Biochimica et biophysica acta *1822*, 1442-1452.

Brookes, P.S., Yoon, Y., Robotham, J.L., Anders, M.W., and Sheu, S.S. (2004). Calcium, ATP, and ROS: a mitochondrial love-hate triangle. American journal of physiology Cell physiology *287*, C817-833.

Brown, D.I., and Griendling, K.K. (2009). Nox proteins in signal transduction. Free radical biology & medicine *47*, 1239-1253.

Bulteau, A.L., Lundberg, K.C., Ikeda-Saito, M., Isaya, G., and Szweda, L.I. (2005). Reversible redox-dependent modulation of mitochondrial aconitase and proteolytic activity during in vivo cardiac ischemia/reperfusion. Proc Natl Acad Sci U S A *102*, 5987-5991.

Bunn, H.F., and Poyton, R.O. (1996). Oxygen sensing and molecular adaptation to hypoxia. Physiol Rev *76*, 839-885.

Bunney, T.D., van Walraven, H.S., and de Boer, A.H. (2001). 14-3-3 protein is a regulator of the mitochondrial and chloroplast ATP synthase. P Natl Acad Sci USA *98*, 4249-4254.

Burchell, V.S., Nelson, D.E., Sanchez-Martinez, A., Delgado-Camprubi, M., Ivatt, R.M., Pogson, J.H., Randle, S.J., Wray, S., Lewis, P.A., Houlden, H.*, et al.* (2013). The Parkinson's disease-linked proteins Fbxo7 and Parkin interact to mediate mitophagy. Nat Neurosci *16*, 1257-1265.

Burre, J., Sharma, M., Tsetsenis, T., Buchman, V., Etherton, M.R., and Sudhof, T.C. (2010). Alpha-synuclein promotes SNARE-complex assembly in vivo and in vitro. Science *329*, 1663-1667.

Buttner, S., Bitto, A., Ring, J., Augsten, M., Zabrocki, P., Eisenberg, T., Jungwirth, H., Hutter, S., Carmona-Gutierrez, D., Kroemer, G.*, et al.* (2008). Functional mitochondria are required for alpha-synuclein toxicity in aging yeast. J Biol Chem *283*, 7554-7560.

Cadenas, E., Boveris, A., Ragan, C.I., and Stoppani, A.O. (1977). Production of superoxide radicals and hydrogen peroxide by NADH-ubiquinone reductase and ubiquinol-cytochrome c reductase from beef-heart mitochondria. Archives of biochemistry and biophysics *180*, 248-257.

Cahn, R.D., Zwilling, E., Kaplan, N.O., and Levine, L. (1962). Nature and Development of Lactic Dehydrogenases: The two major types of this enzyme form molecular hybrids which change in makeup during development. Science *136*, 962-969.

Cairns, R.A., Harris, I.S., and Mak, T.W. (2011). Regulation of cancer cell metabolism. Nat Rev Cancer *11*, 85-95.

Cali, T., Ottolini, D., Soriano, M.E., and Brini, M. (2015). A new split-GFP-based probe reveals DJ-1 translocation into the mitochondrial matrix to sustain ATP synthesis upon nutrient deprivation. Human molecular genetics *24*, 1045-1060.

Canet-Aviles, R.M., Wilson, M.A., Miller, D.W., Ahmad, R., McLendon, C., Bandyopadhyay, S., Baptista, M.J., Ringe, D., Petsko, G.A., and Cookson, M.R. (2004). The Parkinson's

disease protein DJ-1 is neuroprotective due to cysteine-sulfinic acid-driven mitochondrial localization. Proc Natl Acad Sci U S A *101*, 9103-9108.

Cao, J., Lou, S., Ying, M., and Yang, B. (2015a). DJ-1 as a human oncogene and potential therapeutic target. Biochem Pharmacol *93*, 241-250.

Cao, J., Ying, M., Xie, N., Lin, G., Dong, R., Zhang, J., Yan, H., Yang, X., He, Q., and Yang, B. (2014). The oxidation states of DJ-1 dictate the cell fate in response to oxidative stress triggered by 4-hpr: autophagy or apoptosis? Antioxidants & redox signaling *21*, 1443-1459.

Cao, L., Lei, H., Chang, M.Z., Liu, Z.Q., and Bie, X.H. (2015b). Down-regulation of 14-3-3beta exerts anti-cancer effects through inducing ER stress in human glioma U87 cells: Involvement of CHOP-Wnt pathway. Biochem Biophys Res Commun *462*, 389-395.

Carter, P., and Wells, J.A. (1988). Dissecting the catalytic triad of a serine protease. Nature *332*, 564-568.

Celardo, I., Costa, A.C., Lehmann, S., Jones, C., Wood, N., Mencacci, N.E., Mallucci, G.R., Loh, S.H., and Martins, L.M. (2016). Mitofusin-mediated ER stress triggers neurodegeneration in pink1/parkin models of Parkinson's disease. Cell death & disease *7*, e2271.

Chacinska, A., Koehler, C.M., Milenkovic, D., Lithgow, T., and Pfanner, N. (2009). Importing mitochondrial proteins: machineries and mechanisms. Cell *138*, 628-644.

Chan, C.S., Gertler, T.S., and Surmeier, D.J. (2010). A molecular basis for the increased vulnerability of substantia nigra dopamine neurons in aging and Parkinson's disease. Mov Disord *25 Suppl 1*, S63-70.

Chan, D.C. (2006). Mitochondria: dynamic organelles in disease, aging, and development. Cell *125*, 1241-1252.

Chandel, N.S., and Schumacker, P.T. (2000). Cellular oxygen sensing by mitochondria: old questions, new insight. J Appl Physiol (1985) *88*, 1880-1889.

Chandra, D., and Singh, K.K. (2011). Genetic insights into OXPHOS defect and its role in cancer. Biochimica et biophysica acta *1807*, 620-625.

Chandra, S., Gallardo, G., Fernandez-Chacon, R., Schluter, O.M., and Sudhof, T.C. (2005). Alpha-synuclein cooperates with CSPalpha in preventing neurodegeneration. Cell *123*, 383-396.

Chavez, E., Rodriguez, J.S., Garcia, G., Garcia, N., and Correa, F. (2005). Oligomycin strengthens the effect of cyclosporin A on mitochondrial permeability transition by inducing phosphate uptake. Cell Biol Int *29*, 551-558.

Chen, G., Han, Z., Feng, D., Chen, Y., Chen, L., Wu, H., Huang, L., Zhou, C., Cai, X., Fu, C.*, et al.* (2014a). A regulatory signaling loop comprising the PGAM5 phosphatase and CK2 controls receptor-mediated mitophagy. Mol Cell *54*, 362-377.

Chen, H., and Chan, D.C. (2009). Mitochondrial dynamics--fusion, fission, movement, and mitophagy--in neurodegenerative diseases. Human molecular genetics *18*, R169-176.

Chen, J., Li, L., and Chin, L.S. (2010). Parkinson disease protein DJ-1 converts from a zymogen to a protease by carboxyl-terminal cleavage. Human molecular genetics *19*, 2395-2408.

Chen, T.I., Chiu, H.W., Pan, Y.C., Hsu, S.T., Lin, J.H., and Yang, K.T. (2014b). Intermittent hypoxia-induced protein phosphatase 2A activation reduces PC12 cell proliferation and differentiation. J Biomed Sci *21*, 46.

Chen, Y., and Dorn, G.W., 2nd (2013). PINK1-phosphorylated mitofusin 2 is a Parkin receptor for culling damaged mitochondria. Science *340*, 471-475.

Chen, Y.B., Aon, M.A., Hsu, Y.T., Soane, L., Teng, X., McCaffery, J.M., Cheng, W.C., Qi, B., Li, H., Alavian, K.N., *et al.* (2011). Bcl-xL regulates mitochondrial energetics by stabilizing the inner membrane potential. J Cell Biol *195*, 263-276.

Chen, Y.R., Chen, C.L., Pfeiffer, D.R., and Zweier, J.L. (2007). Mitochondrial complex II in the post-ischemic heart: oxidative injury and the role of protein S-glutathionylation. J Biol Chem *282*, 32640-32654.

Chung, K.K., Zhang, Y., Lim, K.L., Tanaka, Y., Huang, H., Gao, J., Ross, C.A., Dawson, V.L., and Dawson, T.M. (2001). Parkin ubiquitinates the alpha-synuclein-interacting protein, synphilin-1: implications for Lewy-body formation in Parkinson disease. Nat Med *7*, 1144-1150.

Clements, C.M., McNally, R.S., Conti, B.J., Mak, T.W., and Ting, J.P. (2006). DJ-1, a cancer- and Parkinson's disease-associated protein, stabilizes the antioxidant transcriptional master regulator Nrf2. Proc Natl Acad Sci U S A *103*, 15091-15096.

Coblitz, B., Wu, M., Shikano, S., and Li, M. (2006). C-terminal binding: an expanded repertoire and function of 14-3-3 proteins. FEBS Lett *580*, 1531-1535.

Cogliati, S., Enriquez, J.A., and Scorrano, L. (2016). Mitochondrial Cristae: Where Beauty Meets Functionality. Trends Biochem Sci *41*, 261-273.

Cole, N.B., Dieuliis, D., Leo, P., Mitchell, D.C., and Nussbaum, R.L. (2008). Mitochondrial translocation of alpha-synuclein is promoted by intracellular acidification. Exp Cell Res *314*, 2076-2089.

Conklin, D.S., Galaktionov, K., and Beach, D. (1995). 14-3-3 proteins associate with cdc25 phosphatases. Proc Natl Acad Sci U S A *92*, 7892-7896.

Connolly, B.S., and Lang, A.E. (2014). Pharmacological treatment of Parkinson disease: a review. JAMA *311*, 1670-1683.

Cookson, M.R. (2010). The role of leucine-rich repeat kinase 2 (LRRK2) in Parkinson's disease. Nature reviews Neuroscience *11*, 791-797.

Cotzias, G.C., Papavasiliou, P.S., and Gellene, R. (1968). Experimental treatment of parkinsonism with L-Dopa. Neurology *18*, 276-277.

Coyle, P., Philcox, J.C., Carey, L.C., and Rofe, A.M. (2002). Metallothionein: the multipurpose protein. Cell Mol Life Sci *59*, 627-647.

Crouch, S.P., Kozlowski, R., Slater, K.J., and Fletcher, J. (1993). The use of ATP bioluminescence as a measure of cell proliferation and cytotoxicity. J Immunol Methods *160*, 81-88.

Cuevas, S., Yang, Y., Konkalmatt, P., Asico, L.D., Feranil, J., Jones, J., Villar, V.A., Armando, I., and Jose, P.A. (2015). Role of nuclear factor erythroid 2-related factor 2 in the oxidative stress-dependent hypertension associated with the depletion of DJ-1. Hypertension *65*, 1251-1257.

da Costa, C.A., Sunyach, C., Giaime, E., West, A., Corti, O., Brice, A., Safe, S., Abou-Sleiman, P.M., Wood, N.W., Takahashi, H., *et al.* (2009). Transcriptional repression of p53 by parkin and impairment by mutations associated with autosomal recessive juvenile Parkinson's disease. Nat Cell Biol *11*, 1370-1375.

Danial, N.N., Gramm, C.F., Scorrano, L., Zhang, C.Y., Krauss, S., Ranger, A.M., Datta, S.R., Greenberg, M.E., Licklider, L.J., Lowell, B.B., *et al.* (2003). BAD and glucokinase reside in a mitochondrial complex that integrates glycolysis and apoptosis. Nature *424*, 952-956.

Datta, S.R., Katsov, A., Hu, L., Petros, A., Fesik, S.W., Yaffe, M.B., and Greenberg, M.E. (2000). 14-3-3 proteins and survival kinases cooperate to inactivate BAD by BH3 domain phosphorylation. Mol Cell *6*, 41-51.

Dauer, W., and Przedborski, S. (2003). Parkinson's disease: mechanisms and models. Neuron *39*, 889-909.

Davidson, W.S., Jonas, A., Clayton, D.F., and George, J.M. (1998). Stabilization of alpha-synuclein secondary structure upon binding to synthetic membranes. J Biol Chem *273*, 9443-9449.

Dawson, T.M., and Dawson, V.L. (2010). The role of parkin in familial and sporadic Parkinson's disease. Mov Disord *25 Suppl 1*, S32-39.

Dawson, T.M., Ko, H.S., and Dawson, V.L. (2010). Genetic animal models of Parkinson's disease. Neuron *66*, 646-661.

de Brito, O.M., and Scorrano, L. (2008). Mitofusin 2 tethers endoplasmic reticulum to mitochondria. Nature *456*, 605-610.

de Kroon, A.I., Dolis, D., Mayer, A., Lill, R., and de Kruijff, B. (1997). Phospholipid composition of highly purified mitochondrial outer membranes of rat liver and Neurospora crassa. Is cardiolipin present in the mitochondrial outer membrane? Biochimica et biophysica acta *1325*, 108-116.

DeBerardinis, R.J., Lum, J.J., Hatzivassiliou, G., and Thompson, C.B. (2008). The biology of cancer: metabolic reprogramming fuels cell growth and proliferation. Cell Metab *7*, 11-20.

Dedkova, E.N., Sigova, A.A., and Zinchenko, V.P. (2000). Mechanism of action of calcium ionophores on intact cells: ionophore-resistant cells. Membr Cell Biol *13*, 357-368.

Del Arco, A., Contreras, L., Pardo, B., and Satrustegui, J. (2016). Calcium regulation of mitochondrial carriers. Biochimica et biophysica acta *1863*, 2413-2421.

DeLong, M.R., and Wichmann, T. (2015). Basal Ganglia Circuits as Targets for Neuromodulation in Parkinson Disease. JAMA Neurol *72*, 1354-1360.

Denton, R.M. (2009). Regulation of mitochondrial dehydrogenases by calcium ions. Biochimica et biophysica acta *1787*, 1309-1316.

Deuschl, G., Schade-Brittinger, C., Krack, P., Volkmann, J., Schafer, H., Botzel, K., Daniels, C., Deutschlander, A., Dillmann, U., Eisner, W.*, et al.* (2006). A randomized trial of deep-brain stimulation for Parkinson's disease. N Engl J Med *355*, 896-908.

Devi, L., Raghavendran, V., Prabhu, B.M., Avadhani, N.G., and Anandatheerthavarada, H.K. (2008). Mitochondrial import and accumulation of alpha-synuclein impair complex I in human dopaminergic neuronal cultures and Parkinson disease brain. J Biol Chem *283*, 9089-9100.

Dexter, D.T., and Jenner, P. (2013). Parkinson disease: from pathology to molecular disease mechanisms. Free radical biology & medicine *62*, 132-144.

DeYoung, M.P., Horak, P., Sofer, A., Sgroi, D., and Ellisen, L.W. (2008). Hypoxia regulates TSC1/2-mTOR signaling and tumor suppression through REDD1-mediated 14-3-3 shuttling. Genes Dev *22*, 239-251.

Di Fonzo, A., Dekker, M.C., Montagna, P., Baruzzi, A., Yonova, E.H., Correia Guedes, L., Szczerbinska, A., Zhao, T., Dubbel-Hulsman, L.O., Wouters, C.H.*, et al.* (2009). FBXO7 mutations cause autosomal recessive, early-onset parkinsonian-pyramidal syndrome. Neurology *72*, 240-245.

Di Maio, R., Barrett, P.J., Hoffman, E.K., Barrett, C.W., Zharikov, A., Borah, A., Hu, X., McCoy, J., Chu, C.T., Burton, E.A.*, et al.* (2016). alpha-Synuclein binds to TOM20 and inhibits mitochondrial protein import in Parkinson's disease. Sci Transl Med *8*, 342ra378.

Dienel, G.A. (2012). Brain lactate metabolism: the discoveries and the controversies. J Cereb Blood Flow Metab *32*, 1107-1138.

Dikiy, I., and Eliezer, D. (2012). Folding and misfolding of alpha-synuclein on membranes. Biochimica et biophysica acta *1818*, 1013-1018.

Ding, W.X., Ni, H.M., Li, M., Liao, Y., Chen, X., Stolz, D.B., Dorn, G.W., 2nd, and Yin, X.M. (2010). Nix is critical to two distinct phases of mitophagy, reactive oxygen species-

mediated autophagy induction and Parkin-ubiquitin-p62-mediated mitochondrial priming. J Biol Chem *285*, 27879-27890.

Dionisi, O., Galeotti, T., Terranova, T., and Azzi, A. (1975). Superoxide radicals and hydrogen peroxide formation in mitochondria from normal and neoplastic tissues. Biochimica et biophysica acta *403*, 292-300.

Dolle, C., Rack, J.G., and Ziegler, M. (2013). NAD and ADP-ribose metabolism in mitochondria. FEBS J *280*, 3530-3541.

Dongworth, R.K., Mukherjee, U.A., Hall, A.R., Astin, R., Ong, S.B., Yao, Z., Dyson, A., Szabadkai, G., Davidson, S.M., Yellon, D.M.*, et al.* (2014). DJ-1 protects against cell death following acute cardiac ischemia-reperfusion injury. Cell death & disease *5*, e1082.

Dowhan, W. (1997). Molecular basis for membrane phospholipid diversity: why are there so many lipids? Annu Rev Biochem *66*, 199-232.

Dudek, J., Rehling, P., and van der Laan, M. (2013). Mitochondrial protein import: common principles and physiological networks. Biochimica et biophysica acta *1833*, 274-285.

Duplan, E., Giaime, E., Viotti, J., Sevalle, J., Corti, O., Brice, A., Ariga, H., Qi, L., Checler, F., and Alves da Costa, C. (2013). ER-stress-associated functional link between Parkin and DJ-1 via a transcriptional cascade involving the tumor suppressor p53 and the spliced X-box binding protein XBP-1. J Cell Sci *126*, 2124-2133.

Dzamko, N., Deak, M., Hentati, F., Reith, A.D., Prescott, A.R., Alessi, D.R., and Nichols, R.J. (2010). Inhibition of LRRK2 kinase activity leads to dephosphorylation of Ser(910)/Ser(935), disruption of 14-3-3 binding and altered cytoplasmic localization. Biochem J *430*, 405-413.

Dzbek, J., and Korzeniewski, B. (2008). Control over the contribution of the mitochondrial membrane potential (DeltaPsi) and proton gradient (DeltapH) to the protonmotive force (Deltap). In silico studies. J Biol Chem *283*, 33232-33239.

Eaton, S., Bartlett, K., and Pourfarzam, M. (1996). Mammalian mitochondrial beta-oxidation. Biochem J *320 (Pt 2)*, 345-357.

Eisner, D., Bode, E., Venetucci, L., and Trafford, A. (2013). Calcium flux balance in the heart. Journal of molecular and cellular cardiology *58*, 110-117.

Ennis, S.R., Kawai, N., Ren, X.D., Abdelkarim, G.E., and Keep, R.F. (1998). Glutamine uptake at the blood-brain barrier is mediated by N-system transport. Journal of neurochemistry *71*, 2565-2573.

Erecinska, M., and Silver, I.A. (2001). Tissue oxygen tension and brain sensitivity to hypoxia. Respir Physiol *128*, 263-276.

Ernster, L., and Schatz, G. (1981). Mitochondria: a historical review. J Cell Biol *91*, 227s-255s.

Exner, N., Lutz, A.K., Haass, C., and Winklhofer, K.F. (2012). Mitochondrial dysfunction in Parkinson's disease: molecular mechanisms and pathophysiological consequences. EMBO J *31*, 3038-3062.

Fan, J., Ren, H., Jia, N., Fei, E., Zhou, T., Jiang, P., Wu, M., and Wang, G. (2008). DJ-1 decreases Bax expression through repressing p53 transcriptional activity. J Biol Chem *283*, 4022-4030.

Fedotcheva, N.I., Sokolov, A.P., and Kondrashova, M.N. (2006). Nonezymatic formation of succinate in mitochondria under oxidative stress. Free radical biology & medicine *41*, 56-64.

Ferguson, S.M., and De Camilli, P. (2012). Dynamin, a membrane-remodelling GTPase. Nature reviews Molecular cell biology *13*, 75-88.

Fong, G.H., and Takeda, K. (2008). Role and regulation of prolyl hydroxylase domain proteins. Cell Death Differ *15*, 635-641.

Foote, M., Qiao, H., Graham, K., Wu, Y., and Zhou, Y. (2015). Inhibition of 14-3-3 Proteins Leads to Schizophrenia-Related Behavioral Phenotypes and Synaptic Defects in Mice. Biol Psychiatry *78*, 386-395.

Freeman, D.J., Li, A.G., Wei, G., Li, H.H., Kertesz, N., Lesche, R., Whale, A.D., Martinez-Diaz, H., Rozengurt, N., Cardiff, R.D.*, et al.* (2003). PTEN tumor suppressor regulates p53 protein levels and activity through phosphatase-dependent and -independent mechanisms. Cancer Cell *3*, 117-130.

Fu, H., Subramanian, R.R., and Masters, S.C. (2000). 14-3-3 proteins: structure, function, and regulation. Annu Rev Pharmacol Toxicol *40*, 617-647.

Fuchs, J., Nilsson, C., Kachergus, J., Munz, M., Larsson, E.M., Schule, B., Langston, J.W., Middleton, F.A., Ross, O.A., Hulihan, M.*, et al.* (2007). Phenotypic variation in a large Swedish pedigree due to SNCA duplication and triplication. Neurology *68*, 916-922.

Fujikawa, M., and Yoshida, M. (2010). A sensitive, simple assay of mitochondrial ATP synthesis of cultured mammalian cells suitable for high-throughput analysis. Biochem Biophys Res Commun *401*, 538-543.

Fujimoto, M., Hayashi, T., and Su, T.P. (2012). The role of cholesterol in the association of endoplasmic reticulum membranes with mitochondria. Biochem Biophys Res Commun *417*, 635-639.

Fusco, G., De Simone, A., Gopinath, T., Vostrikov, V., Vendruscolo, M., Dobson, C.M., and Veglia, G. (2014). Direct observation of the three regions in alpha-synuclein that determine its membrane-bound behaviour. Nat Commun *5*, 3827.

Gabriel, J.L., and Plaut, G.W. (1984). Citrate activation of NAD-specific isocitrate dehydrogenase from bovine heart. J Biol Chem *259*, 1622-1628.

Galvan, A., Devergnas, A., and Wichmann, T. (2015). Alterations in neuronal activity in basal ganglia-thalamocortical circuits in the parkinsonian state. Front Neuroanat *9*, 5.

Gardino, A.K., and Yaffe, M.B. (2011). 14-3-3 proteins as signaling integration points for cell cycle control and apoptosis. Seminars in cell & developmental biology *22*, 688-695.

Gegg, M.E., Cooper, J.M., Chau, K.Y., Rojo, M., Schapira, A.H., and Taanman, J.W. (2010). Mitofusin 1 and mitofusin 2 are ubiquitinated in a PINK1/parkin-dependent manner upon induction of mitophagy. Human molecular genetics *19*, 4861-4870.

Geisler, S., Holmstrom, K.M., Skujat, D., Fiesel, F.C., Rothfuss, O.C., Kahle, P.J., and Springer, W. (2010). PINK1/Parkin-mediated mitophagy is dependent on VDAC1 and p62/SQSTM1. Nat Cell Biol *12*, 119-131.

Gellerich, F.N., Trumbeckaite, S., Opalka, J.R., Seppet, E., Rasmussen, H.N., Neuhoff, C., and Zierz, S. (2000). Function of the mitochondrial outer membrane as a diffusion barrier in health and diseases. Biochem Soc Trans *28*, 164-169.

Gerencser, A.A., Chinopoulos, C., Birket, M.J., Jastroch, M., Vitelli, C., Nicholls, D.G., and Brand, M.D. (2012). Quantitative measurement of mitochondrial membrane potential in cultured cells: calcium-induced de- and hyperpolarization of neuronal mitochondria. J Physiol *590*, 2845-2871.

Giacco, F., and Brownlee, M. (2010). Oxidative stress and diabetic complications. Circulation research *107*, 1058-1070.

Giaime, E., Yamaguchi, H., Gautier, C.A., Kitada, T., and Shen, J. (2012). Loss of DJ-1 does not affect mitochondrial respiration but increases ROS production and mitochondrial permeability transition pore opening. PLoS One *7*, e40501.

Gimenez-Cassina, A., and Danial, N.N. (2015). Regulation of mitochondrial nutrient and energy metabolism by BCL-2 family proteins. Trends Endocrinol Metab *26*, 165-175.

Girotto, S., Sturlese, M., Bellanda, M., Tessari, I., Cappellini, R., Bisaglia, M., Bubacco, L., and Mammi, S. (2012). Dopamine-derived quinones affect the structure of the redox sensor DJ-1 through modifications at Cys-106 and Cys-53. J Biol Chem *287*, 18738-18749.

Gladden, L.B. (2004). Lactate metabolism: a new paradigm for the third millennium. J Physiol *558*, 5-30.

Gleichmann, M., Collis, L.P., Smith, P.J., and Mattson, M.P. (2009). Simultaneous single neuron recording of O2 consumption, [Ca2+]i and mitochondrial membrane potential in glutamate toxicity. Journal of neurochemistry *109*, 644-655.

Gobel, B., Oltmanns, K.M., and Chung, M. (2013). Linking neuronal brain activity to the glucose metabolism. Theor Biol Med Model *10*, 50.

Goedert, M., Spillantini, M.G., Del Tredici, K., and Braak, H. (2013). 100 years of Lewy pathology. Nat Rev Neurol *9*, 13-24.

Gohil, V.M., Sheth, S.A., Nilsson, R., Wojtovich, A.P., Lee, J.H., Perocchi, F., Chen, W., Clish, C.B., Ayata, C., Brookes, P.S.*, et al.* (2010). Nutrient-sensitized screening for drugs that shift energy metabolism from mitochondrial respiration to glycolysis. Nat Biotechnol *28*, 249-255.

Goldberg, J.A., Guzman, J.N., Estep, C.M., Ilijic, E., Kondapalli, J., Sanchez-Padilla, J., and Surmeier, D.J. (2012). Calcium entry induces mitochondrial oxidant stress in vagal neurons at risk in Parkinson's disease. Nat Neurosci *15*, 1414-1421.

Gomez, L., Thiebaut, P.A., Paillard, M., Ducreux, S., Abrial, M., Crola Da Silva, C., Durand, A., Alam, M.R., Van Coppenolle, F., Sheu, S.S.*, et al.* (2016). The SR/ER-mitochondria calcium crosstalk is regulated by GSK3beta during reperfusion injury. Cell Death Differ *23*, 313-322.

Gorlach, A., Bertram, K., Hudecova, S., and Krizanova, O. (2015). Calcium and ROS: A mutual interplay. Redox Biol *6*, 260-271.

Gorner, K., Holtorf, E., Waak, J., Pham, T.T., Vogt-Weisenhorn, D.M., Wurst, W., Haass, C., and Kahle, P.J. (2007). Structural determinants of the C-terminal helix-kink-helix motif essential for protein stability and survival promoting activity of DJ-1. J Biol Chem *282*, 13680-13691.

Gray, M.W. (1989). Origin and evolution of mitochondrial DNA. Annu Rev Cell Biol *5*, 25-50.

Green, D., and Kroemer, G. (1998). The central executioners of apoptosis: caspases or mitochondria? Trends Cell Biol *8*, 267-271.

Green, D.R., and Reed, J.C. (1998). Mitochondria and apoptosis. Science *281*, 1309-1312.

Greggio, E., Zambrano, I., Kaganovich, A., Beilina, A., Taymans, J.M., Daniels, V., Lewis, P., Jain, S., Ding, J., Syed, A.*, et al.* (2008). The Parkinson disease-associated leucine-rich repeat kinase 2 (LRRK2) is a dimer that undergoes intramolecular autophosphorylation. J Biol Chem *283*, 16906-16914.

Gregoire, M., Morais, R., Quilliam, M.A., and Gravel, D. (1984). On auxotrophy for pyrimidines of respiration-deficient chick embryo cells. European journal of biochemistry / FEBS *142*, 49-55.

Gross, A. (2016). BCL-2 family proteins as regulators of mitochondria metabolism. Biochimica et biophysica acta *1857*, 1243-1246.

Grouleff, J., Irudayam, S.J., Skeby, K.K., and Schiott, B. (2015). The influence of cholesterol on membrane protein structure, function, and dynamics studied by molecular dynamics simulations. Biochimica et biophysica acta *1848*, 1783-1795.

Gu, M., Cooper, J.M., Taanman, J.W., and Schapira, A.H. (1998). Mitochondrial DNA transmission of the mitochondrial defect in Parkinson's disease. Annals of neurology *44*, 177-186.

Guda, P., Guda, C., and Subramaniam, S. (2007). Reconstruction of pathways associated with amino acid metabolism in human mitochondria. Genomics Proteomics Bioinformatics *5*, 166-176.

Guerini, D., Coletto, L., and Carafoli, E. (2005). Exporting calcium from cells. Cell calcium *38*, 281-289.

Gutierrez-Aguilar, M., and Baines, C.P. (2013). Physiological and pathological roles of mitochondrial SLC25 carriers. Biochem J *454*, 371-386.

Guzman, J.N., Sanchez-Padilla, J., Wokosin, D., Kondapalli, J., Ilijic, E., Schumacker, P.T., and Surmeier, D.J. (2010). Oxidant stress evoked by pacemaking in dopaminergic neurons is attenuated by DJ-1. Nature *468*, 696-700.

Gwinn, D.M., Shackelford, D.B., Egan, D.F., Mihaylova, M.M., Mery, A., Vasquez, D.S., Turk, B.E., and Shaw, R.J. (2008). AMPK phosphorylation of raptor mediates a metabolic checkpoint. Mol Cell *30*, 214-226.

Hachiya, N., Komiya, T., Alam, R., Iwahashi, J., Sakaguchi, M., Omura, T., and Mihara, K. (1994). Msf, a Novel Cytoplasmic Chaperone Which Functions in Precursor Targeting to Mitochondria. Embo Journal *13*, 5146-5154.

Hague, S., Rogaeva, E., Hernandez, D., Gulick, C., Singleton, A., Hanson, M., Johnson, J., Weiser, R., Gallardo, M., Ravina, B.*, et al.* (2003). Early-onset Parkinson's disease caused by a compound heterozygous DJ-1 mutation. Annals of neurology *54*, 271-274.

Halestrap, A.P., and Wilson, M.C. (2012). The monocarboxylate transporter family--role and regulation. IUBMB Life *64*, 109-119.

Halliday, G.M., Del Tredici, K., and Braak, H. (2006). Critical appraisal of brain pathology staging related to presymptomatic and symptomatic cases of sporadic Parkinson's disease. J Neural Transm Suppl, 99-103.

Halskau, O., Jr., Ying, M., Baumann, A., Kleppe, R., Rodriguez-Larrea, D., Almas, B., Haavik, J., and Martinez, A. (2009). Three-way interaction between 14-3-3 proteins, the N-terminal region of tyrosine hydroxylase, and negatively charged membranes. J Biol Chem *284*, 32758-32769.

Hanukoglu, I., and Gutfinger, T. (1989). cDNA sequence of adrenodoxin reductase. Identification of NADP-binding sites in oxidoreductases. European journal of biochemistry / FEBS *180*, 479-484.

Hao, L.Y., Giasson, B.I., and Bonini, N.M. (2010). DJ-1 is critical for mitochondrial function and rescues PINK1 loss of function. Proc Natl Acad Sci U S A *107*, 9747-9752.

Hartmann, A. (2004). Postmortem studies in Parkinson's disease. Dialogues Clin Neurosci *6*, 281-293.

Hayashi, T., Ishimori, C., Takahashi-Niki, K., Taira, T., Kim, Y.C., Maita, H., Maita, C., Ariga, H., and Iguchi-Ariga, S.M. (2009). DJ-1 binds to mitochondrial complex I and maintains its activity. Biochem Biophys Res Commun *390*, 667-672.

Heifetz, A., Keenan, R.W., and Elbein, A.D. (1979). Mechanism of action of tunicamycin on the UDP-GlcNAc:dolichyl-phosphate Glc-NAc-1-phosphate transferase. Biochemistry *18*, 2186-2192.

Heo, J.Y., Park, J.H., Kim, S.J., Seo, K.S., Han, J.S., Lee, S.H., Kim, J.M., Park, J.I., Park, S.K., Lim, K.*, et al.* (2012). DJ-1 null dopaminergic neuronal cells exhibit defects in mitochondrial function and structure: involvement of mitochondrial complex I assembly. PLoS One *7*, e32629.

Herrera, F.E., Zucchelli, S., Jezierska, A., Lavina, Z.S., Gustincich, S., and Carloni, P. (2007). On the oligomeric state of DJ-1 protein and its mutants associated with Parkinson Disease. A combined computational and in vitro study. J Biol Chem *282*, 24905-24914.

Herrmann, J.M., and Riemer, J. (2010). The intermembrane space of mitochondria. Antioxidants & redox signaling *13*, 1341-1358.

Holmstrom, K.M., and Finkel, T. (2014). Cellular mechanisms and physiological consequences of redox-dependent signalling. Nature reviews Molecular cell biology *15*, 411-421.

Hom, J.R., Quintanilla, R.A., Hoffman, D.L., de Mesy Bentley, K.L., Molkentin, J.D., Sheu, S.S., and Porter, G.A., Jr. (2011). The permeability transition pore controls cardiac mitochondrial maturation and myocyte differentiation. Dev Cell *21*, 469-478.

Honbou, K., Suzuki, N.N., Horiuchi, M., Niki, T., Taira, T., Ariga, H., and Inagaki, F. (2003). The crystal structure of DJ-1, a protein related to male fertility and Parkinson's disease. J Biol Chem *278*, 31380-31384.

Hornbeck, P.V., Kornhauser, J.M., Tkachev, S., Zhang, B., Skrzypek, E., Murray, B., Latham, V., and Sullivan, M. (2012). PhosphoSitePlus: a comprehensive resource for investigating the structure and function of experimentally determined post-translational modifications in man and mouse. Nucleic acids research *40*, D261-270.

Horng, Y.C., Cobine, P.A., Maxfield, A.B., Carr, H.S., and Winge, D.R. (2004). Specific copper transfer from the Cox17 metallochaperone to both Sco1 and Cox11 in the assembly of yeast cytochrome C oxidase. J Biol Chem *279*, 35334-35340.

Hornykiewicz, O. (2002). L-DOPA: from a biologically inactive amino acid to a successful therapeutic agent. Amino Acids *23*, 65-70.

Horvath, S.E., and Daum, G. (2013). Lipids of mitochondria. Prog Lipid Res *52*, 590-614.

Hoshino, A., Mita, Y., Okawa, Y., Ariyoshi, M., Iwai-Kanai, E., Ueyama, T., Ikeda, K., Ogata, T., and Matoba, S. (2013). Cytosolic p53 inhibits Parkin-mediated mitophagy and promotes mitochondrial dysfunction in the mouse heart. Nat Commun *4*, 2308.

Houten, S.M., Violante, S., Ventura, F.V., and Wanders, R.J. (2016). The Biochemistry and Physiology of Mitochondrial Fatty Acid beta-Oxidation and Its Genetic Disorders. Annual review of physiology *78*, 23-44.

Hu, J., Dong, L., and Outten, C.E. (2008). The redox environment in the mitochondrial intermembrane space is maintained separately from the cytosol and matrix. J Biol Chem *283*, 29126-29134.

Huang, H., Hu, X., Eno, C.O., Zhao, G., Li, C., and White, C. (2013). An interaction between Bcl-xL and the voltage-dependent anion channel (VDAC) promotes mitochondrial Ca2+ uptake. J Biol Chem *288*, 19870-19881.

Hulleman, J.D., Mirzaei, H., Guigard, E., Taylor, K.L., Ray, S.S., Kay, C.M., Regnier, F.E., and Rochet, J.C. (2007). Destabilization of DJ-1 by familial substitution and oxidative modifications: implications for Parkinson's disease. Biochemistry *46*, 5776-5789.

Humphrey, S.J., Yang, G., Yang, P., Fazakerley, D.J., Stockli, J., Yang, J.Y., and James, D.E. (2013). Dynamic adipocyte phosphoproteome reveals that Akt directly regulates mTORC2. Cell Metab *17*, 1009-1020.

Hurd, T.R., Requejo, R., Filipovska, A., Brown, S., Prime, T.A., Robinson, A.J., Fearnley, I.M., and Murphy, M.P. (2008). Complex I within oxidatively stressed bovine heart mitochondria is glutathionylated on Cys-531 and Cys-704 of the 75-kDa subunit: potential role of CYS residues in decreasing oxidative damage. J Biol Chem *283*, 24801-24815.

Huttemann, M., Lee, I., Pecinova, A., Pecina, P., Przyklenk, K., and Doan, J.W. (2008). Regulation of oxidative phosphorylation, the mitochondrial membrane potential, and their role in human disease. Journal of bioenergetics and biomembranes *40*, 445-456.

Hyder, F., Herman, P., Bailey, C.J., Moller, A., Globinsky, R., Fulbright, R.K., Rothman, D.L., and Gjedde, A. (2016). Uniform distributions of glucose oxidation and oxygen extraction in gray matter of normal human brain: No evidence of regional differences of aerobic glycolysis. J Cereb Blood Flow Metab *36*, 903-916.

Ibanez, P., De Michele, G., Bonifati, V., Lohmann, E., Thobois, S., Pollak, P., Agid, Y., Heutink, P., Durr, A., Brice, A.*, et al.* (2003). Screening for DJ-1 mutations in early onset autosomal recessive parkinsonism. Neurology *61*, 1429-1431.

Ichas, F., and Mazat, J.P. (1998). From calcium signaling to cell death: two conformations for the mitochondrial permeability transition pore. Switching from low- to high-conductance state. Biochimica et biophysica acta *1366*, 33-50.

Im, J.Y., Lee, K.W., Woo, J.M., Junn, E., and Mouradian, M.M. (2012). DJ-1 induces thioredoxin 1 expression through the Nrf2 pathway. Human molecular genetics *21*, 3013-3024.

Ishikawa, S., Taira, T., Niki, T., Takahashi-Niki, K., Maita, C., Maita, H., Ariga, H., and Iguchi-Ariga, S.M. (2009). Oxidative status of DJ-1-dependent activation of dopamine synthesis through interaction of tyrosine hydroxylase and 4-dihydroxy-L-phenylalanine (L-DOPA) decarboxylase with DJ-1. J Biol Chem *284*, 28832-28844.

Ishikawa, S., Taira, T., Takahashi-Niki, K., Niki, T., Ariga, H., and Iguchi-Ariga, S.M. (2010). Human DJ-1-specific transcriptional activation of tyrosine hydroxylase gene. J Biol Chem *285*, 39718-39731.

Isobe, T., Ichimura, T., Sunaya, T., Okuyama, T., Takahashi, N., Kuwano, R., and Takahashi, Y. (1991). Distinct forms of the protein kinase-dependent activator of tyrosine and tryptophan hydroxylases. Journal of molecular biology *217*, 125-132.

Itagaki, C., Isobe, T., Taoka, M., Natsume, T., Nomura, N., Horigome, T., Omata, S., Ichinose, H., Nagatsu, T., Greene, L.A.*, et al.* (1999). Stimulus-coupled interaction of tyrosine hydroxylase with 14-3-3 proteins. Biochemistry *38*, 15673-15680.

Jackson-Lewis, V., and Przedborski, S. (2007). Protocol for the MPTP mouse model of Parkinson's disease. Nat Protoc *2*, 141-151.

Jacobson, M.D., Weil, M., and Raff, M.C. (1997). Programmed cell death in animal development. Cell *88*, 347-354.

Jain, D., Jain, R., Eberhard, D., Eglinger, J., Bugliani, M., Piemonti, L., Marchetti, P., and Lammert, E. (2012). Age- and diet-dependent requirement of DJ-1 for glucose homeostasis in mice with implications for human type 2 diabetes. Journal of molecular cell biology *4*, 221-230.

Jajoo, R., Jung, Y., Huh, D., Viana, M.P., Rafelski, S.M., Springer, M., and Paulsson, J. (2016). Accurate concentration control of mitochondria and nucleoids. Science *351*, 169-172.

Jang, S.W., Liu, X., Fu, H., Rees, H., Yepes, M., Levey, A., and Ye, K. (2009). Interaction of Akt-phosphorylated SRPK2 with 14-3-3 mediates cell cycle and cell death in neurons. J Biol Chem *284*, 24512-24525.

Jankovic, J. (2008). Parkinson's disease: clinical features and diagnosis. J Neurol Neurosurg Psychiatry *79*, 368-376.

Jastroch, M., Divakaruni, A.S., Mookerjee, S., Treberg, J.R., and Brand, M.D. (2010). Mitochondrial proton and electron leaks. Essays Biochem *47*, 53-67.

Jeggo, P.A., and Lobrich, M. (2007). DNA double-strand breaks: their cellular and clinical impact? Oncogene *26*, 7717-7719.

Jellinger, K.A. (2008). A critical reappraisal of current staging of Lewy-related pathology in human brain. Acta Neuropathol *116*, 1-16.

Johnson, B.N., Berger, A.K., Cortese, G.P., and Lavoie, M.J. (2012). The ubiquitin E3 ligase parkin regulates the proapoptotic function of Bax. Proc Natl Acad Sci U S A *109*, 6283-6288.

Johnson, C., Crowther, S., Stafford, M.J., Campbell, D.G., Toth, R., and MacKintosh, C. (2010). Bioinformatic and experimental survey of 14-3-3-binding sites. Biochem J *427*, 69-78.

Johnson, J.D., Muhonen, W.W., and Lambeth, D.O. (1998). Characterization of the ATP- and GTP-specific succinyl-CoA synthetases in pigeon. The enzymes incorporate the same alpha-subunit. J Biol Chem *273*, 27573-27579.

Jonas, E.A., Buchanan, J., and Kaczmarek, L.K. (1999). Prolonged activation of mitochondrial conductances during synaptic transmission. Science *286*, 1347-1350.

Jonas, E.A., Porter, G.A., Jr., Beutner, G., Mnatsakanyan, N., and Alavian, K.N. (2015). Cell death disguised: The mitochondrial permeability transition pore as the c-subunit of the F(1)F(O) ATP synthase. Pharmacol Res *99*, 382-392.

Jornayvaz, F.R., and Shulman, G.I. (2010). Regulation of mitochondrial biogenesis. Essays Biochem *47*, 69-84.

Joselin, A.P., Hewitt, S.J., Callaghan, S.M., Kim, R.H., Chung, Y.H., Mak, T.W., Shen, J., Slack, R.S., and Park, D.S. (2012). ROS-dependent regulation of Parkin and DJ-1 localization during oxidative stress in neurons. Human molecular genetics *21*, 4888-4903.

Junn, E., Jang, W.H., Zhao, X., Jeong, B.S., and Mouradian, M.M. (2009). Mitochondrial localization of DJ-1 leads to enhanced neuroprotection. Journal of neuroscience research *87*, 123-129.

Kaneko, Y., Shojo, H., Burns, J., Staples, M., Tajiri, N., and Borlongan, C.V. (2014a). DJ-1 ameliorates ischemic cell death in vitro possibly via mitochondrial pathway. Neurobiol Dis *62*, 56-61.

Kaneko, Y., Tajiri, N., Shojo, H., and Borlongan, C.V. (2014b). Oxygen-glucose-deprived rat primary neural cells exhibit DJ-1 translocation into healthy mitochondria: a potent stroke therapeutic target. CNS Neurosci Ther *20*, 275-281.

Kantari, C., and Walczak, H. (2011). Caspase-8 and bid: caught in the act between death receptors and mitochondria. Biochimica et biophysica acta *1813*, 558-563.

Kato, I., Maita, H., Takahashi-Niki, K., Saito, Y., Noguchi, N., Iguchi-Ariga, S.M., and Ariga, H. (2013). Oxidized DJ-1 inhibits p53 by sequestering p53 from promoters in a DNA-binding affinity-dependent manner. Molecular and cellular biology *33*, 340-359.

Kawamoto, Y., Akiguchi, I., Tomimoto, H., Shirakashi, Y., Honjo, Y., and Budka, H. (2006). Upregulated expression of 14-3-3 proteins in astrocytes from human cerebrovascular ischemic lesions. Stroke *37*, 830-835.

Kazlauskaite, A., Kondapalli, C., Gourlay, R., Campbell, D.G., Ritorto, M.S., Hofmann, K., Alessi, D.R., Knebel, A., Trost, M., and Muqit, M.M. (2014). Parkin is activated by PINK1-dependent phosphorylation of ubiquitin at Ser65. Biochem J *460*, 127-139.

Keeney, P.M., Xie, J., Capaldi, R.A., and Bennett, J.P., Jr. (2006). Parkinson's disease brain mitochondrial complex I has oxidatively damaged subunits and is functionally impaired and misassembled. J Neurosci *26*, 5256-5264.

Khacho, M., Tarabay, M., Patten, D., Khacho, P., MacLaurin, J.G., Guadagno, J., Bergeron, R., Cregan, S.P., Harper, M.E., Park, D.S., *et al.* (2014). Acidosis overrides oxygen deprivation to maintain mitochondrial function and cell survival. Nat Commun *5*, 3550.

Kim, I., Rodriguez-Enriquez, S., and Lemasters, J.J. (2007). Selective degradation of mitochondria by mitophagy. Archives of biochemistry and biophysics *462*, 245-253.

Kim, J.M., Jang, H.J., Choi, S.Y., Park, S.A., Kim, I.S., Yang, Y.R., Lee, Y.H., Ryu, S.H., and Suh, P.G. (2014). DJ-1 contributes to adipogenesis and obesity-induced inflammation. Sci Rep *4*, 4805.

Kim, K.S., Kim, J.S., Park, J.Y., Suh, Y.H., Jou, I., Joe, E.H., and Park, S.M. (2013). DJ-1 associates with lipid rafts by palmitoylation and regulates lipid rafts-dependent endocytosis in astrocytes. Human molecular genetics *22*, 4805-4817.

Kim, R.H., Peters, M., Jang, Y., Shi, W., Pintilie, M., Fletcher, G.C., DeLuca, C., Liepa, J., Zhou, L., Snow, B., *et al.* (2005a). DJ-1, a novel regulator of the tumor suppressor PTEN. Cancer Cell *7*, 263-273.

Kim, R.H., Smith, P.D., Aleyasin, H., Hayley, S., Mount, M.P., Pownall, S., Wakeham, A., You-Ten, A.J., Kalia, S.K., Horne, P., *et al.* (2005b). Hypersensitivity of DJ-1-deficient mice to 1-methyl-4-phenyl-1,2,3,6-tetrahydropyrindine (MPTP) and oxidative stress. P Natl Acad Sci USA *102*, 5215-5220.

Kim, S.J., Park, Y.J., Hwang, I.Y., Youdim, M.B., Park, K.S., and Oh, Y.J. (2012). Nuclear translocation of DJ-1 during oxidative stress-induced neuronal cell death. Free radical biology & medicine *53*, 936-950.

Kim, Y.C., Kitaura, H., Taira, T., Iguchi-Ariga, S.M.M., and Ariga, H. (2009). Oxidation of DJ-1-dependent cell transformation through direct binding of DJ-1 to PTEN. International journal of oncology *35*, 1331-1341.

King, M.P., and Attardi, G. (1989). Human cells lacking mtDNA: repopulation with exogenous mitochondria by complementation. Science *246*, 500-503.

Kitada, T., Asakawa, S., Hattori, N., Matsumine, H., Yamamura, Y., Minoshima, S., Yokochi, M., Mizuno, Y., and Shimizu, N. (1998). Mutations in the parkin gene cause autosomal recessive juvenile parkinsonism. Nature *392*, 605-608.

Klawitter, J., Klawitter, J., Agardi, E., Corby, K., Leibfritz, D., Lowes, B.D., Christians, U., and Seres, T. (2013). Association of DJ-1/PTEN/AKT- and ASK1/p38-mediated cell signalling with ischaemic cardiomyopathy. Cardiovasc Res *97*, 66-76.

Kleppe, R., Martinez, A., Doskeland, S.O., and Haavik, J. (2011). The 14-3-3 proteins in regulation of cellular metabolism. Seminars in cell & developmental biology *22*, 713-719.

Klinefelter, G.R., Laskey, J.W., Ferrell, J., Suarez, J.D., and Roberts, N.L. (1997). Discriminant analysis indicates a single sperm protein (SP22) is predictive of fertility following exposure to epididymal toxicants. J Androl *18*, 139-150.

Knudsen, G.M., Paulson, O.B., and Hertz, M.M. (1991). Kinetic analysis of the human blood-brain barrier transport of lactate and its influence by hypercapnia. J Cereb Blood Flow Metab *11*, 581-586.

Kondapalli, C., Kazlauskaite, A., Zhang, N., Woodroof, H.I., Campbell, D.G., Gourlay, R., Burchell, L., Walden, H., Macartney, T.J., Deak, M., *et al.* (2012). PINK1 is activated by mitochondrial membrane potential depolarization and stimulates Parkin E3 ligase activity by phosphorylating Serine 65. Open Biol *2*, 120080.

Kornberg, H. (2000). Krebs and his trinity of cycles. Nature reviews Molecular cell biology *1*, 225-228.

Kosaki, A., Yamada, K., Suga, J., Otaka, A., and Kuzuya, H. (1998). 14-3-3beta protein associates with insulin receptor substrate 1 and decreases insulin-stimulated phosphatidylinositol 3'-kinase activity in 3T3L1 adipocytes. J Biol Chem *273*, 940-944.

Koshiba, T., Detmer, S.A., Kaiser, J.T., Chen, H., McCaffery, J.M., and Chan, D.C. (2004). Structural basis of mitochondrial tethering by mitofusin complexes. Science *305*, 858-862.

Kovacevic, Z. (1977). Mechanism of carrier-mediated glutamine transport across the inner mitochondrial membrane. Curr Probl Clin Biochem *8*, 254-264.

Kovermann, P., Truscott, K.N., Guiard, B., Rehling, P., Sepuri, N.B., Muller, H., Jensen, R.E., Wagner, R., and Pfanner, N. (2002). Tim22, the essential core of the mitochondrial protein insertion complex, forms a voltage-activated and signal-gated channel. Mol Cell *9*, 363-373.

Krebiehl, G., Ruckerbauer, S., Burbulla, L.F., Kieper, N., Maurer, B., Waak, J., Wolburg, H., Gizatullina, Z., Gellerich, F.N., Woitalla, D.*, et al.* (2010). Reduced basal autophagy and impaired mitochondrial dynamics due to loss of Parkinson's disease-associated protein DJ-1. PLoS One *5*, e9367.

Krebs, H.A., and Johnson, W.A. (1980). The role of citric acid in intermediate metabolism in animal tissues. FEBS Lett *117 Suppl*, K1-10.

Kruiswijk, F., Labuschagne, C.F., and Vousden, K.H. (2015). p53 in survival, death and metabolic health: a lifeguard with a licence to kill. Nature reviews Molecular cell biology *16*, 393-405.

Kurup, P.K., Xu, J., Videira, R.A., Ononenyi, C., Baltazar, G., Lombroso, P.J., and Nairn, A.C. (2015). STEP61 is a substrate of the E3 ligase parkin and is upregulated in Parkinson's disease. Proc Natl Acad Sci U S A *112*, 1202-1207.

Kuwana, T., Mackey, M.R., Perkins, G., Ellisman, M.H., Latterich, M., Schneiter, R., Green, D.R., and Newmeyer, D.D. (2002). Bid, Bax, and lipids cooperate to form supramolecular openings in the outer mitochondrial membrane. Cell *111*, 331-342.

LaManna, J.C., Harrington, J.F., Vendel, L.M., Abi-Saleh, K., Lust, W.D., and Harik, S.I. (1993). Regional blood-brain lactate influx. Brain research *614*, 164-170.

Langston, J.W., Ballard, P., Tetrud, J.W., and Irwin, I. (1983). Chronic Parkinsonism in humans due to a product of meperidine-analog synthesis. Science *219*, 979-980.

Lansbury, P.T., and Lashuel, H.A. (2006). A century-old debate on protein aggregation and neurodegeneration enters the clinic. Nature *443*, 774-779.

Lanza, I.R., and Nair, K.S. (2009). Functional assessment of isolated mitochondria in vitro. Methods Enzymol *457*, 349-372.

Larance, M., Ahmad, Y., Kirkwood, K.J., Ly, T., and Lamond, A.I. (2013). Global subcellular characterization of protein degradation using quantitative proteomics. Mol Cell Proteomics *12*, 638-650.

Lavalley, N.J., Slone, S.R., Ding, H., West, A.B., and Yacoubian, T.A. (2016). 14-3-3 Proteins regulate mutant LRRK2 kinase activity and neurite shortening. Human molecular genetics *25*, 109-122.

LaVoie, M.J., Ostaszewski, B.L., Weihofen, A., Schlossmacher, M.G., and Selkoe, D.J. (2005). Dopamine covalently modifies and functionally inactivates parkin. Nat Med *11*, 1214-1221.

Lazarou, M., Sliter, D.A., Kane, L.A., Sarraf, S.A., Wang, C., Burman, J.L., Sideris, D.P., Fogel, A.I., and Youle, R.J. (2015). The ubiquitin kinase PINK1 recruits autophagy receptors to induce mitophagy. Nature *524*, 309-314.

Lee, C., Yen, K., and Cohen, P. (2013). Humanin: a harbinger of mitochondrial-derived peptides? Trends Endocrinol Metab *24*, 222-228.

Lee, J.Y., Song, J., Kwon, K., Jang, S., Kim, C., Baek, K., Kim, J., and Park, C. (2012). Human DJ-1 and its homologs are novel glyoxalases. Human molecular genetics *21*, 3215-3225.

Lee, S.J., Kim, S.J., Kim, I.K., Ko, J., Jeong, C.S., Kim, G.H., Park, C., Kang, S.O., Suh, P.G., Lee, H.S.*, et al.* (2003). Crystal structures of human DJ-1 and Escherichia coli Hsp31, which share an evolutionarily conserved domain. J Biol Chem *278*, 44552-44559.

Lees, A.J., Hardy, J., and Revesz, T. (2009). Parkinson's disease. Lancet *373*, 2055-2066.

Lehninger, A.L. (1974). Role of phosphate and other proton-donating anions in respiration-coupled transport of Ca2+ by mitochondria. Proc Natl Acad Sci U S A *71*, 1520-1524.

Leist, M., Single, B., Castoldi, A.F., Kuhnle, S., and Nicotera, P. (1997). Intracellular adenosine triphosphate (ATP) concentration: a switch in the decision between apoptosis and necrosis. J Exp Med *185*, 1481-1486.

Lemasters, J.J. (2014). Variants of mitochondrial autophagy: Types 1 and 2 mitophagy and micromitophagy (Type 3). Redox Biol *2*, 749-754.

Lemasters, J.J., and Holmuhamedov, E. (2006). Voltage-dependent anion channel (VDAC) as mitochondrial governator--thinking outside the box. Biochimica et biophysica acta *1762*, 181-190.

Lev, N., Barhum, Y., Ben-Zur, T., Aharony, I., Trifonov, L., Regev, N., Melamed, E., Gruzman, A., and Offen, D. (2015). A DJ-1 Based Peptide Attenuates Dopaminergic Degeneration in Mice Models of Parkinson's Disease via Enhancing Nrf2. PLoS One *10*, e0127549.

Li, J., McQuade, T., Siemer, A.B., Napetschnig, J., Moriwaki, K., Hsiao, Y.S., Damko, E., Moquin, D., Walz, T., McDermott, A.*, et al.* (2012). The RIP1/RIP3 necrosome forms a functional amyloid signaling complex required for programmed necrosis. Cell *150*, 339-350.

Li, X., Wang, Q.J., Pan, N., Lee, S., Zhao, Y., Chait, B.T., and Yue, Z. (2011). Phosphorylation-dependent 14-3-3 binding to LRRK2 is impaired by common mutations of familial Parkinson's disease. PLoS One *6*, e17153.

Li, Y., Wu, Y., and Zhou, Y. (2006). Modulation of inactivation properties of CaV2.2 channels by 14-3-3 proteins. Neuron *51*, 755-771.

Liao, W., Wang, S., Han, C., and Zhang, Y. (2005). 14-3-3 proteins regulate glycogen synthase 3beta phosphorylation and inhibit cardiomyocyte hypertrophy. FEBS J *272*, 1845-1854.

Liesa, M., and Shirihai, O.S. (2013). Mitochondrial dynamics in the regulation of nutrient utilization and energy expenditure. Cell Metab *17*, 491-506.

Lin, G., Brownsey, R.W., and MacLeod, K.M. (2009). Regulation of mitochondrial aconitase by phosphorylation in diabetic rat heart. Cell Mol Life Sci *66*, 919-932.

Lin, M.T., and Beal, M.F. (2006). Mitochondrial dysfunction and oxidative stress in neurodegenerative diseases. Nature *443*, 787-795.

Liu, X., Kim, C.N., Yang, J., Jemmerson, R., and Wang, X. (1996). Induction of apoptotic program in cell-free extracts: requirement for dATP and cytochrome c. Cell *86*, 147-157.

Llorente-Folch, I., Rueda, C.B., Pardo, B., Szabadkai, G., Duchen, M.R., and Satrustegui, J. (2015). The regulation of neuronal mitochondrial metabolism by calcium. J Physiol *593*, 3447-3462.

Lloyd, K.G., Davidson, L., and Hornykiewicz, O. (1975). The neurochemistry of Parkinson's disease: effect of L-dopa therapy. The Journal of pharmacology and experimental therapeutics *195*, 453-464.

Los, M., Mozoluk, M., Ferrari, D., Stepczynska, A., Stroh, C., Renz, A., Herceg, Z., Wang, Z.Q., and Schulze-Osthoff, K. (2002). Activation and caspase-mediated inhibition of PARP: a molecular switch between fibroblast necrosis and apoptosis in death receptor signaling. Molecular biology of the cell *13*, 978-988.

Loson, O.C., Song, Z., Chen, H., and Chan, D.C. (2013). Fis1, Mff, MiD49, and MiD51 mediate Drp1 recruitment in mitochondrial fission. Molecular biology of the cell *24*, 659-667.

Lozano, A.M., and Lipsman, N. (2013). Probing and regulating dysfunctional circuits using deep brain stimulation. Neuron *77*, 406-424.

Lu, W., Karuppagounder, S.S., Springer, D.A., Allen, M.D., Zheng, L., Chao, B., Zhang, Y., Dawson, V.L., Dawson, T.M., and Lenardo, M. (2014). Genetic deficiency of the mitochondrial protein PGAM5 causes a Parkinson's-like movement disorder. Nat Commun *5*, 4930.

Lundgaard, I., Li, B., Xie, L., Kang, H., Sanggaard, S., Haswell, J.D., Sun, W., Goldman, S., Blekot, S., Nielsen, M.*, et al.* (2015). Direct neuronal glucose uptake heralds activity-dependent increases in cerebral metabolism. Nat Commun *6*, 6807.

Macaskill, A.F., Rinholm, J.E., Twelvetrees, A.E., Arancibia-Carcamo, I.L., Muir, J., Fransson, A., Aspenstrom, P., Attwell, D., and Kittler, J.T. (2009). Miro1 is a calcium sensor for glutamate receptor-dependent localization of mitochondria at synapses. Neuron *61*, 541-555.

Maehama, T., and Dixon, J.E. (1998). The tumor suppressor, PTEN/MMAC1, dephosphorylates the lipid second messenger, phosphatidylinositol 3,4,5-trisphosphate. J Biol Chem *273*, 13375-13378.

Mahlknecht, P., Gasperi, A., Willeit, P., Kiechl, S., Stockner, H., Willeit, J., Rungger, G., Sawires, M., Nocker, M., Rastner, V.*, et al.* (2016). Prodromal Parkinson's disease as defined per MDS research criteria in the general elderly community. Mov Disord *31*, 1405-1408.

Mailloux, R.J., Jin, X., and Willmore, W.G. (2014). Redox regulation of mitochondrial function with emphasis on cysteine oxidation reactions. Redox Biol *2*, 123-139.

Maita, C., Maita, H., Iguchi-Ariga, S.M., and Ariga, H. (2013). Monomer DJ-1 and its N-terminal sequence are necessary for mitochondrial localization of DJ-1 mutants. PLoS One *8*, e54087.

Majewski, N., Nogueira, V., Bhaskar, P., Coy, P.E., Skeen, J.E., Gottlob, K., Chandel, N.S., Thompson, C.B., Robey, R.B., and Hay, N. (2004). Hexokinase-mitochondria interaction mediated by Akt is required to inhibit apoptosis in the presence or absence of Bax and Bak. Mol Cell *16*, 819-830.

Majmundar, A.J., Wong, W.J., and Simon, M.C. (2010). Hypoxia-inducible factors and the response to hypoxic stress. Mol Cell *40*, 294-309.

Malhotra, D., Thimmulappa, R., Navas-Acien, A., Sandford, A., Elliott, M., Singh, A., Chen, L., Zhuang, X., Hogg, J., Pare, P.*, et al.* (2008). Decline in NRF2-regulated antioxidants in chronic obstructive pulmonary disease lungs due to loss of its positive regulator, DJ-1. American journal of respiratory and critical care medicine *178*, 592-604.

Mannella, C.A. (2006). The relevance of mitochondrial membrane topology to mitochondrial function. Biochimica et biophysica acta *1762*, 140-147.

Marinho, H.S., Real, C., Cyrne, L., Soares, H., and Antunes, F. (2014). Hydrogen peroxide sensing, signaling and regulation of transcription factors. Redox Biol *2*, 535-562.

Markert, C.L. (1984). Lactate dehydrogenase. Biochemistry and function of lactate dehydrogenase. Cell Biochem Funct *2*, 131-134.

Martin, H., Rostas, J., Patel, Y., and Aitken, A. (1994). Subcellular localisation of 14-3-3 isoforms in rat brain using specific antibodies. Journal of neurochemistry *63*, 2259-2265.

Martinat, C., Shendelman, S., Jonason, A., Leete, T., Beal, M.F., Yang, L., Floss, T., and Abeliovich, A. (2004). Sensitivity to oxidative stress in DJ-1-deficient dopamine neurons: an ES- derived cell model of primary Parkinsonism. PLoS Biol *2*, e327.

Matsuda, W., Furuta, T., Nakamura, K.C., Hioki, H., Fujiyama, F., Arai, R., and Kaneko, T. (2009). Single nigrostriatal dopaminergic neurons form widely spread and highly dense axonal arborizations in the neostriatum. J Neurosci *29*, 444-453.

McConnell, J.E., Armstrong, J.F., Hodges, P.E., and Bard, J.B. (1995). The mouse 14-3-3 epsilon isoform, a kinase regulator whose expression pattern is modulated in mesenchyme and neuronal differentiation. Dev Biol *169*, 218-228.

McGeer, P.L., Itagaki, S., Boyes, B.E., and McGeer, E.G. (1988). Reactive microglia are positive for HLA-DR in the substantia nigra of Parkinson's and Alzheimer's disease brains. Neurology *38*, 1285-1291.

McGrath, M.E. (1999). The lysosomal cysteine proteases. Annu Rev Biophys Biomol Struct *28*, 181-204.

McGraw, T.E., and Mittal, V. (2010). Stem cells: Metabolism regulates differentiation. Nat Chem Biol *6*, 176-177.

McNally, R.S., Davis, B.K., Clements, C.M., Accavitti-Loper, M.A., Mak, T.W., and Ting, J.P. (2011). DJ-1 enhances cell survival through the binding of Cezanne, a negative regulator of NF-kappaB. J Biol Chem *286*, 4098-4106.

Meek, S.E., Lane, W.S., and Piwnica-Worms, H. (2004). Comprehensive proteomic analysis of interphase and mitotic 14-3-3-binding proteins. J Biol Chem *279*, 32046-32054.

Meiser, J., Delcambre, S., Wegner, A., Jager, C., Ghelfi, J., d'Herouel, A.F., Dong, X., Weindl, D., Stautner, C., Nonnenmacher, Y.*, et al.* (2016). Loss of DJ-1 impairs antioxidant response by altered glutamine and serine metabolism. Neurobiol Dis *89*, 112-125.

Melin, J., Schulz, C., Wrobel, L., Bernhard, O., Chacinska, A., Jahn, O., Schmidt, B., and Rehling, P. (2014). Presequence recognition by the tom40 channel contributes to precursor translocation into the mitochondrial matrix. Molecular and cellular biology *34*, 3473-3485.

Melser, S., Lavie, J., and Benard, G. (2015). Mitochondrial degradation and energy metabolism. Biochimica et biophysica acta *1853*, 2812-2821.

Mendoza, M.C., Er, E.E., and Blenis, J. (2011). The Ras-ERK and PI3K-mTOR pathways: cross-talk and compensation. Trends Biochem Sci *36*, 320-328.

Mergenthaler, P., Lindauer, U., Dienel, G.A., and Meisel, A. (2013). Sugar for the brain: the role of glucose in physiological and pathological brain function. Trends Neurosci *36*, 587-597.

Metallo, C.M., Gameiro, P.A., Bell, E.L., Mattaini, K.R., Yang, J., Hiller, K., Jewell, C.M., Johnson, Z.R., Irvine, D.J., Guarente, L.*, et al.* (2012). Reductive glutamine metabolism by IDH1 mediates lipogenesis under hypoxia. Nature *481*, 380-384.

Mihara, K., and Omura, T. (1996). Cytosolic factors in mitochondrial protein import. Experientia *52*, 1063-1068.

Minarik, P., Tomaskova, N., Kollarova, M., and Antalik, M. (2002). Malate dehydrogenases--structure and function. Gen Physiol Biophys *21*, 257-265.

Mironov, S.L. (2007). ADP regulates movements of mitochondria in neurons. Biophys J *92*, 2944-2952.

Mitchell, P. (1961). Coupling of phosphorylation to electron and hydrogen transfer by a chemi-osmotic type of mechanism. Nature *191*, 144-148.

Mitsumoto, A., and Nakagawa, Y. (2001). DJ-1 is an indicator for endogenous reactive oxygen species elicited by endotoxin. Free Radic Res *35*, 885-893.

Mitsumoto, A., Nakagawa, Y., Takeuchi, A., Okawa, K., Iwamatsu, A., and Takanezawa, Y. (2001). Oxidized forms of peroxiredoxins and DJ-1 on two-dimensional gels increased in response to sublethal levels of paraquat. Free Radic Res *35*, 301-310.

Miyajima, Y., Sato, Y., Oka, H., Utsuki, S., Kondo, K., Tanizaki, Y., Nagashio, R., Tsuchiya, B., Okayasu, I., and Fujii, K. (2010). Prognostic significance of nuclear DJ-1 expression in astrocytoma. Anticancer Res *30*, 265-269.

Mizuno, Y., Ohta, S., Tanaka, M., Takamiya, S., Suzuki, K., Sato, T., Oya, H., Ozawa, T., and Kagawa, Y. (1989). Deficiencies in complex I subunits of the respiratory chain in Parkinson's disease. Biochem Biophys Res Commun *163*, 1450-1455.

Mnatsakanyan, N., Beutner, G., Porter, G.A., Alavian, K.N., and Jonas, E.A. (2016). Physiological roles of the mitochondrial permeability transition pore. Journal of bioenergetics and biomembranes.

Montero, M., Alonso, M.T., Carnicero, E., Cuchillo-Ibanez, I., Albillos, A., Garcia, A.G., Garcia-Sancho, J., and Alvarez, J. (2000). Chromaffin-cell stimulation triggers fast millimolar mitochondrial Ca2+ transients that modulate secretion. Nat Cell Biol *2*, 57-61.

Moore, D.J., West, A.B., Dikeman, D.A., Dawson, V.L., and Dawson, T.M. (2008). Parkin mediates the degradation-independent ubiquitination of Hsp70. Journal of neurochemistry *105*, 1806-1819.

Morais, V.A., Haddad, D., Craessaerts, K., De Bock, P.J., Swerts, J., Vilain, S., Aerts, L., Overbergh, L., Grunewald, A., Seibler, P.*, et al.* (2014). PINK1 loss-of-function mutations affect mitochondrial complex I activity via NdufA10 ubiquinone uncoupling. Science *344*, 203-207.

Moreno, C.S., Park, S., Nelson, K., Ashby, D., Hubalek, F., Lane, W.S., and Pallas, D.C. (2000). WD40 repeat proteins striatin and S/G(2) nuclear autoantigen are members of a novel family of calmodulin-binding proteins that associate with protein phosphatase 2A. J Biol Chem *275*, 5257-5263.

Morris, A.A. (2005). Cerebral ketone body metabolism. J Inherit Metab Dis *28*, 109-121.

Morrison, D.K. (2009). The 14-3-3 proteins: integrators of diverse signaling cues that impact cell fate and cancer development. Trends Cell Biol *19*, 16-23.

Moscovitz, O., Ben-Nissan, G., Fainer, I., Pollack, D., Mizrachi, L., and Sharon, M. (2015). The Parkinson's-associated protein DJ-1 regulates the 20S proteasome. Nat Commun *6*, 6609.

Murphy, M.P. (2009). How mitochondria produce reactive oxygen species. Biochem J *417*, 1-13.

Muslin, A.J., Tanner, J.W., Allen, P.M., and Shaw, A.S. (1996). Interaction of 14-3-3 with signaling proteins is mediated by the recognition of phosphoserine. Cell *84*, 889-897.

Nagakubo, D., Taira, T., Kitaura, H., Ikeda, M., Tamai, K., Iguchi-Ariga, S.M., and Ariga, H. (1997). DJ-1, a novel oncogene which transforms mouse NIH3T3 cells in cooperation with ras. Biochem Biophys Res Commun *231*, 509-513.

Nakamura, K., Nemani, V.M., Wallender, E.K., Kaehlcke, K., Ott, M., and Edwards, R.H. (2008). Optical reporters for the conformation of alpha-synuclein reveal a specific interaction with mitochondria. J Neurosci *28*, 12305-12317.

Nalls, M.A., Pankratz, N., Lill, C.M., Do, C.B., Hernandez, D.G., Saad, M., DeStefano, A.L., Kara, E., Bras, J., Sharma, M.*, et al.* (2014). Large-scale meta-analysis of genome-wide association data identifies six new risk loci for Parkinson's disease. Nature genetics *46*, 989-993.

Narendra, D., Tanaka, A., Suen, D.F., and Youle, R.J. (2008). Parkin is recruited selectively to impaired mitochondria and promotes their autophagy. J Cell Biol *183*, 795-803.

Narendra, D.P., Jin, S.M., Tanaka, A., Suen, D.F., Gautier, C.A., Shen, J., Cookson, M.R., and Youle, R.J. (2010). PINK1 is selectively stabilized on impaired mitochondria to activate Parkin. PLoS Biol *8*, e1000298.

Narendra, D.P., and Youle, R.J. (2011). Targeting mitochondrial dysfunction: role for PINK1 and Parkin in mitochondrial quality control. Antioxidants & redox signaling *14*, 1929-1938.

Nicholls, D.G. (1978). The regulation of extramitochondrial free calcium ion concentration by rat liver mitochondria. Biochem J *176*, 463-474.

Nichols, R.J., Dzamko, N., Morrice, N.A., Campbell, D.G., Deak, M., Ordureau, A., Macartney, T., Tong, Y., Shen, J., Prescott, A.R.*, et al.* (2010). 14-3-3 binding to LRRK2 is disrupted by multiple Parkinson's disease-associated mutations and regulates cytoplasmic localization. Biochem J *430*, 393-404.

Nikoletopoulou, V., Markaki, M., Palikaras, K., and Tavernarakis, N. (2013). Crosstalk between apoptosis, necrosis and autophagy. Biochimica et biophysica acta *1833*, 3448-3459.

Nunes-Nesi, A., Araujo, W.L., Obata, T., and Fernie, A.R. (2013). Regulation of the mitochondrial tricarboxylic acid cycle. Curr Opin Plant Biol *16*, 335-343.

Obenauer, J.C., Cantley, L.C., and Yaffe, M.B. (2003). Scansite 2.0: Proteome-wide prediction of cell signaling interactions using short sequence motifs. Nucleic acids research *31*, 3635-3641.

Obeso, J.A., Rodriguez-Oroz, M.C., Benitez-Temino, B., Blesa, F.J., Guridi, J., Marin, C., and Rodriguez, M. (2008). Functional organization of the basal ganglia: therapeutic implications for Parkinson's disease. Mov Disord *23 Suppl 3*, S548-559.

Obsil, T., and Obsilova, V. (2011). Structural basis of 14-3-3 protein functions. Seminars in cell & developmental biology *22*, 663-672.

Obsilova, V., Kopecka, M., Kosek, D., Kacirova, M., Kylarova, S., Rezabkova, L., and Obsil, T. (2014). Mechanisms of the 14-3-3 protein function: regulation of protein function through conformational modulation. Physiol Res *63 Suppl 1*, S155-164.

Ogihara, T., Isobe, T., Ichimura, T., Taoka, M., Funaki, M., Sakoda, H., Onishi, Y., Inukai, K., Anai, M., Fukushima, Y.*, et al.* (1997). 14-3-3 protein binds to insulin receptor substrate-1, one of the binding sites of which is in the phosphotyrosine binding domain. J Biol Chem *272*, 25267-25274.

Olzmann, J.A., Li, L., Chudaev, M.V., Chen, J., Perez, F.A., Palmiter, R.D., and Chin, L.S. (2007). Parkin-mediated K63-linked polyubiquitination targets misfolded DJ-1 to aggresomes via binding to HDAC6. J Cell Biol *178*, 1025-1038.

Osbourn, D.M., Sanger, R.H., and Smith, P.J. (2005). Determination of single-cell oxygen consumption with impedance feedback for control of sample-probe separation. Anal Chem *77*, 6999-7004.

Osman, C., Voelker, D.R., and Langer, T. (2011). Making heads or tails of phospholipids in mitochondria. J Cell Biol *192*, 7-16.

Ostrerova, N., Petrucelli, L., Farrer, M., Mehta, N., Choi, P., Hardy, J., and Wolozin, B. (1999). alpha-Synuclein shares physical and functional homology with 14-3-3 proteins. J Neurosci *19*, 5782-5791.

Ott, M., Zhivotovsky, B., and Orrenius, S. (2007). Role of cardiolipin in cytochrome c release from mitochondria. Cell Death Differ *14*, 1243-1247.

Ottmann, C., Yasmin, L., Weyand, M., Veesenmeyer, J.L., Diaz, M.H., Palmer, R.H., Francis, M.S., Hauser, A.R., Wittinghofer, A., and Hallberg, B. (2007). Phosphorylation-

independent interaction between 14-3-3 and exoenzyme S: from structure to pathogenesis. Embo Journal *26*, 902-913.

Ottolini, D., Cali, T., Negro, A., and Brini, M. (2013). The Parkinson disease-related protein DJ-1 counteracts mitochondrial impairment induced by the tumour suppressor protein p53 by enhancing endoplasmic reticulum-mitochondria tethering. Human molecular genetics *22*, 2152-2168.

Pacelli, C., Giguere, N., Bourque, M.J., Levesque, M., Slack, R.S., and Trudeau, L.E. (2015). Elevated Mitochondrial Bioenergetics and Axonal Arborization Size Are Key Contributors to the Vulnerability of Dopamine Neurons. Current biology : CB *25*, 2349-2360.

Palmieri, F. (2004). The mitochondrial transporter family (SLC25): physiological and pathological implications. Pflugers Arch *447*, 689-709.

Paoli, A., Bosco, G., Camporesi, E.M., and Mangar, D. (2015). Ketosis, ketogenic diet and food intake control: a complex relationship. Front Psychol *6*, 27.

Papa, S., and Skulachev, V.P. (1997). Reactive oxygen species, mitochondria, apoptosis and aging. Molecular and cellular biochemistry *174*, 305-319.

Park, J.S., Blair, N.F., and Sue, C.M. (2015). The role of ATP13A2 in Parkinson's disease: Clinical phenotypes and molecular mechanisms. Mov Disord *30*, 770-779.

Parker, W.D., Jr., Boyson, S.J., and Parks, J.K. (1989). Abnormalities of the electron transport chain in idiopathic Parkinson's disease. Annals of neurology *26*, 719-723.

Parsanejad, M., Zhang, Y., Qu, D., Irrcher, I., Rousseaux, M.W., Aleyasin, H., Kamkar, F., Callaghan, S., Slack, R.S., Mak, T.W.*, et al.* (2014). Regulation of the VHL/HIF-1 pathway by DJ-1. J Neurosci *34*, 8043-8050.

Patel, M.S., Nemeria, N.S., Furey, W., and Jordan, F. (2014). The pyruvate dehydrogenase complexes: structure-based function and regulation. J Biol Chem *289*, 16615-16623.

Payne, D.M., Powley, D.G., and Harris, B.G. (1979). Purification, Characterization, and the Presumptive Role of Fumarase in the Energy-Metabolism of Ascaris-Suum. Journal of Parasitology *65*, 833-841.

Pearson, T.A., and Manolio, T.A. (2008). How to interpret a genome-wide association study. JAMA *299*, 1335-1344.

Pellerin, L., and Magistretti, P.J. (1994). Glutamate uptake into astrocytes stimulates aerobic glycolysis: a mechanism coupling neuronal activity to glucose utilization. Proc Natl Acad Sci U S A *91*, 10625-10629.

Pellerin, L., and Magistretti, P.J. (2012). Sweet sixteen for ANLS. J Cereb Blood Flow Metab *32*, 1152-1166.

Penefsky, H.S. (1985). Mechanism of inhibition of mitochondrial adenosine triphosphatase by dicyclohexylcarbodiimide and oligomycin: relationship to ATP synthesis. Proc Natl Acad Sci U S A *82*, 1589-1593.

Perez, R.G., Waymire, J.C., Lin, E., Liu, J.J., Guo, F., and Zigmond, M.J. (2002). A role for alpha-synuclein in the regulation of dopamine biosynthesis. J Neurosci *22*, 3090-3099.

Pfanner, N., van der Laan, M., Amati, P., Capaldi, R.A., Caudy, A.A., Chacinska, A., Darshi, M., Deckers, M., Hoppins, S., Icho, T.*, et al.* (2014). Uniform nomenclature for the mitochondrial contact site and cristae organizing system. J Cell Biol *204*, 1083-1086.

Phan, L., Chou, P.C., Velazquez-Torres, G., Samudio, I., Parreno, K., Huang, Y., Tseng, C., Vu, T., Gully, C., Su, C.H.*, et al.* (2015). The cell cycle regulator 14-3-3sigma opposes and reverses cancer metabolic reprogramming. Nat Commun *6*, 7530.

Phillips, D., Aponte, A.M., French, S.A., Chess, D.J., and Balaban, R.S. (2009). Succinyl-CoA synthetase is a phosphate target for the activation of mitochondrial metabolism. Biochemistry *48*, 7140-7149.

Pickrell, A.M., and Youle, R.J. (2015). The roles of PINK1, parkin, and mitochondrial fidelity in Parkinson's disease. Neuron *85*, 257-273.

Pissadaki, E.K., and Bolam, J.P. (2013). The energy cost of action potential propagation in dopamine neurons: clues to susceptibility in Parkinson's disease. Front Comput Neurosci *7*, 13.

Plotegher, N., Kumar, D., Tessari, I., Brucale, M., Munari, F., Tosatto, L., Belluzzi, E., Greggio, E., Bisaglia, M., Capaldi, S.*, et al.* (2014). The chaperone-like protein 14-3-3eta interacts with human alpha-synuclein aggregation intermediates rerouting the amyloidogenic pathway and reducing alpha-synuclein cellular toxicity. Human molecular genetics *23*, 5615-5629.

Plun-Favreau, H., Klupsch, K., Moisoi, N., Gandhi, S., Kjaer, S., Frith, D., Harvey, K., Deas, E., Harvey, R.J., McDonald, N.*, et al.* (2007). The mitochondrial protease HtrA2 is regulated by Parkinson's disease-associated kinase PINK1. Nat Cell Biol *9*, 1243-1252.

Pochini, L., Scalise, M., Galluccio, M., and Indiveri, C. (2014). Membrane transporters for the special amino acid glutamine: structure/function relationships and relevance to human health. Front Chem *2*, 61.

Poewe, W., Seppi, K., Tanner, C.M., Halliday, G.M., Brundin, P., Volkmann, J., Schrag, A.E., and Lang, A.E. (2017). Parkinson disease. Nat Rev Dis Primers *3*, 17013.

Pogson, J.H., Ivatt, R.M., Sanchez-Martinez, A., Tufi, R., Wilson, E., Mortiboys, H., and Whitworth, A.J. (2014). The complex I subunit NDUFA10 selectively rescues Drosophila pink1 mutants through a mechanism independent of mitophagy. PLoS Genet *10*, e1004815.

Politis, M. (2014). Neuroimaging in Parkinson disease: from research setting to clinical practice. Nat Rev Neurol *10*, 708-722.

Polymeropoulos, M.H., Lavedan, C., Leroy, E., Ide, S.E., Dehejia, A., Dutra, A., Pike, B., Root, H., Rubenstein, J., Boyer, R.*, et al.* (1997). Mutation in the alpha-synuclein gene identified in families with Parkinson's disease. Science *276*, 2045-2047.

Posor, Y., Eichhorn-Grunig, M., and Haucke, V. (2015). Phosphoinositides in endocytosis. Biochimica et biophysica acta *1851*, 794-804.

Postuma, R.B., Berg, D., Stern, M., Poewe, W., Olanow, C.W., Oertel, W., Obeso, J., Marek, K., Litvan, I., Lang, A.E.*, et al.* (2015). MDS clinical diagnostic criteria for Parkinson's disease. Mov Disord *30*, 1591-1601.

Pozuelo Rubio, M., Geraghty, K.M., Wong, B.H., Wood, N.T., Campbell, D.G., Morrice, N., and Mackintosh, C. (2004). 14-3-3-affinity purification of over 200 human phosphoproteins reveals new links to regulation of cellular metabolism, proliferation and trafficking. Biochem J *379*, 395-408.

Pozuelo Rubio, M., Peggie, M., Wong, B.H., Morrice, N., and MacKintosh, C. (2003). 14-3-3s regulate fructose-2,6-bisphosphate levels by binding to PKB-phosphorylated cardiac fructose-2,6-bisphosphate kinase/phosphatase. EMBO J *22*, 3514-3523.

Pozuelo-Rubio, M. (2011). Regulation of autophagic activity by 14-3-3zeta proteins associated with class III phosphatidylinositol-3-kinase. Cell Death Differ *18*, 479-492.

Pridgeon, J.W., Olzmann, J.A., Chin, L.S., and Li, L. (2007). PINK1 protects against oxidative stress by phosphorylating mitochondrial chaperone TRAP1. PLoS Biol *5*, e172.

Puri, P., Myers, K., Kline, D., and Vijayaraghavan, S. (2008). Proteomic analysis of bovine sperm YWHA binding partners identify proteins involved in signaling and metabolism. Biol Reprod *79*, 1183-1191.

Qiao, H., Foote, M., Graham, K., Wu, Y., and Zhou, Y. (2014). 14-3-3 proteins are required for hippocampal long-term potentiation and associative learning and memory. J Neurosci *34*, 4801-4808.

Rabl, R., Soubannier, V., Scholz, R., Vogel, F., Mendl, N., Vasiljev-Neumeyer, A., Korner, C., Jagasia, R., Keil, T., Baumeister, W.*, et al.* (2009). Formation of cristae and crista junctions in mitochondria depends on antagonism between Fcj1 and Su e/g. J Cell Biol *185*, 1047-1063.

Ramakrishnan, G., Davaakhuu, G., Chung, W.C., Zhu, H., Rana, A., Filipovic, A., Green, A.R., Atfi, A., Pannuti, A., Miele, L.*, et al.* (2015). AKT and 14-3-3 regulate Notch4 nuclear localization. Sci Rep *5*, 8782.

Rao, S., Schmidt, O., Harbauer, A.B., Schonfisch, B., Guiard, B., Pfanner, N., and Meisinger, C. (2012). Biogenesis of the preprotein translocase of the outer mitochondrial membrane: protein kinase A phosphorylates the precursor of Tom40 and impairs its import. Molecular biology of the cell *23*, 1618-1627.

Rapoport, M., Saada, A., Elpeleg, O., and Lorberboum-Galski, H. (2008). TAT-mediated delivery of LAD restores pyruvate dehydrogenase complex activity in the mitochondria of patients with LAD deficiency. Mol Ther *16*, 691-697.

Raturi, A., and Simmen, T. (2013). Where the endoplasmic reticulum and the mitochondrion tie the knot: the mitochondria-associated membrane (MAM). Biochimica et biophysica acta *1833*, 213-224.

Reitzer, L.J., Wice, B.M., and Kennell, D. (1979). Evidence that glutamine, not sugar, is the major energy source for cultured HeLa cells. J Biol Chem *254*, 2669-2676.

Ren, H., Fu, K., Wang, D., Mu, C., and Wang, G. (2011). Oxidized DJ-1 interacts with the mitochondrial protein BCL-XL. J Biol Chem *286*, 35308-35317.

Repici, M., Straatman, K.R., Balduccio, N., Enguita, F.J., Outeiro, T.F., and Giorgini, F. (2013). Parkinson's disease-associated mutations in DJ-1 modulate its dimerization in living cells. J Mol Med (Berl) *91*, 599-611.

Requejo-Aguilar, R., Lopez-Fabuel, I., Jimenez-Blasco, D., Fernandez, E., Almeida, A., and Bolanos, J.P. (2015). DJ1 represses glycolysis and cell proliferation by transcriptionally up-regulating Pink1. Biochem J *467*, 303-310.

Reynolds, R., Roncaroli, F., Nicholas, R., Radotra, B., Gveric, D., and Howell, O. (2011). The neuropathological basis of clinical progression in multiple sclerosis. Acta Neuropathol *122*, 155-170.

Rezabkova, L., Man, P., Novak, P., Herman, P., Vecer, J., Obsilova, V., and Obsil, T. (2011). Structural basis for the 14-3-3 protein-dependent inhibition of the regulator of G protein signaling 3 (RGS3) function. J Biol Chem *286*, 43527-43536.

Rhee, S.G. (2006). Cell signaling. H2O2, a necessary evil for cell signaling. Science *312*, 1882-1883.

Richarme, G., Mihoub, M., Dairou, J., Bui, L.C., Leger, T., and Lamouri, A. (2015). Parkinsonism-associated protein DJ-1/Park7 is a major protein deglycase that repairs methylglyoxal- and glyoxal-glycated cysteine, arginine, and lysine residues. J Biol Chem *290*, 1885-1897.

Richter, C. (1993). Pro-oxidants and mitochondrial Ca2+: their relationship to apoptosis and oncogenesis. FEBS Lett *325*, 104-107.

Riemer, J., Bulleid, N., and Herrmann, J.M. (2009). Disulfide formation in the ER and mitochondria: two solutions to a common process. Science *324*, 1284-1287.

Riley, B.E., Lougheed, J.C., Callaway, K., Velasquez, M., Brecht, E., Nguyen, L., Shaler, T., Walker, D., Yang, Y., Regnstrom, K.*, et al.* (2013). Structure and function of Parkin E3 ubiquitin ligase reveals aspects of RING and HECT ligases. Nat Commun *4*, 1982.

Rizzuto, R., Brini, M., Murgia, M., and Pozzan, T. (1993). Microdomains with high Ca2+ close to IP3-sensitive channels that are sensed by neighboring mitochondria. Science *262*, 744-747.

Rizzuto, R., De Stefani, D., Raffaello, A., and Mammucari, C. (2012). Mitochondria as sensors and regulators of calcium signalling. Nature reviews Molecular cell biology *13*, 566-578.

Ross, C.A., and Poirier, M.A. (2004). Protein aggregation and neurodegenerative disease. Nat Med *10 Suppl*, S10-17.

Ruderman, N.B., Ross, P.S., Berger, M., and Goodman, M.N. (1974). Regulation of glucose and ketone-body metabolism in brain of anaesthetized rats. Biochem J *138*, 1-10.

Rutter, J., Winge, D.R., and Schiffman, J.D. (2010). Succinate dehydrogenase - Assembly, regulation and role in human disease. Mitochondrion *10*, 393-401.

Sacchetti, S., Alavian, K.N., Lazrove, E., and Jonas, E.A. (2013). F1FO ATPase vesicle preparation and technique for performing patch clamp recordings of submitochondrial vesicle membranes. J Vis Exp, e4394.

Santo-Domingo, J., and Demaurex, N. (2010). Calcium uptake mechanisms of mitochondria. Biochimica et biophysica acta *1797*, 907-912.

Sato, M., and Sato, K. (2013). Maternal inheritance of mitochondrial DNA by diverse mechanisms to eliminate paternal mitochondrial DNA. Biochimica et biophysica acta *1833*, 1979-1984.

Sato, S., Chiba, T., Sakata, E., Kato, K., Mizuno, Y., Hattori, N., and Tanaka, K. (2006). 14-3-3eta is a novel regulator of parkin ubiquitin ligase. EMBO J *25*, 211-221.

Sato, S., Fujita, N., and Tsuruo, T. (2002). Regulation of kinase activity of 3-phosphoinositide-dependent protein kinase-1 by binding to 14-3-3. J Biol Chem *277*, 39360-39367.

Sazanov, L.A., and Jackson, J.B. (1994). Proton-translocating transhydrogenase and NAD- and NADP-linked isocitrate dehydrogenases operate in a substrate cycle which contributes to fine regulation of the tricarboxylic acid cycle activity in mitochondria. FEBS Lett *344*, 109-116.

Scarpulla, R.C., Vega, R.B., and Kelly, D.P. (2012). Transcriptional integration of mitochondrial biogenesis. Trends Endocrinol Metab *23*, 459-466.

Schaar, C.E., Dues, D.J., Spielbauer, K.K., Machiela, E., Cooper, J.F., Senchuk, M., Hekimi, S., and Van Raamsdonk, J.M. (2015). Mitochondrial and cytoplasmic ROS have opposing effects on lifespan. PLoS Genet *11*, e1004972.

Schapira, A.H. (2008). Mitochondria in the aetiology and pathogenesis of Parkinson's disease. Lancet neurology *7*, 97-109.

Schapira, A.H. (2011). Aetiopathogenesis of Parkinson's disease. Journal of neurology *258*, S307-310.

Schapira, A.H. (2015). Glucocerebrosidase and Parkinson disease: Recent advances. Mol Cell Neurosci *66*, 37-42.

Schapira, A.H., Cooper, J.M., Dexter, D., Jenner, P., Clark, J.B., and Marsden, C.D. (1989). Mitochondrial complex I deficiency in Parkinson's disease. Lancet *1*, 1269.

Schapira, A.H., and Jenner, P. (2011). Etiology and pathogenesis of Parkinson's disease. Mov Disord *26*, 1049-1055.

Schindelin, J., Arganda-Carreras, I., Frise, E., Kaynig, V., Longair, M., Pietzsch, T., Preibisch, S., Rueden, C., Saalfeld, S., Schmid, B.*, et al.* (2012). Fiji: an open-source platform for biological-image analysis. Nat Methods *9*, 676-682.

Schmidt, O., Harbauer, A.B., Rao, S., Eyrich, B., Zahedi, R.P., Stojanovski, D., Schonfisch, B., Guiard, B., Sickmann, A., Pfanner, N., *et al.* (2011). Regulation of mitochondrial protein import by cytosolic kinases. Cell *144*, 227-239.

Schoenwaelder, S.M., Darbousset, R., Cranmer, S.L., Ramshaw, H.S., Orive, S.L., Sturgeon, S., Yuan, Y., Yao, Y., Krycer, J.R., Woodcock, J., *et al.* (2016). 14-3-3zeta regulates the mitochondrial respiratory reserve linked to platelet phosphatidylserine exposure and procoagulant function. Nat Commun *7*, 12862.

Schwarz, T.L. (2013). Mitochondrial trafficking in neurons. Cold Spring Harb Perspect Biol *5*.

Scorrano, L., Ashiya, M., Buttle, K., Weiler, S., Oakes, S.A., Mannella, C.A., and Korsmeyer, S.J. (2002). A distinct pathway remodels mitochondrial cristae and mobilizes cytochrome c during apoptosis. Dev Cell *2*, 55-67.

Sekito, A., Koide-Yoshida, S., Niki, T., Taira, T., Iguchi-Ariga, S.M., and Ariga, H. (2006). DJ-1 interacts with HIPK1 and affects H2O2-induced cell death. Free Radic Res *40*, 155-165.

Semenza, G.L. (2014). Oxygen sensing, hypoxia-inducible factors, and disease pathophysiology. Annu Rev Pathol *9*, 47-71.

Sentelle, R.D., Senkal, C.E., Jiang, W., Ponnusamy, S., Gencer, S., Selvam, S.P., Ramshesh, V.K., Peterson, Y.K., Lemasters, J.J., Szulc, Z.M., *et al.* (2012). Ceramide targets autophagosomes to mitochondria and induces lethal mitophagy. Nat Chem Biol *8*, 831-838.

Sepe, S., Milanese, C., Gabriels, S., Derks, K.W., Payan-Gomez, C., van, I.W.F., Rijksen, Y.M., Nigg, A.L., Moreno, S., Cerri, S., *et al.* (2016). Inefficient DNA Repair Is an Aging-Related Modifier of Parkinson's Disease. Cell Rep *15*, 1866-1875.

Sermeus, A., and Michiels, C. (2011). Reciprocal influence of the p53 and the hypoxic pathways. Cell death & disease *2*, e164.

Sharp, M.G., Adams, S.M., Walker, R.A., Brammar, W.J., and Varley, J.M. (1992). Differential expression of the mitochondrial gene cytochrome oxidase II in benign and malignant breast tissue. J Pathol *168*, 163-168.

Shchepina, L.A., Pletjushkina, O.Y., Avetisyan, A.V., Bakeeva, L.E., Fetisova, E.K., Izyumov, D.S., Saprunova, V.B., Vyssokikh, M.Y., Chernyak, B.V., and Skulachev, V.P. (2002). Oligomycin, inhibitor of the F0 part of H+-ATP-synthase, suppresses the TNF-induced apoptosis. Oncogene *21*, 8149-8157.

Shendelman, S., Jonason, A., Martinat, C., Leete, T., and Abeliovich, A. (2004). DJ-1 is a redox-dependent molecular chaperone that inhibits alpha-synuclein aggregate formation. PLoS Biol *2*, e362.

Sheng, Z.H. (2014). Mitochondrial trafficking and anchoring in neurons: New insight and implications. J Cell Biol *204*, 1087-1098.

Sheng, Z.H., and Cai, Q. (2012). Mitochondrial transport in neurons: impact on synaptic homeostasis and neurodegeneration. Nature reviews Neuroscience *13*, 77-93.

Shi, S.Y., Lu, S.Y., Sivasubramaniyam, T., Revelo, X.S., Cai, E.P., Luk, C.T., Schroer, S.A., Patel, P., Kim, R.H., Bombardier, E., *et al.* (2015). DJ-1 links muscle ROS production with metabolic reprogramming and systemic energy homeostasis in mice. Nat Commun *6*, 7415.

Shi, Y., Chen, J., Weng, C., Chen, R., Zheng, Y., Chen, Q., and Tang, H. (2003). Identification of the protein-protein contact site and interaction mode of human VDAC1 with Bcl-2 family proteins. Biochem Biophys Res Commun *305*, 989-996.

Shimada, T., Fournier, A.E., and Yamagata, K. (2013). Neuroprotective function of 14-3-3 proteins in neurodegeneration. Biomed Res Int *2013*, 564534.

Shimura, H., Schlossmacher, M.G., Hattori, N., Frosch, M.P., Trockenbacher, A., Schneider, R., Mizuno, Y., Kosik, K.S., and Selkoe, D.J. (2001). Ubiquitination of a new form of alpha-synuclein by parkin from human brain: implications for Parkinson's disease. Science *293*, 263-269.

Shin, J.H., Ko, H.S., Kang, H., Lee, Y., Lee, Y.I., Pletinkova, O., Troconso, J.C., Dawson, V.L., and Dawson, T.M. (2011). PARIS (ZNF746) repression of PGC-1alpha contributes to neurodegeneration in Parkinson's disease. Cell *144*, 689-702.

Shinoda, S., Skradski, S.L., Araki, T., Schindler, C.K., Meller, R., Lan, J.Q., Taki, W., Simon, R.P., and Henshall, D.C. (2003). Formation of a tumour necrosis factor receptor 1 molecular scaffolding complex and activation of apoptosis signal-regulating kinase 1 during seizure-induced neuronal death. Eur J Neurosci *17*, 2065-2076.

Shojaee, S., Sina, F., Banihosseini, S.S., Kazemi, M.H., Kalhor, R., Shahidi, G.A., Fakhrai-Rad, H., Ronaghi, M., and Elahi, E. (2008). Genome-wide linkage analysis of a Parkinsonian-pyramidal syndrome pedigree by 500 K SNP arrays. Am J Hum Genet *82*, 1375-1384.

Shulman, J.M., De Jager, P.L., and Feany, M.B. (2011). Parkinson's disease: genetics and pathogenesis. Annu Rev Pathol *6*, 193-222.

Shumway, S.D., Li, Y., and Xiong, Y. (2003). 14-3-3beta binds to and negatively regulates the tuberous sclerosis complex 2 (TSC2) tumor suppressor gene product, tuberin. J Biol Chem *278*, 2089-2092.

Sidransky, E., Nalls, M.A., Aasly, J.O., Aharon-Peretz, J., Annesi, G., Barbosa, E.R., Bar-Shira, A., Berg, D., Bras, J., Brice, A., *et al.* (2009). Multicenter analysis of glucocerebrosidase mutations in Parkinson's disease. N Engl J Med *361*, 1651-1661.

Siebert, G., Carsiotis, M., and Plaut, G.W. (1957). [The enzymatic properties of isocitric dehydrogenase]. J Biol Chem *226*, 977-991.

Sies, H. (2014). Role of metabolic H2O2 generation: redox signaling and oxidative stress. J Biol Chem *289*, 8735-8741.

Simpson, I.A., Carruthers, A., and Vannucci, S.J. (2007). Supply and demand in cerebral energy metabolism: the role of nutrient transporters. J Cereb Blood Flow Metab *27*, 1766-1791.

Sinha, S., and Levine, B. (2008). The autophagy effector Beclin 1: a novel BH3-only protein. Oncogene *27 Suppl 1*, S137-148.

Skulachev, V.P. (2001). Mitochondrial filaments and clusters as intracellular power-transmitting cables. Trends Biochem Sci *26*, 23-29.

Skulachev, V.P. (2006). Bioenergetic aspects of apoptosis, necrosis and mitoptosis. Apoptosis *11*, 473-485.

Slone, S.R., Lavalley, N., McFerrin, M., Wang, B., and Yacoubian, T.A. (2015). Increased 14-3-3 phosphorylation observed in Parkinson's disease reduces neuroprotective potential of 14-3-3 proteins. Neurobiol Dis *79*, 1-13.

Sluchanko, N.N., Artemova, N.V., Sudnitsyna, M.V., Safenkova, I.V., Antson, A.A., Levitsky, D.I., and Gusev, N.B. (2012). Monomeric 14-3-3zeta has a chaperone-like activity and is stabilized by phosphorylated HspB6. Biochemistry *51*, 6127-6138.

Sluchanko, N.N., and Gusev, N.B. (2012). Oligomeric structure of 14-3-3 protein: what do we know about monomers? FEBS Lett *586*, 4249-4256.

Smith, Y., Wichmann, T., Factor, S.A., and DeLong, M.R. (2012). Parkinson's disease therapeutics: new developments and challenges since the introduction of levodopa. Neuropsychopharmacology *37*, 213-246.

Sofroniew, M.V., and Vinters, H.V. (2010). Astrocytes: biology and pathology. Acta Neuropathol *119*, 7-35.

Solaini, G., Baracca, A., Lenaz, G., and Sgarbi, G. (2010). Hypoxia and mitochondrial oxidative metabolism. Biochimica et biophysica acta *1797*, 1171-1177.

Solignac, M., Genermont, J., Monnerot, M., and Mounolou, J.C. (1987). Drosophila Mitochondrial Genetics: Evolution of Heteroplasmy through Germ Line Cell Divisions. Genetics *117*, 687-696.

Song, I.K., Lee, J.J., Cho, J.H., Jeong, J., Shin, D.H., and Lee, K.J. (2016). Degradation of Redox-Sensitive Proteins including Peroxiredoxins and DJ-1 is Promoted by Oxidation-induced Conformational Changes and Ubiquitination. Sci Rep *6*, 34432.

Spillantini, M.G., Crowther, R.A., Jakes, R., Hasegawa, M., and Goedert, M. (1998). alpha-Synuclein in filamentous inclusions of Lewy bodies from Parkinson's disease and dementia with lewy bodies. Proc Natl Acad Sci U S A *95*, 6469-6473.

Stafa, K., Trancikova, A., Webber, P.J., Glauser, L., West, A.B., and Moore, D.J. (2012). GTPase activity and neuronal toxicity of Parkinson's disease-associated LRRK2 is regulated by ArfGAP1. PLoS Genet *8*, e1002526.

Stambolic, V., Suzuki, A., de la Pompa, J.L., Brothers, G.M., Mirtsos, C., Sasaki, T., Ruland, J., Penninger, J.M., Siderovski, D.P., and Mak, T.W. (1998). Negative regulation of PKB/Akt-dependent cell survival by the tumor suppressor PTEN. Cell *95*, 29-39.

Stamer, K., Vogel, R., Thies, E., Mandelkow, E., and Mandelkow, E.M. (2002). Tau blocks traffic of organelles, neurofilaments, and APP vesicles in neurons and enhances oxidative stress. J Cell Biol *156*, 1051-1063.

Stephens, L., Anderson, K., Stokoe, D., Erdjument-Bromage, H., Painter, G.F., Holmes, A.B., Gaffney, P.R., Reese, C.B., McCormick, F., Tempst, P.*, et al.* (1998). Protein kinase B kinases that mediate phosphatidylinositol 3,4,5-trisphosphate-dependent activation of protein kinase B. Science *279*, 710-714.

Stewart, J.B., and Chinnery, P.F. (2015). The dynamics of mitochondrial DNA heteroplasmy: implications for human health and disease. Nat Rev Genet *16*, 530-542.

Strain, J., Lorenz, C.R., Bode, J., Garland, S., Smolen, G.A., Ta, D.T., Vickery, L.E., and Culotta, V.C. (1998). Suppressors of superoxide dismutase (SOD1) deficiency in Saccharomyces cerevisiae. Identification of proteins predicted to mediate iron-sulfur cluster assembly. J Biol Chem *273*, 31138-31144.

Strauss, M., Hofhaus, G., Schroder, R.R., and Kuhlbrandt, W. (2008). Dimer ribbons of ATP synthase shape the inner mitochondrial membrane. EMBO J *27*, 1154-1160.

Su, Y.C., Guo, X., and Qi, X. (2015). Threonine 56 phosphorylation of Bcl-2 is required for LRRK2 G2019S-induced mitochondrial depolarization and autophagy. Biochimica et biophysica acta *1852*, 12-21.

Subramaniam, S.R., and Chesselet, M.F. (2013). Mitochondrial dysfunction and oxidative stress in Parkinson's disease. Progress in neurobiology *106-107*, 17-32.

Suen, D.F., Norris, K.L., and Youle, R.J. (2008). Mitochondrial dynamics and apoptosis. Genes Dev *22*, 1577-1590.

Sullivan, L.B., Gui, D.Y., Hosios, A.M., Bush, L.N., Freinkman, E., and Vander Heiden, M.G. (2015). Supporting Aspartate Biosynthesis Is an Essential Function of Respiration in Proliferating Cells. Cell *162*, 552-563.

Sulzer, D. (2010). Clues to how alpha-synuclein damages neurons in Parkinson's disease. Mov Disord *25 Suppl 1*, S27-31.

Surmeier, D.J., Guzman, J.N., Sanchez-Padilla, J., and Schumacker, P.T. (2011). The role of calcium and mitochondrial oxidant stress in the loss of substantia nigra pars compacta dopaminergic neurons in Parkinson's disease. Neuroscience *198*, 221-231.

Surmeier, D.J., and Schumacker, P.T. (2013). Calcium, bioenergetics, and neuronal vulnerability in Parkinson's disease. J Biol Chem *288*, 10736-10741.

Surmeier, D.J., Schumacker, P.T., Guzman, J.D., Ilijic, E., Yang, B., and Zampese, E. (2016). Calcium and Parkinson's disease. Biochem Biophys Res Commun.

Susin, S.A., Lorenzo, H.K., Zamzami, N., Marzo, I., Snow, B.E., Brothers, G.M., Mangion, J., Jacotot, E., Costantini, P., Loeffler, M.*, et al.* (1999). Molecular characterization of mitochondrial apoptosis-inducing factor. Nature *397*, 441-446.

Szabo, I., Bernardi, P., and Zoratti, M. (1992). Modulation of the mitochondrial megachannel by divalent cations and protons. J Biol Chem *267*, 2940-2946.

Taipa, R., Pereira, C., Reis, I., Alonso, I., Bastos-Lima, A., Melo-Pires, M., and Magalhaes, M. (2016). DJ-1 linked parkinsonism (PARK7) is associated with Lewy body pathology. Brain : a journal of neurology *139*, 1680-1687.

Taira, T., Iguchi-Ariga, S.M., and Ariga, H. (2004a). Co-localization with DJ-1 is essential for the androgen receptor to exert its transcription activity that has been impaired by androgen antagonists. Biol Pharm Bull *27*, 574-577.

Taira, T., Saito, Y., Niki, T., Iguchi-Ariga, S.M., Takahashi, K., and Ariga, H. (2004b). DJ-1 has a role in antioxidative stress to prevent cell death. EMBO Rep *5*, 213-218.

Tait, S.W., and Green, D.R. (2010). Mitochondria and cell death: outer membrane permeabilization and beyond. Nature reviews Molecular cell biology *11*, 621-632.

Takahashi, Y. (2003). The 14-3-3 proteins: gene, gene expression, and function. Neurochem Res *28*, 1265-1273.

Tamura, Y., Endo, T., Iijima, M., and Sesaki, H. (2009). Ups1p and Ups2p antagonistically regulate cardiolipin metabolism in mitochondria. J Cell Biol *185*, 1029-1045.

Tang, C.C., Poston, K.L., Dhawan, V., and Eidelberg, D. (2010). Abnormalities in metabolic network activity precede the onset of motor symptoms in Parkinson's disease. J Neurosci *30*, 1049-1056.

Tanti, G.K., and Goswami, S.K. (2014). SG2NA recruits DJ-1 and Akt into the mitochondria and membrane to protect cells from oxidative damage. Free radical biology & medicine *75*, 1-13.

Thomas, K.J., McCoy, M.K., Blackinton, J., Beilina, A., van der Brug, M., Sandebring, A., Miller, D., Maric, D., Cedazo-Minguez, A., and Cookson, M.R. (2011). DJ-1 acts in parallel to the PINK1/parkin pathway to control mitochondrial function and autophagy. Human molecular genetics *20*, 40-50.

Thomas, R.E., Andrews, L.A., Burman, J.L., Lin, W.Y., and Pallanck, L.J. (2014). PINK1-Parkin pathway activity is regulated by degradation of PINK1 in the mitochondrial matrix. PLoS Genet *10*, e1004279.

Thornberry, N.A., and Lazebnik, Y. (1998). Caspases: enemies within. Science *281*, 1312-1316.

Tiede, L.M., Cook, E.A., Morsey, B., and Fox, H.S. (2011). Oxygen matters: tissue culture oxygen levels affect mitochondrial function and structure as well as responses to HIV viroproteins. Cell death & disease *2*, e246.

Tomas, A., Futter, C.E., and Eden, E.R. (2014). EGF receptor trafficking: consequences for signaling and cancer. Trends Cell Biol *24*, 26-34.

Toyo-oka, K., Shionoya, A., Gambello, M.J., Cardoso, C., Leventer, R., Ward, H.L., Ayala, R., Tsai, L.H., Dobyns, W., Ledbetter, D.*, et al.* (2003). 14-3-3epsilon is important for neuronal migration by binding to NUDEL: a molecular explanation for Miller-Dieker syndrome. Nature genetics *34*, 274-285.

Traba, J., Del Arco, A., Duchen, M.R., Szabadkai, G., and Satrustegui, J. (2012). SCaMC-1 promotes cancer cell survival by desensitizing mitochondrial permeability

transition via ATP/ADP-mediated matrix Ca(2+) buffering. Cell Death Differ *19*, 650-660.

Trachootham, D., Lu, W., Ogasawara, M.A., Nilsa, R.D., and Huang, P. (2008). Redox regulation of cell survival. Antioxidants & redox signaling *10*, 1343-1374.

Trempe, J.F., and Fon, E.A. (2013). Structure and Function of Parkin, PINK1, and DJ-1, the Three Musketeers of Neuroprotection. Front Neurol *4*, 38.

Trempe, J.F., Sauve, V., Grenier, K., Seirafi, M., Tang, M.Y., Menade, M., Al-Abdul-Wahid, S., Krett, J., Wong, K., Kozlov, G.*, et al.* (2013). Structure of parkin reveals mechanisms for ubiquitin ligase activation. Science *340*, 1451-1455.

Tzivion, G., Shen, Y.H., and Zhu, J. (2001). 14-3-3 proteins; bringing new definitions to scaffolding. Oncogene *20*, 6331-6338.

Usami, Y., Hatano, T., Imai, S., Kubo, S., Sato, S., Saiki, S., Fujioka, Y., Ohba, Y., Sato, F., Funayama, M.*, et al.* (2011). DJ-1 associates with synaptic membranes. Neurobiol Dis *43*, 651-662.

Vaishnavi, S.N., Vlassenko, A.G., Rundle, M.M., Snyder, A.Z., Mintun, M.A., and Raichle, M.E. (2010). Regional aerobic glycolysis in the human brain. Proc Natl Acad Sci U S A *107*, 17757-17762.

Valente, E.M., Abou-Sleiman, P.M., Caputo, V., Muqit, M.M., Harvey, K., Gispert, S., Ali, Z., Del Turco, D., Bentivoglio, A.R., Healy, D.G.*, et al.* (2004). Hereditary early-onset Parkinson's disease caused by mutations in PINK1. Science *304*, 1158-1160.

van der Brug, M.P., Blackinton, J., Chandran, J., Hao, L.Y., Lal, A., Mazan-Mamczarz, K., Martindale, J., Xie, C., Ahmad, R., Thomas, K.J.*, et al.* (2008). RNA binding activity of the recessive parkinsonism protein DJ-1 supports involvement in multiple cellular pathways. Proc Natl Acad Sci U S A *105*, 10244-10249.

van der Laan, M., Meinecke, M., Dudek, J., Hutu, D.P., Lind, M., Perschil, I., Guiard, B., Wagner, R., Pfanner, N., and Rehling, P. (2007). Motor-free mitochondrial presequence translocase drives membrane integration of preproteins. Nat Cell Biol *9*, 1152-1159.

Van Laar, V.S., and Berman, S.B. (2013). The interplay of neuronal mitochondrial dynamics and bioenergetics: implications for Parkinson's disease. Neurobiol Dis *51*, 43-55.

Van Laar, V.S., Mishizen, A.J., Cascio, M., and Hastings, T.G. (2009). Proteomic identification of dopamine-conjugated proteins from isolated rat brain mitochondria and SH-SY5Y cells. Neurobiol Dis *34*, 487-500.

Vance, J.E. (2014). MAM (mitochondria-associated membranes) in mammalian cells: lipids and beyond. Biochimica et biophysica acta *1841*, 595-609.

Vance, J.E., and Tasseva, G. (2013). Formation and function of phosphatidylserine and phosphatidylethanolamine in mammalian cells. Biochimica et biophysica acta *1831*, 543-554.

Vanden Berghe, T., Linkermann, A., Jouan-Lanhouet, S., Walczak, H., and Vandenabeele, P. (2014). Regulated necrosis: the expanding network of non-apoptotic cell death pathways. Nature reviews Molecular cell biology *15*, 135-147.

Vander Haar, E., Lee, S.I., Bandhakavi, S., Griffin, T.J., and Kim, D.H. (2007). Insulin signalling to mTOR mediated by the Akt/PKB substrate PRAS40. Nat Cell Biol *9*, 316-323.

Vander Heiden, M.G., Cantley, L.C., and Thompson, C.B. (2009). Understanding the Warburg effect: the metabolic requirements of cell proliferation. Science *324*, 1029-1033.

Vanderperre, B., Bender, T., Kunji, E.R., and Martinou, J.C. (2015). Mitochondrial pyruvate import and its effects on homeostasis. Curr Opin Cell Biol *33*, 35-41.

Vasseur, S., Afzal, S., Tardivel-Lacombe, J., Park, D.S., Iovanna, J.L., and Mak, T.W. (2009). DJ-1/PARK7 is an important mediator of hypoxia-induced cellular responses. Proc Natl Acad Sci U S A *106*, 1111-1116.

Villinger, S., Briones, R., Giller, K., Zachariae, U., Lange, A., de Groot, B.L., Griesinger, C., Becker, S., and Zweckstetter, M. (2010). Functional dynamics in the voltage-dependent anion channel. Proc Natl Acad Sci U S A *107*, 22546-22551.

Vives-Bauza, C., Zhou, C., Huang, Y., Cui, M., de Vries, R.L., Kim, J., May, J., Tocilescu, M.A., Liu, W., Ko, H.S.*, et al.* (2010). PINK1-dependent recruitment of Parkin to mitochondria in mitophagy. Proc Natl Acad Sci U S A *107*, 378-383.

Voigt, A., Berlemann, L.A., and Winklhofer, K.F. (2016). The mitochondrial kinase PINK1: functions beyond mitophagy. Journal of neurochemistry.

Waak, J., Weber, S.S., Gorner, K., Schall, C., Ichijo, H., Stehle, T., and Kahle, P.J. (2009). Oxidizable residues mediating protein stability and cytoprotective interaction of DJ-1 with apoptosis signal-regulating kinase 1. J Biol Chem *284*, 14245-14257.

Wagenfeld, A., Gromoll, J., and Cooper, T.G. (1998). Molecular cloning and expression of rat contraception associated protein 1 (CAP1), a protein putatively involved in fertilization. Biochem Biophys Res Commun *251*, 545-549.

Wagner, B.A., Venkataraman, S., and Buettner, G.R. (2011). The rate of oxygen utilization by cells. Free radical biology & medicine *51*, 700-712.

Wagner, O.I., Lifshitz, J., Janmey, P.A., Linden, M., McIntosh, T.K., and Leterrier, J.F. (2003). Mechanisms of mitochondria-neurofilament interactions. J Neurosci *23*, 9046-9058.

Wahl, D.R., Byersdorfer, C.A., Ferrara, J.L., Opipari, A.W., Jr., and Glick, G.D. (2012). Distinct metabolic programs in activated T cells: opportunities for selective immunomodulation. Immunol Rev *249*, 104-115.

Walker, J.E. (2013). The ATP synthase: the understood, the uncertain and the unknown. Biochem Soc Trans *41*, 1-16.

Wallace, D.C. (2012). Mitochondria and cancer. Nat Rev Cancer *12*, 685-698.

Wallings, R., Manzoni, C., and Bandopadhyay, R. (2015). Cellular processes associated with LRRK2 function and dysfunction. FEBS J *282*, 2806-2826.

Wang, B., Qin, H., Wang, Y., Chen, W., Luo, J., Zhu, X., Wen, W., and Lei, W. (2014). Effect of DJ-1 overexpression on the proliferation, apoptosis, invasion and migration of laryngeal squamous cell carcinoma SNU-46 cells through PI3K/AKT/mTOR. Oncol Rep *32*, 1108-1116.

Wang, X., and Schwarz, T.L. (2009). The mechanism of Ca2+ -dependent regulation of kinesin-mediated mitochondrial motility. Cell *136*, 163-174.

Wang, X., Winter, D., Ashrafi, G., Schlehe, J., Wong, Y.L., Selkoe, D., Rice, S., Steen, J., LaVoie, M.J., and Schwarz, T.L. (2011). PINK1 and Parkin target Miro for phosphorylation and degradation to arrest mitochondrial motility. Cell *147*, 893-906.

Wang, X., Yan, M.H., Fujioka, H., Liu, J., Wilson-Delfosse, A., Chen, S.G., Perry, G., Casadesus, G., and Zhu, X. (2012). LRRK2 regulates mitochondrial dynamics and function through direct interaction with DLP1. Human molecular genetics *21*, 1931-1944.

Wang, Y., Chandran, J.S., Cai, H., and Mattson, M.P. (2008). DJ-1 is essential for long-term depression at hippocampal CA1 synapses. Neuromolecular Med *10*, 40-45.

Wang, Y., Liu, W., He, X., and Zhou, F. (2013). Parkinson's disease-associated DJ-1 mutations increase abnormal phosphorylation of tau protein through Akt/GSK-3beta pathways. J Mol Neurosci *51*, 911-918.

Warburg, O. (1956). On the origin of cancer cells. Science *123*, 309-314.

Watanabe, M., Isobe, T., Ichimura, T., Kuwano, R., Takahashi, Y., and Kondo, H. (1993). Molecular cloning of rat cDNAs for beta and gamma subtypes of 14-3-3 protein and developmental changes in expression of their mRNAs in the nervous system. Brain Res Mol Brain Res *17*, 135-146.

Weerasekara, V.K., Panek, D.J., Broadbent, D.G., Mortenson, J.B., Mathis, A.D., Logan, G.N., Prince, J.T., Thomson, D.M., Thompson, J.W., and Andersen, J.L. (2014). Metabolic-stress-induced rearrangement of the 14-3-3zeta interactome promotes autophagy via a ULK1- and AMPK-regulated 14-3-3zeta interaction with phosphorylated Atg9. Molecular and cellular biology *34*, 4379-4388.

Wenz, T. (2011). Mitochondria and PGC-1alpha in Aging and Age-Associated Diseases. J Aging Res *2011*, 810619.

West, A.B., Kapatos, G., O'Farrell, C., Gonzalez-de-Chavez, F., Chiu, K., Farrer, M.J., and Maidment, N.T. (2004). N-myc regulates parkin expression. J Biol Chem *279*, 28896-28902.

Westermann, B. (2012). Bioenergetic role of mitochondrial fusion and fission. Biochimica et biophysica acta *1817*, 1833-1838.

Wheaton, W.W., and Chandel, N.S. (2011). Hypoxia. 2. Hypoxia regulates cellular metabolism. American journal of physiology Cell physiology *300*, C385-393.

Wider, E.A., and Tigier, H.A. (1970). Properties and regulatory effect on tetrapyrrole biosynthesis of succinyl CoA synthetase isolated from soybean callus tissue system. FEBS Lett *9*, 30-32.

Williams, A., Gill, S., Varma, T., Jenkinson, C., Quinn, N., Mitchell, R., Scott, R., Ives, N., Rick, C., Daniels, J.*, et al.* (2010). Deep brain stimulation plus best medical therapy versus best medical therapy alone for advanced Parkinson's disease (PD SURG trial): a randomised, open-label trial. Lancet neurology *9*, 581-591.

Williams, D.M., Ecroyd, H., Goodwin, K.L., Dai, H., Fu, H., Woodcock, J.M., Zhang, L., and Carver, J.A. (2011). NMR spectroscopy of 14-3-3zeta reveals a flexible C-terminal extension: differentiation of the chaperone and phosphoserine-binding activities of 14-3-3zeta. Biochem J *437*, 493-503.

Williamson, J.R., and Cooper, R.H. (1980). Regulation of the citric acid cycle in mammalian systems. FEBS Lett *117 Suppl*, K73-85.

Winklhofer, K.F., Tatzelt, J., and Haass, C. (2008). The two faces of protein misfolding: gain- and loss-of-function in neurodegenerative diseases. EMBO J *27*, 336-349.

Wise, D.R., Ward, P.S., Shay, J.E., Cross, J.R., Gruber, J.J., Sachdeva, U.M., Platt, J.M., DeMatteo, R.G., Simon, M.C., and Thompson, C.B. (2011). Hypoxia promotes isocitrate dehydrogenase-dependent carboxylation of alpha-ketoglutarate to citrate to support cell growth and viability. Proc Natl Acad Sci U S A *108*, 19611-19616.

Witt, A.C., Lakshminarasimhan, M., Remington, B.C., Hasim, S., Pozharski, E., and Wilson, M.A. (2008). Cysteine pKa depression by a protonated glutamic acid in human DJ-1. Biochemistry *47*, 7430-7440.

Wong, E.S., Tan, J.M., Wang, C., Zhang, Z., Tay, S.P., Zaiden, N., Ko, H.S., Dawson, V.L., Dawson, T.M., and Lim, K.L. (2007). Relative sensitivity of parkin and other cysteine-containing enzymes to stress-induced solubility alterations. J Biol Chem *282*, 12310-12318.

Wu, H., Xue, D., Chen, G., Han, Z., Huang, L., Zhu, C., Wang, X., Jin, H., Wang, J., Zhu, Y.*, et al.* (2014). The BCL2L1 and PGAM5 axis defines hypoxia-induced receptor-mediated mitophagy. Autophagy *10*, 1712-1725.

Wu, Z., Puigserver, P., Andersson, U., Zhang, C., Adelmant, G., Mootha, V., Troy, A., Cinti, S., Lowell, B., Scarpulla, R.C.*, et al.* (1999). Mechanisms controlling mitochondrial

biogenesis and respiration through the thermogenic coactivator PGC-1. Cell *98*, 115-124.

Wurtele, M., Jelich-Ottmann, C., Wittinghofer, A., and Oecking, C. (2003). Structural view of a fungal toxin acting on a 14-3-3 regulatory complex. EMBO J *22*, 987-994.

Xiong, H., Wang, D., Chen, L., Choo, Y.S., Ma, H., Tang, C., Xia, K., Jiang, W., Ronai, Z., Zhuang, X.*, et al.* (2009). Parkin, PINK1, and DJ-1 form a ubiquitin E3 ligase complex promoting unfolded protein degradation. The Journal of clinical investigation *119*, 650-660.

Xu, Z., Graham, K., Foote, M., Liang, F., Rizkallah, R., Hurt, M., Wang, Y., Wu, Y., and Zhou, Y. (2013). 14-3-3 protein targets misfolded chaperone-associated proteins to aggresomes. J Cell Sci *126*, 4173-4186.

Yacoubian, T.A., Slone, S.R., Harrington, A.J., Hamamichi, S., Schieltz, J.M., Caldwell, K.A., Caldwell, G.A., and Standaert, D.G. (2010). Differential neuroprotective effects of 14-3-3 proteins in models of Parkinson's disease. Cell death & disease *1*, e2.

Yaffe, M.B., Rittinger, K., Volinia, S., Caron, P.R., Aitken, A., Leffers, H., Gamblin, S.J., Smerdon, S.J., and Cantley, L.C. (1997). The structural basis for 14-3-3:phosphopeptide binding specificity. Cell *91*, 961-971.

Yamada, K., Takahashi, S., Karube, F., Fujiyama, F., Kobayashi, K., Nishi, A., and Momiyama, T. (2016). Neuronal circuits and physiological roles of the basal ganglia in terms of transmitters, receptors and related disorders. J Physiol Sci.

Yamano, K., and Youle, R.J. (2013). PINK1 is degraded through the N-end rule pathway. Autophagy *9*, 1758-1769.

Yang, X., Lee, W.H., Sobott, F., Papagrigoriou, E., Robinson, C.V., Grossmann, J.G., Sundstrom, M., Doyle, D.A., and Elkins, J.M. (2006). Structural basis for protein-protein interactions in the 14-3-3 protein family. Proc Natl Acad Sci U S A *103*, 17237-17242.

Yano, M., Nakamuta, S., Wu, X.J., Okumura, Y., and Kido, H. (2006). A novel function of 14-3-3 protein: 14-3-3 zeta is a heat-shock-related molecular chaperone that dissolves thermal-aggregated proteins. Molecular biology of the cell *17*, 4769-4779.

Ye, B., Maret, W., and Vallee, B.L. (2001). Zinc metallothionein imported into liver mitochondria modulates respiration. Proc Natl Acad Sci U S A *98*, 2317-2322.

Yoshida, K., Yamaguchi, T., Natsume, T., Kufe, D., and Miki, Y. (2005). JNK phosphorylation of 14-3-3 proteins regulates nuclear targeting of c-Abl in the apoptotic response to DNA damage. Nat Cell Biol *7*, 278-285.

Youle, R.J., and Narendra, D.P. (2011). Mechanisms of mitophagy. Nature reviews Molecular cell biology *12*, 9-14.

Youle, R.J., and van der Bliek, A.M. (2012). Mitochondrial fission, fusion, and stress. Science *337*, 1062-1065.

Young, J.C., Hoogenraad, N.J., and Hartl, F.U. (2003). Molecular chaperones Hsp90 and Hsp70 deliver preproteins to the mitochondrial import receptor Tom70. Cell *112*, 41-50.

Yu, S.W., Wang, H., Poitras, M.F., Coombs, C., Bowers, W.J., Federoff, H.J., Poirier, G.G., Dawson, T.M., and Dawson, V.L. (2002). Mediation of poly(ADP-ribose) polymerase-1-dependent cell death by apoptosis-inducing factor. Science *297*, 259-263.

Yu, W., Sun, Y., Guo, S., and Lu, B. (2011). The PINK1/Parkin pathway regulates mitochondrial dynamics and function in mammalian hippocampal and dopaminergic neurons. Human molecular genetics *20*, 3227-3240.

Yuan, Z., Agarwal-Mawal, A., and Paudel, H.K. (2004). 14-3-3 binds to and mediates phosphorylation of microtubule-associated tau protein by Ser9-phosphorylated glycogen synthase kinase 3beta in the brain. J Biol Chem *279*, 26105-26114.

Zha, J., Harada, H., Yang, E., Jockel, J., and Korsmeyer, S.J. (1996). Serine phosphorylation of death agonist BAD in response to survival factor results in binding to 14-3-3 not BCL-X(L). Cell *87*, 619-628.

Zhang, C., Lin, M., Wu, R., Wang, X., Yang, B., Levine, A.J., Hu, W., and Feng, Z. (2011). Parkin, a p53 target gene, mediates the role of p53 in glucose metabolism and the Warburg effect. Proc Natl Acad Sci U S A *108*, 16259-16264.

Zhang, L., Shimoji, M., Thomas, B., Moore, D.J., Yu, S.W., Marupudi, N.I., Torp, R., Torgner, I.A., Ottersen, O.P., Dawson, T.M.*, et al.* (2005). Mitochondrial localization of the Parkinson's disease related protein DJ-1: implications for pathogenesis. Human molecular genetics *14*, 2063-2073.

Zhang, Y., Gong, X.G., Wang, Z.Z., Sun, H.M., Guo, Z.Y., Hu, J.H., Ma, L., Li, P., and Chen, N.H. (2016). Overexpression of DJ-1/PARK7, the Parkinson's disease-related protein, improves mitochondrial function via Akt phosphorylation on threonine 308 in dopaminergic neuron-like cells. Eur J Neurosci *43*, 1379-1388.

Zhong, N., and Xu, J. (2008). Synergistic activation of the human MnSOD promoter by DJ-1 and PGC-1alpha: regulation by SUMOylation and oxidation. Human molecular genetics *17*, 3357-3367.

Zhou, R., Yazdi, A.S., Menu, P., and Tschopp, J. (2011). A role for mitochondria in NLRP3 inflammasome activation. Nature *469*, 221-225.

Zhou, W., and Freed, C.R. (2005). DJ-1 up-regulates glutathione synthesis during oxidative stress and inhibits A53T alpha-synuclein toxicity. J Biol Chem *280*, 43150-43158.

Zhou, W., Zhu, M., Wilson, M.A., Petsko, G.A., and Fink, A.L. (2006). The oxidation state of DJ-1 regulates its chaperone activity toward alpha-synuclein. Journal of molecular biology *356*, 1036-1048.

Zhu, J., Aja, S., Kim, E.K., Park, M.J., Ramamurthy, S., Jia, J., Hu, X., Geng, P., and Ronnett, G.V. (2012). Physiological oxygen level is critical for modeling neuronal metabolism in vitro. Journal of neuroscience research *90*, 422-434.

Zick, M., Rabl, R., and Reichert, A.S. (2009). Cristae formation-linking ultrastructure and function of mitochondria. Biochimica et biophysica acta *1793*, 5-19.

Zimprich, A., Biskup, S., Leitner, P., Lichtner, P., Farrer, M., Lincoln, S., Kachergus, J., Hulihan, M., Uitti, R.J., Calne, D.B.*, et al.* (2004). Mutations in LRRK2 cause autosomal-dominant parkinsonism with pleomorphic pathology. Neuron *44*, 601-607.

Zondler, L., Miller-Fleming, L., Repici, M., Goncalves, S., Tenreiro, S., Rosado-Ramos, R., Betzer, C., Straatman, K.R., Jensen, P.H., Giorgini, F.*, et al.* (2014). DJ-1 interactions with alpha-synuclein attenuate aggregation and cellular toxicity in models of Parkinson's disease. Cell death & disease *5*, e1350.

9 Addendum

–

Effect of 14-3-3β on DJ-1 localisation in primary neurons

9.1 Introduction

DJ-1 and 14-3-3β are highly expressed in the brain, where they positively contribute to cell viability (Bonifati et al., 2003; Cao et al., 2015). As shown in the chapters 3 and 4 of this study, 14-3-3β exerts a negative effect on mitochondrial localisation of DJ-1 in a human embryonic kidney cell line (HEK). Mitochondrial DJ-1 has been proposed to be neuroprotective after stroke (Kaneko et al., 2014a; Kaneko et al., 2014b) and under oxidative stress conditions (Junn et al., 2009). Furthermore, mitochondrial dysfunction is thought to be a key pathologic event in Parkinson's disease, the second most common neurodegenerative disorder (Bindoff et al., 1989; Langston et al., 1983; Parker et al., 1989; Schapira et al., 1990). Restoring mitochondrial function by targeting neuronal DJ-1 to mitochondria could provide a new therapeutic avenue to neuroprotection in PD. I therefore asked whether reduction of 14-3-3β enhances the level of mitochondrial DJ-1 in neurons.

9.2 Material and Methods

9.2.1 Neuronal isolation and culture

All animal procedures were carried out according to the guidelines of Imperial College London Central Biomedical Services and the Home Office. The evening before neuronal isolation 10 cm cell culture dishes were coated with poly-D-lysine over night at room temperature followed by two washes with PBS. An E18 pregnant Sprague Dawley rat was sacrificed according to the Home Office Schedule 1 procedure using CO_2 inhalation followed by cervical dislocation. E18 embryos were dissected out of the amniotic sacs and culled by decapitation. The sculls were transferred to cold dissection medium. The following steps were performed under aseptic conditions in a laminar flow hood using a low magnification dissection microscope and sterile micro-dissection forceps. Using fresh dissection medium in a petri dish on ice the brains were removed from the scull. The cortical hemispheres were isolated and the hippocampi and meninges were removed. The cortices were minced in a fresh petri dish in dissection medium using sterile scissors, transferred to a 15 ml conical

tube and left to settle for 1 min on ice. The dissection medium was removed and the cortices were incubated with 5 ml papain for 2 min in a 37ºC water bath. During the incubation, the tube was regularly inverted to increase papain penetration into the tissue. The tissue was placed back on ice and left to settle for 1 min. The papain was removed, 5 ml inactivation medium was added and the tube was inverted. The tissue was left to settle for 2 min on ice before inactivation medium was removed. 2 ml complete neurobasal medium was added and neurons were dissociated by pipetting 10 times through a fire-polished glass Pasteur pipette. Medium was topped up to 5 ml and the cells were spun for 5 min at 400xg and 4ºC to remove all papain. The supernatant was removed, the cells were resuspended in 10 ml complete neurobasal medium and filtered through a cell strainer to remove any remaining tissue clumps. Cells were counted and adjusted to 450,000 cells/ml. 10 ml cell suspension was plated per 10 cm dish and maintained at 37ºC and 5% CO_2. At DIV3 and DIV6 half the medium was replaced with fresh complete neurobasal medium.

Table 9.1: Plasmids used for cloning and lentivirus pseudo-particle production

ID	insert	promotor	source
pL-Crispr.EFS.GFP	Cas9 endonuclease Scrambled guideRNA GFP	EFS (Cas9), U6 (gRNA)	Addgene ID: 57818
pL-Crispr.EFS.GFP-r1433β2	Cas9 endonuclease r1433β guideRNA #2 GFP	EFS (Cas9), U6 (gRNA)	cloned
pcDNA3.1-Gag/Pol	HIV Gag/Pol polyprotein	CMV	Elizabeth Jonas, Yale University
pcDNA3.1-VSV-G	VSV glycoprotein	CMV	Elizabeth Jonas, Yale University

HIV: human immunodeficiency virus, VSV: Vesicular stomatitis virus

Table 9.2: 14-3-3β guideRNA and primers used for pL-Crispr.EFS.GFP-r1433β cloning

#	guideRNA sequence	Sense primer	Antisense primer
1	GTAGGTGCCCGCCGTTCTTCC	CACCGTAGGTGCCCGCCGTTCTTCC	AAACGGAAGAACGGCGGGCACCTAC
2	TGACTCGCCAGGAAGAACGG	CACCGTGACTCGCCAGGAAGAACGG	AAACCCGTTCTTCCTGGCGAGTCAC
3	GATGCTGGAGATGACTCGCC	CACCGATGCTGGAGATGACTCGCC	AAACGGCGAGTCATCTCCAGCATC
4	GCCTACACACCCGATTCGCCT	CACCGCCTACACACCCGATTCGCCT	AAACAGGCGAATCGGGTGTGTAGGC

9.2.2 Cloning of rat 14-3-3β targeting Crispr/Cas9 vectors

The design of guideRNAs targeting rat 14-3-3β was performed with the online tool available at http://crispr.mit.edu/. As input the complete coding sequence from 14-3-3β was used (Gene bank ID: D17446.1). Four of the top scoring gRNAs were selected, #1-3 targeting exon1 and #4 targeting exon3 (Table 9.2). Where the gRNA sequence starts with A, T, or C, a G nucleotide was added to the 5' end for efficient transcription from the U6 promotor. This core sequence served as template for the forward primer, which was generated by fusing the short sequence CACC to the 5' end. For the reverse primer the reverse complement of the core sequence including the additional G (were applicable) was generated and the short sequence ACCC was fused to the 5' end.

To insert the gRNA sequences into the Cas9 vector 2 µg pL-Crispr.EFS.GFP plasmid was digested with 1 µl Esp3I FastDigest endonuclease for 45 min at 37 ºC in 20 µl final volume containing 2 µl 10x FastDigest buffer and 1 mM DTT. Re-annealing was prevented by addition of 1 µl FastAlkaline phosphatase (1U) and incubation for 15 min at 37 ºC. The digested plasmid was purified on a 1% agarose gel for 1h at 100V. The gel was stained in ethidium bromide for 30 min at room temperate and the DNA was visualised on a UV transilluminator. The corresponding band was cut out and purified using the GeneJet Gel extraction and DNA cleanup kit according to the manufacturer's protocol. For the primer annealing reaction, sense and antisense primer pairs were mixed 1:1 at a final concentration of 100 µM/primer in a final volume of 10 µl containing 1 µl 10x T4 DNA Ligase buffer and 0.5 µl T4 polynucleotide kinase (5U). The reaction was performed using the annealing program outlined in Table 9.3. The annealed primer duplex was diluted 1:500 in molecular biology grade H_2O and 1 µl was mixed with 40 ng Esp3I-digested Cas9 vector in a final volume of 5 µl containing 0.5 µl 10x T4 DNA ligase buffer and 0.5 µl T4 DNA ligase (2.5U). The ligation reaction was performed at room temperature for 120 min. The product of this ligation was directly transformed into Ca^{2+}-competent *E.coli* Top10 as described in section 2.5.1. Plasmid DNA was purified from positive colonies and the correct insertion of the gRNA sequence was

assessed by Sanger Sequencing as described in section 2.5.2 using the following sequencing primer: primer U6_Seq_fw: TTTGCTGTACTTTCTATAGTG.

Table 9.3: PCR program for primer annealing

PCR program	step	temperature	duration
Primer annealing	1	37 ºC	45 min
	2	95ºC	2.5 min
	3	Ramp at 0.1ºC/s to 22ºC	pause

9.2.3 Lentiviral pseudo-particle production

For the production of lentiviral pseudo-particles, a 2nd generation lentiviral packaging system was used. The system included a transfer plasmid containing the gene of interest (pL-Crispr plasmid) and two plasmids containing the essential components necessary for pseudo-particle production, the envelope plasmid pcDNA3.1-VSV-G and the packaging plasmid pcDNA3.1-Gag/Pol (Table 9.1). pcDNA3.1-VSV-G contains the gene coding for the envelope glycoprotein derived from vesicular stomatitis virus (VSV-G). The pcDNA3.1-Gag/Pol vector encodes the HIV-derived proteins group-specific antigen (Gag) and reverse transcriptase polyprotein (Pol).

To produce lentiviral pseudo-particles HEK293T cells were co-transfected with either control pL-Crispr.EFS.GFP or knockout plasmid pL-Crispr.EFS.GFP-r1433b#2 together with pcDNA3.1-Gag/Pol and pcDNA3.1-VSV-G plasmids using the calcium phosphate reverse transfection method. The reverse transfection is based on the conventional $CaPO_4$ transfection described in part 2.1.4 with the main difference that cell seeding and transfection is done at the same time. A single cell suspension was prepared as described under section 2.1.3. The cell suspension was adjusted to a concentration of 1.2 x10^6 cells/ml in complete DMEM. The DNA/$CaPO_4$ mix was prepared for transfection of a 150 mm round cell culture plate as described in 2.1.4 using the volumes given in Table 9.4. After precipitation of the DNA the transfection mix was diluted in 10 ml complete DMEM and placed into the cell

culture vessel. 16 ml of the adjusted single cell suspension was quickly added to the diluted DNA/$CaPO_4$ mix and the dish was placed into the cell culture incubator. After 12 to 16 h the medium was replaced with fresh complete DMEM. Two days after medium change the cell supernatant was filtered through a 0.45 µm polyethane sulfon filter (Stericup, EMD Millipore) using a vacuum pump (Thermo Brand) to yield non-concentrated viral pseudo-particles. The non-concentrated viral pseudo-particles were precipitated over night at 4ºC by adding 5xLenti concentrator solution (Origene) to a final concentration of 20%. The precipitated pseudo-particles were spun at 3500xg for 30 min at 4ºC, the supernatant was discarded and the pellet was spun as above for 5 min to remove the remaining liquid. The pellet was resuspended in 1/100 of the original volume in cold PBS to yield concentrated viral pseudo-particles and stored at 4ºC for up to one week. Pseudo-particles were prepared freshly before every experiment.

Table 9.4: DNA/$CaPO_4$ transfection mix for lentiviral particle production. The quantities are given for transfection of one 150 mm round cell culture plate.

Reagent	Volume/amount	
DNA		
pL-Crispr	26 µg	Component 1
pcDNA3.1-Gag/Pol	6.6 µg	
pcDNA3.1-VSV-G	2.17 µg	
$CaCl_2$	183 µl	
H_2O	ad 1.5 ml	
2xHBS	1.5 ml	Component 2
Total volume	3.0 ml	

9.2.4 N27 cell culture and Crispr knockdown validation

The N27 cell line is a rat dopaminergic neuron-like cell line. N27 cells were cultured in complete RPMI and were sub-cultured every 2 to 3 days. For Crispr-mediated knockdown of 14-3-3β, cells were seeded at 5000 cells/cm^2 in a 6-well plate. 24h post-seeding 2.5 ml of the

non-concentrated viral pseudo-particles was added to the cell culture medium. After 24h medium was replaced with fresh complete RPMI. 48h after medium change cells were harvested by scraping on ice in cold PBS. Cells were spun down at 400xg for 5 min and 4ºC. The supernatant was removed and the cells were lysed in TX lysis buffer and the protein concentration was determined by Bradford assay (chapter 2). 10 µg protein was used for western blot analysis of 14-3-3β knockdown and the protein level was determined relative to α-tubulin, serving as loading control.

9.2.5 Subcellular fractionation of primary neurons

For each cell fractionation 2x10 cm-dishes of cortical neurons were washed with cold 0.9% NaCl solution and harvested by scraping on ice in cold 0.9% NaCl solution. A tenth of the cell suspension was placed into a separate microtube, pelleted at 1000xg for 5 min at 4ºC and stored at -80ºC for protein expression analysis. The subcellular fractionation was performed using Qproteome mitochondrial isolation kit according to the manufacturers protocol. In brief, cells were spun for 10 min at 500xg and 4ºC. The supernatant was removed and the cells were resuspended in 0.5 ml lysis buffer freshly supplemented with protease inhibitor solution. Cells were incubated for 10 min at 4ºC under rotation and spun at 1000xg for 10 min at 4ºC. The supernatant containing the cytosolic fraction was recovered and stored at -80ºC. The pellet containing permeabilised cells was resuspended in 1 ml disruption buffer freshly supplemented with protease inhibitor solution and cells were disrupted by drawing 10 times through a G23 blunt end needle. Disrupted cells were spun at 1000xg for 10 min at 4ºC. The supernatant containing the mitochondrial and microsomal fraction was recovered and spun at 6000xg for 10 min at 4ºC. The resulting pellet containing the crude mitochondrial fraction was resuspended in 1 ml mitochondrial storage buffer and spun at 6000xg for 20 min at 4ºC. The final mitochondrial pellet was stored at -80ºC. For protein analysis the total cell pellet and mitochondrial pellet were lysed in 20 µl mitochondrial lysis buffer for 30 min on ice with occasional vortexing. The lysates were sonicated for 30 sec in a water bath and cleared by centrifugation at 1000xg for 5 min at 4ºC. The protein content of all fractions was analysed by Bradford assay (see Material and Methods chapter 2.6.1).

9.2.6 Reagents and kits

All reagents were purchased from Sigma if not stated otherwise.

Reagents

Dissection medium (DM): 33mM glucose (Gibco) in Hank's buffered salt solution

Papain stock: 10 mg/ml in H_2O, sterile filtered, stable at 4ºC for 1 year

Papain working solution: 0.1 mg/ml in DM, freshly prepared from papain stock

Inactivation medium: 50% FBS in DM

Complete neurobasal medium: Neurobasal medium (Gibco), 1xB27 supplement (Gibco), 2 mM glutamine (Gibco), 1 mM lactate

Borate buffer: 0.1M borate in ddH_2O

poly-D-lysine, MW: 70k-150k: 10 µg/ml in borate buffer

Mitochondrial lysis buffer (pH 7.5): 50 mM Tris, 250 mM NaCl, 10 mM EDTA, 1% (v/v) TritonX-100

Complete RPMI: RPMI (Gibco), 10% FBS

Complete DMEM: DMEM-AQ (Sigma), 10% FBS

TX lysis buffer (pH 7.5): 1% (w/v) TritonX-100 in TBS

FastDigest Esp3I (BsmBI) (ThermoFisher, FD0454)

T4 Polynucleotide Kinase (ThermoFisher, EK0031)

T4 DNA ligase (ThermoFisher, EL0011), also contains the 10x T4 DNA ligase buffer

FastAP (ThermoFisher, EF0654)

1xTris borate EDTA buffer (TBE) (ThermoFisher, B52): 1:10 dilution in ddH_2O

Agarose (ThermoFisher, R0492): 1% (w/v) in TBE, agarose suspension was heated in a microwave until entirely dissolved, poured into a gel container and left to solidify at room temperature

Ethidium bromide (ThermoFisher, 15585011): 0.5 µg/ml in ddH_2O

Kits

GeneJet Gel extraction and DNA cleanup kit (ThermoFisher, K0831)

Qproteome Mitochondria isolation kit (Qiagen, #37612)

9.3 Results: The effect of 14-3-3β on mitochondrial localisation of DJ-1 is cell type-dependent

9.3.1 Primary neuronal culture from rat cortex

In order to test whether 14-3-3β sequesters DJ-1 in neurons a primary culture system using E18 rat cortical neurons was established. The neurons were cultured for seven days in vitro (DIV) to allow synapse formation without compromising neuronal viability (Ichikawa et al., 1993). During the culture period neurite outgrowth became apparent as early as DIV1 and gradually extended into large and dense networks at DIV7 (Figure 9.1).

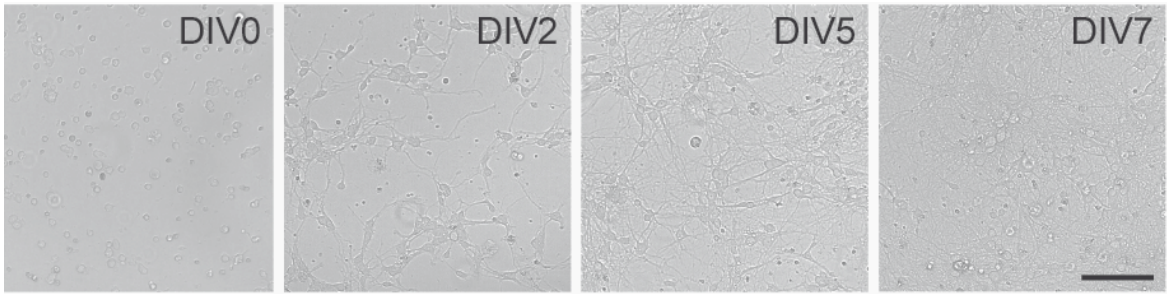


Figure 9.1 – Primary neuronal culture from E18 rat cortex. Phase contrast images of rat cortical neurons at various days in vitro (DIV) after isolation at day 0. Cultures were maintained for 7 days prior to fractionation. Neurite outgrowth is first observed on DIV 1 (not shown). On DIV 2 small neuronal clusters became apparent and grew larger over the culture period into highly connected dense networks on DIV 7. Scale bar: 100 µm.

9.3.2 Cas9-mediated gene depletion of rat 14-3-3β

To achieve efficient reduction of 14-3-3β protein levels in primary neurons we employed the Crispr/Cas9 mediated gene disruption. Previous shRNA-mediated knockdown attempts failed to sufficiently deplete 14-3-3β levels (data not shown). For this approach four different guideRNAs (gRNA) against rat 14-3-3β were cloned into the pL-Crispr.EFS.GFP vector replacing the original non-targeting gRNA of the host vector. The original vector (Ctl) and the four r14-3-3β-targeting vectors were used to produce lentiviral particles and the efficiency of gene disruption was tested by transducing N27 cells, a rat dopaminergic neuron-like cell line.

Three days post-transduction the cells were harvested and the 14-3-3β protein levels were assessed by western blot (Figure 9.2). gRNA# 2 was most efficient and reduced 14-3-3β protein to 35.4±17.6% relative to Ctl (mean±SEM) in three independent experiments.

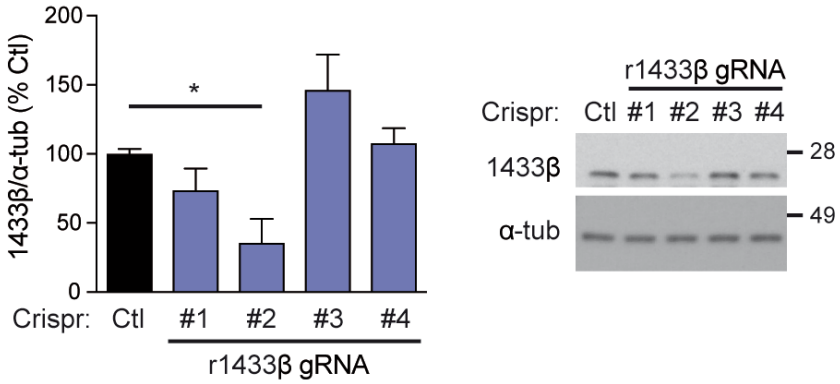


Figure 9.2 – Cas9-mediated depletion of 14-3-3β in rat N27 cells. N27 cells were transduced with Crispr/Cas9 control vector (Ctl) or Crispr/Cas9 vector co-expressing rat 14-3-3β targeting guideRNAs (gRNA). Reduction of 14-3-3β protein levels was assessed by western blot and normalised against α-tubulin. gRNA #2 consistently reduced 14-3-3β levels and was chosen for knockdown in subsequent neuronal experiments. Data is derived from 3 independent experiments and presented as mean±SEM of % Ctl (n=3, unpaired t-test, *p=0.0228).

Next, Cas9-mediated knockdown was assessed in neuronal cultures. For this purpose the concentrated viral pseudo-particles were titrated onto the cortical neurons at DIV4. At DIV7 neurons were harvested and gene disruption was assessed at protein level using western blot. At the highest concentration corresponding to 10 µl concentrated viral pseudo-particles/ml medium the level of 14-3-3β was reduced to 38.8% relative to untreated neurons (Figure 9.3, derived from a single experiment). A dose of 10 µl concentrated viral pseudo-particles/ml medium was used for subsequent fractionation experiments.

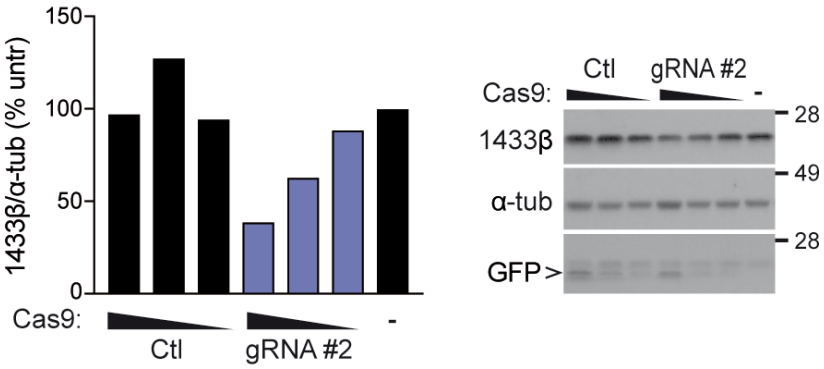


Figure 9.3 – Cas9-mediated depletion of 14-3-3β in cortical neurons. Neurons were transduced with Crispr/Cas9 control vector (Ctl) or Crispr/Cas9 vector co-expressing rat 14-3-3β-targeting gRNA #2 at varying concentrations (10, 5, 2.5 µl concentrated viral pseudo-particles/ml medium) at DIV4. At DIV7 14-3-3β protein levels were assessed by western blot and quantified relative to α-tubulin. The highest dose reduced 14-3-3β levels to 38.8% of untreated neurons (-). The data is derived from a single experiment. 10 µl concentrated viral pseudo-particles/ml medium was used for all subsequent experiments.

9.3.3 14-3-3β enhances mitochondrial DJ-1 levels in primary cortical neurons

To test the effect of 14-3-3β on the localisation of DJ-1 in primary neurons the cultures were transduced with the Cas9 vector carrying r14-3-3β gRNA#2 or non-targeting gRNA control vector (Ctl). Using 10 µl concentrated viral particles/ml medium, as determined in the preliminary experiment (Figure 9.3), resulted in reliable reduction of 14-3-3β protein to 22.9±7.5% relative to Ctl (mean±SEM, unpaired t-test, n=4, p=0.0004; Figure 9.4 A). Transduced neurons were harvested on DIV7 and separated into cytosolic and mitochondrial fractions. Western blot analysis of DJ-1 and the cytosolic marker GAPDH showed no effect of 14-3-3β on protein expression (total) or cytosolic levels of DJ-1. However, 14-3-3β had a significant effect on mitochondrial levels of DJ-1 normalised to the mitochondrial marker Hsp60 (Figure 9.4 B). To our surprise, 14-3-3β knockdown reduced mitochondrial DJ-1 to 66.8±9.4% of Ctl (mean±SEM, unpaired t-test, *p=0.0191). This is contradictory to the effect of 14-3-3β in HEK cells, where the expression level of 14-3-3β negatively correlated with the levels of mitochondrial DJ-1 (chapter 4, Figures 4.4 and 4.5). This result indicates that the

role of 14-3-3β in regulating the localisation of DJ-1 is cell type-dependent. It further demonstrates the requirement of validating novel mechanisms in primary cells.

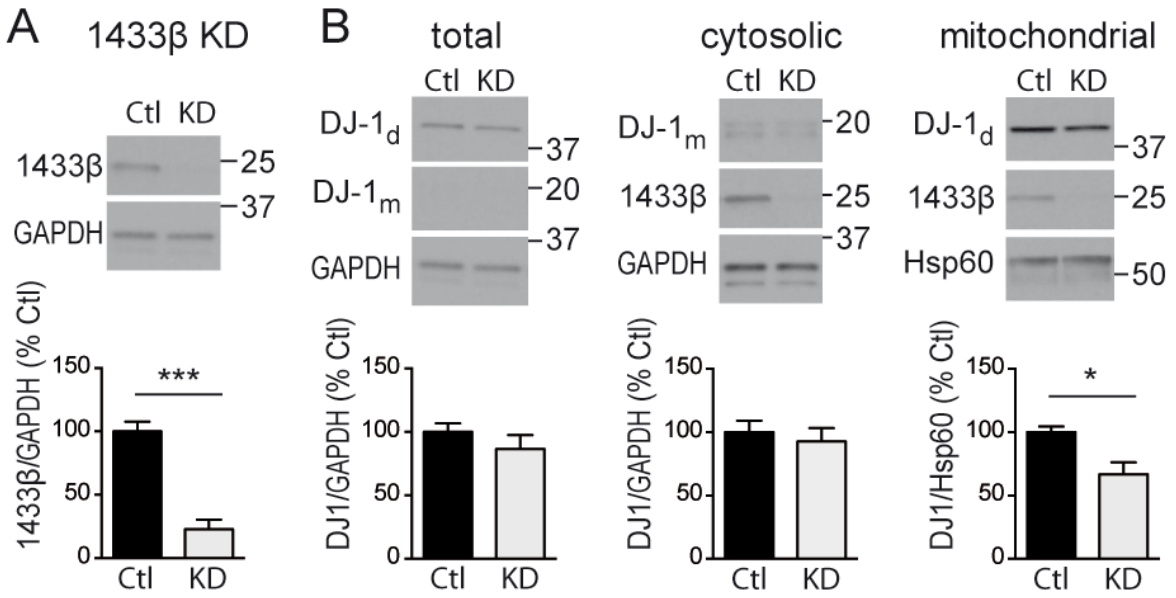


Figure 9.4 – Effect of 14-3-3β depletion on localisation of DJ-1 in neurons. 14-3-3β was downregulated in primary rat cortical neurons using lentiviral delivery of r14-3-3β targeting Cas9 (KD) or non-targeting control vector (Ctl) and protein depletion was quantified by Western blot (A). 14-3-3β levels in KD neurons were 22.9±7.5% that of Ctl neurons (mean±SEM, n=4, unpaired t-test, ***p=0.0004). 14-3-3β knockdown did not alter the total or cytosolic levels of DJ-1 in primary neurons but decreased the amount of mitochondrial DJ-1 (B) to 66.8±9.4% of Ctl (mean±SEM, n=4, unpaired t-test, *p=0.0191).

9.3.4 Cell type-specific expression of DJ-1 in mitochondria correlates with mitochondrial 14-3-3β

Importantly, the subcellular distribution of DJ-1 is profoundly different between neurons and HEK cells. We found DJ-1 mostly localised to mitochondria in neurons under basal conditions. In contrast, DJ-1 in HEK cells was more cytosolic and only accumulated in mitochondria after hypoxia or depletion of 14-3-3β. Interestingly, the compartmentalisation of 14-3-3β also showed differences between HEK cells and neurons. In HEK cells a very small fraction of 14-3-3β was found in mitochondria. In neurons, however, a significant portion of 14-3-3β was localised to mitochondria. To address whether there is a correlation between

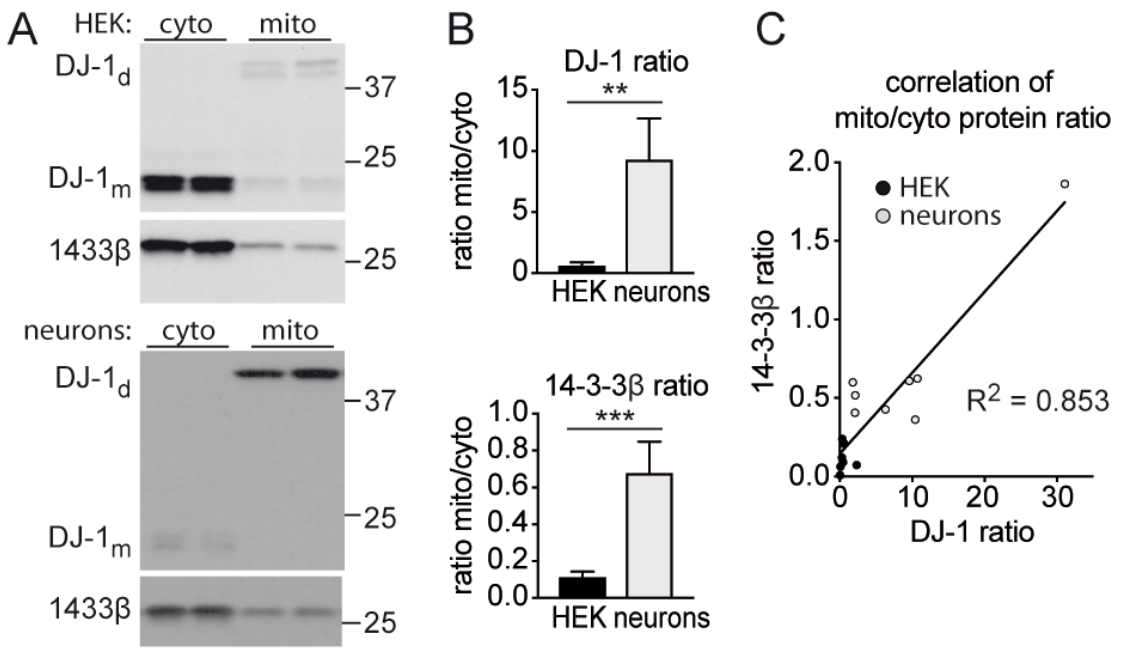


Figure 9.5 – Cell type-specific expression of mitochondrial DJ-1 and 14-3-3β correlates. The basal levels of cytosolic and mitochondrial DJ-1 and 14-3-3β from untreated HEK cells and primary cortical neurons was compared by western blot (A). For comparison between cell types the ratio of mitochondrial over cytosolic protein was analysed showing higher mitochondrial localisation of both proteins in neurons compared to HEK cells (mean ± SEM of mitochondrial over cytosolic protein ratio; Mann-Whitney test; n=7 for HEK, n=8 for neurons; DJ-1 in HEK: 0.59±0.30 and neurons: 9.27±3.40, Mann-Whitney U = 3; 14-3-3β in HEK: 0.11±0.03 and neurons: 0.56±0.19, Mann-Whitney U = 0; **p=0.0022, ***p=0.0003). Furthermore, mitochondrial over cytosolic ratio of DJ-1 positively correlates with 14-3-3β ratios (C; Linear regression of correlation, R^2=0.853).

the level of mitochondrial DJ-1 and 14-3-3β, unstimulated HEK cells and neurons were separated in cytosolic and mitochondrial fractions. The level of DJ-1 and 14-3-3β was assessed in both fractions by western blot and the ratio of mitochondrial over cytosolic protein was used as an expression of relative distribution (Figure 9.5). Indeed, the level of mitochondrial DJ-1 is significantly higher in neurons compared to HEK cells (mean±SEM; neurons: 9.27±3.40, n=8; HEK: 0.59±0.30, n=7). Similarly, the fraction of mitochondrial 14-3-3β is significantly higher in neurons compared to HEK cells (mean±SEM; neurons: 0.56±0.19, n=8; HEK: 0.11±0.03, n=7; Figure 9.5 B). Correlation analysis further demonstrates that mitochondrial DJ-1 is high in those cells, particularly neurons, where 14-3-3β is most enriched in mitochondria (Figure 9.5 C). This result together with the knockdown

experiment suggests that 14-3-3β positively regulates the mitochondrial localisation of DJ-1 in neurons, possibly through binding of DJ-1 in mitochondria.

9.4 Discussion and future direction

Using primary cortical neurons as model system our results have shown a preferential localisation of DJ-1 in mitochondria in these cells (Figure 9.5). This is profoundly different to the HEK cell line, where DJ-1 only accumulated in mitochondria after hypoxia or depletion of 14-3-3β. Given the positive effect of DJ-1 on mitochondrial energy production (chapter 5), we speculate that the different sub-cellular distribution of DJ-1 reflects the diverging energetic profiles of these two cell types. HEK cells are highly glycolytic (Henry et al., 2011), whereas neurons rely on OXPHOS as main energy supply (Kasischke et al., 2004; Llorente-Folch et al., 2015; Lundgaard et al., 2015). We speculate that mitochondrial localisation of DJ-1 is necessary for efficient ATP production in neurons. Loss of function mutations of DJ-1 are the cause of rare cases of familial Parkinson's disease (Bonifati et al., 2003), a disorder characterised by mitochondrial dysfunction (Bindoff et al., 1989; Parker et al., 1989; Schapira et al., 1990). The etiology of PD is unclear but energetic failure as cause of neurodegeneration is among the hypothesis that is being discussed in the field (Dranka et al., 2012; Exner et al., 2012; Matsuda et al., 2009; Pacelli et al., 2015; Pissadaki and Bolam, 2013; Van Laar and Berman, 2013). Genetic mutations account for up to 10% of PD prevalence (Shulman et al., 2011) and most of the genetic defects were shown to cause mitochondrial dysfunction (Canet-Aviles et al., 2004; Chen and Dorn, 2013; Devi et al., 2008; Di Maio et al., 2016; Hayashi et al., 2009; Lazarou et al., 2015; Morais et al., 2014; Ottolini et al., 2013; Shi et al., 2015; Su et al., 2015; Wang et al., 2012). The majority of PD cases, however, develop sporadically and deficits in OXPHOS have been shown in both post-mortem brain sections (Mizuno et al., 1989; Schapira et al., 1989) as well as platelets (Parker et al., 1989) of PD patients. Interestingly, 14-3-3 proteins have a molecular link to PD pathology. Several 14-3-3 isoforms, including 14-3-3β, where shown to accumulate in Lewy bodies (LB) both in mouse (Shirakashi et al., 2006) and human brain (Berg et al., 2003; Kawamoto et al., 2002) and higher levels of secreted 14-3-3 has been suggested as CSF biomarker for neurodegeneration (Shimada et al., 2013). This raises the question whether segregation of 14-3-3 protein into LBs or secretion into the CSF might lower the availability of

14-3-3 in other, functional parts of the cell. If this were the case, the depletion of 14-3-3β could reduce levels of mitochondrial DJ-1 in neurons, similar to the gene depletion in primary neuronal cultures (Figure 9.4). This in turn would lower the efficiency of mitochondrial energy production, thereby causing significant energetic stress to neuronal cells. Under conditions of low mitochondrial activity cells tend to acidify due to lactate production (Gladden, 2004). An acidic intracellular pH increases the tendency for α-synuclein to form oligomers (McClendon et al., 2009), the precursors of the pathologic LBs. Unfortunately, little is known regarding the subcellular localisation of DJ-1 in the substantia nigra of PD patients but one could imagine how the lack of mitochondrial DJ-1 could fuel a viscous cycle of detrimental events that ultimately lead to neurodegeneration.

We haven't specifically tested whether the interaction between DJ-1 and 14-3-3β occurs in the cytosol or in mitochondria. Of note, immunoprecipitated DJ-1 in HEK cells was observed as monomer, whereas the endogenous IP from rat brain exclusively immunoprecipitated dimeric DJ-1 (Figure 3.1). In the fractionation experiments cytosolic DJ-1 is typically resolved as monomer by western blot, whereas it appears to form stable dimers in mitochondria. This suggests that the DJ1-1433β complex was likely immunoprecipitated from the cytosol in HEK cells, but from mitochondria when using brain lysate. To address this question in detail, IP's could be performed on mitochondrial and cytosolic isolations from HEK cells and brain tissue. Alternatively, the proximity ligation assay could be used on fixed cells and brain tissue to study close proximity of endogenous DJ-1 and 14-3-3β. The assay uses an immunofluorescence read out, which can be combined with conventional staining of subcellular markers for mitochondria and the cytosol.

Another intriguing question is whether the preferred mitochondrial localisation of DJ-1 is specific to neurons. Given the important role of DJ-1 for efficient mitochondrial function, one might speculate that oxidative tissues show higher mitochondrial levels of DJ-1 than glycolytic tissues. Finally, in view of the crucial role of DJ-1 for the viability of dopaminergic

neurons of the substantia nigra, I speculate that impaired localisation of DJ-1 contributes to the energetic deficit and neurodegeneration in sporadic PD patients. I propose to use sub-cellular immunofluorescence analysis of post-mortem human brain tissue to get a deeper understanding of the role of neuronal DJ-1 in healthy ageing and during neurodegeneration.

9.5 References

Berg, D., Riess, O., and Bornemann, A. (2003). Specification of 14-3-3 proteins in Lewy bodies. Annals of neurology *54*, 135.

Bindoff, L.A., Birch-Machin, M., Cartlidge, N.E., Parker, W.D., Jr., and Turnbull, D.M. (1989). Mitochondrial function in Parkinson's disease. Lancet *2*, 49.

Bonifati, V., Rizzu, P., Squitieri, F., Krieger, E., Vanacore, N., van Swieten, J.C., Brice, A., van Duijn, C.M., Oostra, B., Meco, G.*, et al.* (2003). DJ-1(PARK7), a novel gene for autosomal recessive, early onset parkinsonism. Neurol Sci *24*, 159-160.

Canet-Aviles, R.M., Wilson, M.A., Miller, D.W., Ahmad, R., McLendon, C., Bandyopadhyay, S., Baptista, M.J., Ringe, D., Petsko, G.A., and Cookson, M.R. (2004). The Parkinson's disease protein DJ-1 is neuroprotective due to cysteine-sulfinic acid-driven mitochondrial localization. Proc Natl Acad Sci U S A *101*, 9103-9108.

Cao, L., Lei, H., Chang, M.Z., Liu, Z.Q., and Bie, X.H. (2015). Down-regulation of 14-3-3beta exerts anti-cancer effects through inducing ER stress in human glioma U87 cells: Involvement of CHOP-Wnt pathway. Biochem Biophys Res Commun *462*, 389-395.

Chen, Y., and Dorn, G.W., 2nd (2013). PINK1-phosphorylated mitofusin 2 is a Parkin receptor for culling damaged mitochondria. Science *340*, 471-475.

Devi, L., Raghavendran, V., Prabhu, B.M., Avadhani, N.G., and Anandatheerthavarada, H.K. (2008). Mitochondrial import and accumulation of alpha-synuclein impair complex I in human dopaminergic neuronal cultures and Parkinson disease brain. J Biol Chem *283*, 9089-9100.

Di Maio, R., Barrett, P.J., Hoffman, E.K., Barrett, C.W., Zharikov, A., Borah, A., Hu, X., McCoy, J., Chu, C.T., Burton, E.A.*, et al.* (2016). alpha-Synuclein binds to TOM20 and inhibits mitochondrial protein import in Parkinson's disease. Sci Transl Med *8*, 342ra378.

Dranka, B.P., Zielonka, J., Kanthasamy, A.G., and Kalyanaraman, B. (2012). Alterations in bioenergetic function induced by Parkinson's disease mimetic compounds: lack of correlation with superoxide generation. Journal of neurochemistry *122*, 941-951.

Exner, N., Lutz, A.K., Haass, C., and Winklhofer, K.F. (2012). Mitochondrial dysfunction in Parkinson's disease: molecular mechanisms and pathophysiological consequences. EMBO J *31*, 3038-3062.

Gladden, L.B. (2004). Lactate metabolism: a new paradigm for the third millennium. J Physiol *558*, 5-30.

Hayashi, T., Ishimori, C., Takahashi-Niki, K., Taira, T., Kim, Y.C., Maita, H., Maita, C., Ariga, H., and Iguchi-Ariga, S.M. (2009). DJ-1 binds to mitochondrial complex I and maintains its activity. Biochem Biophys Res Commun *390*, 667-672.

Henry, O., Jolicoeur, M., and Kamen, A. (2011). Unraveling the metabolism of HEK-293 cells using lactate isotopomer analysis. Bioprocess Biosyst Eng *34*, 263-273.

Ichikawa, M., Muramoto, K., Kobayashi, K., Kawahara, M., and Kuroda, Y. (1993). Formation and maturation of synapses in primary cultures of rat cerebral cortical cells: an electron microscopic study. Neurosci Res *16*, 95-103.

Junn, E., Jang, W.H., Zhao, X., Jeong, B.S., and Mouradian, M.M. (2009). Mitochondrial localization of DJ-1 leads to enhanced neuroprotection. Journal of neuroscience research *87*, 123-129.

Kaneko, Y., Shojo, H., Burns, J., Staples, M., Tajiri, N., and Borlongan, C.V. (2014a). DJ-1 ameliorates ischemic cell death in vitro possibly via mitochondrial pathway. Neurobiol Dis *62*, 56-61.

Kaneko, Y., Tajiri, N., Shojo, H., and Borlongan, C.V. (2014b). Oxygen-glucose-deprived rat primary neural cells exhibit DJ-1 translocation into healthy mitochondria: a potent stroke therapeutic target. CNS Neurosci Ther *20*, 275-281.

Kasischke, K.A., Vishwasrao, H.D., Fisher, P.J., Zipfel, W.R., and Webb, W.W. (2004). Neural activity triggers neuronal oxidative metabolism followed by astrocytic glycolysis. Science *305*, 99-103.

Kawamoto, Y., Akiguchi, I., Nakamura, S., Honjyo, Y., Shibasaki, H., and Budka, H. (2002). 14-3-3 proteins in Lewy bodies in Parkinson disease and diffuse Lewy body disease brains. J Neuropathol Exp Neurol *61*, 245-253.

Langston, J.W., Ballard, P., Tetrud, J.W., and Irwin, I. (1983). Chronic Parkinsonism in humans due to a product of meperidine-analog synthesis. Science *219*, 979-980.

Lazarou, M., Sliter, D.A., Kane, L.A., Sarraf, S.A., Wang, C., Burman, J.L., Sideris, D.P., Fogel, A.I., and Youle, R.J. (2015). The ubiquitin kinase PINK1 recruits autophagy receptors to induce mitophagy. Nature *524*, 309-314.

Llorente-Folch, I., Rueda, C.B., Pardo, B., Szabadkai, G., Duchen, M.R., and Satrustegui, J. (2015). The regulation of neuronal mitochondrial metabolism by calcium. J Physiol *593*, 3447-3462.

Lundgaard, I., Li, B., Xie, L., Kang, H., Sanggaard, S., Haswell, J.D., Sun, W., Goldman, S., Blekot, S., Nielsen, M.*, et al.* (2015). Direct neuronal glucose uptake heralds activity-dependent increases in cerebral metabolism. Nat Commun *6*, 6807.

Matsuda, W., Furuta, T., Nakamura, K.C., Hioki, H., Fujiyama, F., Arai, R., and Kaneko, T. (2009). Single nigrostriatal dopaminergic neurons form widely spread and highly dense axonal arborizations in the neostriatum. J Neurosci *29*, 444-453.

McClendon, S., Rospigliosi, C.C., and Eliezer, D. (2009). Charge neutralization and collapse of the C-terminal tail of alpha-synuclein at low pH. Protein Sci *18*, 1531-1540.

Mizuno, Y., Ohta, S., Tanaka, M., Takamiya, S., Suzuki, K., Sato, T., Oya, H., Ozawa, T., and Kagawa, Y. (1989). Deficiencies in complex I subunits of the respiratory chain in Parkinson's disease. Biochem Biophys Res Commun *163*, 1450-1455.

Morais, V.A., Haddad, D., Craessaerts, K., De Bock, P.J., Swerts, J., Vilain, S., Aerts, L., Overbergh, L., Grunewald, A., Seibler, P.*, et al.* (2014). PINK1 loss-of-function mutations affect mitochondrial complex I activity via NdufA10 ubiquinone uncoupling. Science *344*, 203-207.

Ottolini, D., Cali, T., Negro, A., and Brini, M. (2013). The Parkinson disease-related protein DJ-1 counteracts mitochondrial impairment induced by the tumour suppressor protein p53 by enhancing endoplasmic reticulum-mitochondria tethering. Human molecular genetics *22*, 2152-2168.

Pacelli, C., Giguere, N., Bourque, M.J., Levesque, M., Slack, R.S., and Trudeau, L.E. (2015). Elevated Mitochondrial Bioenergetics and Axonal Arborization Size Are Key Contributors to the Vulnerability of Dopamine Neurons. Current biology : CB *25*, 2349-2360.

Parker, W.D., Jr., Boyson, S.J., and Parks, J.K. (1989). Abnormalities of the electron transport chain in idiopathic Parkinson's disease. Annals of neurology *26*, 719-723.

Pissadaki, E.K., and Bolam, J.P. (2013). The energy cost of action potential propagation in dopamine neurons: clues to susceptibility in Parkinson's disease. Front Comput Neurosci *7*, 13.

Schapira, A.H., Cooper, J.M., Dexter, D., Clark, J.B., Jenner, P., and Marsden, C.D. (1990). Mitochondrial complex I deficiency in Parkinson's disease. Journal of neurochemistry *54*, 823-827.

Schapira, A.H., Cooper, J.M., Dexter, D., Jenner, P., Clark, J.B., and Marsden, C.D. (1989). Mitochondrial complex I deficiency in Parkinson's disease. Lancet *1*, 1269.

Shi, S.Y., Lu, S.Y., Sivasubramaniyam, T., Revelo, X.S., Cai, E.P., Luk, C.T., Schroer, S.A., Patel, P., Kim, R.H., Bombardier, E.*, et al.* (2015). DJ-1 links muscle ROS production with metabolic reprogramming and systemic energy homeostasis in mice. Nat Commun *6*, 7415.

Shimada, T., Fournier, A.E., and Yamagata, K. (2013). Neuroprotective function of 14-3-3 proteins in neurodegeneration. Biomed Res Int *2013*, 564534.

Shirakashi, Y., Kawamoto, Y., Tomimoto, H., Takahashi, R., and Ihara, M. (2006). alpha-Synuclein is colocalized with 14-3-3 and synphilin-1 in A53T transgenic mice. Acta Neuropathol *112*, 681-689.

Shulman, J.M., De Jager, P.L., and Feany, M.B. (2011). Parkinson's disease: genetics and pathogenesis. Annu Rev Pathol *6*, 193-222.

Su, Y.C., Guo, X., and Qi, X. (2015). Threonine 56 phosphorylation of Bcl-2 is required for LRRK2 G2019S-induced mitochondrial depolarization and autophagy. Biochimica et biophysica acta *1852*, 12-21.

Van Laar, V.S., and Berman, S.B. (2013). The interplay of neuronal mitochondrial dynamics and bioenergetics: implications for Parkinson's disease. Neurobiol Dis *51*, 43-55.

Wang, X., Yan, M.H., Fujioka, H., Liu, J., Wilson-Delfosse, A., Chen, S.G., Perry, G., Casadesus, G., and Zhu, X. (2012). LRRK2 regulates mitochondrial dynamics and function through direct interaction with DLP1. Human molecular genetics *21*, 1931-1944.